THESIS

LIVE-BED FAILURE MODES OF BENDWAY WEIRS AND ROCK VANES IN ALLUVIAL CHANNELS

Submitted by

Alex Wittmershaus

Department of Civil and Environmental Engineering

In partial fulfillment of the requirements

For the Degree of Master of Science

Colorado State University

Fort Collins, Colorado

Summer 2022

Master's Committee:

Advisor: Robert Ettema
Co-Advisor: Christopher Thornton

Stephanie Kampf

ABSTRACT

LIVE-BED FAILURE MODES OF BENDWAY WEIRS AND ROCK VANES IN ALLUVIAL CHANNELS

Bendway weirs and rock vanes are instream rock structures primarily used for managing the alignment of a channel's thalweg. Built from rock, bendway weirs and rock vanes are intended to function by directing flow away from a channel's outer bank and thereby reducing flow velocity along the outer bank. The present study investigated how bendway weirs and rock vanes placed in curved, alluvial channels subject to live-bed flow conditions (active bed-sediment transport) may fail. Further, the experiments then sought to recommend design dimensions so that bendway weirs and rock vanes accommodate failure (and loss of rock), thereby enabling them to continue performing as intended.

A curved flume was constructed in Colorado State University's Hydraulics Laboratory to conduct experiments that illuminated the failure modes and to confirm (or modify) preliminary design recommendations obtained from experiments using a straight flume fitted with three bendway weirs or rock vanes. The curved flume experiments involved a series of six bendway weirs or rock vanes and used a hydrograph procedure to simulate the rising limb of a hydrograph of flow along a medium sized river like the Middle Rio Grande; the proportions of the flume were like selected bends in that river. Six bendway weirs or rock vanes were needed to direct flow around the curved flume, as opposed to the need for three bendway weirs or rock vanes in the experiments in the straight flume. Two sizes of non-uniform bed sediment also were used (a medium sand and very coarse sand) for the experiments. The two sands were used to see if bed sediment size affected the failure modes.

The experimental results showed that bendway weirs and rock vanes experienced rock dislodgement primarily via contraction scour, which undermines the end, or tip, of these instream structures. Destabilized rock then tumbles into the scour zone along the channel's shifted thalweg, armoring the bed. This observation was observed for both the beds comprised of medium sand and very coarse sand. As flow depth increased above the mean elevation of the bendway weirs or rock vanes, contraction of flow reduced as more flow passed over the structures. The flow field at each bendway weir or rock vane changed.

The hydrograph procedure yielded similar changes in bed bathymetry for beds of medium sand and very coarse sand over the rising limb of the hydrograph. When $(\Delta y+H)/H = 0.75$, a deep scour hole formed in between the first two structures in the configuration within about 15 minutes. Then, when $(\Delta y+H)/H = 1.25$, the scour hole was partially filled with sediment and extended downstream largely along the series of bendway weirs or rock vanes. Further, when $(\Delta y+H)/H = 2.0$, the scour hole was again partially filled with sediment, but scour extended along the entire configuration of bendway weirs or rock vanes, thereby delineating a defined thalweg. As the flow depth increased, the maximum scour depth along the thalweg decreased for the experiments.

The bendway weirs and rock vanes experienced structural deformation due to rock dislodgement primarily from contraction scour. Less rock dislodgement occurred for these instream structures placed on the medium sand than when on the very coarse sand. Also, the rock vanes experienced less rock dislodgement than did the bendway weirs in general. This finding is attributed to upwards slope of the crest of rock vanes; the sloped crest directed more flow around each rock vane and over the already armored bed.

The results from using the hydrograph procedure in a curved flume confirmed the preliminary design recommendations from the straight flume. The design recommendations

required that bendway weirs or rock vanes be lengthened by $2d_{100}$ and their crests be widened by d_{100}; here d_{100} is the diameter of the largest rock used to build bendway weirs or rock vanes. This lengthening and widening accounts for the shortening and narrowing of bendway weirs or rock vanes subject to scour. A prior study recommended the size of rock chosen in design to form bendway weirs or rock vanes.

ACKNOWLEDGEMENTS

First, I would like to thank my advisor, Dr. Robert Ettema, and co-advisor, Dr. Chris Thornton for giving me the opportunity to work in the Hydraulics Laboratory and learn from them on this project. Their knowledge and guidance have been invaluable to me in completing this project, my academic studies, and starting my professional career. I would also like to thank my third committee member, Dr. Stephanie Kampf for her time and input.

A special thanks also goes out to Parker Maddocks for welcoming me when I joined the project and to Jeff Ellis for helping trouble shoot problems as they arose and helping organize testing logistics within the lab. I'd also like to thank the general lab crew who helped with the construction and maintenance of the flume and Alisher Khazratov for helping me with the LSPIV analysis.

Finally, I would like to thank my family for their support and encouragement over the last year and half. Specifically, I would like to thank my wife, Anna, for her daily love and support, which encouraged me to accomplish all that I am capable of. I would also like to thank my parents for their support and encouragement all the way from Wisconsin.

TABLE OF CONTENTS

LIST OF TABLES

LIST OF FIGURES

LIST OF SYMBOLS

A^* = percentage of baseline cross-sectional flow area blocked by structure

D_b = average thalweg depth in bend before the installation of structures

D = hydraulic depth

d_{50} = median particle diameter

H = height of BW crest, or height of crest at tip of RV

Δz = elevation difference between the baseline water surface and structure crest at the tip

L_c = length of the structure crest, measured as the distance along the structure crest from the waterline at the design flowrate to the tip of the crest

L_{proj} = projected length of the structure, defined as the shortest distance from the tip of the structure crest to the waterline along the outer bank

L_{arc} = arc length along the bank between the centerline of adjacent structures

m = slope of the structure toe, given as mH:1V (1 for bendway weirs)

$tan\phi$ = slope of the structure crest; $tan\phi = 0$ for bendway weirs

R_c = radius of curvature of channel bend centerline

T_w = average top-width of channel in the bend at the design flowrate before the installation of structures

α *or* θ = structure planform angle measured from the bank on the upstream side of the structure to the structure crest

W = width of structure crest

y = flow depth

Δy = change in flow depth

Y = flow depth at top of bank

CHAPTER 1. INTRODUCTION

1.1 Introduction

Colorado State University's Hydraulics Laboratory (CSU) has been working with the Bureau of Reclamation (BOR) since the early 2000s to improve the design layout and dimensions of bendway weirs and rock vanes, used as in-stream structures to manage thalweg alignment along alluvial-channel bends (Heintz 2002; Darrow 2004; Cox 2005; Kasper 2005; Kinzli 2005; Schmidt 2005; Walker 2009; Scurlock et al. 2014; Shin et al. 2018; Garfield 2019; Hogan 2019; Siefken et al. 2021; Maddocks 2021). In this regard, physical and numerical hydraulic models were used to investigate the effectiveness of the layout configuration of these structures. Also, field data from a sinuous reach of the Middle Rio Grande, New Mexico were used in the development of both the physical and numerical models. Additionally, the present study concerned alluvial channels with similar geometry to that of the Middle Rio Grande. An important aspect of improved design is ascertaining how bendway weirs and rock vanes fail when in alluvial channels.

The present study was funded by the BOR's Albuquerque Office (AO), New Mexico, with technical oversight and guidance given by BOR's Technical Advisory Center (TAC) in Lakewood, Colorado. Engineers from AO and TAC visited CSU in November 2021, and they discussed and confirmed some of the project's findings.

A major source of the data for the models was a large (1:12-scale for length) model of a representative reach of the Middle Rio Grande. Figure 1 shows the physical model, which provided data on water velocity, water-surface elevation, and observations on flow-field behavior. These data were also used to calibrate numerical computational fluid dynamic (CFD) models developed in the commonly available codes FLOW-3D and SRH-2D (Scurlock et al. 2014; Garfield and Ettema 2021; Hogan 2019; and Siefken et al. 2021). The models created with FLOW-3D simulated

steady-state, 3-dimenisonal flow fields whereas the model created with SRH-2D simulated 2-dimensional or depth-averaged flows.

Figure 1. Physical hydraulic model of a representative reach of the Middle Rio Grande. The model was located in CSU's Hydraulics Lab at the Engineering Research Center (Scurlock et al. 2014). This photo shows an early configuration of the reach fitted with a trapezoidal cross section.

The present study is focused on failure modes, and therefore, on producing design guidelines for the dimensions of these rock structures that ensure their stability and performance under live-bed conditions in alluvial channels. Initially, a single bendway weir was placed in an outdoor flume at CSU's hydraulics lab to study its stability under clearwater scour conditions. It was found that the clearwater conditions only produced minor failure of the bendway weir, rock failed locally at the base of the tip or end of the structure and did not cause the side slope of the structure to fail. BOR confirmed the results of this test and noted that field observations indicated more severe failure of these structures occurred under live-bed conditions. Therefore, it was determined that further experiments on bendway weir and rock vane failure should be conducted in a flume that could produce live-bed conditions to replicate the observed live-bed field conditions that caused the structure failure.

1.2 Objectives

This thesis study had the following primary objectives:

- Determine the main mode whereby bendway weirs and rock vanes fail owing to scour in curved alluvial channels.
- Ascertain how the maximum depth of scour at bendway weirs and rock vanes varies with flow stage (water level) relative to average crest height of bendway weirs or rock vanes.
- Determine the design dimensions of bendway weirs and rock vanes placed in alluvial channels with active sediment transport, such that live-bed scour would occur at these transverse instream-structures.

Attaining these objectives involved building a curved flume whose geometry was like a selected bend of the Rio Grande, then running a sequence of flows that mimicked flows in that bend. In this regard, the sequence had in to include flow conditions typical of when bendway weirs and rock vanes would be constructed. Additionally, the procedure just mentioned was done for two sizes of bed sediment (a medium sand and a very coarse sand), because a concern existed regarding the stability of bendway weirs and rock vanes placed on beds of finer sediment and on beds of coarser sediment, as this thesis elaborates.

Therefore, two additional objectives of this study were:

- Assess how experiment procedure affects the stability of rock structures
- Evaluate how some alluvial processes, such as dune formation and point-bar formation, may affect bendway weir or rock-vane performance.

CHAPTER 2. BACKGROUND

Rock vanes and bendway weirs are extensively used, transverse (across channel) rock structures placed in streams for channel management, particularly management of a channel's thalweg position. This chapter reviews bendway weir and rock vane use and design, concentrating specifically on current information regarding bendway weir and rock vane design and how these structures individually fail owing to scour of the alluvial bed on which they are placed.

2.1 Geometry of Rock Vanes and Bendway Weirs

Rock vanes and bendway weirs are designed to protrude into a channel from the outer bank. Rock vanes are characterized by their crest sloping down toward the center of the channel, as shown in Figure 2 whereas bendway weirs have flat crests. The sloped crest increases the area of flow blocked as the water level increases, providing a progressive hydraulic effect as discharge increases (NRCS 2005). Well-designed rock vanes should provide sufficient velocity reduction along the outer bank of a bend to prevent erosion, usually at a lower cost and with less environmental impact than a riprap revetment (Baird et al. 2015).

Figure 2. Rock vane installation (NRCS 2007).

The terms used to define the geometric variables of bendway weirs and rock vanes are complicated often by angled orientation of these rock structures placed in an alluvial-channel bend. This study adopts the following definitions for the variables (modified slightly [e.g., Δy instead of Δz]) from the definitions given by Baird et al. (2015).

D_b = average thalweg depth in bend before the installation of structures

L_c = length of the structure crest, measured as the distance along the structure crest from the waterline at the design flowrate to the tip of the crest

L_{proj} = projected length of the structure, defined as the shortest distance from the tip of the structure crest to the waterline along the outer bank

L_{arc} = arc length along the bank between the centerline of adjacent structures

m = slope of the structure toe, given as mH:1V

R_c = radius of curvature of channel bend centerline

T_w = average top-width of channel in the bend at the design flowrate before the installation of structures

W = width of structure crest

Δy = elevation difference between the baseline water surface and structure crest at its tip

θ = structure planform angle measured from the bank on the upstream side of the structure to the structure crest

$\tan\phi$ = slope of the structure's crest; with $\tan\phi = 0$ for bendway weirs

The projected length of rock vanes has been defined as $L_{proj} = L_c \sin\theta$ from previous studies. However, when these structures are constructed at small angles to a channels outer bank, and a bend has a small radius of curvature, this definition yields projected lengths significantly larger

than the distance from the outer bank to the structure's tip, as shown in Figure 3. Instead, Equation 1 should be used for these structures, as this equation calculates the exact distance from the outer bank to the structure tip for a channel with constant top-width and radius of curvature.

$$L_{proj} = R_c + \frac{T_w}{2} - \sqrt{L_c^2 + \left(R_c + \frac{T_w}{2}\right)^2 - 2L_c\left(R_c + \frac{T_w}{2}\right)\sin\theta} \quad (1)$$

Note that Equation 1 simplifies to $L_{proj} = L_c \sin\theta$ for $\theta = 90°$, or for R_c approaching infinity.

Being able to calculate the required crest length for a given projected length is useful when determining rock vane configuration. Equation 2 calculates the crest length as a function of projected length, planform angle, top-width, and radius of curvature.

$$L_c = \left(R_c + \frac{T_w}{2}\right) sin\theta - \sqrt{L_{proj}^2 - 2L_{proj}\left(R_c + \frac{T_w}{2}\right) + \left(R_c + \frac{T_w}{2}\right)^2 \sin^2\theta} \quad (2)$$

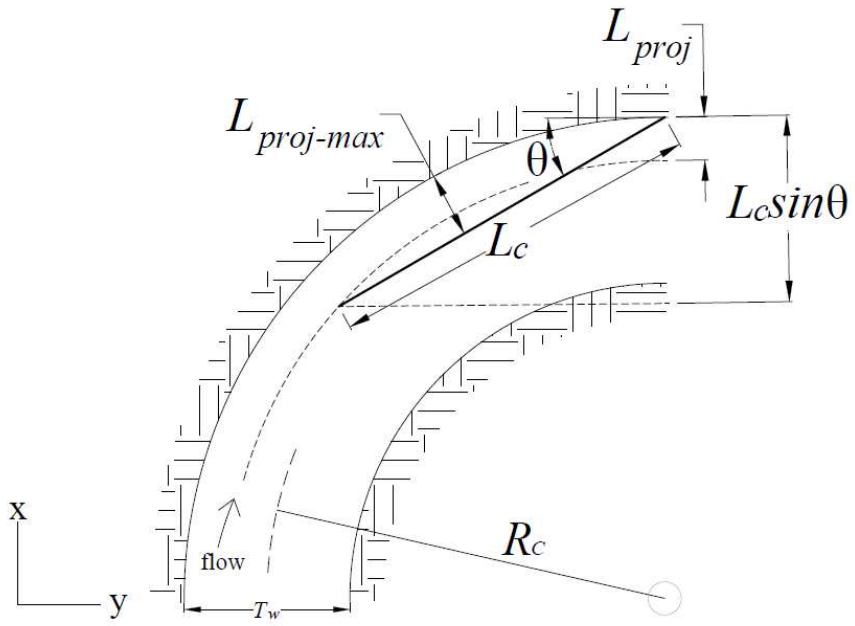

Figure 3. The effect of curvature on the projected length of a rock vane (Scurlock et al. 2014)

As assumed by Siefken et al. (2021), it is assumed here, that the crest of a rock vane intersects the bank at the design water surface elevation. The submergence of the vane tip, Δy, is typically related to the crest length and slope of the rock vane, $\tan\phi$, as defined by Equation 3.

$$\Delta y = L_c tan\phi \tag{3}$$

The area of flow blocked by a bendway weir or rock vane structure is important to consider. The flow blockage is defined as follows:

$$A^* = \frac{A_{structure}}{A_{flow}} \tag{4}$$

where, A^* = the percentage of baseline cross-sectional flow area blocked by structure, A_{flow} = the baseline area of flow before the installation of structures at a cross-section perpendicular to the direction of flow located at the root of the structure, and $A_{structure}$, is determined by projecting the structure onto the cross-section perpendicular to the flow direction, as shown in Figure 4.

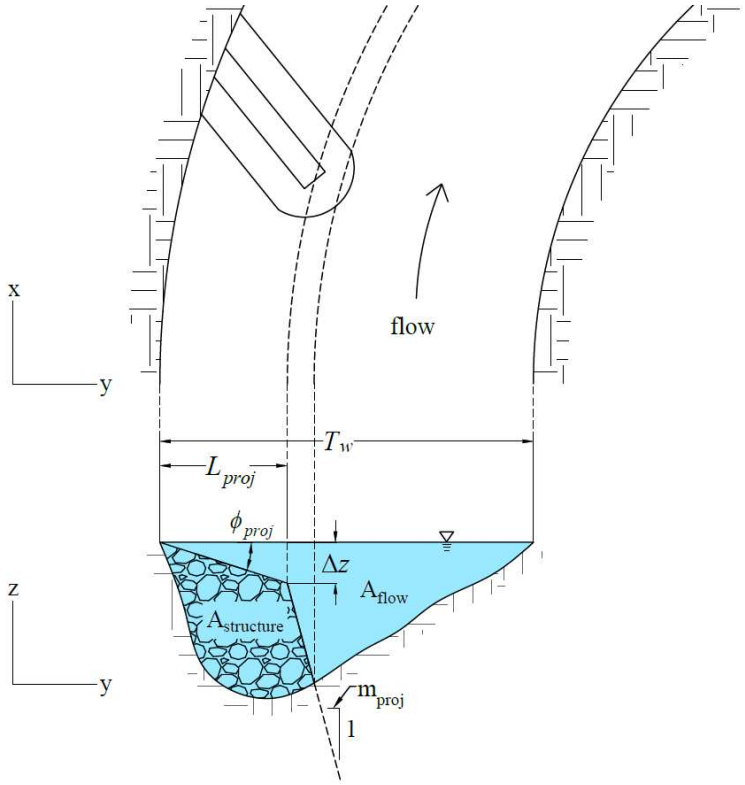

Figure 4. Projection of a rock structure onto a perpendicular cross-section (Siefken 2019).

The projection of the structure onto the cross-section results in the projected toe slope (m_{proj}H:1V) being steeper than the actual toe slope of the installed structure and the projected crest slope of rock vanes ($\tan\phi_{proj}$) is also steeper than the installed structure's crest slope. An exact projection would result in crest and toe slopes with small variations along the structure but is small enough to disregard in practical calculations. The mean projected crest is calculated in Equation 5 by dividing the projected length by the submergence of the structure tip.

$$\tan(\phi_{proj}) = \frac{L_{proj}}{\Delta y} \tag{5}$$

As the area blocked under the crest is large compared to the area blocked under the toe of the structure, the projected toe slope can be approximated by Equation 6.

$$m_{proj} \approx m * \sin\theta \tag{6}$$

2.3 Design Guidelines for Rock Vane Configurations

The most recent design guidelines for rock vane configurations are available in Siefken et al. (2021), which gives the following dimensions so that rock vane configurations perform as intended in design:

- Upstream angles ranging from 45° to 85° to the outer bank.
- Selection of crest slope is a balance between hydraulic performance and volume of rock required for construction. Decreasing the rock vane's crest slope reduces velocity along the outer bank.
- Optimal projected crest length ranges from 0.2 to 0.3 times the channel top width (bank-full flow).
- Optimal spacing was 0.75 times the channel top width. Reducing spacing below 0.5 times the top width produces no further reductions in outer bank velocity.
- For rock vanes installed at small planform angles in tightly curved bends, Seifken et al. (2021) recommends using Equation 1 to compute the projected length.
- Equation 8 (Seifken et al. 2021) gives preliminary estimates of reductions in flow velocities near the outer bank.

Seifken et al.'s (2021) guidelines are based on extensive numerical modeling using FLOW 3D, with the numerical models calibrated and validated with data from the physical hydraulic model shown in Figure 1.

The main attention regarding rock vane configuration is on determining vane length, spacing, and planform angle. It should be noted that Siefken et al. (2021) has no recommendation for rock vane height at the crest tip relative to the bank-full depth flow. Rock vanes, though extend upwards to the top of a channel's bank.

Table 1, taken from Maddocks (2021), summarizes geometric design guidelines for rock vanes. The guidelines are proposed in nine publications, including the guidelines suggested by Siefken et al. (2021). Whereas these guidelines provide general ranges of acceptable design parameters, the guidelines proposed before Siefken et al. are largely anecdotal and based on laboratory observations (e.g., Thornton et al. 2016) and have no verification via physical or numerical modeling. Several of the design guidelines report on field experience but little has been done to comparatively test the different designs.

Table 1. Summary of various design guidelines for rock vanes (Maddocks 2021).

	Length		Length Type	Spacing		θ		Crest slope	
Source	min	max		min	max	min	max	min	max
WSDOT (2017)	$T_w/3$		Projected	$4L_{proj}$		50°		10%	
NRCS (2013)	Length based on designed thalweg location, not to exceed $T_w/3$		Crest	Line from DS structure tip, parallel to bank tangent at tie-in, to intersection of US bank		20°	30°	5%	8%
NRCS (2010)	$T_w/10$	$0.35T_w$	Crest, but called effective length	Flow direction analysis		50°	80°	3%	10%
NRCS (2009)	Must cross thalweg, dependent upon horizontal angle, not to exceed baseflow $T_w/2$		Crest	$4L_c$	$5L_c$	50°	80°	0%	n/a
NRCS (2007)	$T_w/10$	$T_w/4$	Projected	$4L_{proj}$	$5L_{proj}$	<20°	45°	20%	

Source	Length		Length Type	Spacing		θ		Crest slope	
	min	max		min	max	min	max	min	max
NRCS (2005)	Must cross thalweg, dependent upon horizontal angle, not to exceed $T_w/3$		Crest	Line from DS structure tip, parallel to bank tangent at tie-in, to intersection of US bank		20°	30°	5%	8%
Johnson et al. (2001)	$T_w/4$	$T_w/3$	Projected	n/a	n/a	20°	30°	n/a	n/a
Maryland (2000)	n/a	$T_w/3$	Projected	$5T_w$	$7T_w$	20°	30°	3%	7%

2.4 Design Guidelines for Bendway Weir Configurations

The most recent design guidelines for bendway weir configurations also are available in Siefken et al. (2021). The guidelines give the following dimensions enabling bendway weir configurations to perform as intended in design:

- Upstream angles ranging from 45° to 85° to the outer bank.
- Optimal spacing was 0.75 times the channel top width. Reducing spacing below 0.5 times the top width produces no further reductions in outer bank velocity.
- Optimal projected crest length ranges from 0.2 to 0.3 times the channel top width (bank-full flow).
- Most bendway-weir configurations are largely ineffective at protecting the outer bank in comparison to configurations of rock-vanes. The optimal bendway weir configuration used a projected crest length of 0.25 times the channel top width and an upstream angle of 70°.

The geometric parameters for bendway weirs are defined the same as rock vanes, as shown in Figure 4. The crest of a bendway weir is designed to be submerged at design flow, which distinguishes it from a rock vane. Therefore, the bendway weir crest intersects the bank below the design water surface elevation unlike rock vanes, which have a sloped crest that intersects the bank at the design water surface elevation. It should be noted that, as with rock vanes, Siefken et al. (2021) does not recommend a value of bendway weir crest height relative to the bank-full depth of flow.

Bendway weirs were originally developed to improve navigation in river systems but have also been found to mitigate erosion of the outer bank in a curved channel (Biedenharn et al. 1997). A summary of existing design guidelines for bendway weirs from NCHRP Report 544 (McCullah and Gray 2005), Hydraulic Engineering Circular (HEC) 23 (Lagasse et al. 2009), and Julien and Duncan (2003) are in Table 2. The recommended design values vary considerably from one guide to another, with recommend length ranging from $T_w/10$ to $T_w/2$ and spacing from $1.5L_c$ to $5L_c$ (Maddocks 2021).

Table 2. Summary of existing design guidelines for bendway weirs (after Scurlock et al. 2014b). Height is given in terms of hydraulic depth (*D*) or bank full depth (BF) (Maddocks 2021).

Source	Length min	Length max	Length Type	Spacing min	Spacing max	θ min	θ max	Height min	Height max
NCHRP 544 (2005)	$T_w/3$	$T_w/2$	crest	$1.5L_c$		70°	80°	$D/2$	D
HEC 23 (2009)	$T_w/10$*	$T_w/3$	crest	$4L_c$	$5L_c$	60°	80°	0.3BF	0.5BF
Julien and Duncan (2003)	case-by-case		N/A	$2L$	$3L$	60°		Max permitting navigation	

*HEC 23 further recommends that the crest be long enough to cross the thalweg

The geometric design criteria for bendway weirs (and rock vanes) are limited in their approach by failing to consider the approach velocity of flow in the river bend (Baird et al. 2015). Regression equations have been developed by researchers in attempts to overcome this shortfall in BW and RV design. Scurlock et al. (2011(a) created a regression equation based on physical model studies at CSU's hydraulics lab in the Engineering Research Center and Shin et al. (2018) created a similar equation based on a numerical model study. It should be noted that official design guides have not adopted these equations.

2.5 Failure of Rock Vanes and Bendway Weirs

Scant few studies have examined rock vanes or bendway weirs placed in alluvial beds subject to live-bed conditions of sediment transport. The following summary of studies is based on compilation prepared by Maddocks (2021) and is elaborated here:

- Papanicolaou et al. (2018) used a *y/H* of 0.98 to 2.53 with barb dimensions from WSDOT. Their study focused on gravel bed scour development around barbs rather than failure of the barbs themselves. However, scour development was found to be a component in bendway weir and rock vane failure. Here, and below, *Y* is bank-full depth of flow, *H* is the height of a barb's mid-crest elevation, and *y* is flow depth.
- The study by Cunningham and Lyn (2016) used a *y/H* of 0.95 to 2.00 and took bendway weir design guidelines from HEC-23. Results of their study did not concentrate on bendway weir failure modes but provided useful insight into components causing failure such as the effect of *y/H* on scour development was more significant at 1.25 than 2.00.

- Garfield and Ettema (2021) report the findings of clearwater scour experiments on a single bendway weir, within CSU's large outdoor flume. The study used a *y/H* of 1.25 to 2.00 and assessed two-dimensional numerical modeling supported by flume data. The practical implications of using 2D versus a 3D model were briefly assessed by them. They report that 2D models were found suitable for designing bendway weirs to manage thalweg position, but inadequate for estimating near-bank velocities. Garfield and Ettema (2021) did not primarily focus on bendway weir or rock vane failure modes but provided useful insight into components affecting failure.

While bendway weirs and rock vanes placed in alluvial channels in flows producing live-bed conditions have not been extensively studied, abutments under the same conditions have due to their importance for waterway bridge stability. Abutments have a similar flow field to bendway weirs, even though flow overtops bendway weirs. Studies from Kwan (1984), Ettema et al. (2010), Jia et al. (2009), and Jamieson et al. (2011) show scour effects of flow field structure from abutment installation which can be attributed to scour effects observed around bendway weir and rock vane installation.

The most recent study on bendway weir and rock vane failure under live-bed conditions is documented by Maddocks (2021), who focused on studying these structures in a straight flume (2 ft wide) at CSU's hydraulics lab. His study preceded the present study and in various ways (e.g., obtaining initial insights into live-bed scour at bendway weir and rock vanes) was preliminary to the present study. A summary of his results from the straight flume is given below.

- The failure mode of contraction scour was more severe for $y/H = 1.25$ than when $y/H = 2.0$

- The approach of dune troughs led to structure failure by lowering the bed level at the upstream side slopes. The condition $y/H = 2.0$ was more problematic than when $y/H = 1.25$ because larger flow depths produce larger bed forms, in this case dunes.
- For both structure types, sediment accumulation caused slope reductions along the downstream side of the structure and would typically extend to the upstream side of the adjacent downstream structure. Such accumulation of sediment should not be considered a failure mode, because sediment accumulation reflected a reduction in flow velocity between adjacent structures.
- Both structure types experienced the same failure modes.
- As experimental conditions reached equilibrium (channel bathymetry remained stable) the rock structures experienced reduction in length, width, and slope but did not breach. Additional scour around the structures was prevented from rock dislodgement armoring the surrounding bed.

Maddock's study also conducted some preliminary experiments in the same curved flume used in this study. His preliminary findings are summarized below.

- The failure modes observed in the straight flume were verified by the results from the curved flume (bendway weirs and rock vanes experienced the same failure mechanisms).
- The lateral variation of bed bathymetry requires that a parameter used for the straight channel be re-defined: instead of y/H use $(\Delta y+H)/H$, where Δy is the depth of water above the crest tip of a bendway weir or rock vane; and H is the height of the crest tip above the local elevation of the bed.
- Failure modes were more severe for $(\Delta y+H)/H = 1.25$ than when $(\Delta y+H)/H = 2.0$ for the curved flume experiments.

- Contraction scour was the prevalent failure mechanism.
- For bendway weirs, sediment accumulation caused slope reductions along the downstream side of the structures, where experiments with $(\Delta y+H)/H$ = 1.25 displayed a greater reduction in slope. Slope reduction due to sediment accumulation was less severe for curved flume experiments relative to straight flume experiments. Sediment accumulation around the structures was not considered a failure but showed the structures were functioning properly.
- As the experiments approached equilibrium structures were reduced in size and were less abrupt along the downstream side of the structure. Further scour around the structures was prevented from dislodged rock armoring the surrounding bed.

The results from the straight- and curved-flume experiments provided useful insights into bendway weir and rock vane failure modes. The design recommendations in Figure 5 and Figure 6 were developed in collaboration with BOR (Maddocks 2021). These designs incorporate "sacrificial" rock into the design that is intended to dislodge with the failure mechanisms, armor the bed, and allow the structures to perform as designed.

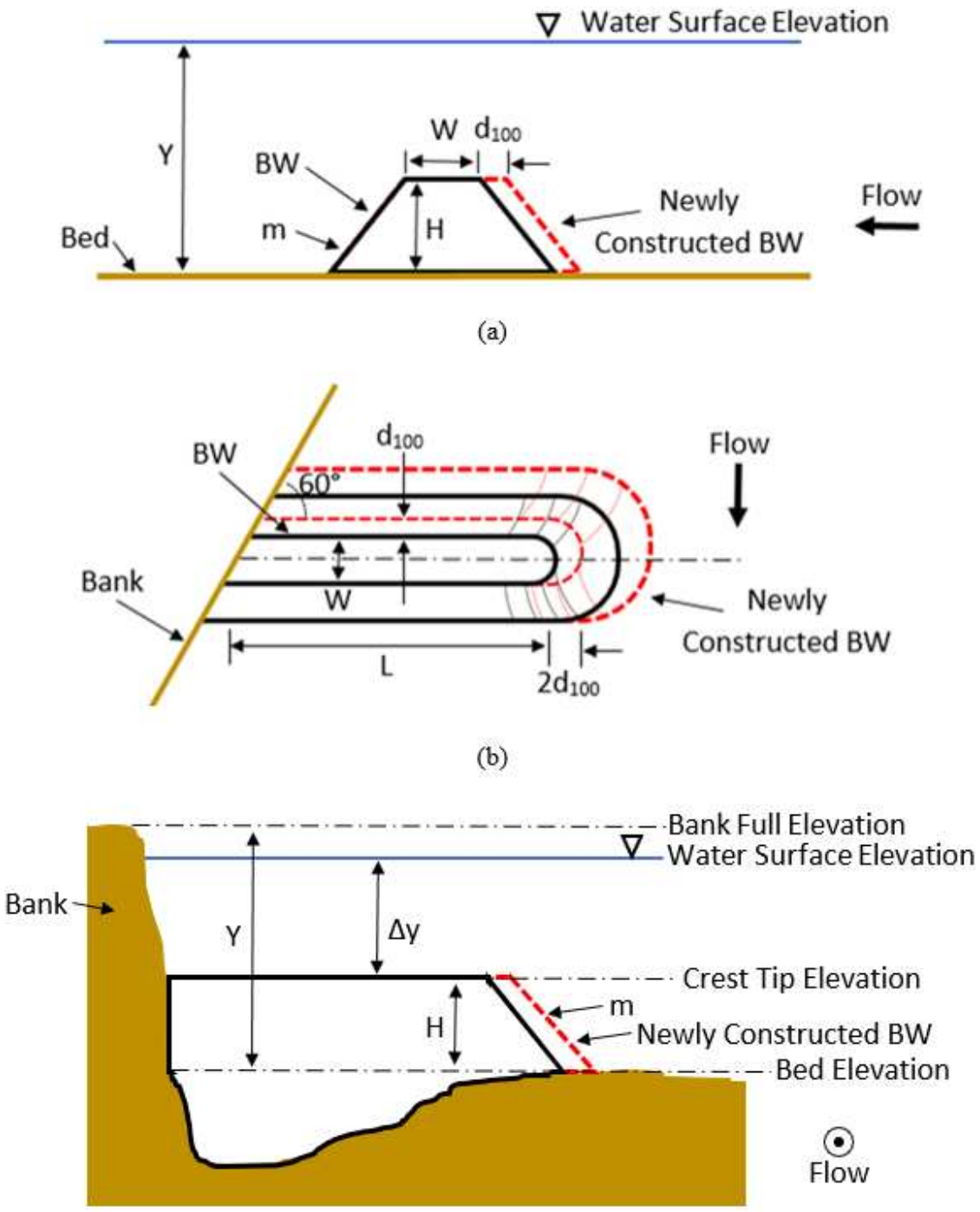

Figure 5. Design recommendation applied to a bendway weir: (a) cross-section view of the applied design recommendation; (b) plan view of the applied design recommendation; and (c) centerline elevation view of the design recommendation (Maddocks 2021).

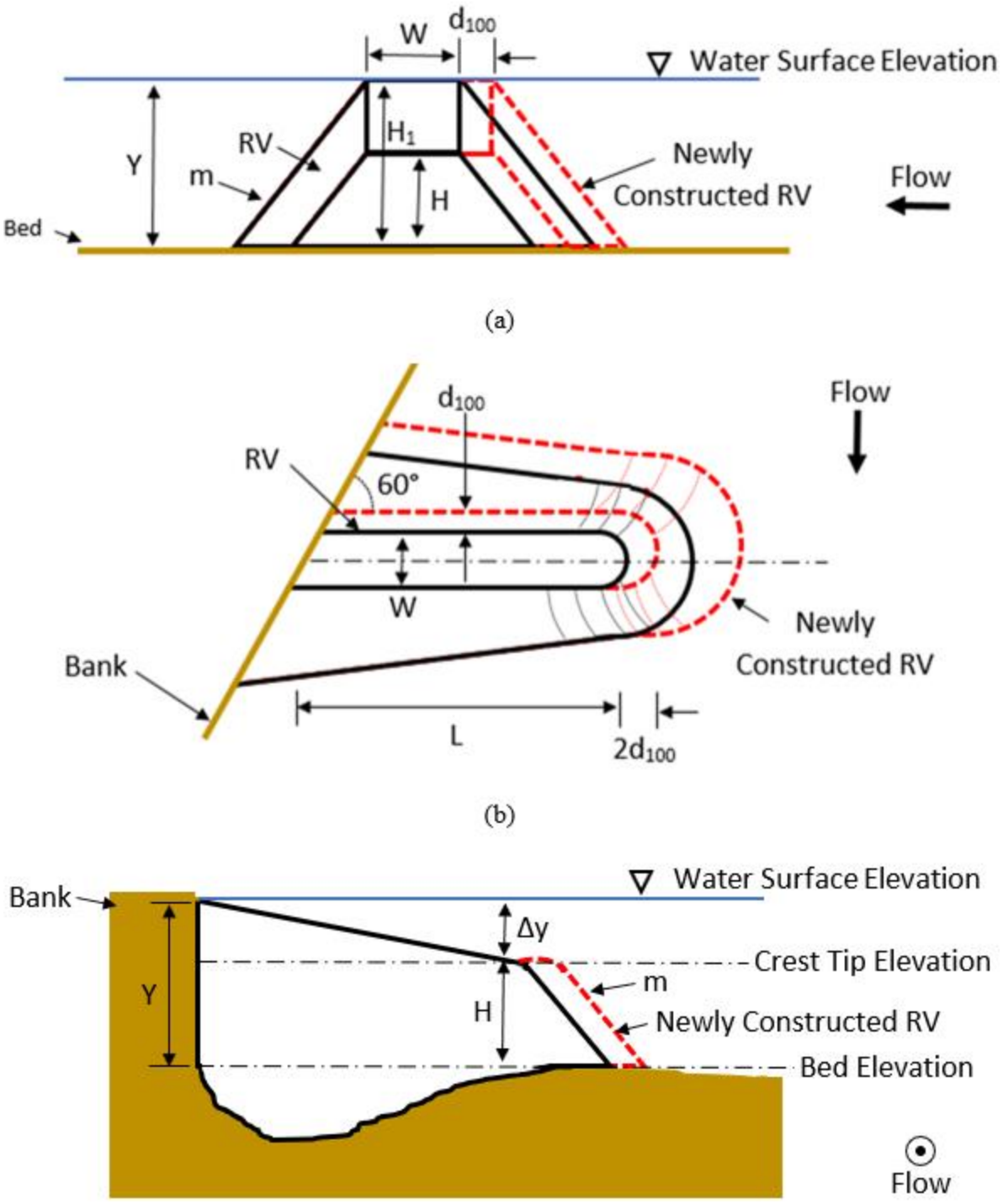

Figure 6. Design recommendation applied to a rock vane: (a) cross-section view of the applied design recommendation; (b) plan view of the applied design recommendation; and (c) centerline elevation view of the design recommendation (Maddocks 2021).

2.6 Conclusions from Literature Review

The conclusions from this literature review can be summarized as indicated below:

- Few studies have been conducted on failure modes of bendway weirs and rock vanes in alluvial channels under live-bed flows. Maddocks (2021) provides useful insights and design recommendations to preserve structure function under failure conditions.
- Despite development of numerous design guidelines in Table 1 and Table 2. Little comparative testing has been conducted regarding design guidelines and no design recommendations have been made to prevent the scour-related failure of individual rock vanes or bendway weirs (Maddocks 2021).

CHAPTER 3. EXPERIMENT SETUP

3.1 Introduction

This chapter presents the experimental setup and procedure used to meet the objectives described in Chapter 1. Details regarding the flume used for flow control, and live-bed setup, bendway weir and rock vane arrangements, program of experiments, instrumentation, and procedure are also covered in this chapter.

3.2 The Curved Flume

A 1.22 m wide (4.0-ft-wide) curved flume was specifically constructed for this study. The curved flume was constructed in a 6.1 m wide (20.0-ft-wide) indoor basin located in the Hydraulics Laboratory at CSU's Engineering Research Center. The geometric dimensions of the curved flume are described here and shown in the plan view given as Figure 7. The flume had trapezoidal cross-section geometry, a 1.22 m (4.0 ft) base width, and a bed consisting of 24.4 cm (10.0 in) thick layer of sand. The radius of curvature was based on channel bend dimensions given by the Bureau of Reclamation (Maddocks 2021).

Additional purposes of experiments were to check whether bendway weirs and rock vanes have the same failure modes as in the narrower, straight flume used by Maddocks, and to check the design recommendations from Maddocks (2021) regarding bendway weirs and rock vanes. The curved flume, being wider than the straight flume (and curved) may alter some of the failure modes observed in the straight flume. Additionally, the present study involved two sands: a medium sand and very coarse sand.

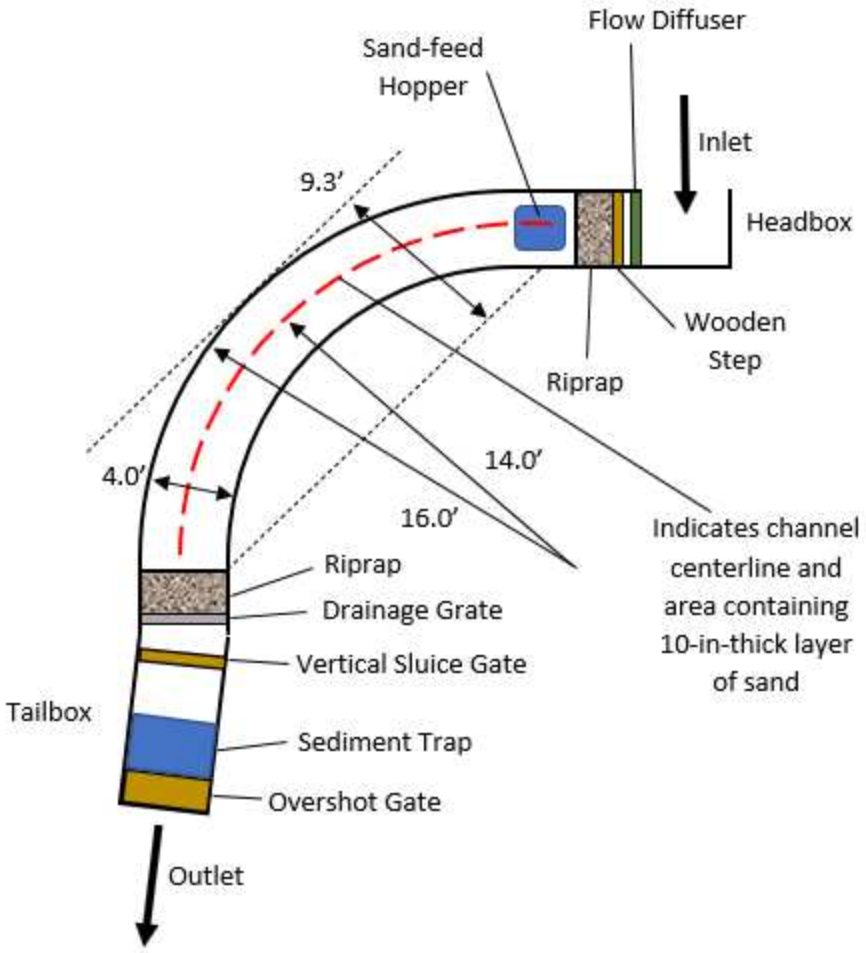

Figure 7. Curved flume dimensions. Note that sand was dispensed via the upstream side of the sand-feed hopper.

As the curved flume was purposely built for this study, the flume was constructed in a short period of time using an alternative, inexpensive construction method. The flume was built with materials recycled from previous (completed) projects on existing infrastructure and was comparatively inexpensive to building a new flume for this study. The remainder of this section, and the subsequent sections, detail the construction of the flume and supporting features.

The extents of the flume were defined within the 6.1 m basin and the lower walls were constructed using two layers of concrete blocks which were used to form the rectangular portion of the flume's bed. Sandbags were stacked to form the 1.5H:1.0V sloped banks. A black matting

was placed between the sandbags and concrete blocks to prevent the sandbags and pond liner from tearing as shown in Figure 8.

Figure 8. Completed curved flume channel walls without the rubber pond-liner and the Pyramat® cover. This figure shows how the flume's curved channel was built.

Once the curved walls were formed by the concrete blocks and sandbags, wood walls were framed and used to construct the head- and tail-boxes for the flume. The test flows would be guided into the flume through the head-box and out through the tail-box. Downstream, a sediment trap was constructed after the tail-box to collect sediment and prevent it from entering the laboratory's sump. The sediment trap consisted of an overshot gate and sudden channel expansion to decrease the water velocity and capture bed particles and cause suspended particles to settle out of the water column. At the flume's upstream end, a flow-diffuser (Figure 9) made from green Propex Pyramat® was placed after the head-box at the entrance of the flume to ensure the flow entering the channel was uniform.

Figure 9. Green Propex Pyramat® diffuser at the entrance of the flume.

An impermeable 15.2 m (50 ft) x 6.1 m (20 ft), 40-mil pond-liner (Figure 10) was installed to prevent leaking during test runs after the flume was fully formed. Rubber clamps and sandbags were used to keep the liner in place and prevent it from tearing. A green Propex Pyramat® (like that used for the diffuser) was placed over top of the pond-liner to give it relatively uniform texture and surface roughness.

Figure 10. Fitting the thick pond-liner (black) along the fume.

Once the pond-liner and Pyramat® were correctly placed into the flume, the flume was filled with sand to form the flume's bed. The Pyramat® was anchored by the sand and paracord anchors so small adjustments could be made readily. Small concrete blocks were used as temporary anchors to hold the Pyramat® in place as shown in Figure 11. The arrangement enabled the flume to be filled sand by means of a Bobcat (skid-steer), as Figure 11 indicates. Rakes and shovels were used to manually distribute and place the sand evenly along the entire flume. Figure 12 shows the flume completed and ready to run experiments.

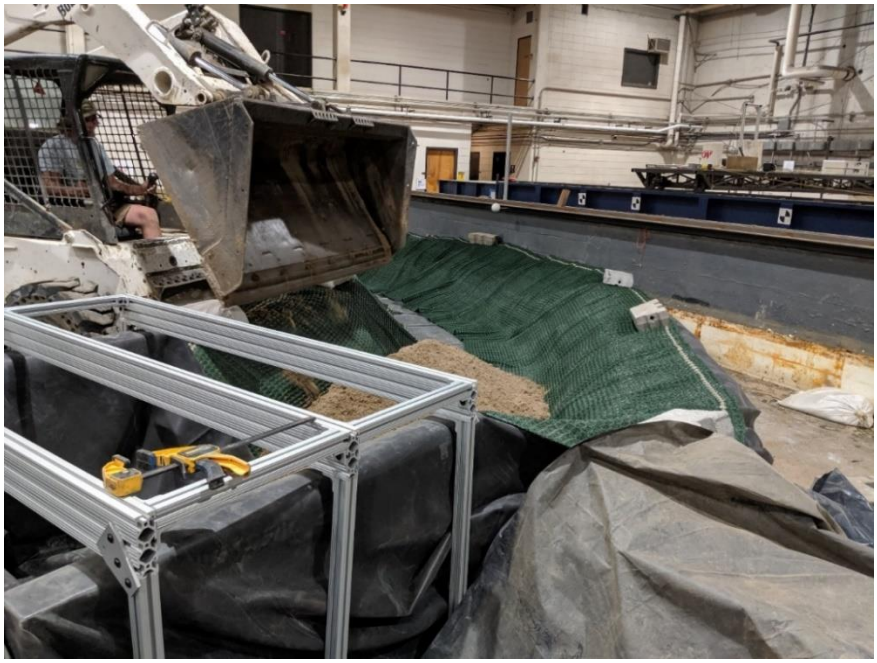

Figure 11. Use of a Bobcat to fill the curved flume with the sand, forming the flume's bed. Note that the concrete blocks positioned along the top of the sloping wall were temporary anchors, used until the sand had been placed in the curved channel.

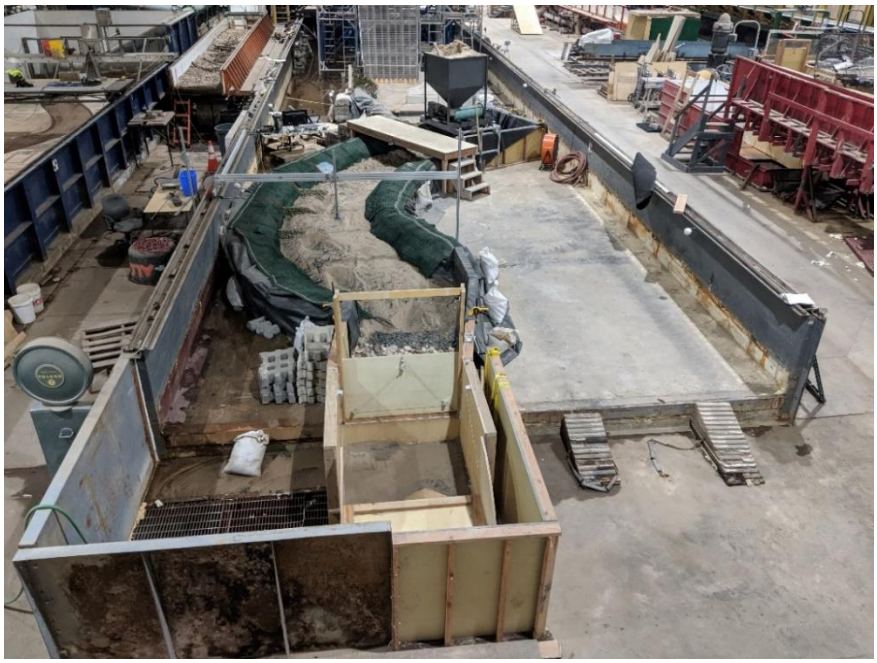

Figure 12. A view of the completed curved flume. The view also shows a configuration of bendway weirs placed in the flume.

3.2.1 Flow Control

Water was supplied to the curved flume via a 56 kW (75 HP) pump. Volumetric flowrate to the flume was regulated by a bypass valve located near the pump or a valve controlled by an electronic motor. An electromagnetic flowrate meter (Endress + Hauser Promag 53 W) positioned between the bypass and electronic valve was used to check the flowrate being supplied to the flume.

Two gates located at the downstream end of the flume were used to control the flow depth along the curved flume for each experiment. The first gate, a vertical sluice gate (Figure 13), was used to control the flow depth during test runs of $(\Delta y+H)/H = 0.75$ and was placed upstream of the tail-box and sediment trap. It was also used to avoid critical flow conditions while filling and draining the flume to maintain bedforms. The second gate, an overshot gate (Figure 14, also known as a tilting weir gate), was used to control the flow depth at $(\Delta y+H)/H = 1.25$, and $(\Delta y+H)/H = 2.0$

and prevent sand from entering the laboratory's sump. It was placed immediately downstream of the tail-box and sediment trap.

Figure 13. The vertical sluice gate used for flow depth control.

Figure 14. The overshot gate (or tilting weir gate) used for flow depth control.

A vertical sluice gate was chosen to control flow and avoid critical flow conditions because it was easier to seal to prevent leaking and was able to pass low amounts of flow required to maintain the flow depth for $(\Delta y+H)/H = 0.75$. Correctly filling and draining the flume was essential for comparison of the rock structures and bed conditions in the flume between each experiment. An overshot gate was chosen to control the flow depth for $(\Delta y+H)/H = 1.25$ and $(\Delta y+H)/H = 2.0$ because it created a vertical channel expansion which created a large channel cross-section that enabled sediment to settle out and discharged flow at the water surface.

A riprap filter was installed at the end of the curved flume before the flow entered the tail-box as shown in Figure 15 and was held in place by a perforated metal grate. The filter was used to prevent head-cutting from occurring during the slow process of filling and draining the flume. Particle size of the filter decreases in the upstream direction to prevent sediment loss in the flume. Ensuring the flume drained properly was vital for capturing LiDAR scans depicting the bed conditions.

Figure 15. Upstream view of riprap and drainage at the downstream end of the flume's curved channel.

3.2.2 Sediment Size

Two types of sand were selected for the experiments conducted in the curved flume. The first sand, a medium sand (Figure 16) was the same as the sand used in the straight-flume experiments conducted in Maddocks (2021). The second sand was in the category of very coarse sand (Figure 17), which is representative of the Middle Rio Grande River.

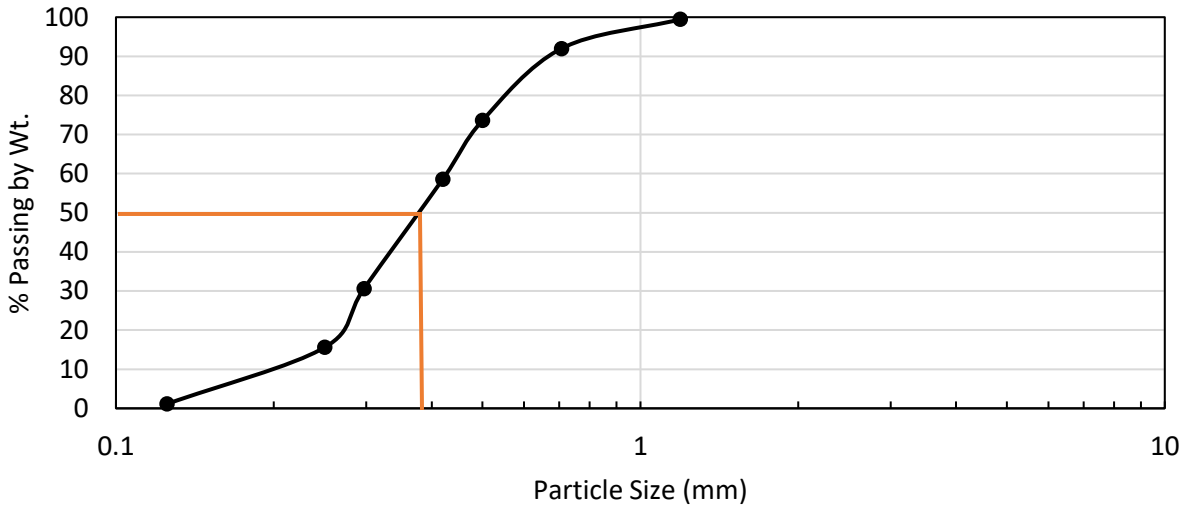

Figure 16. Medium sand particle size distribution curve (d_{50} = 0.38 mm, σ_g = 1.52).

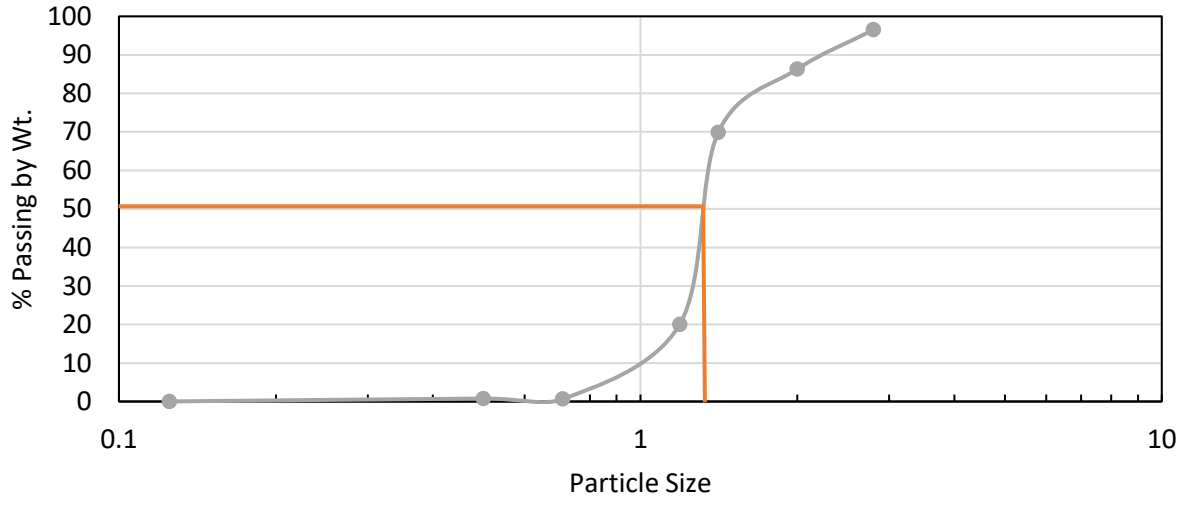

Figure 17. Very coarse sand particle size distribution curve (d_{50} = 1.3 mm, σ_g = 1.29).

The medium sand was 1-2% by weight magnetite (black sand) and the very coarse sand was 0-1% by weight magnetite. The specific gravity of magnetite is 5.2 compared to both sand's 2.65 (Keating & Knight 2008). Also, the d_{50} of magnetite sand was approximately 0.02-0.1 mm. As the concentration of magnetite was very small in the volume of sand used; therefore, it did not cause any armoring of the bed, but instead helped identify zones of higher shear stress on the bed. The shear stress associated with incipient motion of magnetite sand was estimated to be $\tau_c = 0.26$ (Julien 2010).

A hopper (Figure 18) was placed at the upstream end of the flume to discharge sand into the channel because the flume did not have a sediment recirculation system. A metal diffuser was fabricated and installed on the upstream side of the hopper to evenly distribute the sand along the width of the flume (Figure 19). The feed rates for the medium and very coarse sands were estimated using estimates obtained from the Meyer-Peter & Müller method (Julien 2010) and adjusted using the flume itself. The sediment feed rates were used to find the sediment discharge for the medium and very coarse sands as shown in Figure 20 and Figure 21. The feed rate of the hopper was tuned by measuring the rate at which sand was discharged, then by measuring the volume of sand retained in the tail-box and compared with the calculated volume of sand discharged into the flume. The difference in volume was calculated to be about 4% which could be attributed to sand being stored in the point bar formed on the inner bank of the flume and sand suspended in flow passing the overshot gate (Maddocks 2021).

Figure 18. The sediment hopper used to feed sand into the approach to the curved flume.

Figure 19. Sediment diffuser located at the base of the sand-feed hopper.

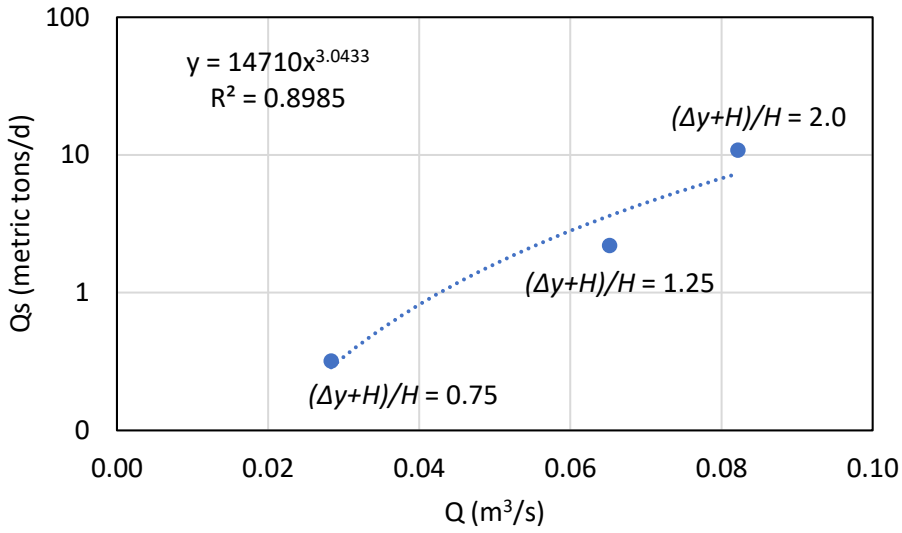

Figure 20. Medium sand sediment discharge diagram.

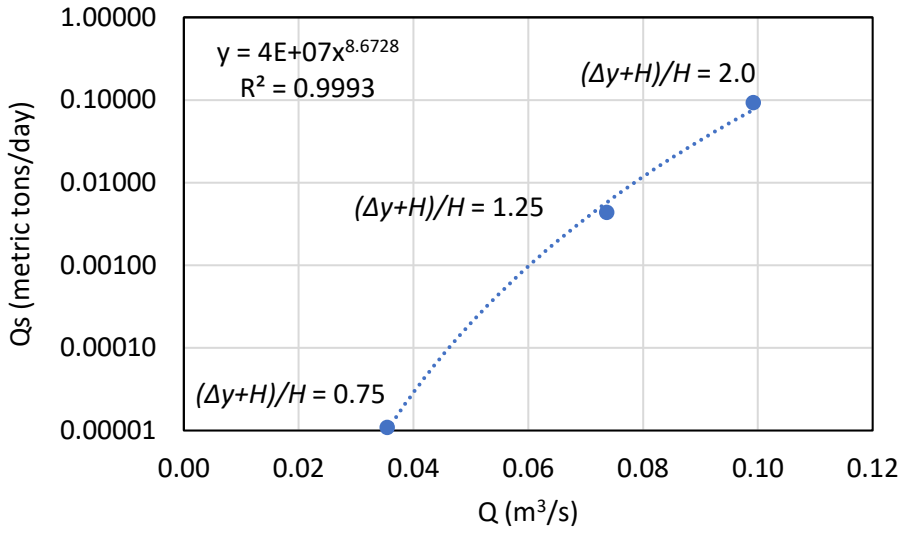

Figure 21. Very coarse sand sediment discharge diagram.

Five arbitrary points along the flume bed were monitored to ensure sediment equilibrium occurred toward the end of each experiment. The elevation of each point was measured every 5 minutes for the first 30 minutes and every 10 minutes after for the remainder of each experiment. Large changes in in the bed elevation occurred in the first 15 min with the sediment approaching

equilibrium conditions at 30 minutes. Fluctuations in the bed elevation after 30 minutes into the test can be attributed to bedforms moving along the bed due to the live-bed conditions.

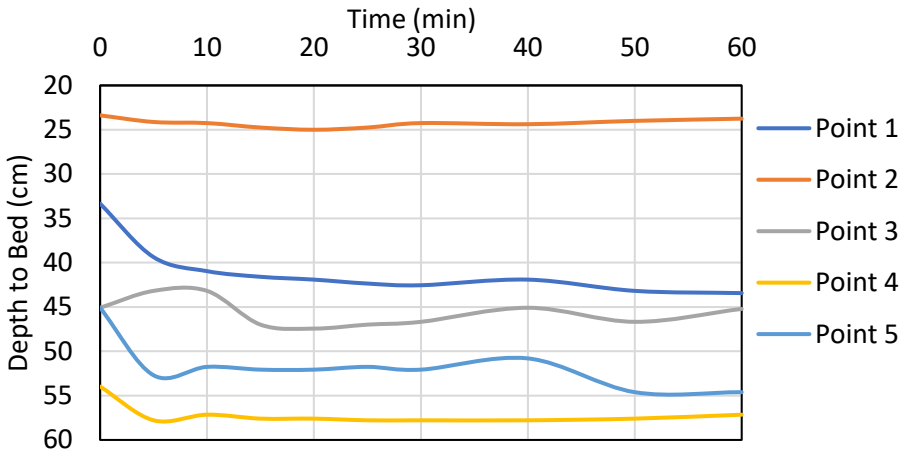

Figure 22. Monitored flume bed points to check sediment equilibrium.

3.2.3 Bendway Weir and Rock Vane Rock Size

The rock used to construct bendway weirs and rock vanes used in this study was sized using the methods outlined in Ettema et al. (2020). The particle size distribution of the rock is shown in Figure 23, where d_{50} = 12.5 mm and $d_{100} \approx$ 25 mm.Figure 23. Grading curve of the rock used to construct the bendway weirs and rock vanes used in this study (d_{50} = 12.5 mm, $d_{100} \approx$ 25 mm, σ_g = 1.60).

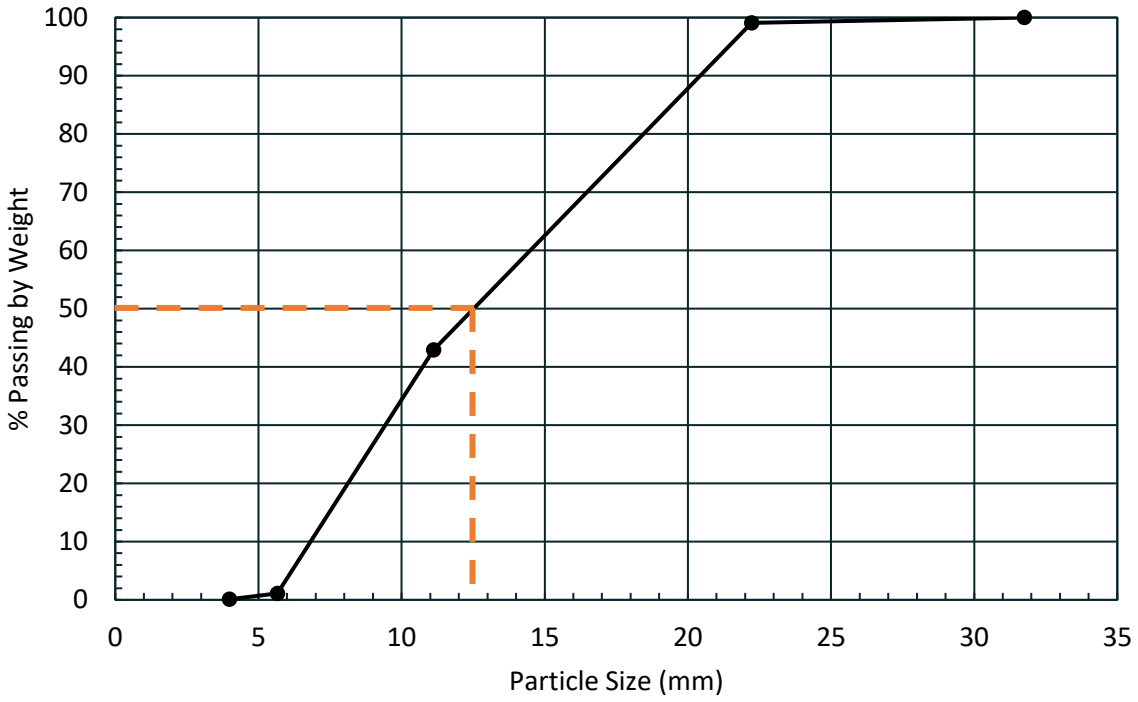

Figure 23. Grading curve of the rock used to construct the bendway weirs and rock vanes used in this study (d_{50} = 12.5 mm, $d_{100} \approx$ 25 mm, σ_g = 1.60).

3.2.4 Program of Experiment

Table 3 outlines the experiments conducted for this study. The first eight experiments were preliminary and the subsequent sixteen experiments tested the design recommendations via the hydrograph procedure from Maddocks (2021). Appendix a contains the results from every experiment.

Table 3. Program of experiments conducted in this study.

EXPT #	Structure	d_{50} (mm)	Q (m^3/s)	y (cm)	Shear stress ratio τ_0/τ_c	$(\Delta y+H)/H$	Design α (Degrees)	Design W (cm)	Design L (cm)	Design H (cm)	S_0
Preliminary Experiments											
1a	3BW	0.38	0.08	15.2	7.7	2.0	90	7.62	20.3	7.62	0.0012
2a	4BW	0.38	0.08	15.2	7.7	2.0	90	7.62	40.6	7.62	0.0012
3a	4BW	0.38	0.08	15.2	7.7	2.0	90	7.62	40.6	7.62	0.0012
4a	4BW	0.38	0.07	9.53	4.8	1.25	90	7.62	40.6	7.62	0.0012
5a	4BW	0.38	0.07	9.53	4.8	1.25	90	7.62	40.6	7.62	0.0012
6a	6RV	0.38	0.07	9.53	4.8	1.25	90	7.62	40.6	7.62	0.0012
7a	6RV	0.38	0.08	15.2	7.7	2.0	90	7.62	40.6	7.62	0.0012
8a	6RV	0.38	0.03	5.72	2.9	0.75	90	7.62	40.6	7.62	0.0012
Main Experiments											
9a	-	1.3	0.07	9.53	1.6	1.25	60	7.62	52.1	7.62	0.0012
10a	6BW	1.3	0.04	5.72	0.9	0.75	60	7.62	52.1	7.62	0.0012
11a	6BW	1.3	0.07	9.53	1.6	1.25	60	7.62	52.1	7.62	0.0012
12a	6BW	1.3	0.10	15.2	2.5	2.0	60	7.62	52.1	7.62	0.0012
13a	-	1.3	0.07	9.53	1.6	1.25	60	7.62	52.1	7.62	0.0012
14a	6RV	1.3	0.04	5.72	0.9	0.75	60	7.62	52.1	7.62	0.0012
15a	6RV	1.3	0.07	9.53	1.6	1.25	60	7.62	52.1	7.62	0.0012
16a	6RV	1.3	0.10	15.2	2.5	2.0	60	7.62	52.1	7.62	0.0012
17a	-	0.38	0.07	9.53	4.8	1.25	60	7.62	52.1	7.62	0.0012
18a	6BW	0.38	0.04	5.72	2.9	0.75	60	7.62	52.1	7.62	0.0012
19a	6BW	0.38	0.07	9.53	4.8	1.25	60	7.62	52.1	7.62	0.0012
20a	6BW	0.38	0.08	15.2	7.7	2.0	60	7.62	52.1	7.62	0.0012

21a	-	0.38	0.07	9.53	4.8	1.25	60	7.62	52.1	7.62	0.0012
22a	6RV	0.38	0.04	5.72	2.9	0.75	60	7.62	52.1	7.62	0.0012
23a	6RV	0.38	0.07	9.53	4.8	1.25	60	7.62	52.1	7.62	0.0012
24a	6RV	0.38	0.08	15.2	7.7	2.0	60	7.62	52.1	7.62	0.0012

Note:

- The experiments referenced henceforth in this thesis follow the numbering system indicated in the first column.

3.2.5 Data Collection

Throughout this study, various data were collected via a variety of different methods. The methods include LiDAR scans of the flume bed, Large-Scale Particle Image Velocimetry (LSPIV), Acoustic-Doppler-Velocimeter (ADV), structure measurements (via a tape measure), and water surface (via Massa acoustic probes) and bed elevation measurements (via Massa acoustic probes, tape measure, and LiDAR). The ensuing paragraphs of this section will discuss the methods used to collect the data.

LiDAR scans of the curved flume were collected using a TOPCON GLS-2000 3D Laser Scanner. The flume's bed was scanned before and after each experiment to compare the changes in bend bathymetry. The TOPCON Scanner was placed at two different locations, one upstream on the bridge and the other downstream by the riprap filter (Figure 24) to get complete coverage of the bed and rock structures. The scanner was surveyed into the Hydraulics Laboratory's existing coordinate system to avoid distortion in the results. The data from the scanner were transferred to a computer via an SD card and post-processed in the computer program Magnet collage where it was output as an Autodesk Recap file for viewing. Autodesk Recap was used to removed excess data points and scale the scan based on elevation.

Figure 24. The LiDAR instrument used to scan the curved channel bed after a completed experiment.

Surface water velocity was recorded using Large-Scale Particle Image Velocimetry (LSPIV). This method involved dispersing shredded paper (mean diameter of 5 mm), using a video camera to record its passage through the flume, then post-processing the video. Figure 25 shows the video camera used to record the paper particles passing through the flume. LSPIV data are documented here in Appendix B of this thesis.

Figure 25. Setup used to record the video for LSPIV.

Data on the maximum velocity of flow at the tip of bendway weirs and rock vanes were collected using an Acoustic-Doppler-Velocimeter (ADV). Specifically, a SonTek FlowTracker Handheld ADV was used to collect velocity at the BW and RV tips (as seen in Figure 26) in addition to collecting velocity at the outer bank when no structures were present. The ADV provided 3-dimensional velocity data that was manually imputed into Microsoft Excel to produce results for this study. ADV data are in this thesis' Appendix C.

Figure 26. Bendway weir tip velocity being measured with a SonTek FlowTracker Handheld ADV for (Δy+H)/H = 1.25

Measurements of the rock structures (bendway weir and rock vane) were taken after each experiment in the hydrograph sequence of testing. These measurements included crest length, crest slope (RVs only), height, width, orientation, structure tip scour depth, and maximum scour depth. A tape measure was used to collect the various measurements. The scour depth as measured by placing a thin piece of wood at the base of the structure, extending it over the scour hole as shown in Figure 27, and measuring the distance between it and the bottom of the hole. Once the data were collected in was manually input into Microsoft Excel for processing. The structure measurement data are in this thesis' Appendix D.

Figure 27. Rock vane tip scour being measured in very coarse sand.

Massa ultrasonic sensors were used to collect the water surface and bed surface elevations. Two Massa probes were placed along the flume, one of them being permanently located on the bridge (Figure 28. Massa probes (ultrasonic sensors) used for collecting bed surface and water-surface elevation (WSE): (a) the stationary Massa probe; and (b) a mobile Massa probe was used for collecting data at different locations along the flume.) and the other located on a mobile frame (Figure 22b) that moved over the flume. Five points along the channel were selected to record the water surface elevation for every experiment. The Massa probes were connected to a data station that enabled them to communicate with the computer program NI LabVIEW which was used to process the measurements. After processing the measurements, the results were recorded using Microsoft Excel. The Massa probe data are in this thesis' Appendix E.

(a)

(b)

Figure 28. Massa probes (ultrasonic sensors) used for collecting bed surface and water-surface elevation (WSE): (a) the stationary Massa probe; and (b) a mobile Massa probe was used for collecting data at different locations along the flume.

3.2.6 Procedure used for Preliminary Curved Flume Experiments

The procedure outlined below was used to conduct the preliminary experiments using the curved flume.

1. Before the initial bed forming flow was run, the bed was refilled with sediment and leveled. The sediment trap was emptied, and the hopper refilled with dry sand as needed.
2. The pump was turned on at a lower flow rate than desired to slowly fill the flume. Once the flume was filled, the pump was set to the required flowrate for the initial bed forming flow conditions, the sluice and overshot gates were opened and adjusted to maintain the appropriate flow depth. Additionally, the hopper was turned on and set to the sediment feed rate required for the flow conditions.
3. The water surface elevation was monitored and recorded for the selected five points along the flume throughout the duration of the experiment.
4. After running the flume 2-4 hours to reach bedform equilibrium, the sluice gate was closed, and pump and hopper were shut off. Closing the sluice gate enabled the flume to slowly drain and prevent bedforms from washing out.
5. Rock structures were installed in the flume and the bed was LiDAR scanned.
6. Again, the pump was turned on at a lower flow rate than desired to slowly fill the flume to prevent damaging the structures. When the flume was filled, the pump was set to the required flowrate for the experiment, the sluice and overshot gates were opened and adjusted to maintain the appropriate flow depth. Additionally, the hopper was turned on and set to the sediment feed rate required for the flow conditions.

7. The water surface elevation was monitored and recorded for the selected five points along the flume throughout the duration of the experiment. Photos also were taken during the experiments.
8. After running the flume 2-4 hours to reach bedform equilibrium, the sluice gate was closed, and pump and hopper were shut off. Closing the sluice gate let the flume slowly drain and prevent bedforms from washing out.
9. The bed was LiDAR scanned and photos were taken of the channel.

3.2.7 Procedure used for Main Curved Flume Experiments

The procedure outlined below was used to conduct the hydrograph procedure in the curved flume.

1. Before the initial bed forming flow was run, the bed was refilled with sediment and leveled. The sediment trap was emptied, and the hopper refilled with dry sand as needed.
2. The pump was turned on at a lower flow rate than desired to slowly fill the flume. When the flume was filled, the pump was set to the flowrate for the initial bed forming flow conditions ($(\Delta y+H)/H = 1.25$), the sluice and overshot gates were opened and adjusted to maintain the appropriate flow depth. Additionally, the hopper was turned on and set to the feed rate required for the flow conditions.
3. The water surface elevation was monitored and recorded for the selected five points along the flume throughout the duration of the experiment.
4. At the end of the experiment, the LSPIV data were collected.
5. After running the flume 4 hours to reach bedform equilibrium, the sluice gate was closed, and pump and hopper were shut off. Closing the sluice gate let the flume slowly drain and

prevent bedforms from washing out. Additionally, a sump pump in the headbox was used to drain the flume from the head-box as well.

6. Rock structures were installed in the flume and the bed was LiDAR scanned.
7. Again, the pump was turned on at a lower flow rate than desired to slowly fill the flume to prevent damaging the structures. Once the flume was filled, the pump was set to the required flowrate for the flow conditions of $(\Delta y+H)/H = 0.75$, the sluice and overshot gates were opened and adjusted to maintain the appropriate flow depth. Additionally, the hopper was turned on and set to the sediment feed rate required for $(\Delta y+H)/H = 0.75$.
8. The water surface elevation was monitored and recorded for the selected five points along the flume throughout the duration of the experiment. Photos were also taken of the channel during the experiments.
9. At the end of the experiment, the LSPIV data were collected.
10. After running the flume 4 hours to reach bedform equilibrium, the sluice gate was closed, and the pump and hopper were shut off. Closing the sluice gate let the flume slowly drain and prevent bedforms from washing out. Additionally, a sump pump in the headbox was used to drain the flume from the upstream end as well.
11. The bed was LiDAR scanned, structure measurements and photos of the channel were taken.
12. The hopper was refilled as needed.
13. Steps 7-12 were repeated for $(\Delta y+H)/H = 1.25$ and $(\Delta y+H)/H = 2.0$.

Figure 29 and Figure 30 show the hydrograph procedures used for the medium and very coarse sands, respectively.

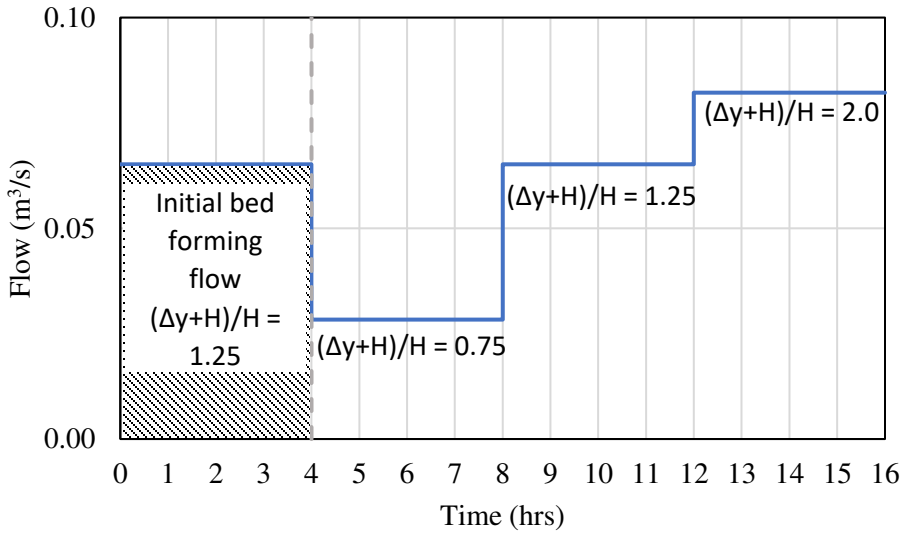

Figure 29. Sequence of discharges used in the hydrograph procedure for conducting experiments with medium sand.

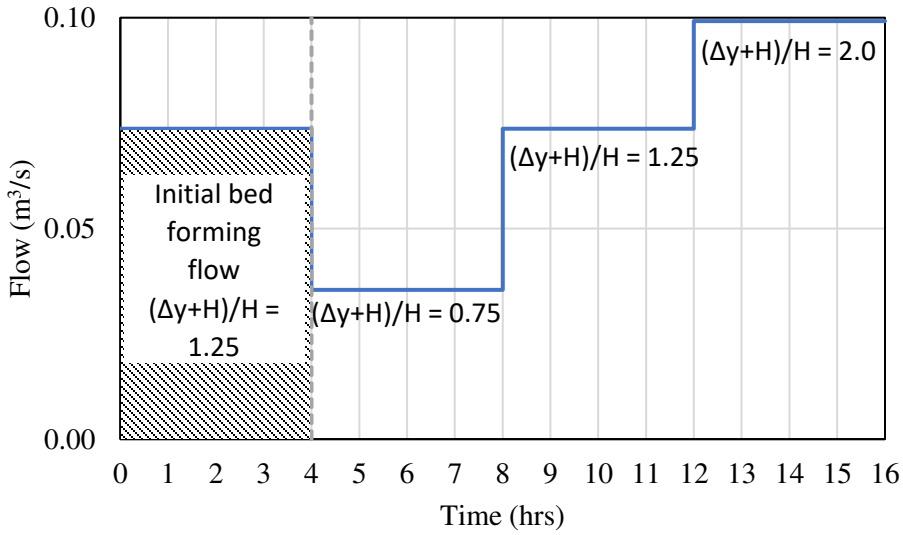

Figure 30. Sequence of discharges used in the hydrograph procedure for conducting experiments with very coarse sand.

CHAPTER 4. EXPERIMENT RESULTS

4.1 Introduction

This chapter presents the results from the experiments conducted in this study. Only the main results are presented in the following sections. Observations and data mentioned are from select experiments representative of the main findings from this study. Findings from the preliminary experiments are presented and discussed first. Then, the results of the main experiments are presented and discussed.

The preliminary experiments were conducted with bendway weirs and rock vanes placed on the bed of medium sand to determine if the bendway weir and rock vane experience the failure mechanisms reported by Maddocks (2021). His observations using the straight flume applied to these structures placed in curved alluvial channels bend subject to live-bed flows. Maddocks (2021), assisted by the author of this thesis, reported on the findings of bendway weirs in these conditions and found that bendway weirs experience the same main primary failure mechanisms, though a dune trough is present at the upstream face at the upstream face of the first bendway weir. The preliminary results of this study therefore focus on a series of rock vanes using the configuration recommended in Seifken et al. (2021) in an alluvial channel bend under live-bed flows because it has not been reported whether the failure mechanisms observed in Maddocks (2021) occur at these structures.

Once the preliminary experiments were concluded, subsequent experiments were conducted using a hydrograph procedure and a series of 6 bendway weirs or rock vanes (using the layout configurations from Seifken et al. 2021) to test the design recommendations from

Maddocks (2021) in conditions typical of those found in Middle Rio Grande or similar mid-sized rivers.

4.2 Preliminary Results: Before and After Procedure

As mentioned in Chapter 1, the objective of the preliminary experiments was to verify the main failure mode observed in the straight flume (Maddocks 2021) occur for rock vanes in an alluvial channel bend subject to live-bed flows. EXPTs 6a (see Table 3) is representative of the findings regarding rock vanes in a curved alluvial channel under live-bed flows. A configuration of 6 rock vanes installed normal (90˚) to the flume's outer bank with each structure having the same dimensions was used in this experiment. EXPT 6a was ran at $(\Delta y+H)/H = 1.25$.

EXPT 6a showed the same failure mechanisms from the straight flume and preliminary curved flume experiments from Maddocks (2021). The first rock vane (number 1 in **Figure 31**a) experienced rock dislodgement on the upstream side and at the structure tip due to contraction scour. The remaining rock vanes (numbers 2 – 6) primarily experienced rock dislodgement at their structure tips due to contraction scour. Herein, the numbering system is used to name each rock vane in an experiment series (e.g., 1 refers to the first bendway weir or rock vane in the series of 6 structures).

Sediment deposition behind rock vane 1 (Figure 31a) and subsequent rock vanes led to a decrease in downstream slope. Structures also experienced a decrease in upstream slope when sediment deposition occurred behind the structure upstream of them, this occurred for all structures in the rock vane configuration with rock vanes 1 and 6 being the only exception as seen in Figure 31 and Figure 32.

Figure 32 also shows the movement of the channel thalweg and point bar. Figure 32a shows the flume bed after initial bed forming flow conditions with structures installed on it.

Figure 32b shows the flume bed after running EXPT 6a where $(\Delta y+H)/H$ = 1.25. The channel thalweg moved from the outer bank of the channel to the structure tips with the old thalweg being filled in with sediment. The point bar also narrows and is pushed downstream by the configuration of six rock vanes.

(a)

(b)

Figure 31. Photos of Rock vanes from EXPT 6a where $(\Delta y+H)/H$ = 1.25: (a) shows rock vanes 1-3; and (b) shows rock vanes 4-6.

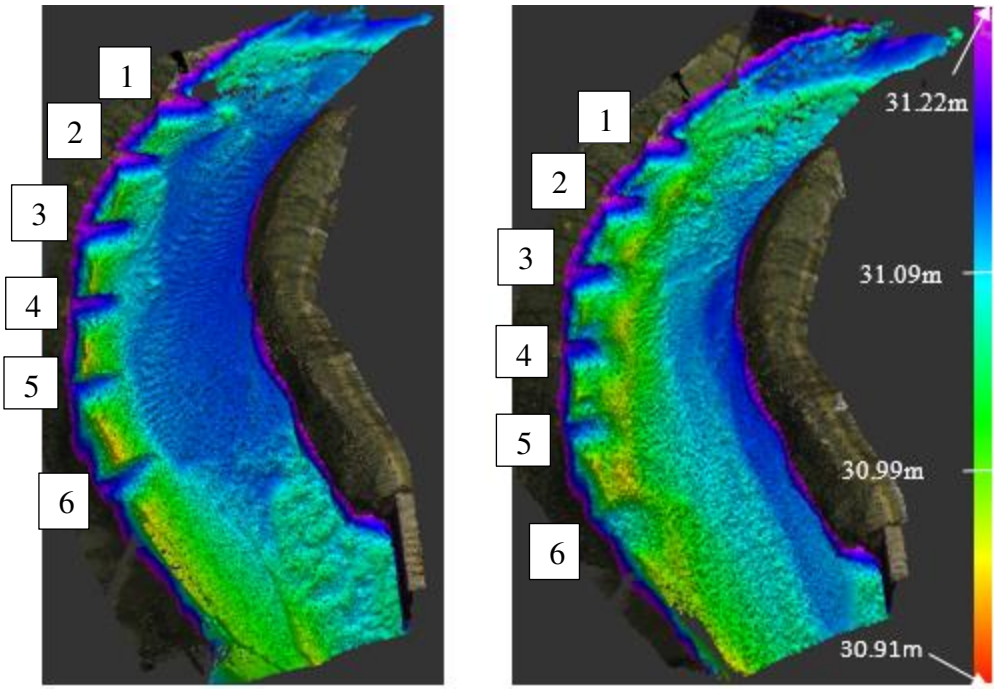

(a) (b)

Figure 32. Lidar scans associated with EXPT 6a: (a) before and (b) after. Note some of the deep areas on the outer bank filled with sediment, the thalweg shifted to the structure tips, and the point bar has narrowed and shifted downstream.

4.3 Main Experiments: Hydrograph Procedure

The main experiments used the hydrograph procedure and were conducted to address the primary objectives of this study and thereby to test the design recommendations proposed in Maddocks (2021). EXPTs 13a – 16a are representative of the results obtained for bendway weirs and rock vanes placed on the beds of very coarse sand and medium sand.

EXPTs 13a – 16a were conducted with six rock vanes placed on the bed of very coarse sand. The rock vanes were constructed using the design recommendations proposed by Maddocks (2021) for individual structures: the length of the structure was increased by $2d_{100}$ and the structure's width increased by d_{100}.

The primary mechanism for rock dislodgement throughout this first series of experiments was contraction scour, as indeed seen in the preliminary tests. However, the extent of contraction scour along the configuration of rock vanes varied for the hydrograph procedure compared to the

preliminary tests, because the extent of contraction could vary along the curved flume. For $(\Delta y+H)/H = 0.75$, contraction scour primarily occurred between the first two structures (bendway weirs or rock vanes), forming a relatively deep scour hole that was the deepest observed during the experiments (Figure 33b). When $(\Delta y+H)/H = 1.25$, contraction scour extended further all the way along all six structures but had varying amounts of scour depth (Figure 33c). Then, when $(\Delta y+H)/H = 2.0$, contraction scour occurred along all six structure and was relatively uniform in depth (Figure 33d); i.e., scour depth was about the same at the tip of each of the six structures.

Figure 33 compares the LiDAR scans from each step of the hydrograph procedure using rock vanes and very coarse sand to show the changes in bed bathymetry over time. The scans confirm that, over the series of experiments, the thalweg shifted from the outer bank to a line along the structure's tips and the point bar was pushed downstream.

Sediment deposition primarily occurred behind the first five structures (Figure 34a 1-5) for $(\Delta y+H)/H = 0.75$, the first three structures (Figure 34b 1-3) for $(\Delta y+H)/H = 1.25$, and the first two structures (Figure 34c 1-2) for $(\Delta y+H)/H = 2.0$ as shown in Figure 34. The LiDAR scans also show that while sediment deposition did occur behind structures 1 and 2 for $(\Delta y+H)/H = 1.25$ and 2.0, scour occurred behind structures 3 – 6 when the water level exceeded the height of the rock vane's crest tip.

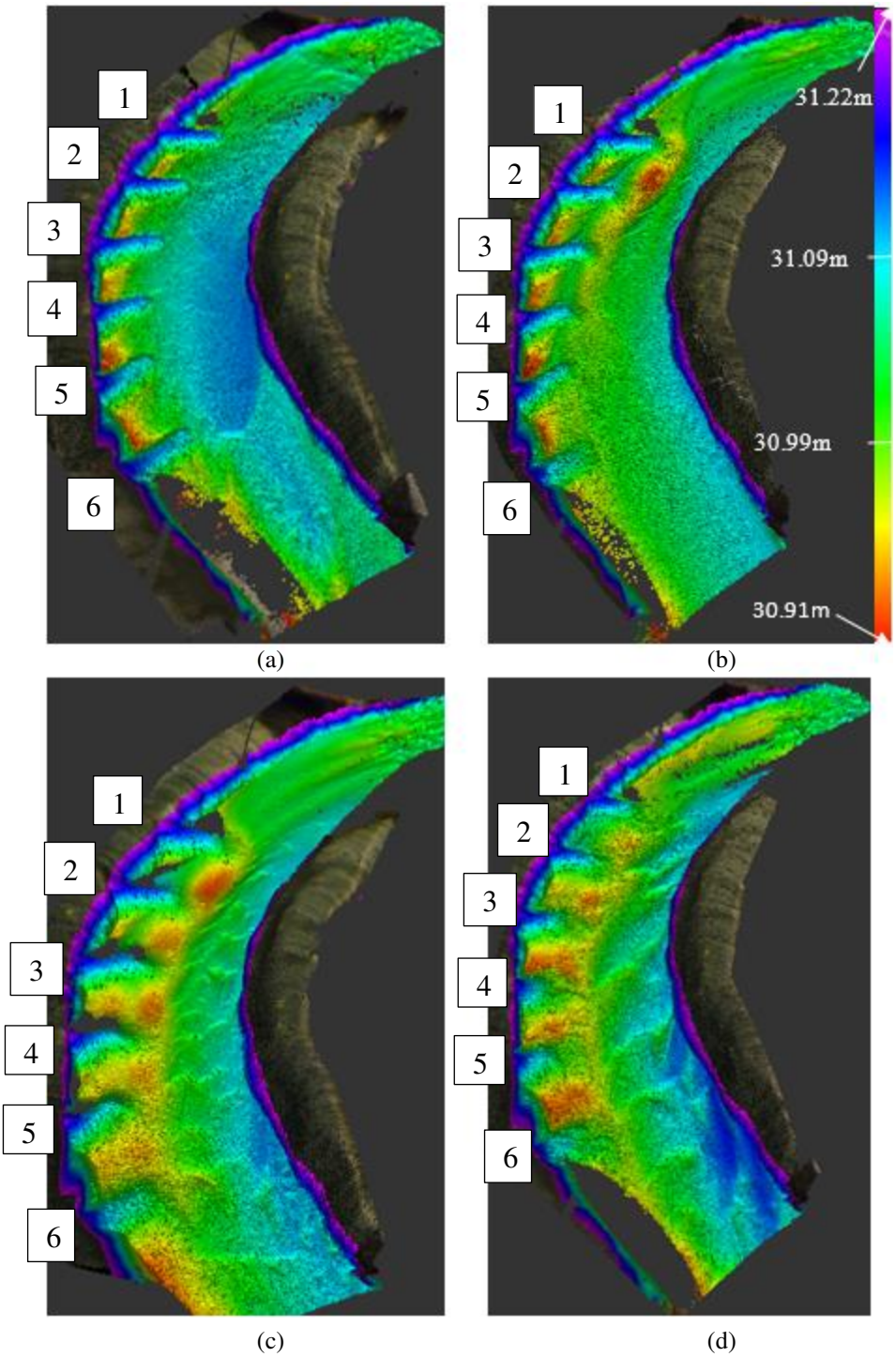

Figure 33. LiDAR scans of the flume bed from (a) after running the initial bed forming conditions of $(\Delta y+H)/H = 1.25$ in EXPT 13a and installing rock vanes, (b) after running at $(\Delta y+H)/H = 0.75$ in EXPT 14a, (c) after running at $(\Delta y+H)/H = 1.25$ in EXPT 15a, and (d) after running at $(\Delta y+H)/H = 2.0$ in EXPT 16a. Note that the initial scour is deep but fills in and lengthens over time. Some deposition occurs between the structures and the point bar also gets pushed downstream.

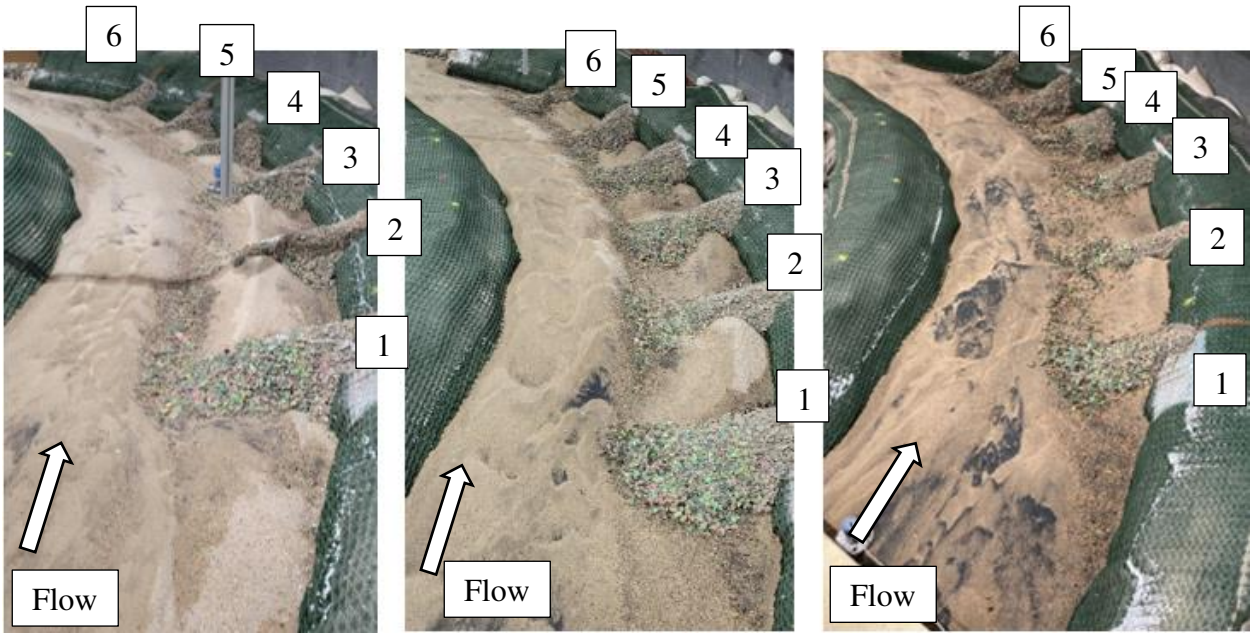

(a) (b) (c)

Figure 34. Photos of results from (a) EXPT 14a, (b) EXPT 15a, and (c) EXPT 16a (see Table 3 for numbering of experiments).

Figure 35 shows the variation in scour depth versus the nominal value $(\Delta y+H)/H$. The values were measured along the configuration of rock vanes used in EXPTs 14a – 16a, and they confirm the bathymetry variations shown by LiDAR scans in Figure 33. The scour depth is deepest for $(\Delta y+H)/H = 0.75$ and gradually changes until there is relatively uniform scour depth across the entire rock vane configuration after $(\Delta y+H)/H = 2.0$.

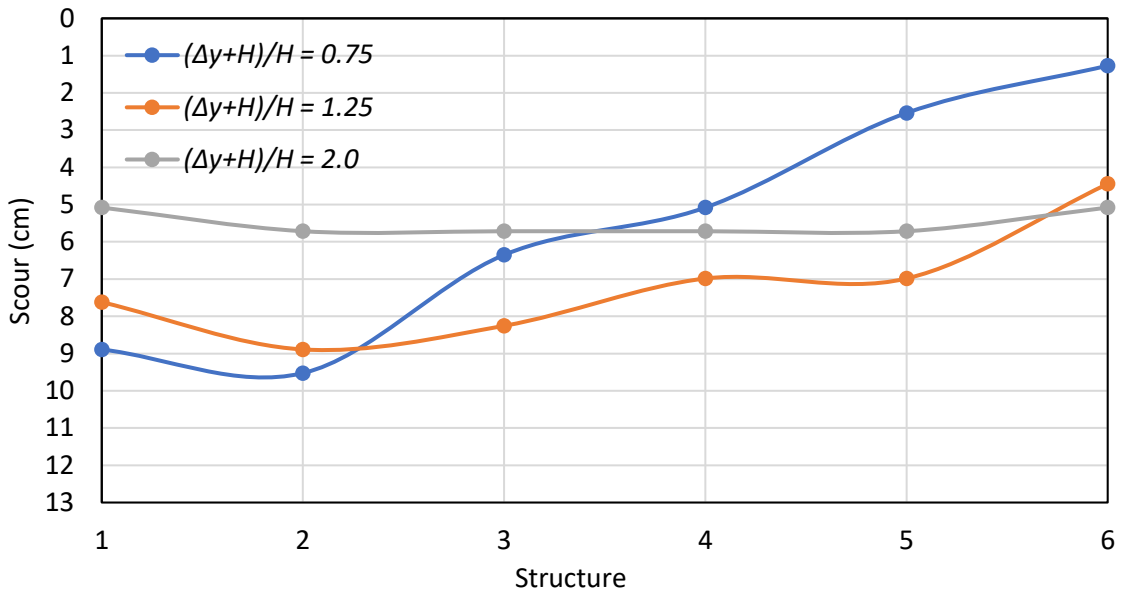

Figure 35. Rock vane tip scour over varying flow depths in a curved flume with very coarse sand.

Rock dislodgement changed structure dimensions as the bed scoured around the structure tips. Figure 36 shows the crest length as a percentage of the design crest length versus flow depth. The greatest reduction in rock vane crest length occurred in the middle of the configuration at rock vanes 3 and 4. This shortening was due to flow being directed away from the outer bank by the first two rock vanes in the configuration and then flow heading back towards the outer bank, as seen in Figure 37.

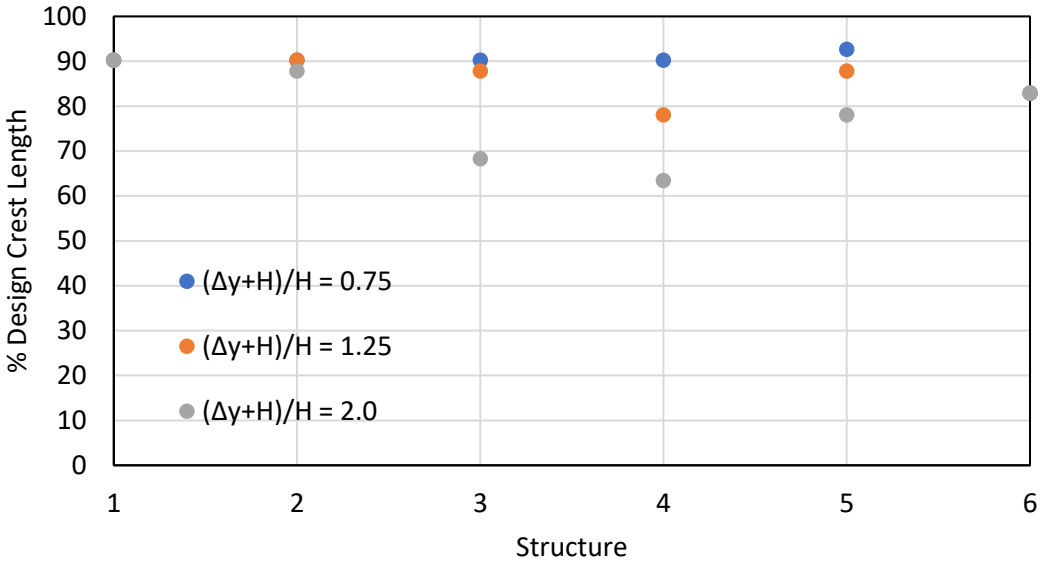

Figure 36. Rock vane crest length variation with flow depth as a percent of the design crest length in a curved flume with very coarse sand.

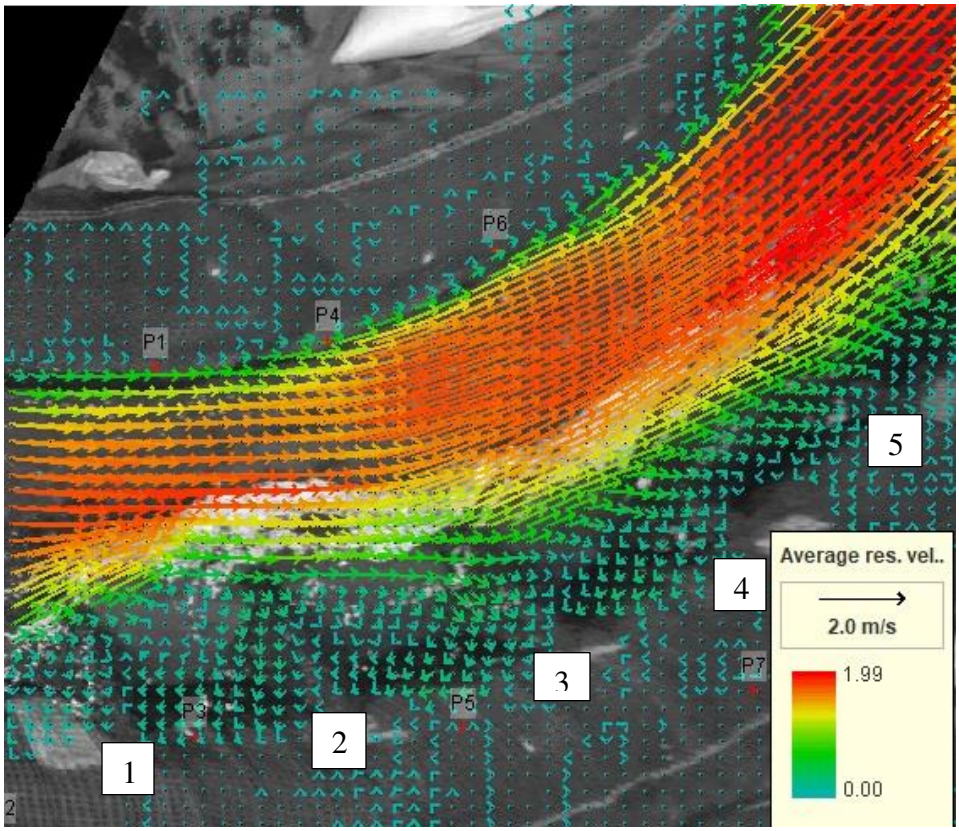

Figure 37. Surface water velocity for $(\Delta y+H)/H$ = 0.75 during EXPT 14a.

The maximum velocity of water flow at the tip of each rock vane was measured during every phase of the hydrograph procedure, including during the initial bed forming flows when no rock vanes were present. The ratio of outer bank velocity to structure tip velocity was calculated and averaged over time for each structure for a given flow condition. For $(\Delta y+H)/H = 1.25$, the average velocity ratio was typically 0.9 – 1.3 for bendway weirs and rock vanes placed on beds of both sediment sizes (Figure 38 and Figure 39). When $(\Delta y+H)/H = 2.0$, the typical value of the average velocity ratio was 1.0 – 1.4 for bendway weirs and rock vanes placed on the bed of medium sand. Outlying points in this dataset occur at structure 5 in the 6-structure configuration. The large increase in velocity ratio was due to effects of the changing bed bathymetry and changes in channel geometry around the bend.

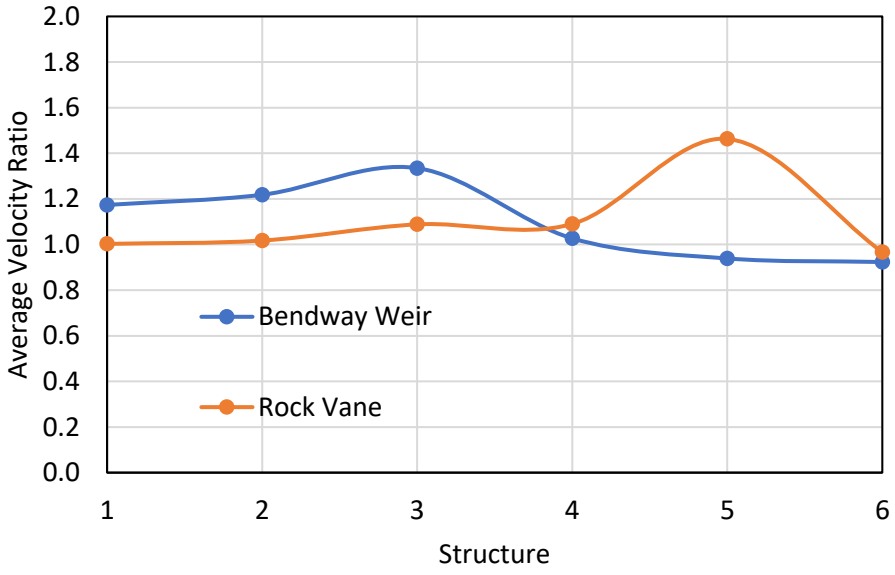

Figure 38. Comparison of average velocity ratio of tip velocity to outer bank velocity (with no structures) for $(\Delta y+H)/H = 1.25$ for bendway weirs or rock vanes placed on the bed of very coarse sand. The ratios were estimated at the end of each experiment.

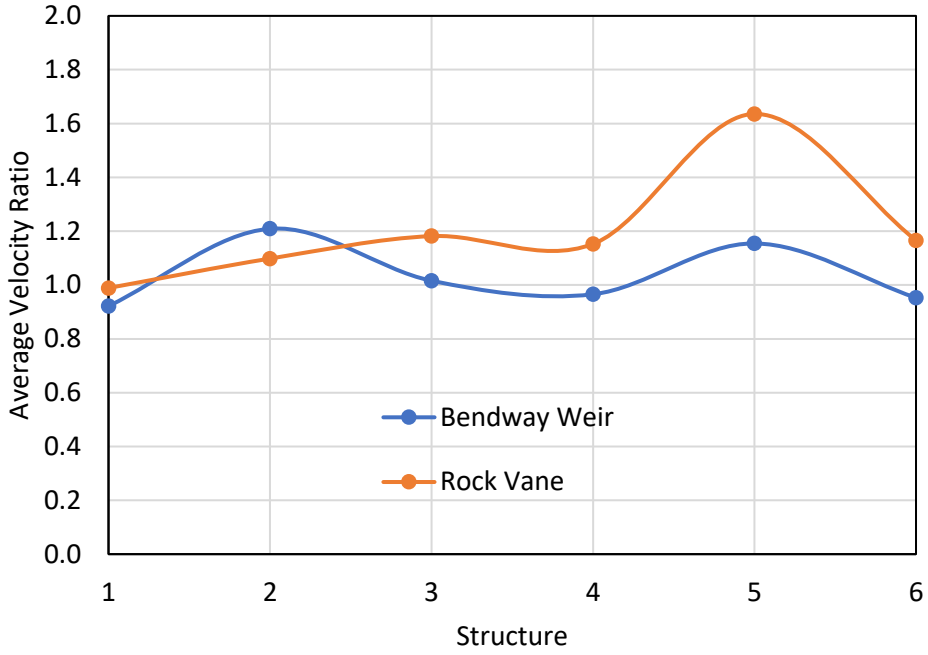

Figure 39. Comparison of average velocity ratio of tip velocity to outer bank velocity (with no structures) for $(\Delta y+H)/H$ = 1.25 for bendway weirs and rock vanes placed on the bed of very coarse sand. The ratios were estimated at the end of each experiment.

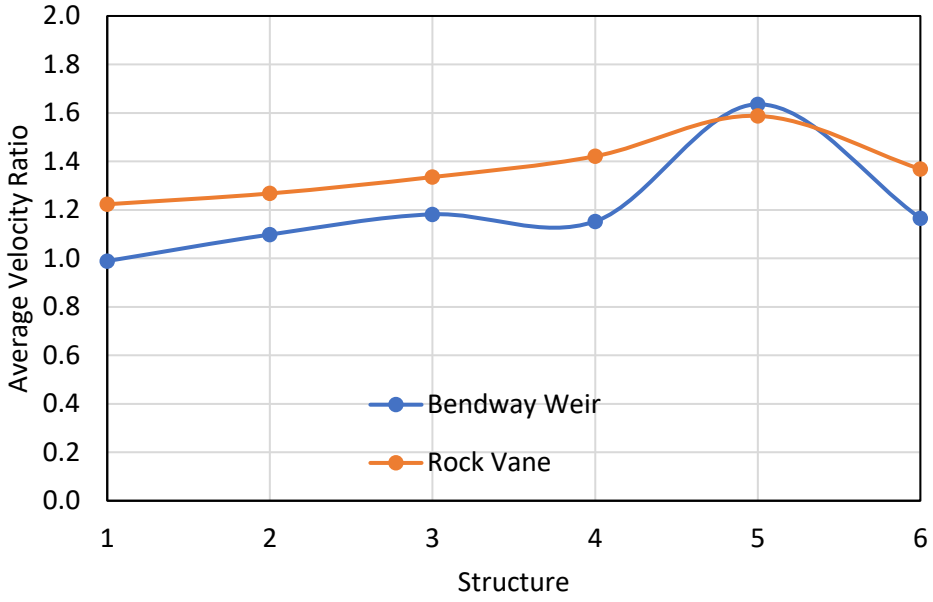

Figure 40. Comparison of average velocity ratio tip velocity to outer bank velocity (with no structures) for $(\Delta y+H)/H$ = 2.0 for bendway weirs and rocks vanes placed on very coarse sand. The ratios were estimated at the end of each experiment.

Figure 41 and Figure 42 show that the maximum scour depth along the thalweg (at the structure tips, not in between the structures) of the channel is inversely proportional to the flow depth. Also, the maximum depth of scour at the structure crest tips was greater in the very coarse sand compared to the medium sand. The value of D/d was greater for the bed of very coarse sand, such that dislodged rock from the bendway weirs or rock vanes moved further on the bed before armoring the bed. This process enabled the bed to scour more before rock dislodgement occurred and the channel became armored, preventing further scour. Bendway weirs and rock vanes placed on the bed of very coarse sand experienced near identical values of maximum scour depth, whereas there was about 1 cm difference in maximum depth of scour in medium sand for the corresponding flow conditions. This aspect requires further investigation, as the manner whereby dislodged rock moved on the sand bed differed somewhat for the two bed sediments. Also, some variation could occur, depending on uncertainties in how the dislodged rock landed.

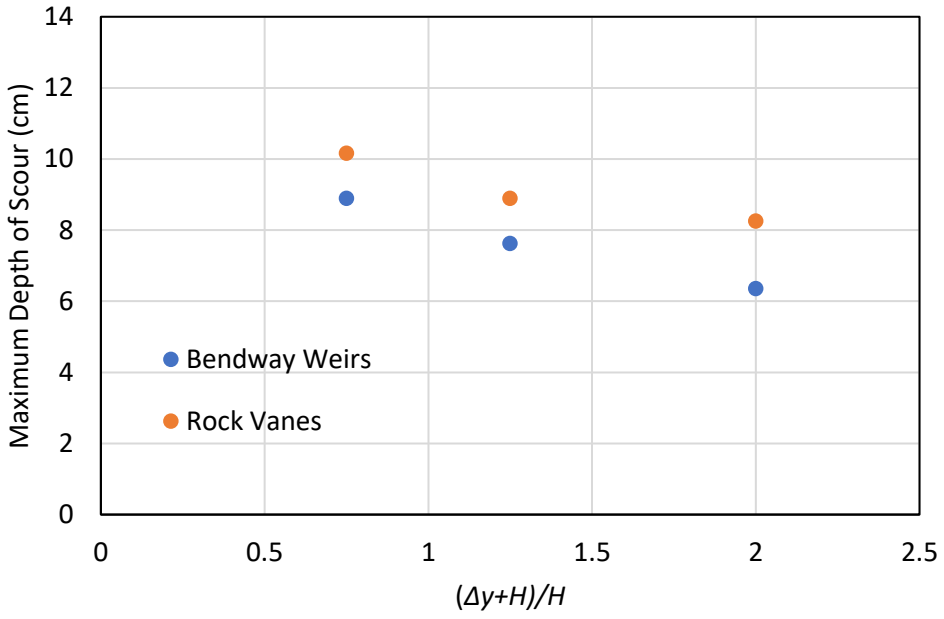

Figure 41. Maximum scour versus $(\Delta y+H)/H$ (or essentially flow depth relative to height of bendway weir or rock vane tips) in medium sand.

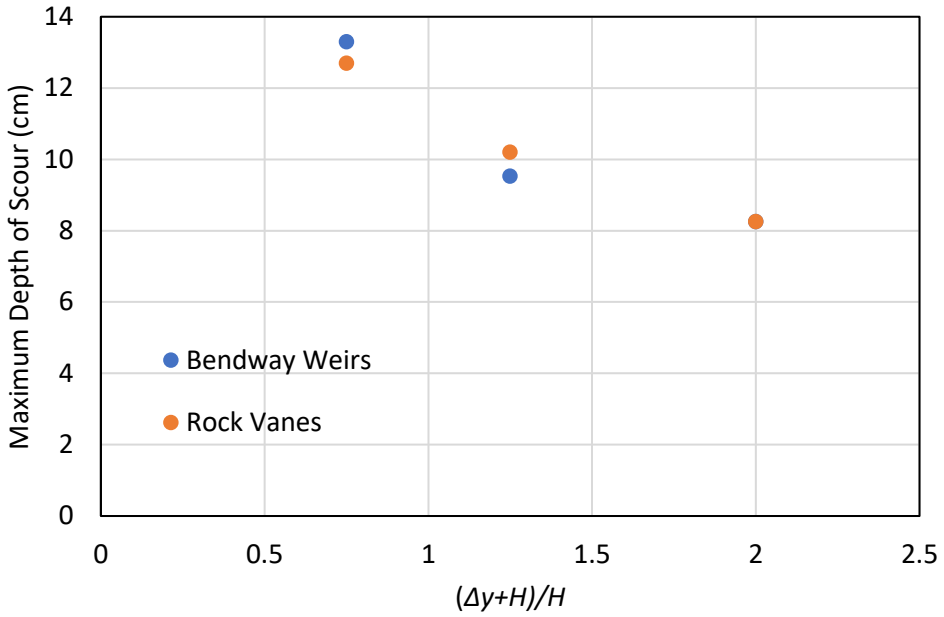

Figure 42. Maximum scour versus *(Δy+H)/H* (or essentially flow depth relative to height of bendway weir or rock vane tips) in very coarse sand.

CHAPTER 5. CONCLUSIONS AND RECOMMENDATIONS

This chapter summarizes the principal conclusions from the main experiments involving bendway weirs and rock vanes (instream structures) as conducted for this thesis.

5.1 Principal Conclusions

The principal conclusions from the hydrograph procedure in the curved flume are as follows:

- The main mode of failure experienced by the bendway weirs and rock vanes was attributable to contraction scour at the tip of each of these instream structures, especially the first instream structure. The contraction scour occurred as flow contracted around the tip of these instream structures.
- When $(\Delta y+H)/H = 0.75$, the initial scour hole formed between the first two structures (numbers 1 and 2) in approximately 15-30 min. regardless of structure type (bendway weir or rock vane) or sediment size.
- Initially, when flow did not pass over the crests of the bendway weirs or rock vanes, this scour occurred in the region of greatest contraction, between structures 1 and 2. As flow passed over the crest of a bendway weir or rock vane, the proportion of flow contracted decreased, the scour extended further downstream along the tips of the series of these instream structures. For the largest depth used in the experiments ($(\Delta y+H)/H = 2.0$), the scour zone (and thus the thalweg) extended at approximately the same depth along all the instream structures.
- The hydrograph procedure in the curved flume confirmed the design recommendations in Maddocks (2021). This procedure entailed successively increasing $(\Delta y+H)/H$ from 0.75 to 2.0, with the bathymetry of the initial bed formed when $(\Delta y+H)/H = 1.25$. In design,

bendway weirs and rock vanes should be lengthened by about $2d_{100}$ (the largest rock used for building the instream structures) and their crest widened by about d_{100}.

- For the range of values of $(\Delta y+H)/H$ used in the experiments, the maximum scour depth varied inversely with $(\Delta y+H)/H$, because as $(\Delta y+H)/H$ exceeded one, more flow went over the crest of the bendway weirs or rock vanes, thereby easing flow contraction.
- The rock vanes experienced less rock dislodgement than did the bendway weirs. This conclusion holds for both the very coarse and medium sands used in the experiments.
- The bendway weirs and rock vanes experienced less rock dislodgement when placed on the bed of medium sand than when they were placed on the bed of very coarse sand, as deeper scour developed in the bed of very coarse sand than in the bed of medium sand. Rock dislodged from the bendway weirs or rock vanes embedded sooner and more effectively armored the bed of medium sand.
- Bedforms did not dominate the structures in the hydrograph procedure as they did in the preliminary experiments. Those experiments were conducted using the before-after-procedure for each value of $(\Delta y+H)/H$. Therefore, the procedure used in conducting experiments is important.

5.2 Design Guidelines

The results of this study were used to revise the bendway weir and rock vane design guidelines reported in Siefken et al. (2021). Table 4 and the subsequent text outlines the updated guidelines below:

Table 4. Revised bendway weir and rock vane design (structure) guidelines.

Layout of Structures in Channel	
Planform Angle Relative to Bank (Pointing Upstream)	45˚ - 85˚
Optimal Projected Crest Length	0.2 – 0.3 T_w
Optimal Spacing	0.75 T_w
Height at Tip	0.3Y
Sideslope	1.5H:1.0V
Individual Structures	
Crest Length	Increase design crest length by 2d_{100} (Allow for sacrificial rock at structure tip)
Crest Width	Increase design crest width by d_{100} (Allow for sacrificial rock at structure width)
Rock Size for Individual Structures	
Structure Rock	See Ettema et al. (2020) for design curve

- Decreasing the crest slope of rock vanes reduced the velocity along the outer bank. Selection of crest slope is a balance between hydraulic performance and the volume of rock required for construction.
- Longer projected crest lengths did not provide substantial velocity reduction along the outer bank compared with optimal range.
- Reducing spacing to $0.5T_w$ produced no further reductions in outer bank velocity.
- Rock vanes are more effective than bendway weirs in reducing velocity near the outer bank. However, the use of either rock structure still may require protection of the outer bank between structures if flow velocity over the crests of these structures is sufficiently large to erode the bank.

5.3 Recommendations for Further Research

The results of this study provided insights into how bendway weirs and rock vanes behave in an alluvial channel bend when subject to live-bed flows and how the design recommendations originally stemming from Maddocks (2021) performed in a curved flume. The following recommendations for research are needed to develop further insights regarding how rock structures like bendway weirs and rock vanes interact with live-bed, loose-boundary hydrodynamics of flow in curved alluvial channels:

- The influence of bar formation on flow fields at bendway weirs and rock vanes and how the flow fields impact rock dislodgement.
- The impact of bed sediment size in combination with flow depth on scour formation.
- The influence of multiple consecutive meanders on structure performance and scour formation.
- The influence of scaling on structure tip scour and rock dislodgement.

- The effects of varying for $(\Delta y+H)/H$ on scour behind structures and the ability of bendway weirs and rock vanes to protect the outer bank from erosion.

5.4 Limitations

This study focused on the failure mechanisms of bendway weirs and rock vanes in an alluvial channel bend. It built off the findings from Maddocks (2021) and tested the recommended hydrograph procedure and design guidelines. While bendway weir or rock vane performance regarding thalweg management was not explicitly studied, this study can be used as a steppingstone for future studies reporting on it.

The curved flume was designed with medium sand in consideration, not the very coarse sand. Therefore, slight scaling issues occurred with flow discharge, flow depth, and getting adequate bed shear stress ratios for the very coarse sand.

The abrupt change in channel geometry where the flume enters the tail-box is not representative of typical field conditions for medium sized rivers. This abrupt change affects the flow field around the last structure in the 6-structure configuration. However, the data from the last structure may be useful in certain instances that occur outside of natural rivers, such as a series of bendway weirs or rock vanes that are placed near an off-take structure.

REFERENCES

Baird, D., Fotherby, L., Klumpp, C., and Sculock, S. M. (2015). *Bank stabilization design guidelines*. Bureau of Reclamation, Denver, CO.

Biedenharn, D. S., Elliott, C. M., and Watson, C. C. (1997). *The WES stream investigation and streambank stabilization handbook*. US Army Engineer Waterways Experiment Station, Vicksburg, MS.

Cox, A. L. (2005). *A Study of In-stream Rehabilitation Structures in Sand-bed Channels*. M.S. Thesis, Colorado State University, Department of Civil Engineering, Fort Collins, CO.

Cunningham, R. and Lyn, D.A (2016). *A laboratory study of bendway weirs as a bank erosion countermeasure*. Purdue e-Pubs. JTRP Technical Reports. FHWA/IN/JTRP-2010/24.

Darrow, J. D. (2004). *Effects of Bendway Weir Characteristics on Resulting Flow Conditions.*Thesis, Colorado State University, Fort Collins, CO.

Ettema, R., AuBuchon, J., Holste, N., Varyu, D., Baird, D., Padilla, R., Posner, A., & Thornton, C. (2020). *Large-flume tests on flow dislodgment of rocks forming Bendway Weirs*. Journal of Hydraulic Engineering, 146(4), 04020008. https://doi.org/10.1061/(asce)hy.1943-7900.0001702

Ettema, R., Nakato, T., and Muste, M. (2010). *Estimation of scour depth at bridge abutments*. NCHRP 24-20, National Cooperative Highway Research Program, National Transportation Board, 436.

Garfield, M. (2019). *The Effects of Scour on the Flow Field at a Bendway Weir*. M.S. Thesis, Colorado State University, Department of Civil Engineering, Fort Collins, CO.

Garfield, M. and Ettema R. (2021). *Effect of clearwater scour on the flow field at a single bendway weir: Two-dimensional numerical modeling supported by flume data*. ASCE, Journal of Irrigation and Drainage, Vol. 147 (2).

Heintz, M. L. (2002). *Investigation of bendway weir spacing.* Fort Collins, CO: Colorado State University.

Hogan, A. T. (2019). *Investigating the effects of bend radius of curvature on the flow around bendway weirs*. M.S. Thesis, Colorado State University, Department of Civil Engineering, Fort Collins, CO.

Jamieson, E. C., Rennie, C. D., Jacobson, R. B., and Townsend, R. D. (2011). *3-D flow and scour near a submerged wing dike: ADCP measurements on the Missouri River: 3-D FLOW and scour near a submerged wing dike*. Water Resources Research, 47(7). https://doi.org/10.1029/2010WR010043

Jia Y., Scott S., Xu Y., and Wang S. S. Y. (2009). *Numerical study of flow affected by bendway weirs in Victoria Bendway, the Mississippi River*. Journal of Hydraulic Engineering, 135(11), 902–916. https://doi.org/10.1061/(ASCE)0733-9429(2009)135:11(902)

Johnson, P.A., Hey, R.D., Tessier, M., and Rosgen, D.L. (2001). *Use of vanes for control of scour at vertical wall abutments*. Journal of Hydraulic Engineering. 127(9). 772-778.

Julien, P. Y., & Duncan, J. R. (2003). *Optimal design criteria of bendway weirs from numerical simulations and physical model studies.* Colorado State University, Fort Collins, CO.

Julien, P.Y. (2010). *Erosion and sedimentation.* Second Edition, Cambridge University Press, UK.

Kasper, K. E. (2005). *Accuracy of HEC-RAS to Calculated flow depths and total energy loss with and without bendway weirs in a meander mend*. M.S. Thesis, Colorado State University, Department of Civil Engineering, Fort Collins, CO.

Keating, K. and Knight, R. (2008). *A Laboratory study of the effect of magnetite on NMR relaxation rates*. Journal of Applied Geophysics, Volume 66, pp. 188-196.

Kinzli, K. (2005). *Effects of bendway weir characteristics on resulting eddy and channel flow conditions*. M.S. Thesis, Colorado State University, Department of Civil Engineering, Fort Collins, CO.

Kwan, T.F. (1984). *Study of abutment scour*. School of Engineering, Report No. 328. The University of Auckland, Auckland, New Zealand.

Lagasse, P.F., Clopper, P.E., Pagan-Ortiz, J.E., Zevenbergen, L.W., Arneson, L.A., Schall, J.D., and Girard, L.G. (2009). *Bridge scour and stream instability countermeasures: experience, selection, and design guidance*. 3rd ed. HEC-23. Federal Highway Administration. FHWA-NHI-09-111.

Maddocks, P. (2021). *Live-bed failure modes of bendway weirs and rock vanes in alluvial channels.* M.S. Thesis, Colorado State University, Department of Civil Engineering, Fort Collins, CO.

Maryland Department of the Environment (2000). *Maryland's waterway construction guidelines*. Water Management Administration, Baltimore, ML.

McCullah, J.A. and Gray, D. (2005). *Environmentally sensitive channel- and bank-protection measures*. NCHRP Report 544, Transportation Research Board, National Academies of Science, Washington, D.C.

NRCS (Natural Resources Conservation Service). (2005). *Design of stream barbs*. Technical Note 23, Version 2.0. Portland, OR: US Dept. of Agriculture.

NRCS (Natural Resources Conservation Service). (2007). *Flow changing techniques*. Part 65: National engineering handbook. Technical Supplement 14H. NRCS, Washington, D.C.

NRCS (Natural Resources Conservation Service). (2009). *Streambank and shoreline protection*. Chap. 16 in Wisconsin supplement engineering field handbook. NRCS, Washington, D.C.

NRCS (Natural Resources Conservation Service). (2010). *Design of stream barbs for low gradient streams*. Minnesota Technical Note No. 8. NRCS, Washington, D.C.

NRCS (Natural Resources Conservation Service). (2013). *Kansas engineering technical note No. KS-1 (Revision 1)*. NRCS, Washington, D.C.

Papanicolaou, A. N., Bressan, F., Fox, J., Kramer C., & Kjos L. (2018). *Role of structure submergence on scour evolution in gravel bed rivers: Application to slope-crested structures*. ASCE, Journal of Hydraulic Engineering, 144(2), 03117008. https://doi.org/10.1061/(ASCE)HY.1943-7900.0001411

Schmidt, P. G. (2005). *Effects of bendway weir field geometric characteristics on channel flow conditions*. M.S. Thesis, Colorado State University, Department of Civil Engineering, Fort Collins, CO.

Scurlock, S., M., Baird, C., D., Cox, L., A., & Thornton, I., C. (2012). *Bendway weir design - Rio Grande Physical Model. Bureau of Reclamation*, Denver, CO.

Scurlock, S. M., Cox, A. L., Thornton, C. I., & Abt, S. R. (2014). *Calibration and validation of a numerical model forevaluation of transverse in-stream structure research.* Bureau of Reclamation, Denver, CO.

Scurlock, S. M., Thornton, C. I., & Abt, S. R. (2014). *Evaluation of bendway-weir structures within the native topography channel.* Denver, CO: Bureau of Reclamation.

Shin, K., Ettema, R., & Thornton, C. I. (2018). *Native channel topography and rock-weir structure channel-maintenance techniques.* Colorado State University, Fort Collins, CO.

Siefken, S. A. (2019). *Computational fluid dynamics models of Rio Grande bends fitted with rock vanes or bendway weirs*. M.S. thesis, Dept. of Civil and Environmental Engineering, Colorado State University.

Siefken, S.A. (2021). *Optimal configuration of rock vanes and bendway weirs for river bends: Numerical-Model Insights*. ASCE, Journal of Hydraulic Engineering, 147(5).

Thornton, C. I., James, M., & Shin, K. (2016). *Testing of instream vane structures within the native-topography channel*. Colorado State University, Fort Collins, CO.

Walker, K. G. (2009). *Comparison of a generalized trapezoidal hydraulic model to a native topography patterned bed Surface model of the Rio Grande*. M.S. Thesis, Colorado State University, Department of Civil and Environmental Engineering, Fort Collins, CO.

WSDOT (Washington State Department of Transportation). (2017). *Hydraulics manual*. Washington, DC: WSDOT.

APPENDIX A. EXPERIMENT RESULTS

Table 5a. Preliminary curved flume experiments with medium sand.

EXPT #	**Structure**	**Q** (m^3/s)	**y** (cm)	**Shear stress ratio** τ_0/τ_c	$(\Delta y+H)/H$	**Design α** (Degrees)	**Design W** (cm)	**Design L** (cm)	**Design H** (cm)	S_0
1a	3BW	0.08	15.2	7.7	2.0	90	7.62	20.3	7.62	0.0012
2a	4BW	0.08	15.2	7.7	2.0	90	7.62	40.6	7.62	0.0012
3a	4BW	0.08	15.2	7.7	2.0	90	7.62	40.6	7.62	0.0012
4a	4BW	0.07	9.53	4.8	1.25	90	7.62	40.6	7.62	0.0012
5a	4BW	0.07	9.53	4.8	1.25	90	7.62	40.6	7.62	0.0012
6a	6RV	0.07	9.53	4.8	1.25	90	7.62	40.6	7.62	0.0012
7a	6RV	0.08	15.2	7.7	2.0	90	7.62	40.6	7.62	0.0012
8a	6RV	0.03	5.72	2.9	0.75	90	7.62	40.6	7.62	0.0012

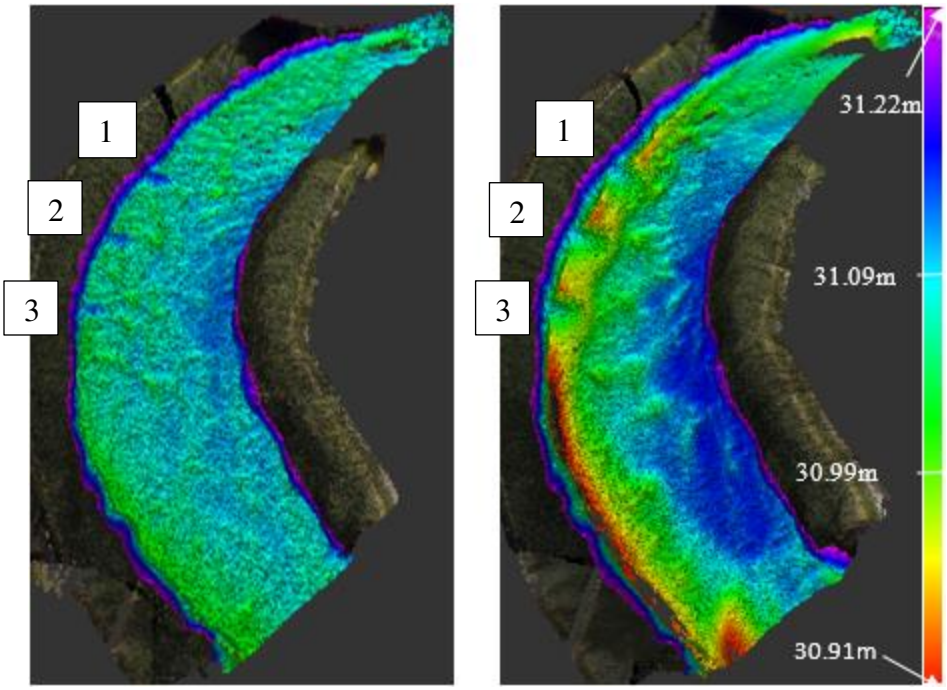

(a) (b)

Figure 43. Lidar from (a) before and (b) after EXPT 1a.

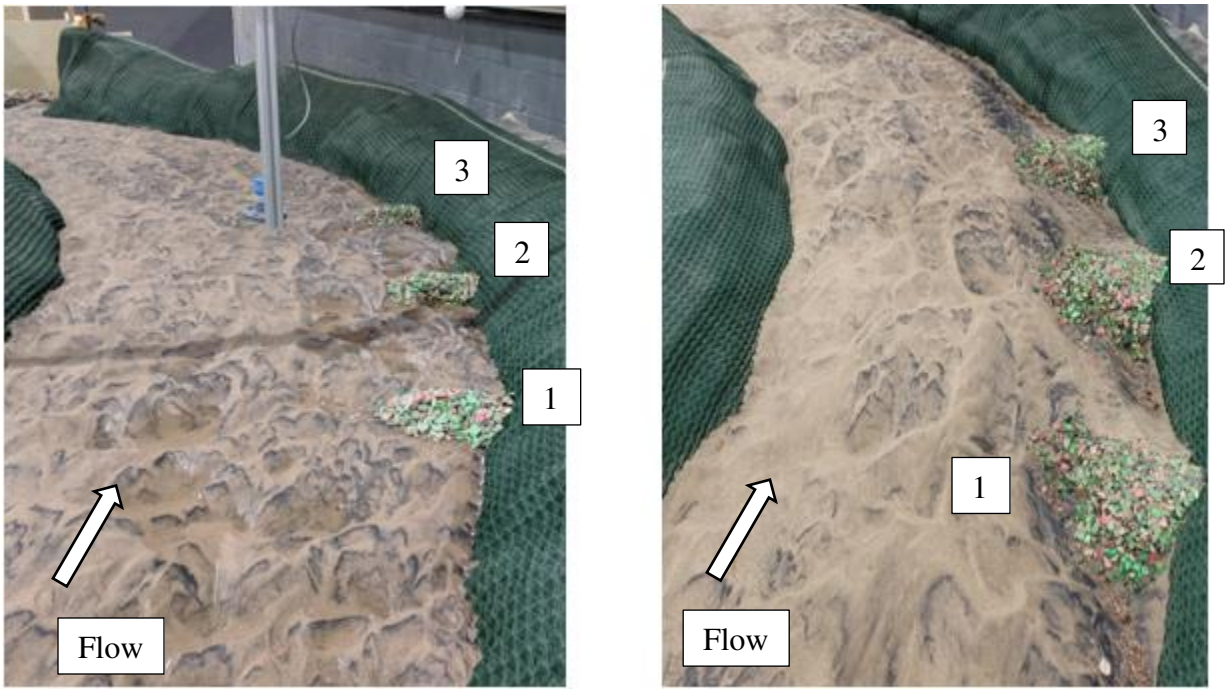

(a) (b)

Figure 44. Photos from (a) before and (b) after EXPT 1a.

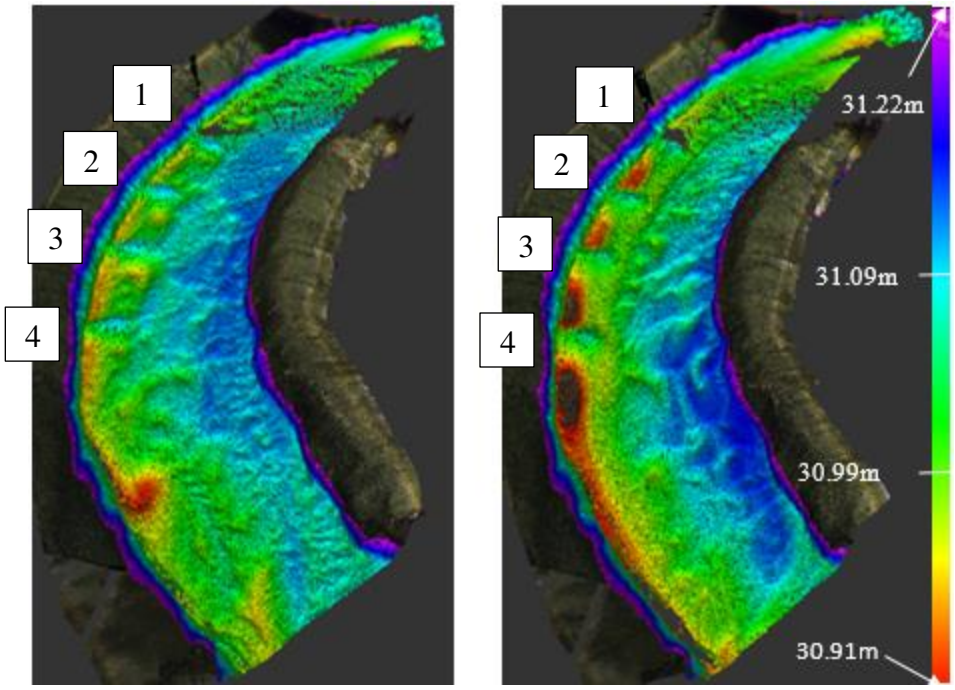

(a) (b)

Figure 45. Lidar from (a) before and (b) after EXPT 2a.

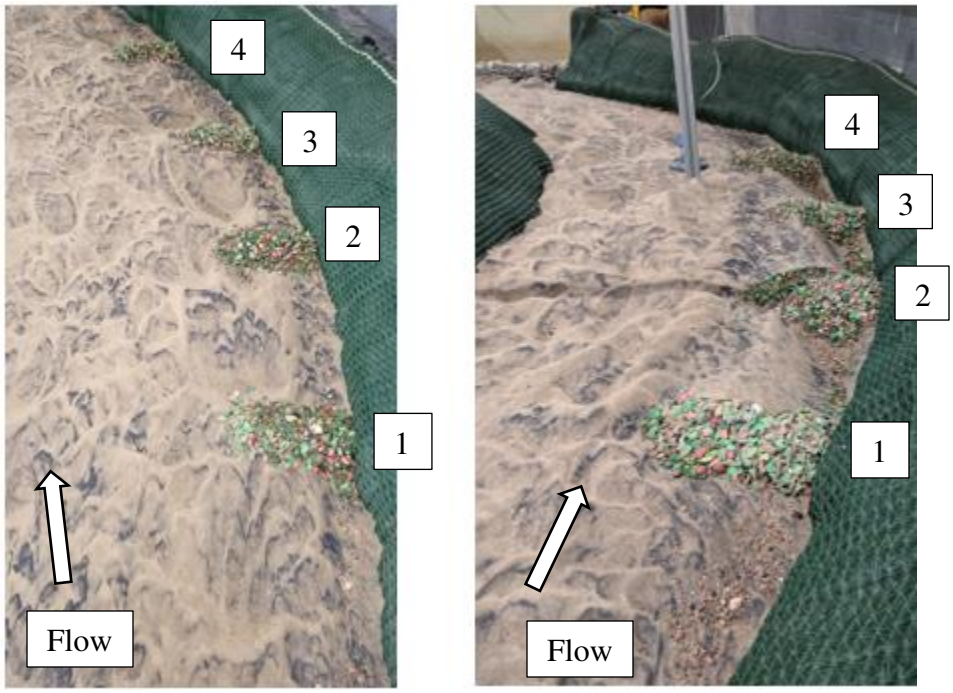

(a) (b)

Figure 46. Photos from (a) before and (b) after EXPT 2a.

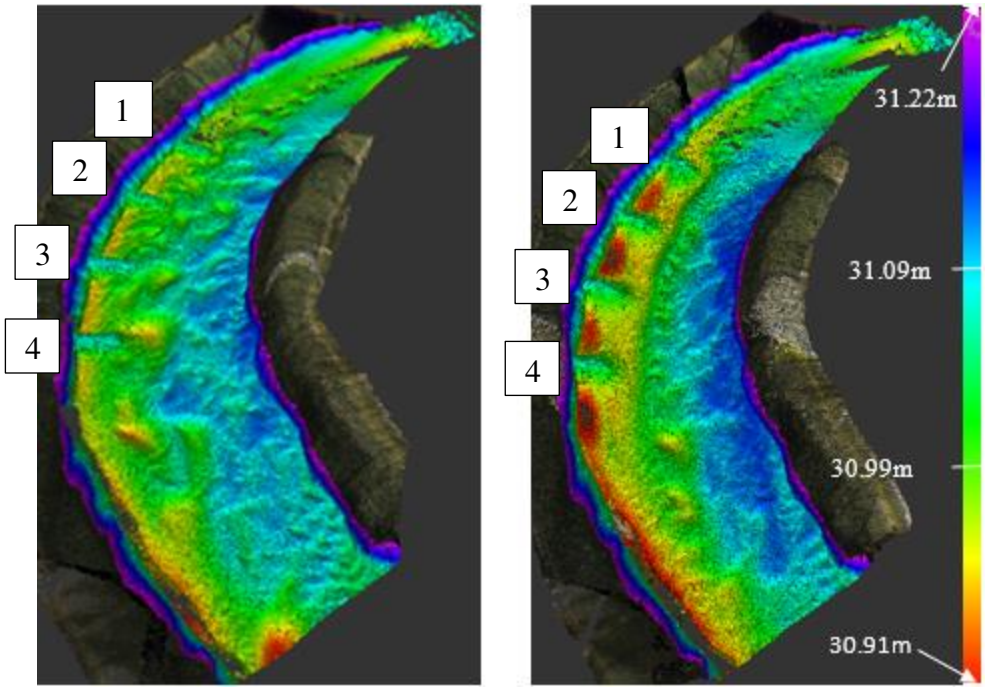

(a) (b)

Figure 47. Lidar from (a) before and (b) after EXPT 3a.

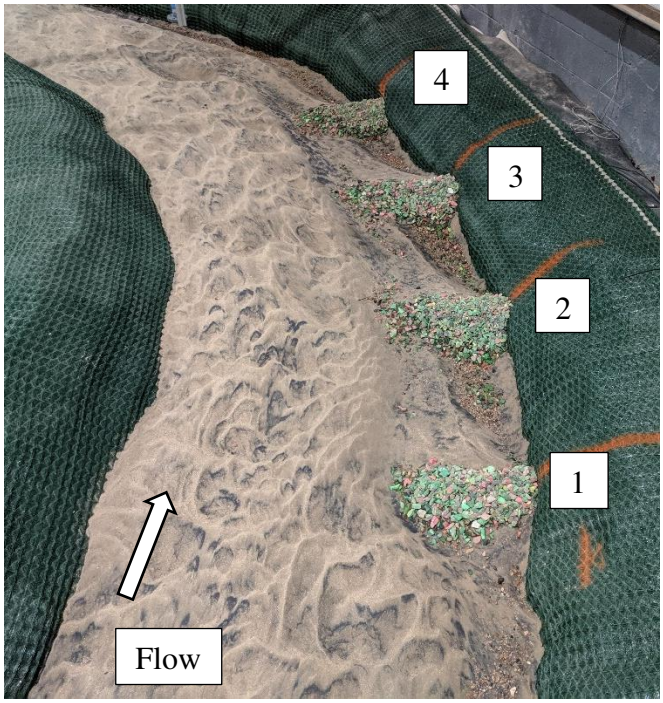

Figure 48. Photo from after EXPT 3a.

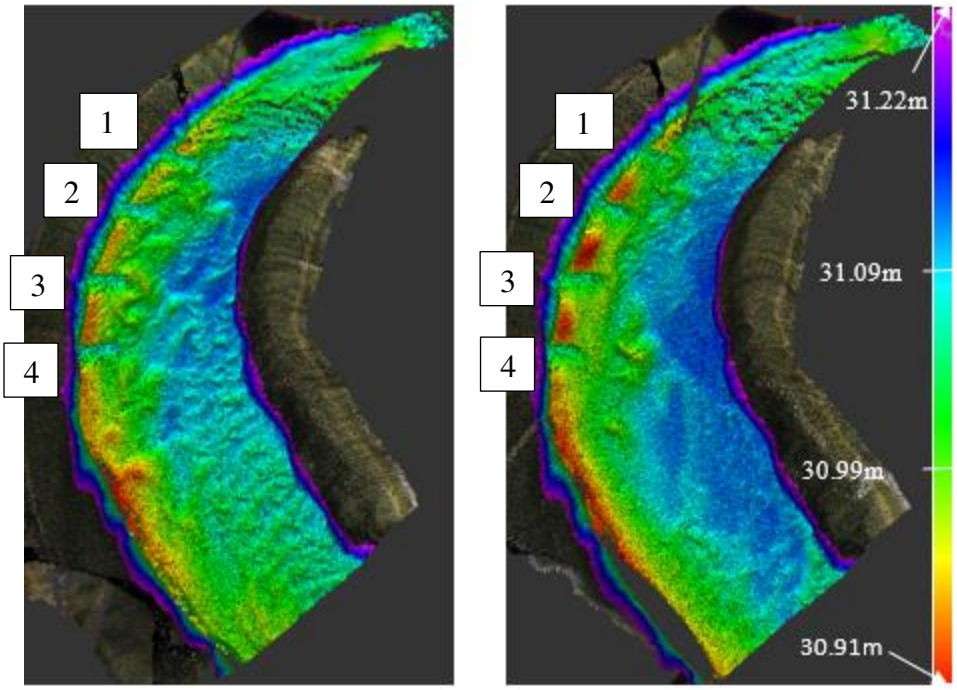

(a) (b)

Figure 49. Lidar from (a) before and (b) after EXPT 4a.

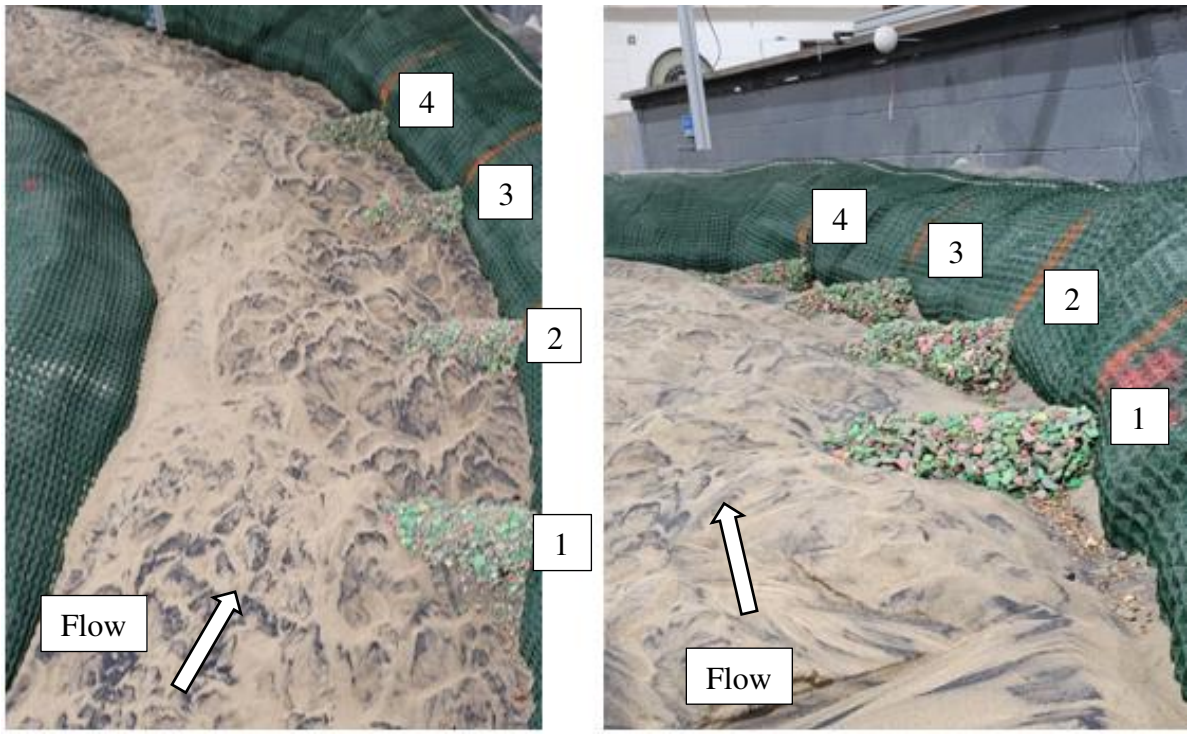

(a) (b)

Figure 50. Photos from (a) before and (b) after EXPT 4a.

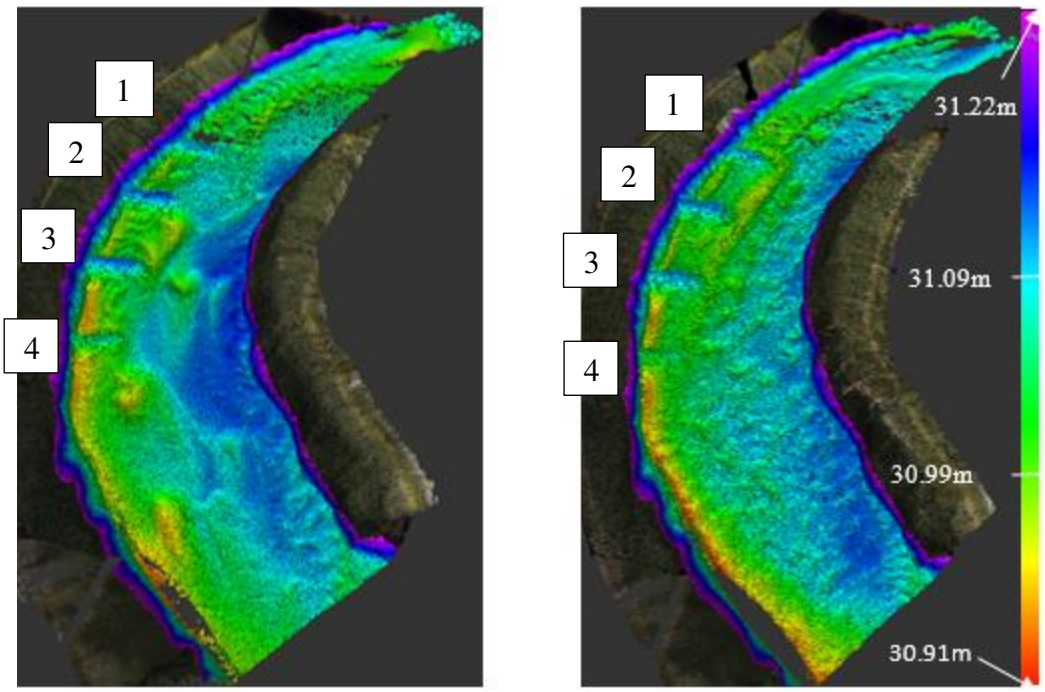

(a) (b)

Figure 51. Lidar from (a) before and (b) after EXPT 5a.

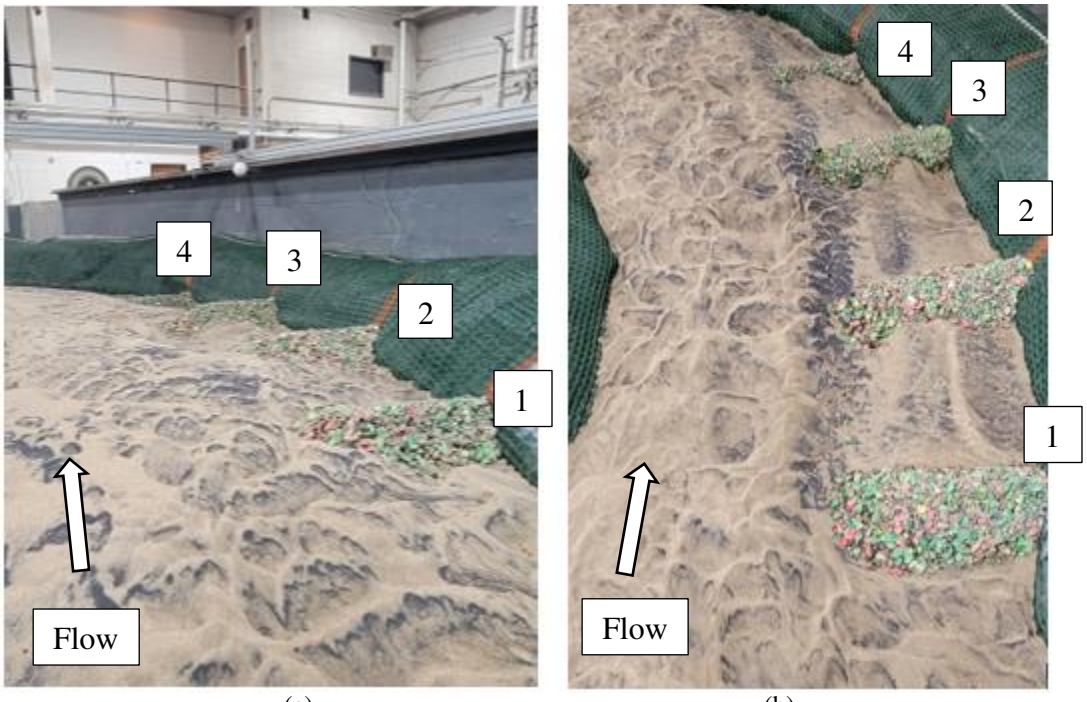

(a) (b)

Figure 52. Photos from (a) before and (b) after EXPT 5a.

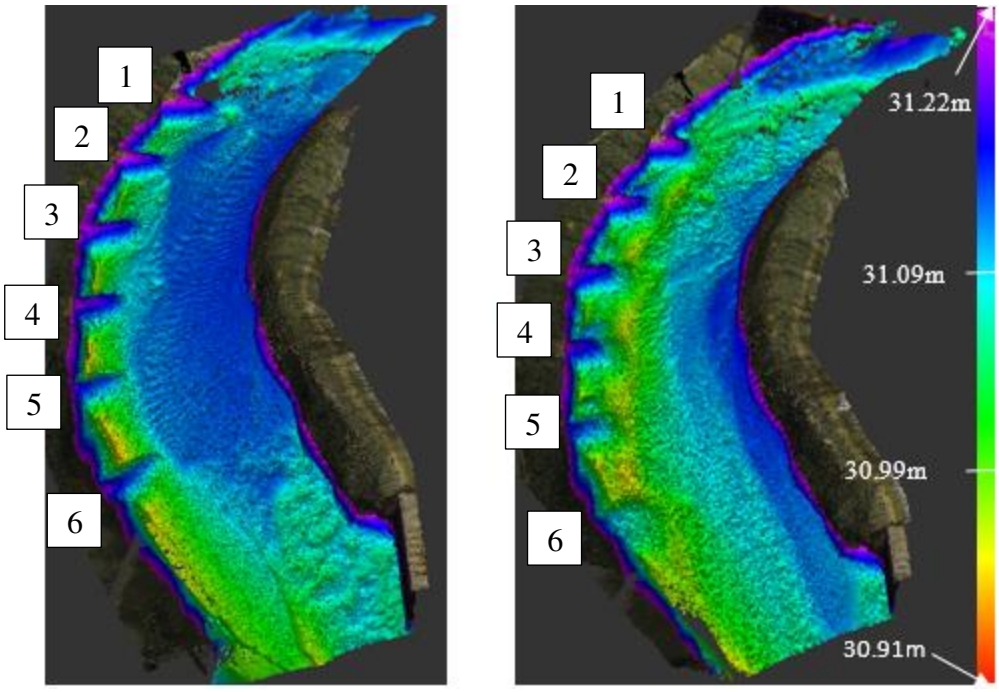

(a) (b)

Figure 53. LiDAR from (a) before and (b) after EXPT 6a.

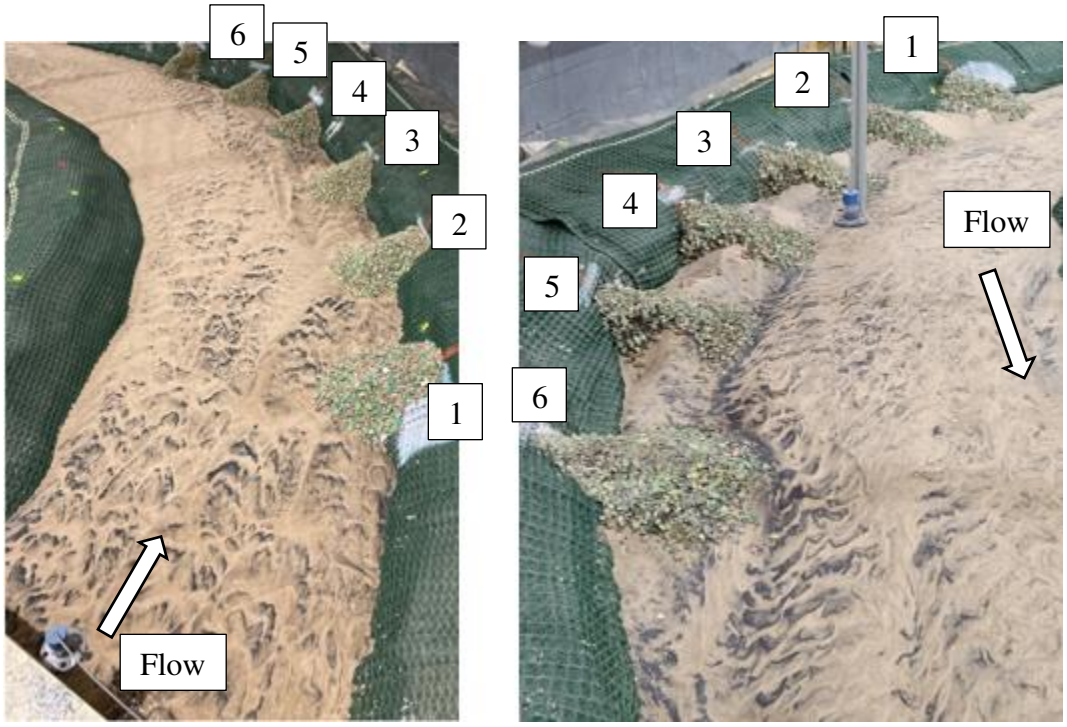

(a) (b)

Figure 54. Photos from (a) before (downstream view) and (b) after (upstream view) EXPT 6a.

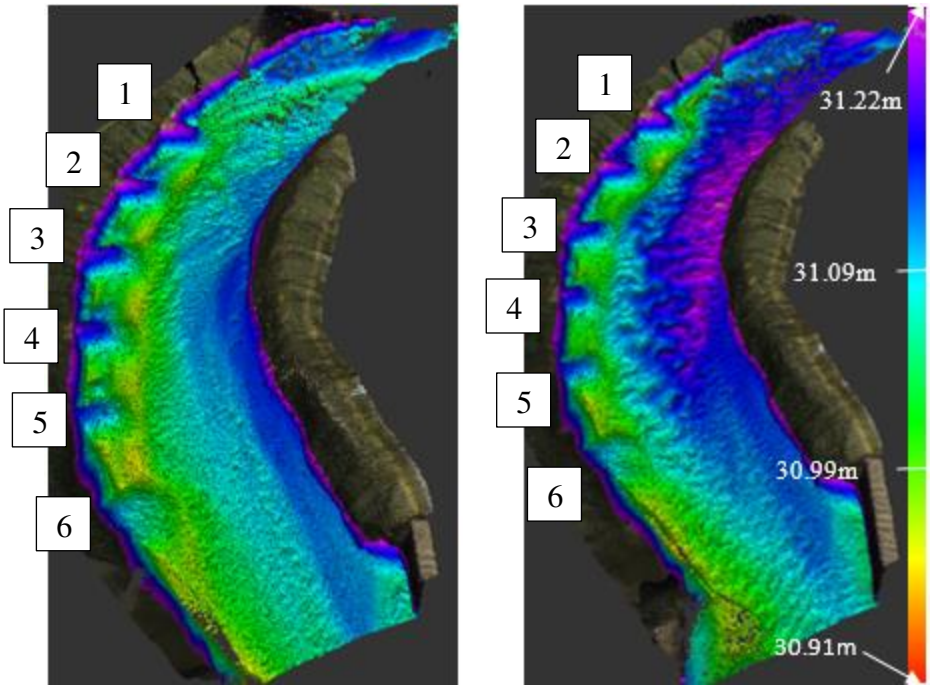

(a) (b)

Figure 55. LiDAR from (a) before EXPT 6a and (b) after EXPT 7a.

Figure 56. Photo (upstream view) after EXPT 7a.

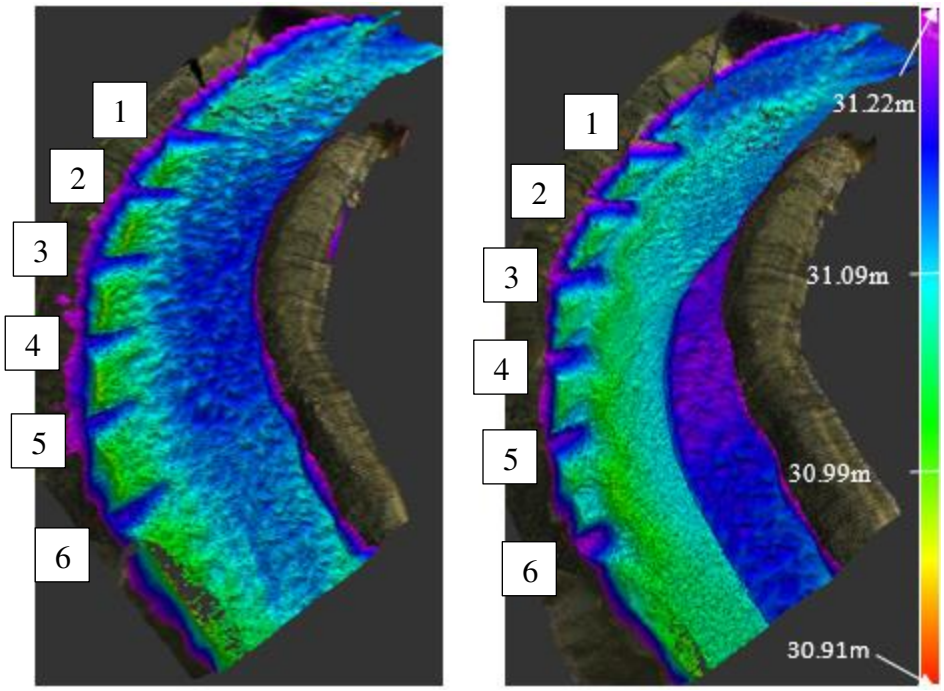

(a) (b)

Figure 57. LiDAR from (a) before and (b) after EXPT 8a.

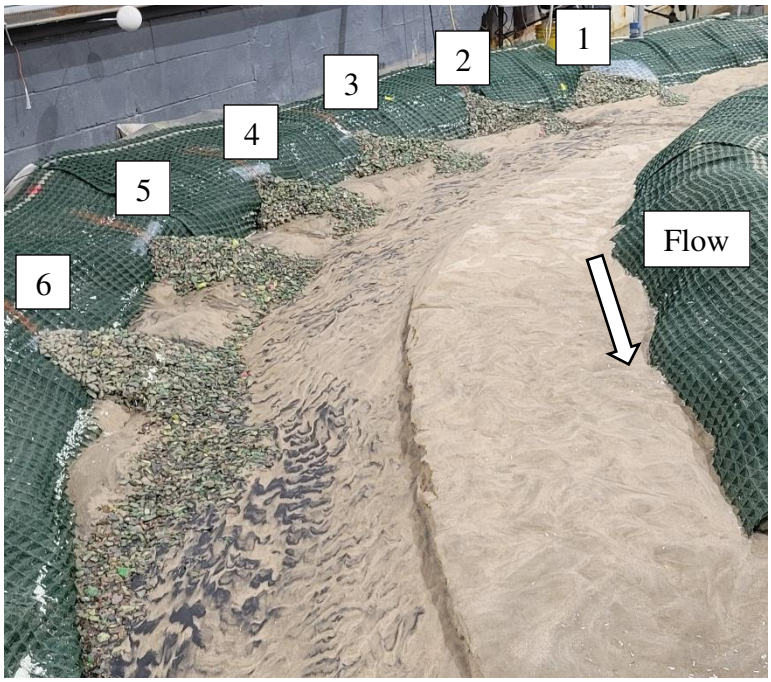

Figure 58. Photo (upstream view) after EXPT 8a.

Table 6a. Curved flume hydrograph procedure experiments with very coarse sand.

EXPT #	**Structure**	**Q** (m^3/s)	**y** (cm)	**Shear stress ratio** τ_0/τ_c	$(\Delta y+H)/H$	**Design α** (Degrees)	**Design W** (cm)	**Design L** (cm)	**Design H** (cm)	S_0
9a	-	0.07	9.53	1.6	1.25	60	7.62	52.1	7.62	0.0012
10a	6BW	0.04	5.72	0.9	0.75	60	7.62	52.1	7.62	0.0012
11a	6BW	0.07	9.53	1.6	1.25	60	7.62	52.1	7.62	0.0012
12a	6BW	0.10	15.2	2.5	2.0	60	7.62	52.1	7.62	0.0012
13a	-	0.07	9.53	1.6	1.25	60	7.62	52.1	7.62	0.0012
14a	6RV	0.04	5.72	0.9	0.75	60	7.62	52.1	7.62	0.0012
15a	6RV	0.07	9.53	1.6	1.25	60	7.62	52.1	7.62	0.0012
16a	6RV	0.10	15.2	2.5	2.0	60	7.62	52.1	7.62	0.0012

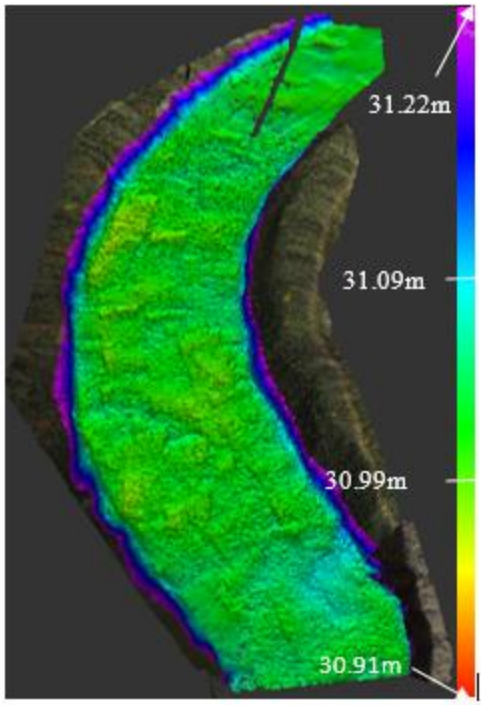

Figure 59. LiDAR of the curved flume before EXPT 9a.

Figure 60. Photo of the curved flume before EXPT 9a.

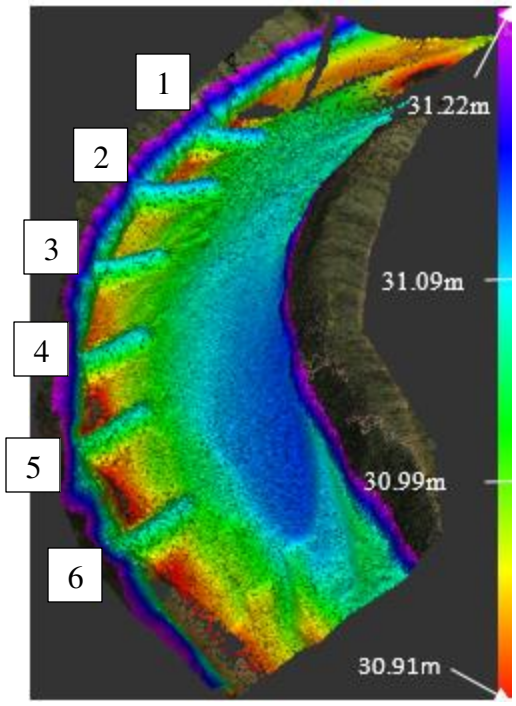

Figure 61. LiDAR of the curved flume after EXPT 9a ($(\Delta y+H)/H$ = 1.25) with bendway weirs constructed after the experiment.

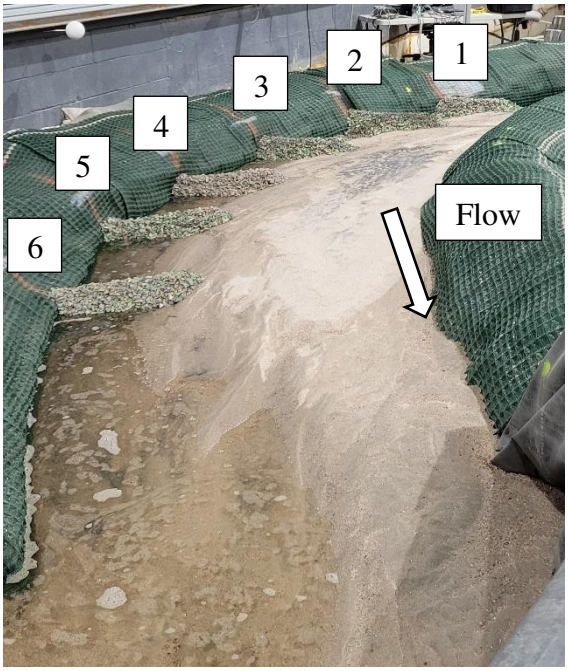

Figure 62. Photo of the curved flume after EXPT 9a ($(\Delta y+H)/H$ = 1.25). Note the flume is being filled for the next EXPT.

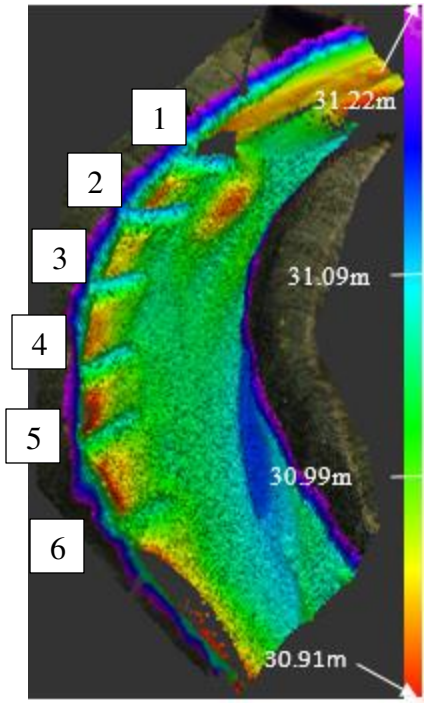

Figure 63. LiDAR of the curved flume after EXPT 10a ($(\Delta y+H)/H$ = 0.75).

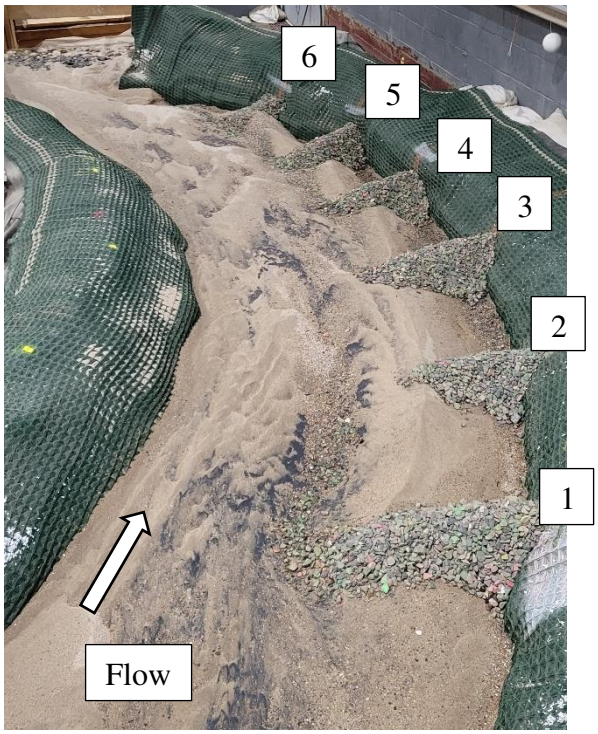

Figure 64. Photo of the curved flume after EXPT 10a ($(\Delta y+H)/H$ = 0.75).

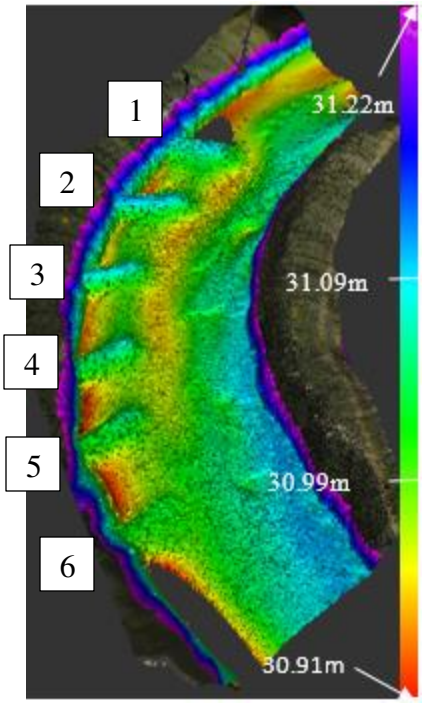

Figure 65. LiDAR of the curved flume after EXPT 11a ((*Δy*+*H*)/*H* = 1.25).

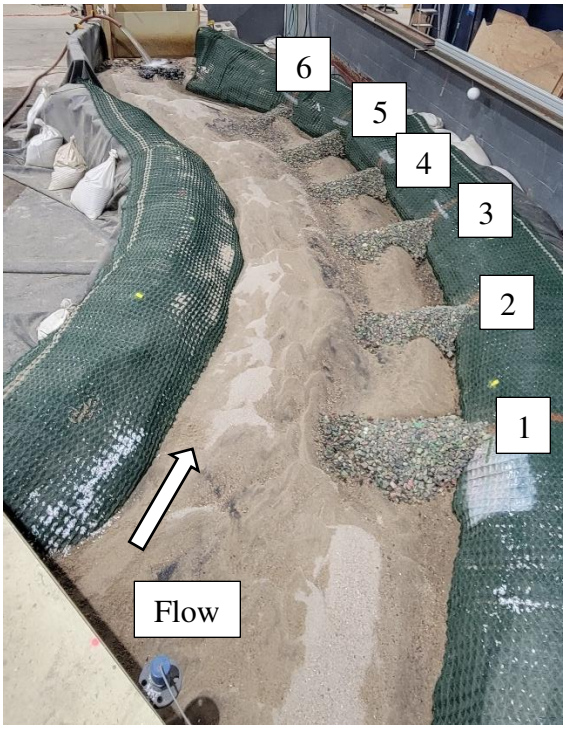

Figure 66. Photo of the curved flume after EXPT 11a ((*Δy*+*H*)/*H* = 1.25).

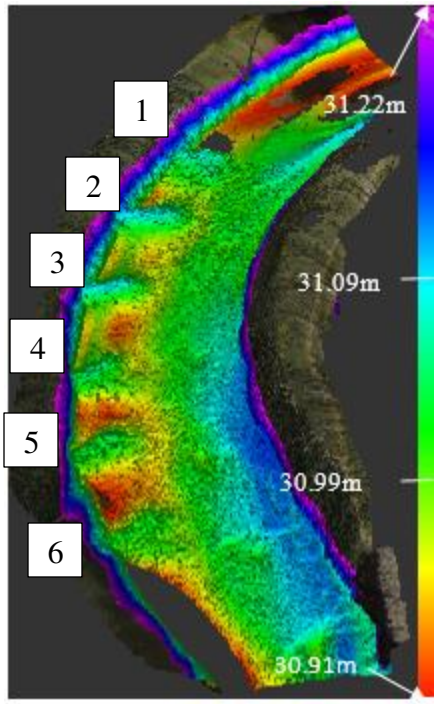

Figure 67. LiDAR of the curved flume after EXPT 12a ((*Δy*+*H*)/*H* = 2.0).

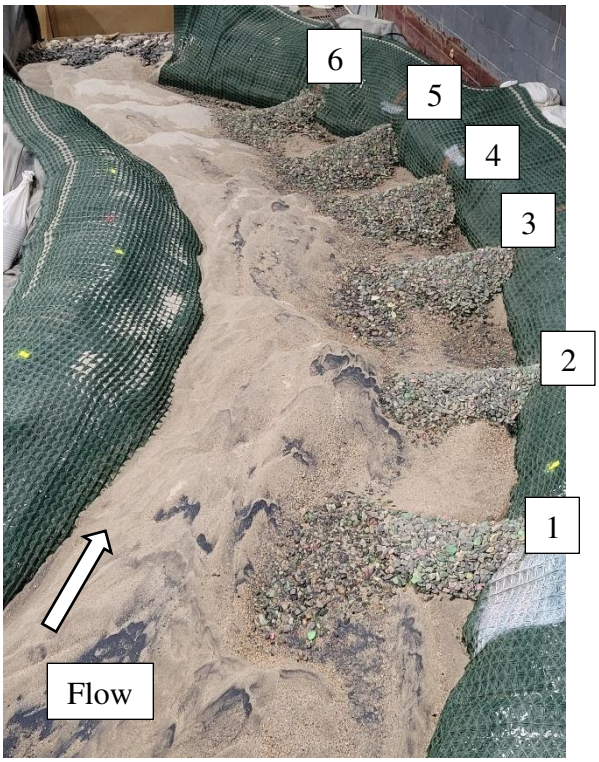

Figure 68. Photo of the curved flume after EXPT 12a ((*Δy*+*H*)/*H* = 2.0).

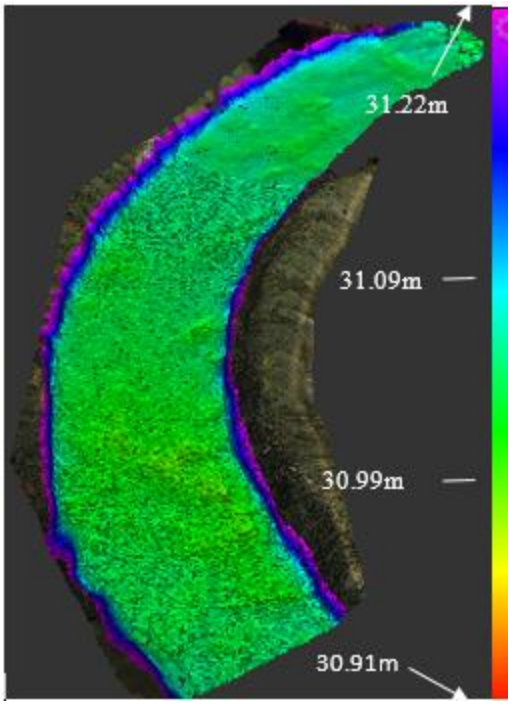

Figure 69. LiDAR of the curved flume before EXPT 13a.

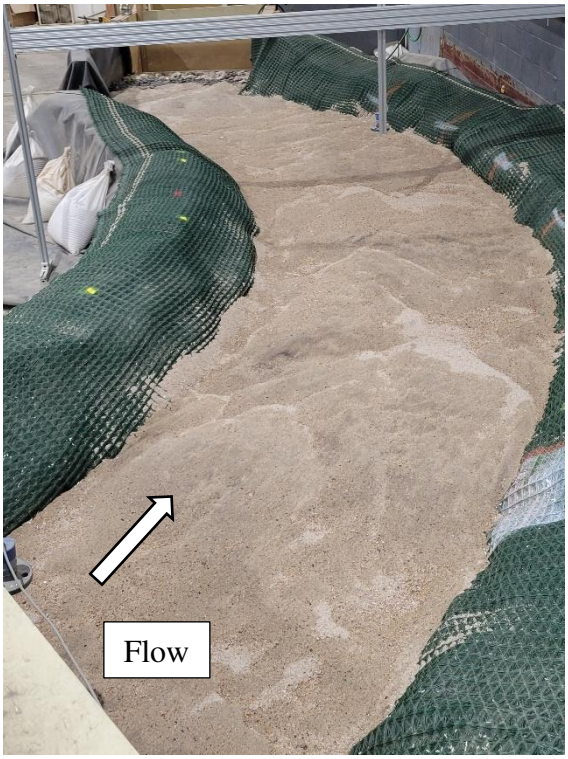

Figure 70. Photo of the curved flume before EXPT 13a.

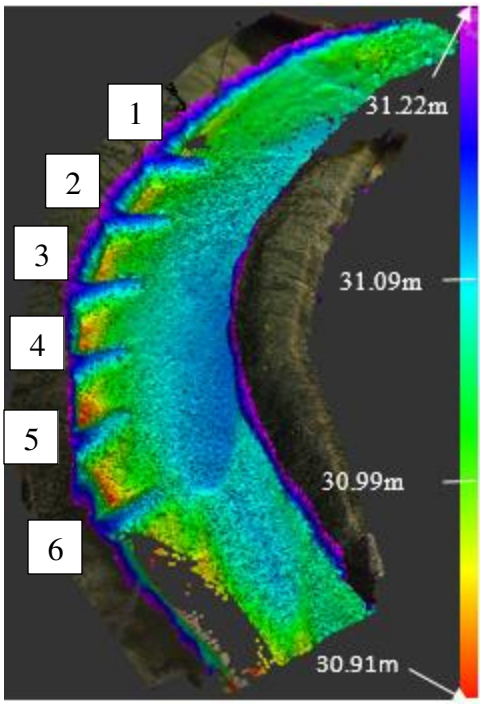

Figure 71. LiDAR of the curved flume after EXPT 13a ((*Δy*+*H*)/*H* = 1.25) with rock vanes constructed after the experiment.

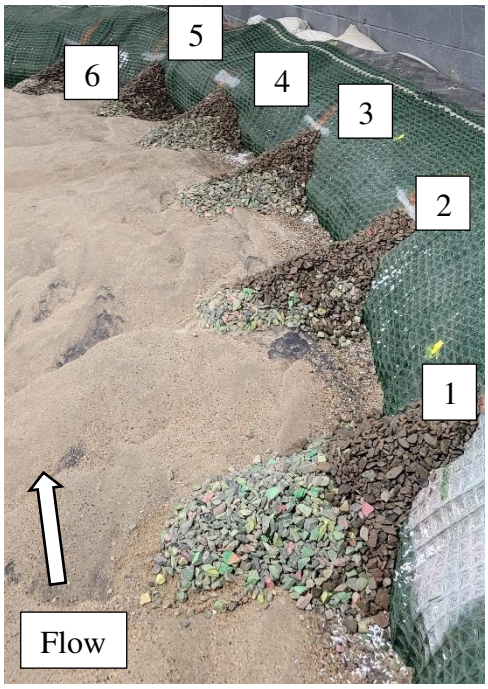

Figure 72. Photo of the curved flume after EXPT 13a ((*Δy*+*H*)/*H* = 1.25) with rock vanes constructed after the experiment.

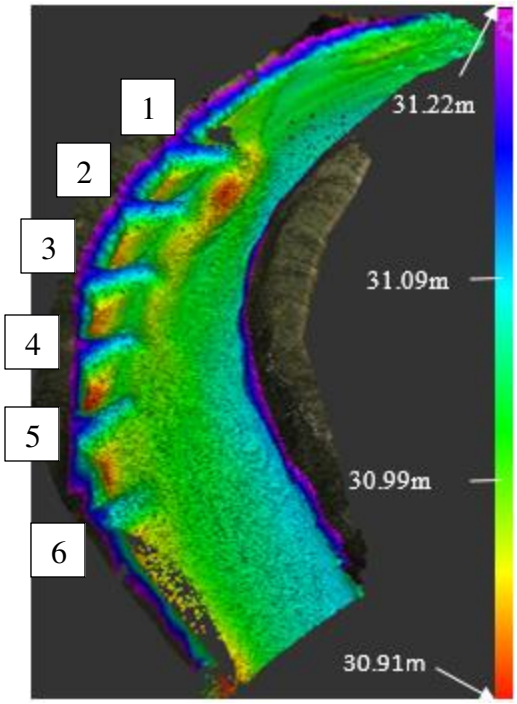

Figure 73. LiDAR of the curved flume after EXPT 14a ((*Δy*+*H*)/*H* = 0.75).

Figure 74. Photo of the curved flume after EXPT 14a ((*Δy*+*H*)/*H* = 0.75).

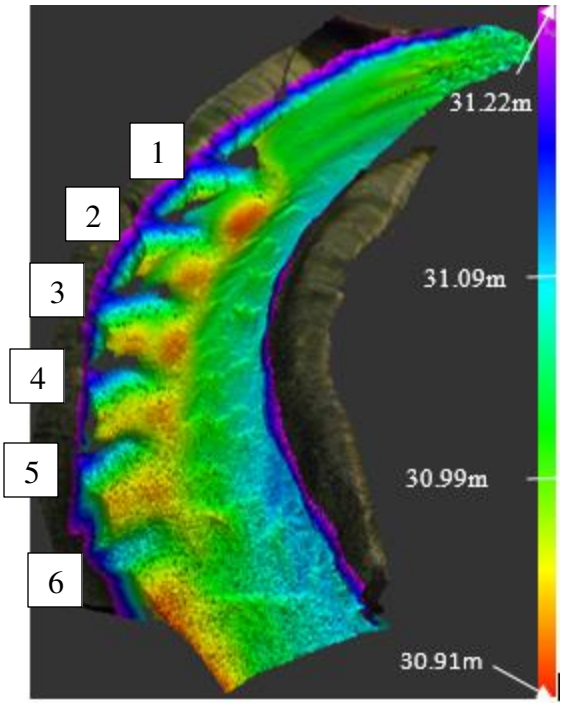

Figure 75. LiDAR of the curved flume after EXPT 15a ((*Δy*+*H*)/*H* = 1.25).

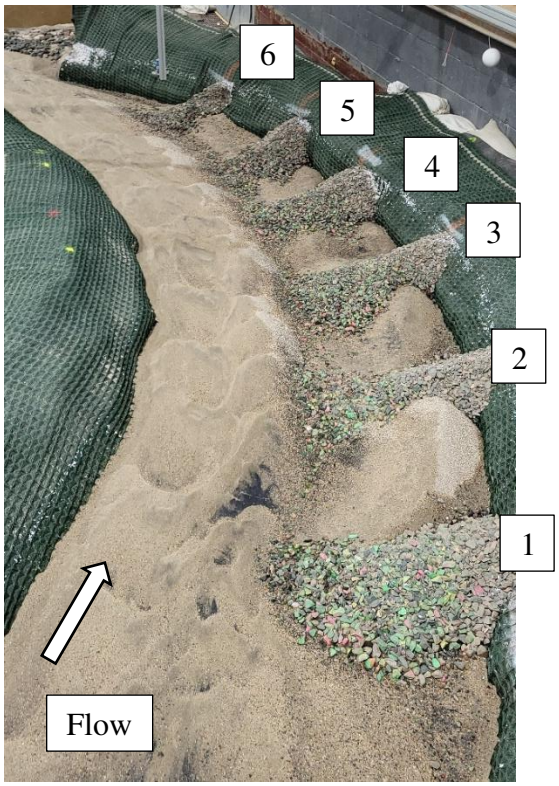

Figure 76. Photo of the curved flume after EXPT 15a ((*Δy*+*H*)/*H* = 1.25).

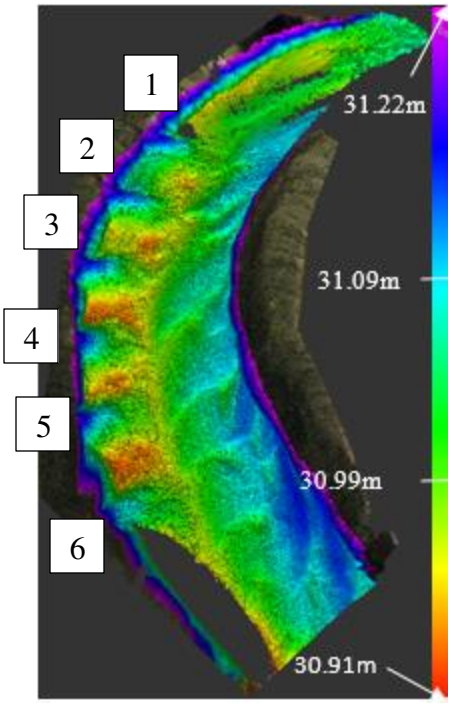

Figure 77. LiDAR of the curved flume after EXPT 16a ((*Δy*+*H*)/*H* = 2.0).

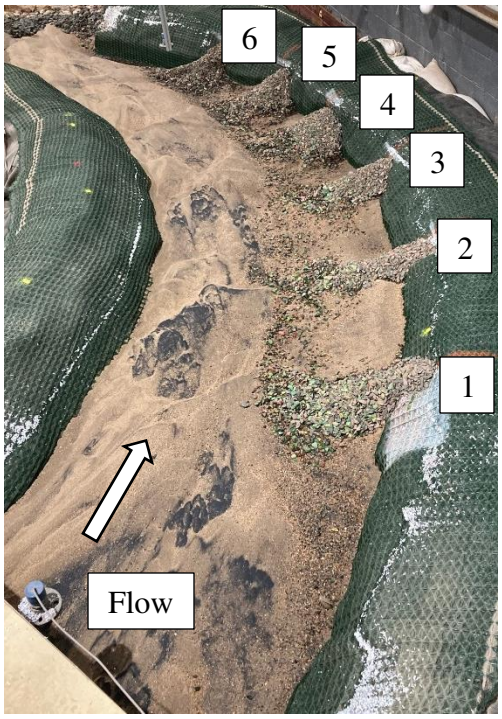

Figure 78. Photo of the curved flume after EXPT 16a ((*Δy*+*H*)/*H* = 2.0).

Table 7a. Curved flume hydrograph procedure experiments with medium sand.

EXPT #	**Structure**	**Q** (m^3/s)	**y** (cm)	**Shear stress ratio** τ_0/τ_c	$(\Delta y+H)/H$	**Design α** (Degrees)	**Design W** (in)	**Design L** (in)	**Design H** (in)	S_0
17a	-	0.07	9.53	4.8	1.25	60	7.62	52.1	7.62	0.0012
18a	6BW	0.04	5.72	2.9	0.75	60	7.62	52.1	7.62	0.0012
19a	6BW	0.07	9.53	4.8	1.25	60	7.62	52.1	7.62	0.0012
20a	6BW	0.08	15.2	7.7	2.0	60	7.62	52.1	7.62	0.0012
21a	-	0.07	9.53	4.8	1.25	60	7.62	52.1	7.62	0.0012
22a	6RV	0.04	5.72	2.9	0.75	60	7.62	52.1	7.62	0.0012
23a	6RV	0.07	9.53	4.8	1.25	60	7.62	52.1	7.62	0.0012
24a	6RV	0.08	15.2	7.7	2.0	60	7.62	52.1	7.62	0.0012

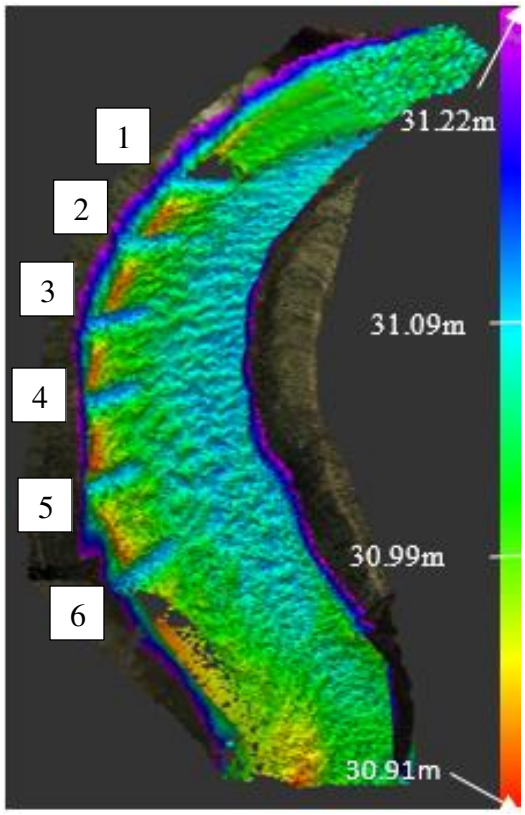

Figure 79. LiDAR of the curved flume after EXPT 17a ($(\Delta y+H)/H$ = 1.25) with bendway weirs constructed after the experiment.

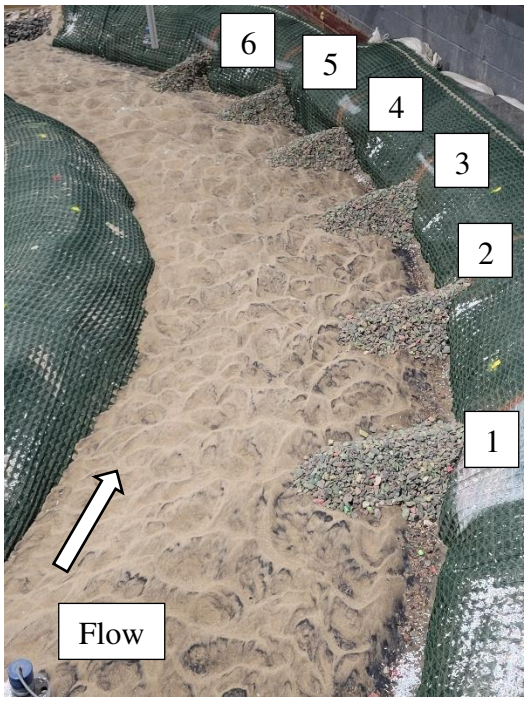

Figure 80. Photo of the curved flume after EXPT 17a ($(\Delta y+H)/H$ = 1.25) with bendway weirs constructed after the experiment.

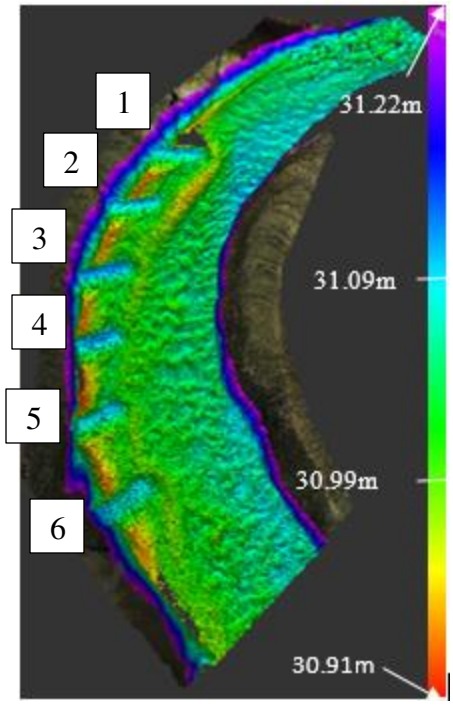

Figure 81. LiDAR of the curved flume after EXPT 18a ($(\Delta y+H)/H$ = 0.75).

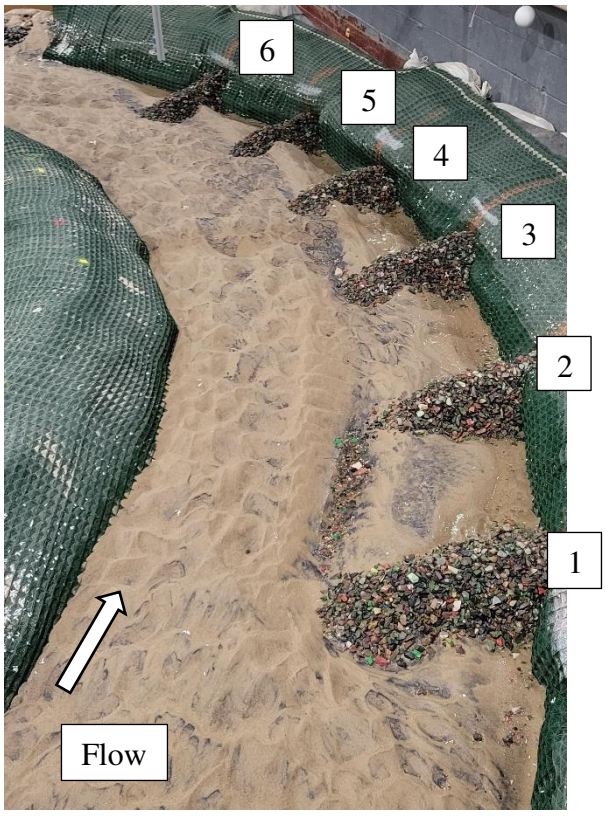

Figure 82. Photo of the curved flume after EXPT 18a ($(\Delta y+H)/H$ = 0.75).

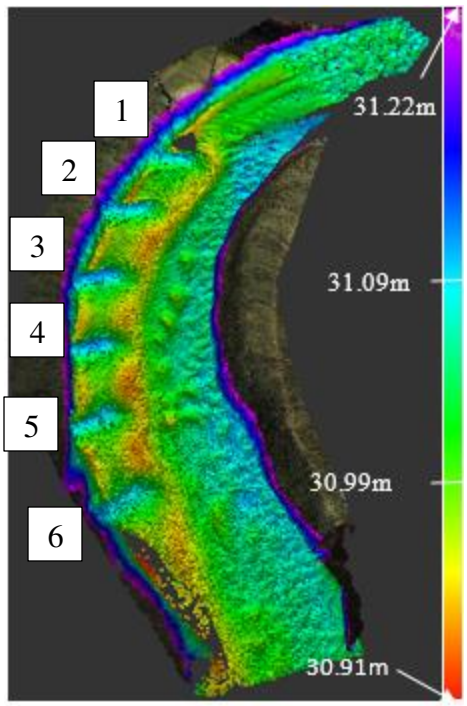

Figure 83. LiDAR of the curved flume after EXPT 19a ($(\Delta y+H)/H$ = 1.25).

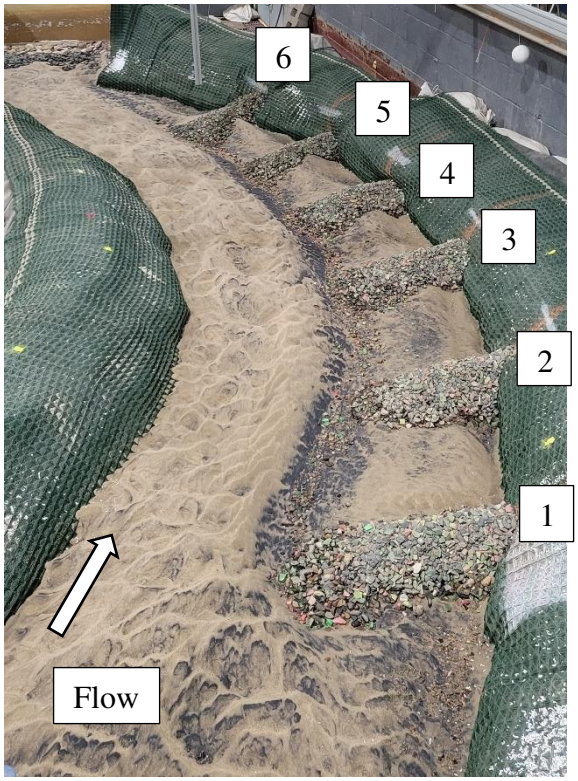

Figure 84. Photo of the curved flume after EXPT 19a ($(\Delta y+H)/H$ = 1.25).

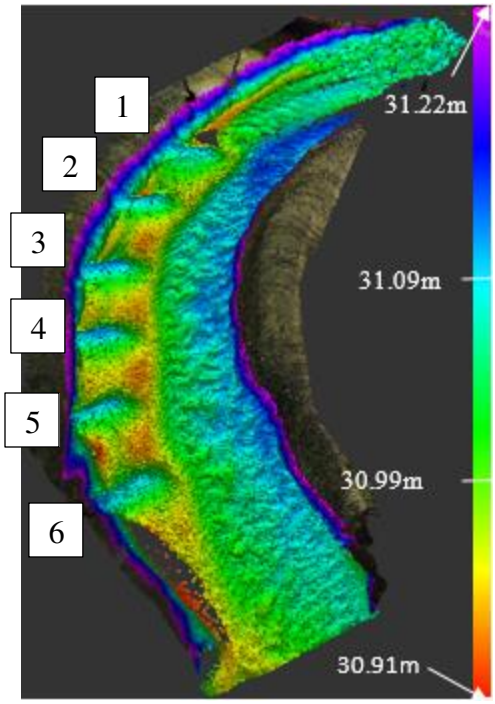

Figure 85. LiDAR of the curved flume after EXPT 20a ((*Δy*+*H*)/*H* = 2.0).

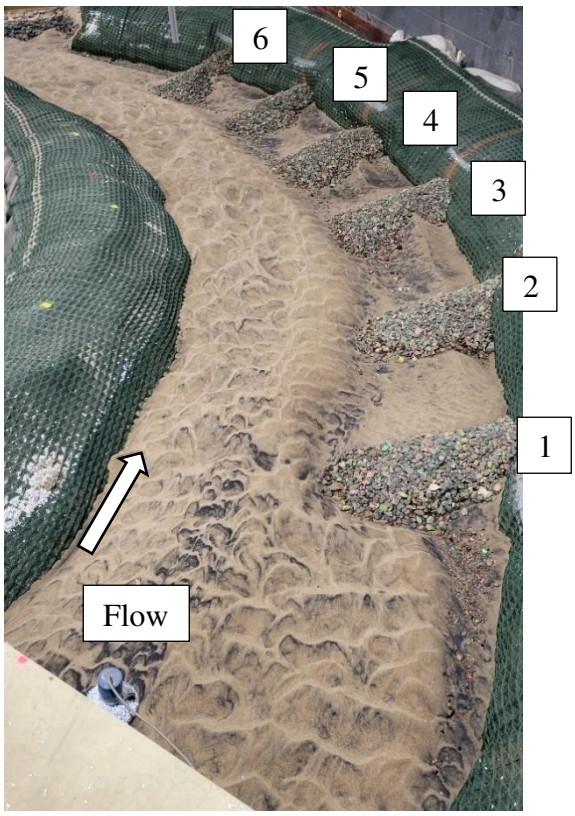

Figure 86. Photo of the curved flume after EXPT 20a ((*Δy*+*H*)/*H* = 2.0).

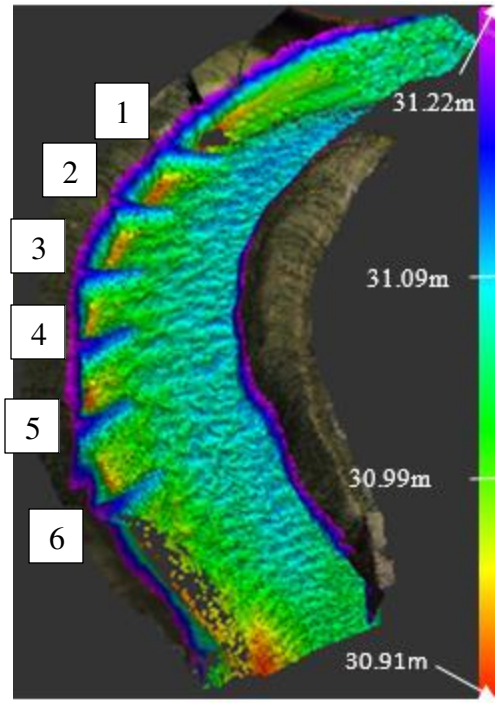

Figure 87. LiDAR of the curved flume after EXPT 21a ($(\Delta y+H)/H$ = 1.25) with bendway weirs constructed after the experiment.

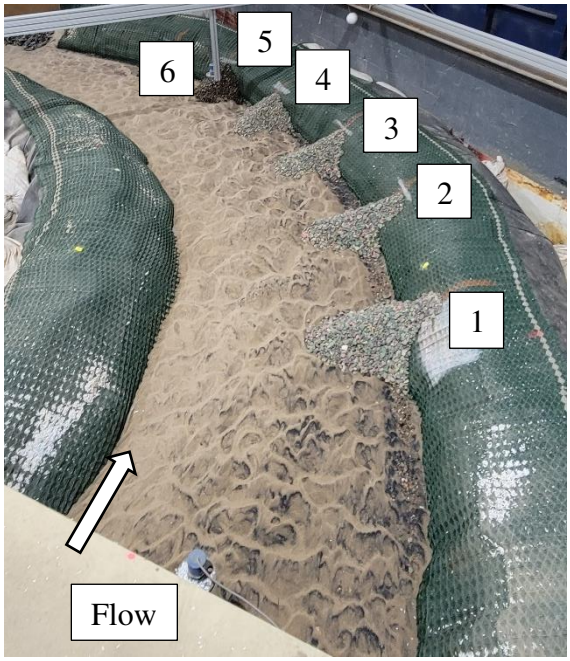

Figure 88. Photo of the curved flume after EXPT 21a ($(\Delta y+H)/H$ = 1.25) with bendway weirs constructed after the experiment.

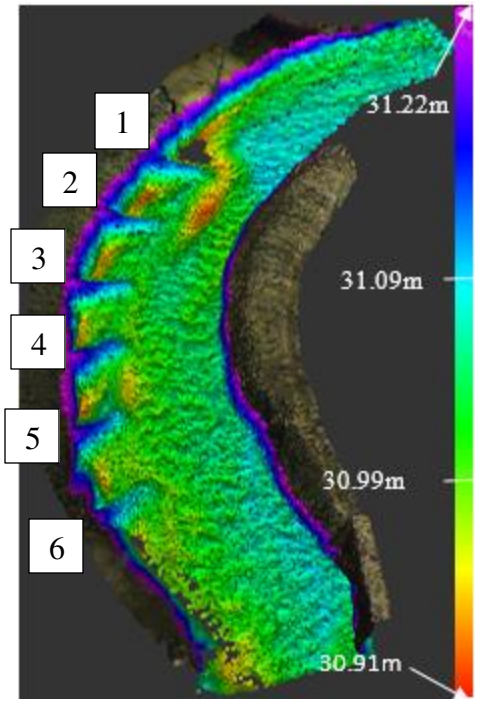

Figure 89. LiDAR of the curved flume after EXPT 22a ((*Δy*+*H*)/*H* = 0.75).

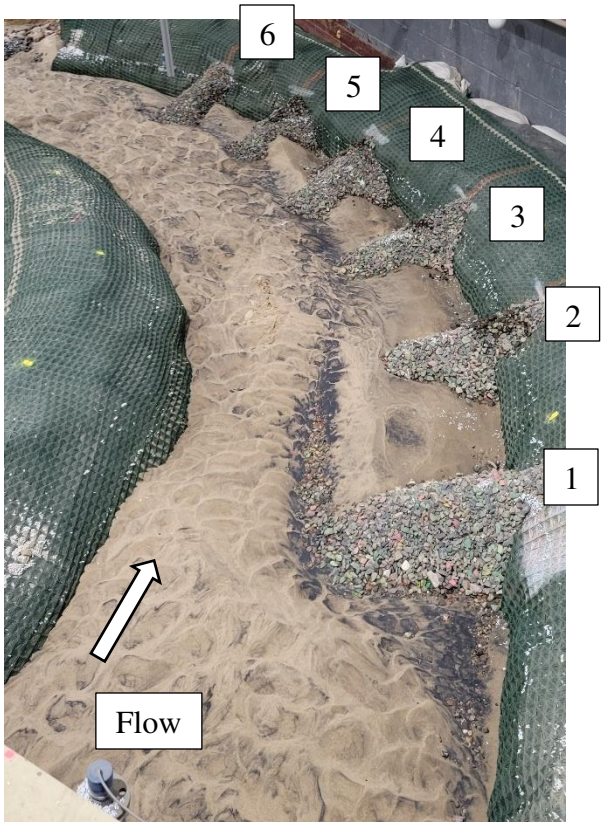

Figure 90. Photo of the curved flume after EXPT 22a ((*Δy*+*H*)/*H* = 0.75).

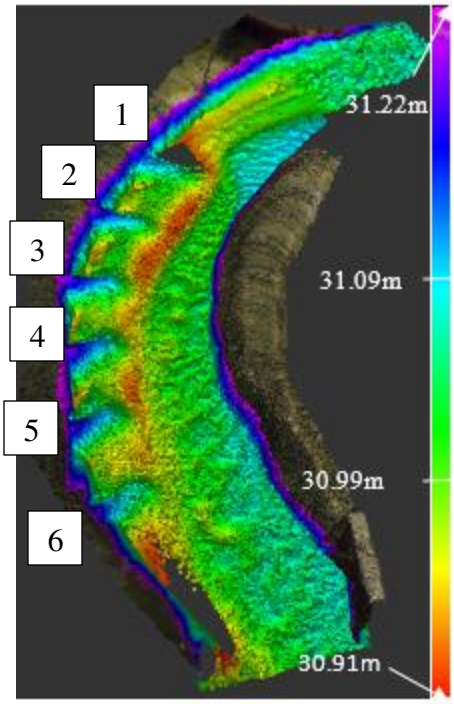

Figure 91. LiDAR of the curved flume after EXPT 23a ((*Δy*+*H*)/*H* = 1.25).

Figure 92. Photo of the curved flume after EXPT 23a ((*Δy*+*H*)/*H* = 1.25).

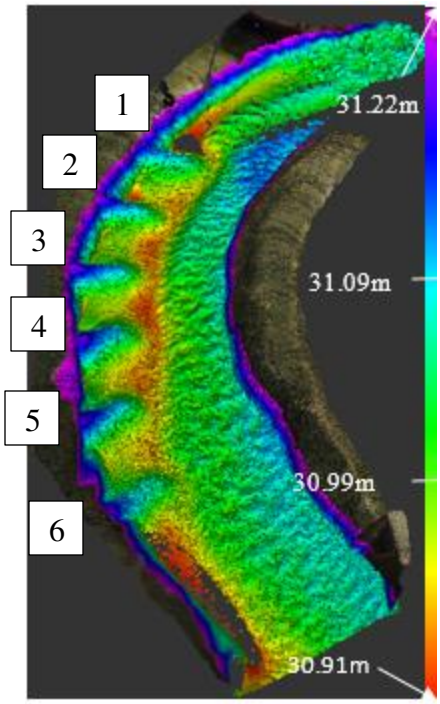

Figure 93. LiDAR of the curved flume after EXPT 24a ((*Δy*+*H*)/*H* = 2.0).

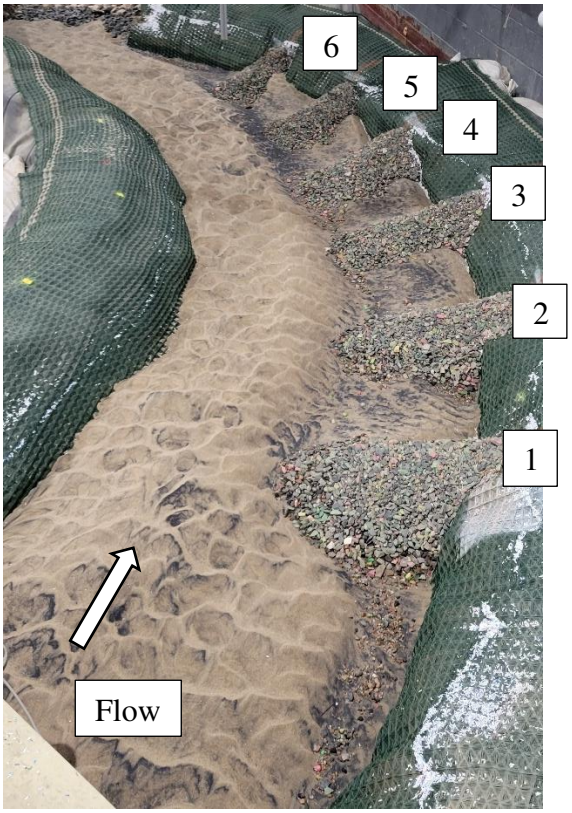

Figure 94. Photo of the curved flume after EXPT 24a ((*Δy*+*H*)/*H* = 2.0).

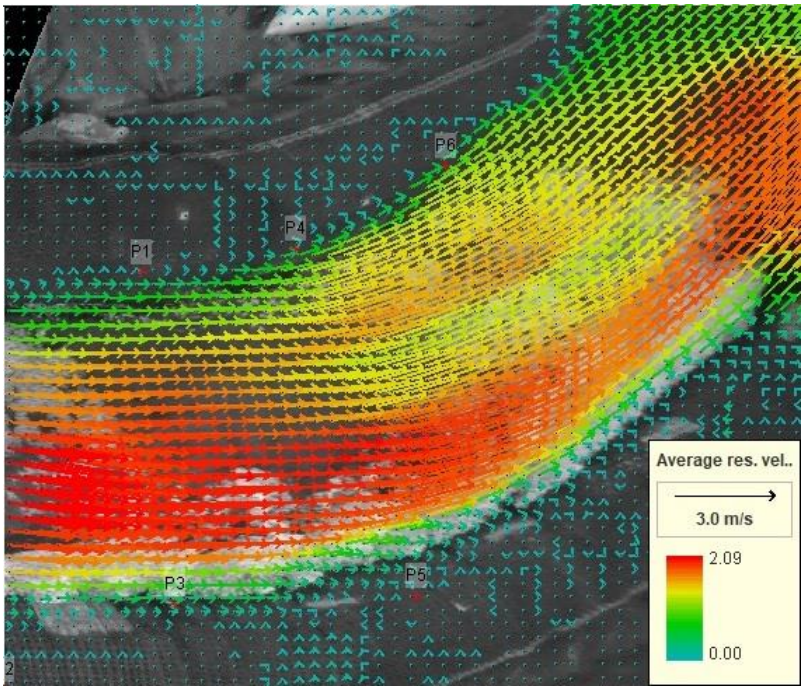

Figure 95. Surface water velocity of the initial bed forming flow ((*Δy*+*H*)/*H* = 1.25) during EXPT 9a.

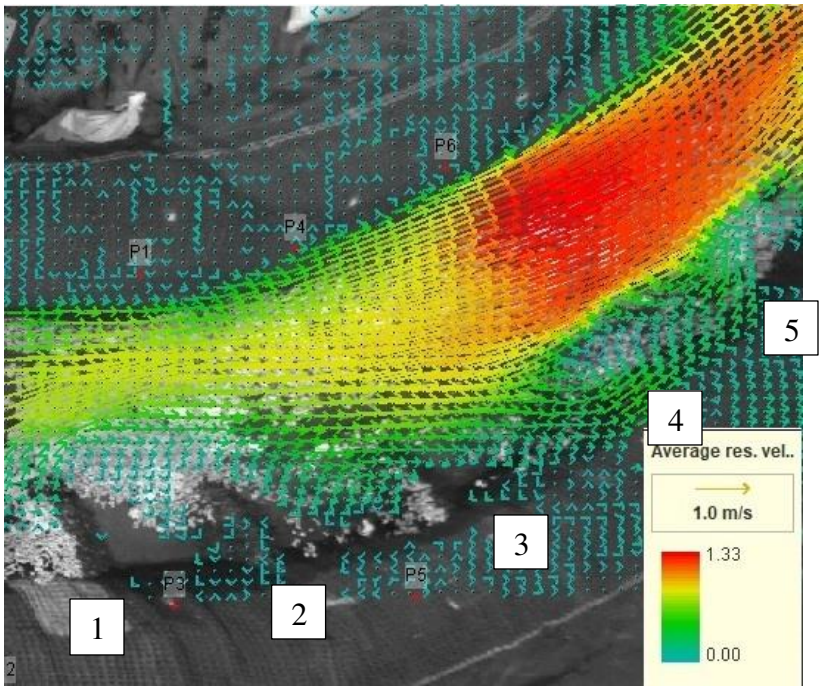

Figure 96. Surface water velocity for (*Δy*+*H*)/*H* = 0.75 during EXPT 10a.

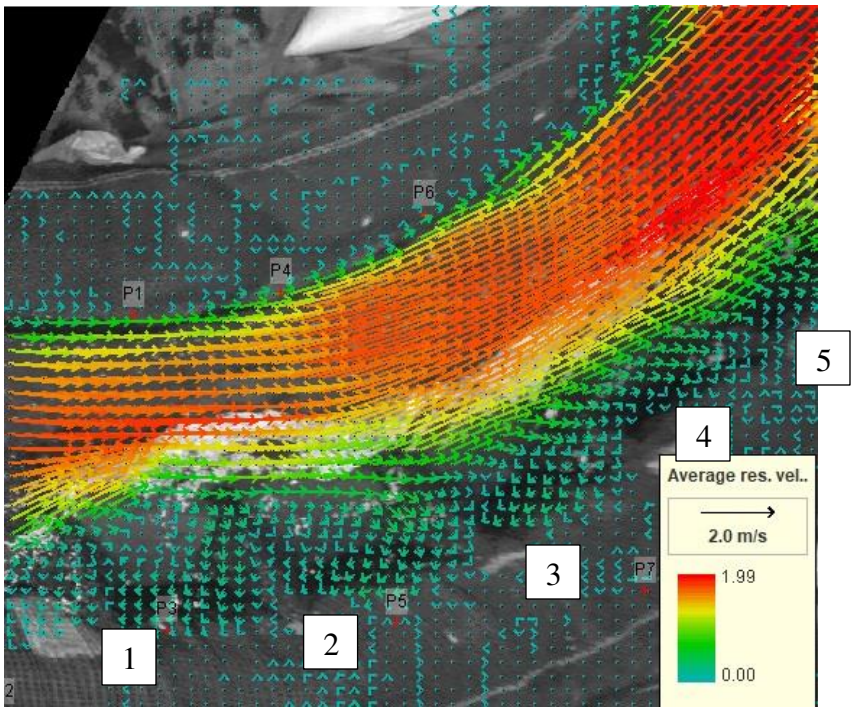

Figure 97. Surface water velocity for ($\Delta y+H$)/H = 1.25 during EXPT 11a.

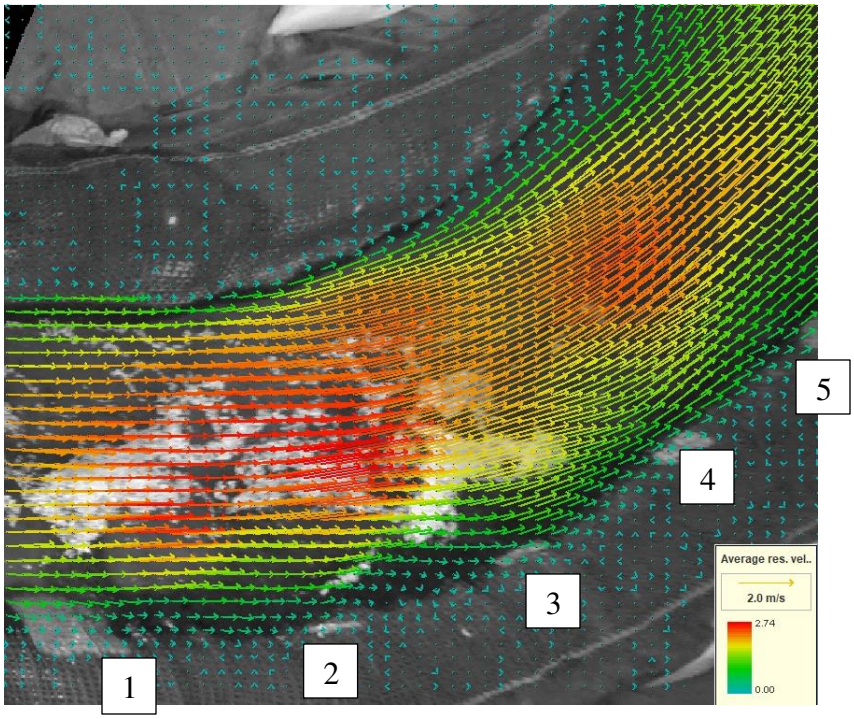

Figure 98. Surface water velocity for ($\Delta y+H$)/H = 2.0 during EXPT 12a.

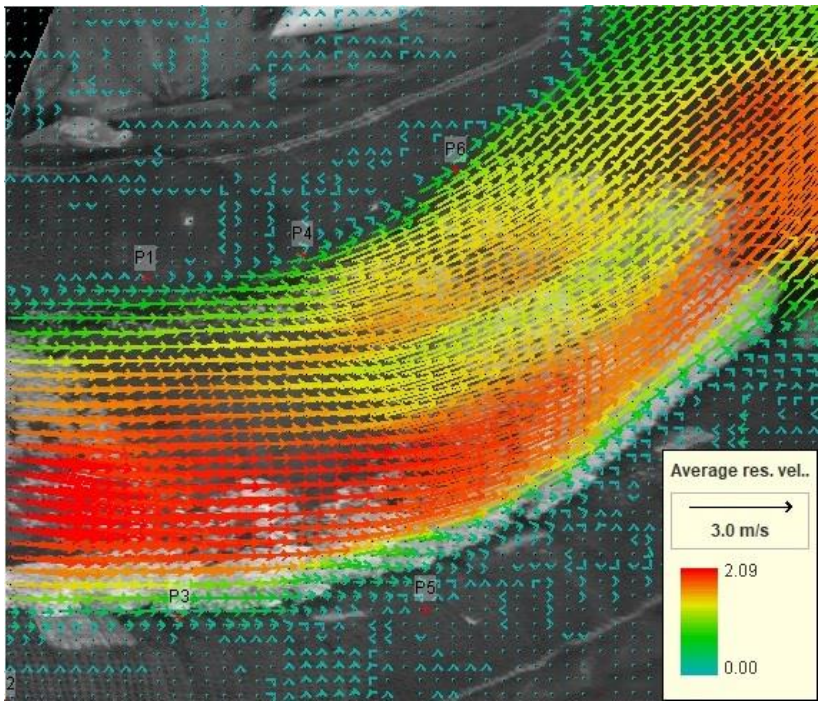

Figure 99. Surface water velocity for initial bed forming flow ((*Δy*+*H*)/*H* = 1.25) during EXPT 13a.

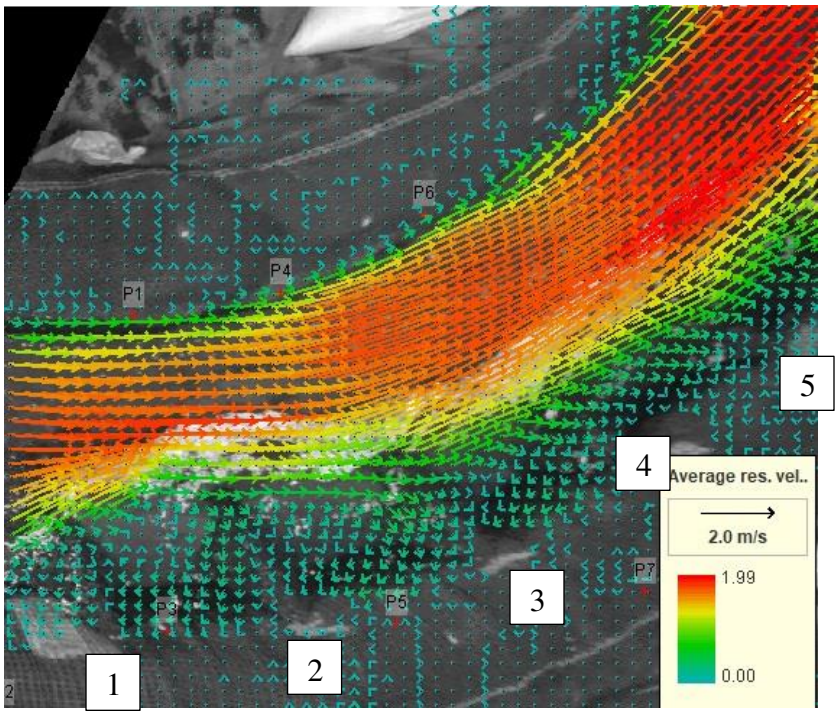

Figure 100. Surface water velocity for (*Δy*+*H*)/*H* = 0.75 during EXPT 14a.

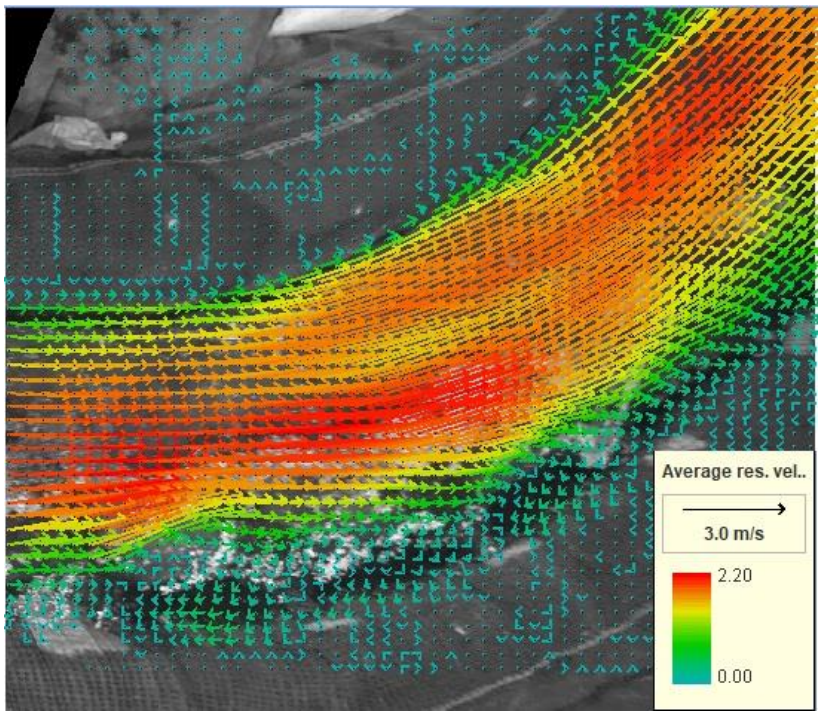

Figure 101. Surface water velocity for $(\Delta y+H)/H$ = 1.25 during EXPT 15a.

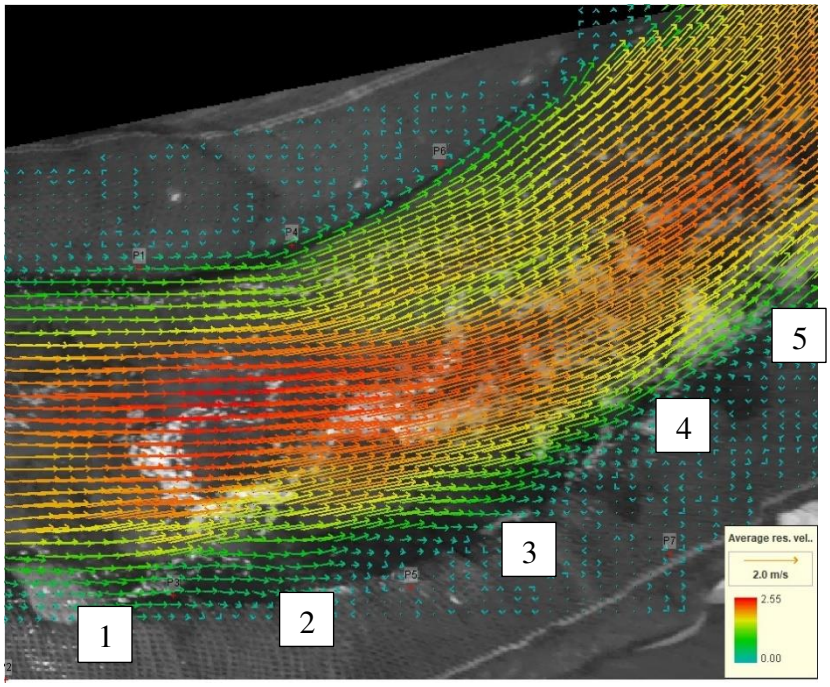

Figure 102. Surface water velocity for $(\Delta y+H)/H$ = 2.0 during EXPT 16a.

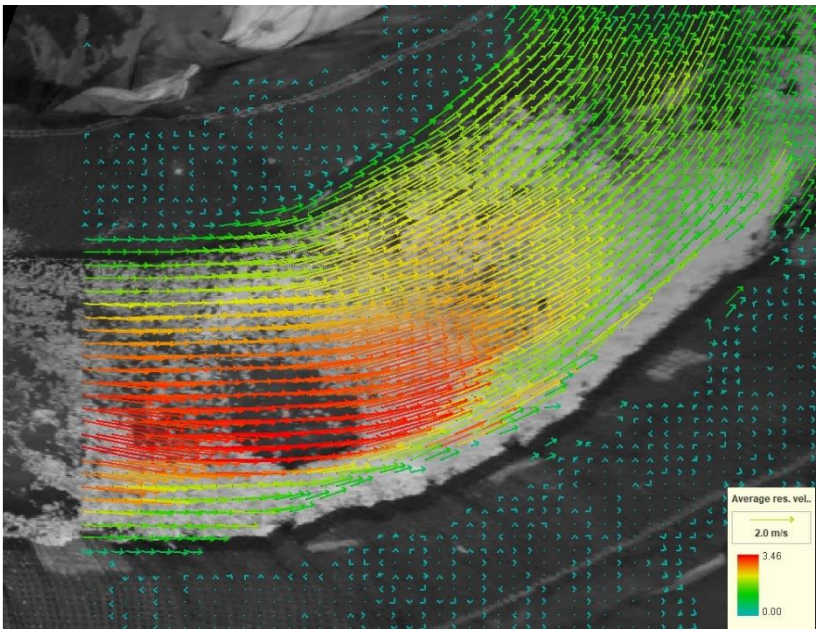

Figure 103. Surface water velocity of the initial bed forming flow ($(\Delta y+H)/H$ = 1.25) during EXPT 17a.

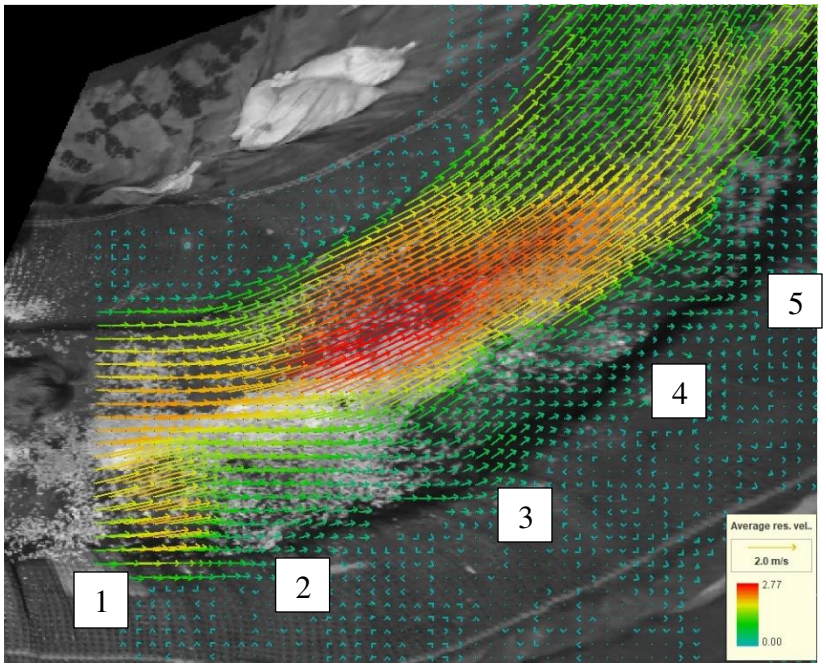

Figure 104. Surface water velocity for $(\Delta y+H)/H$ = 0.75 during EXPT 18a.

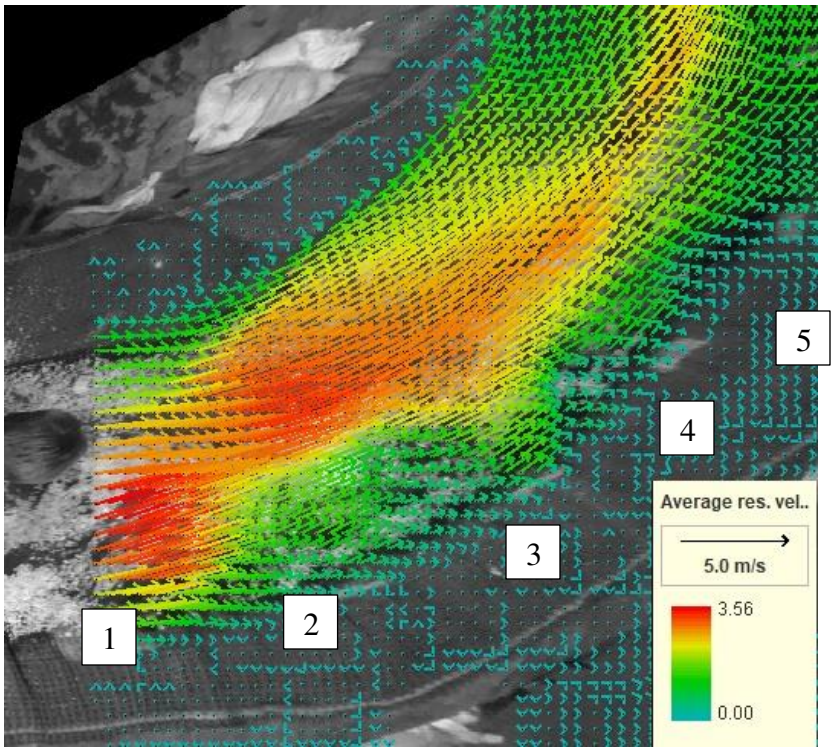

Figure 105. Surface water velocity for ($\Delta y+H$)/H = 1.25 during EXPT 19a.

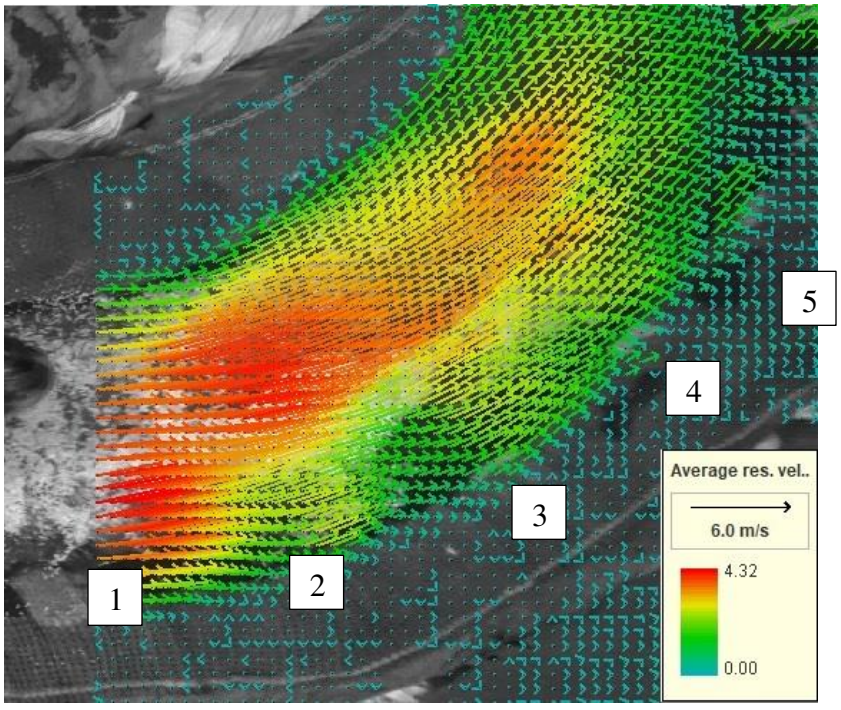

Figure 106. Surface water velocity for ($\Delta y+H$)/H = 2.0 during EXPT 20a.

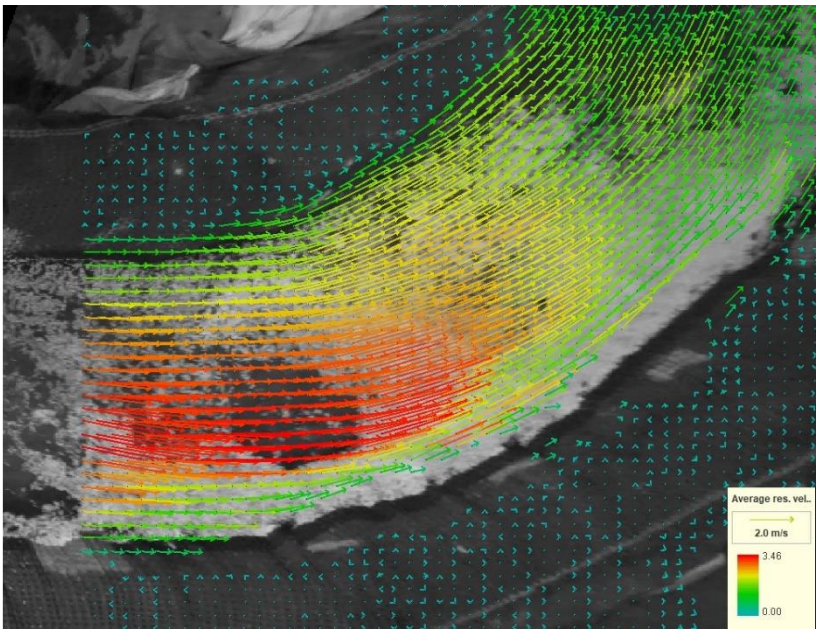

Figure 107. Surface water velocity of the initial bed forming flow ((*Δy*+*H*)/*H* = 1.25) during EXPT 21a.

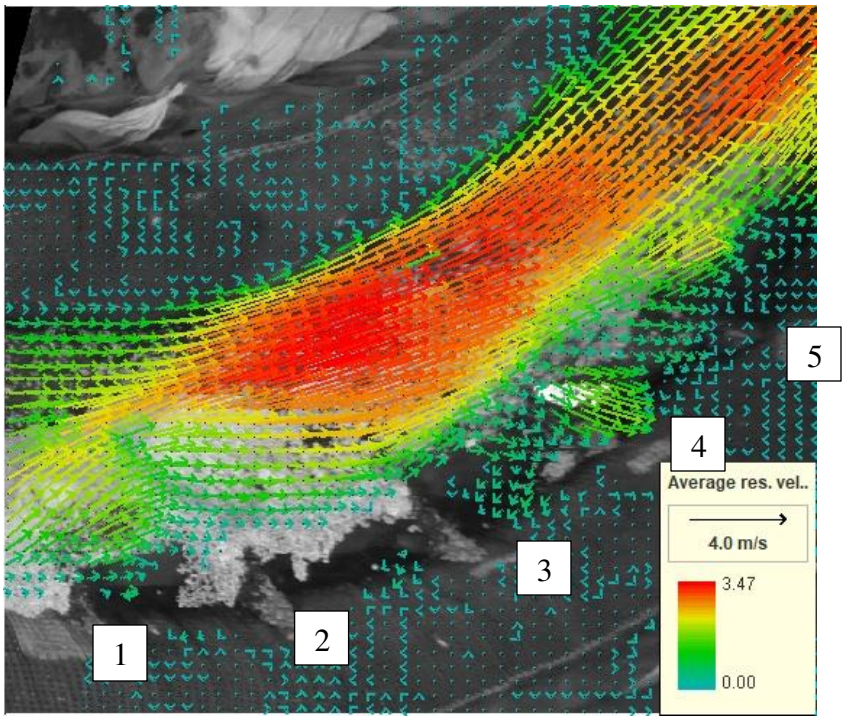

Figure 108. Surface water velocity for (*Δy*+*H*)/*H* = 0.75 during EXPT 22a.

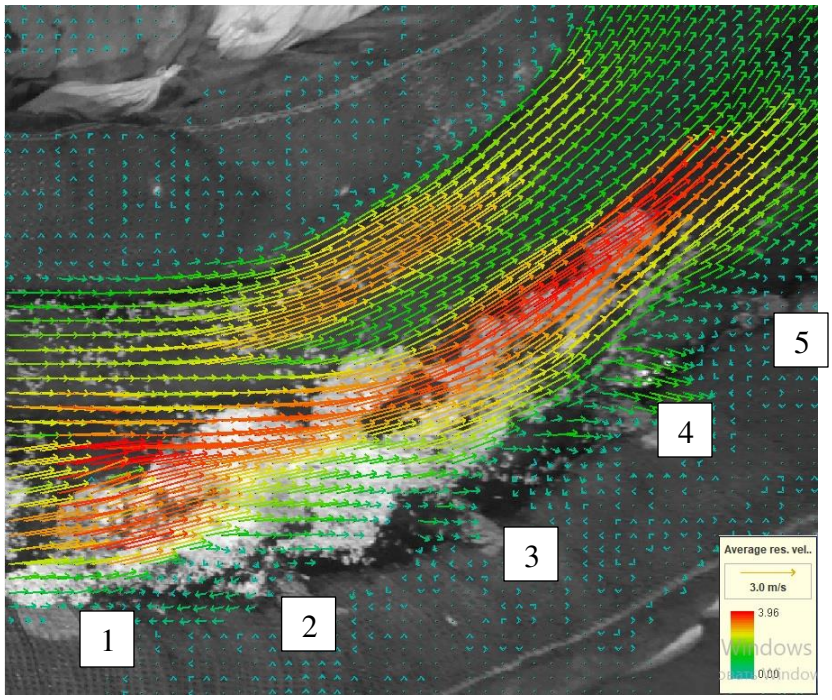

Figure 109. Surface water velocity for ($\Delta y+H$)/H = 1.25 during EXPT 23a.

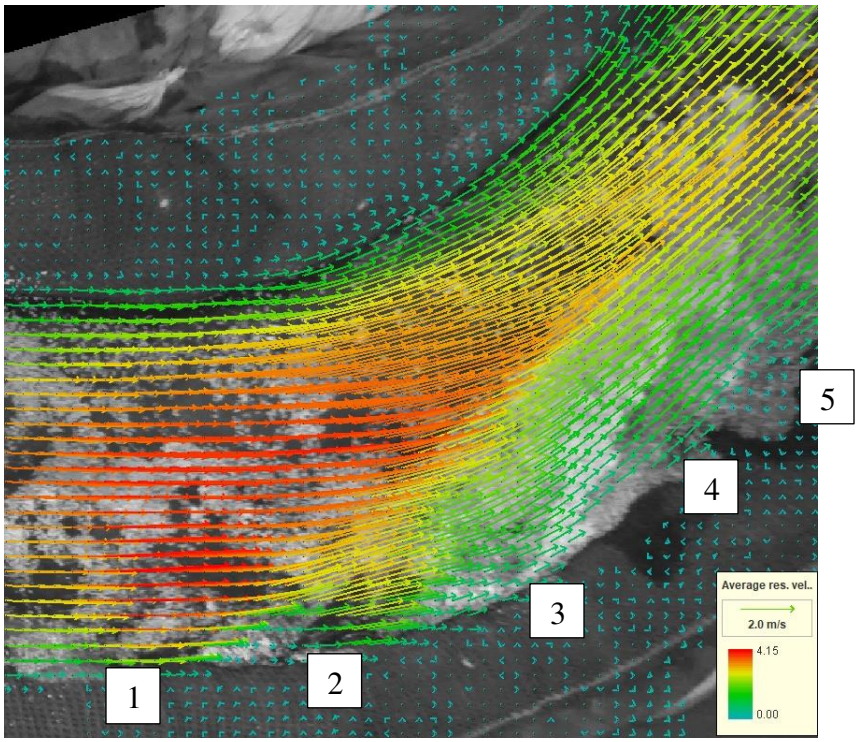

Figure 110. Surface water velocity for ($\Delta y+H$)/H = 2.0 during EXPT 24a.

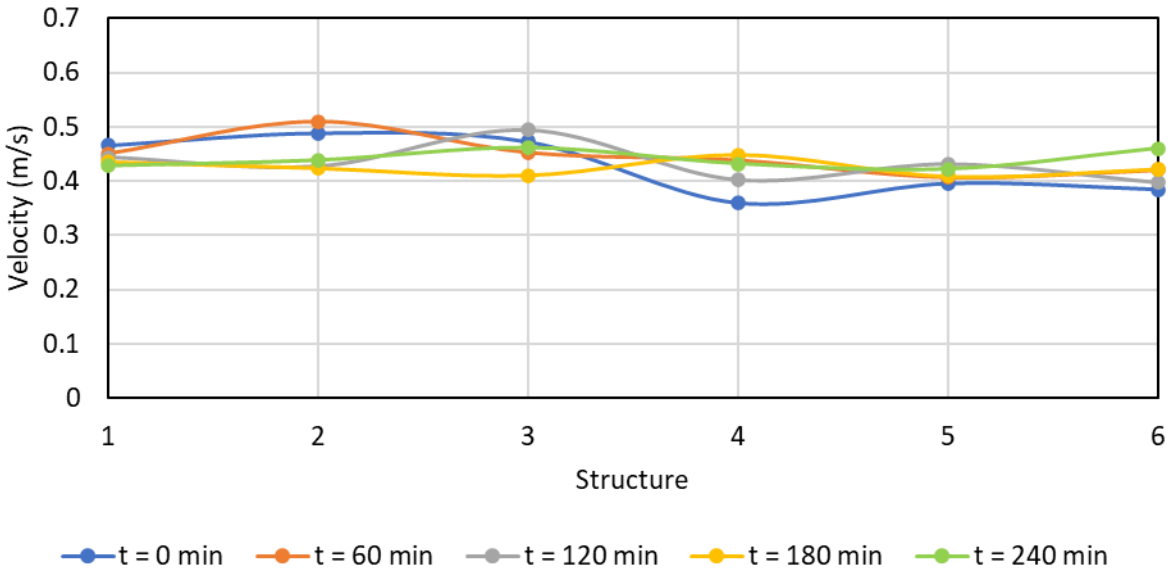

Figure 111. Outer bank x-velocity over time for the initial bed forming flow ($(\Delta y+H)/H$ = 1.25) in the curved flume from EXPT 9a.

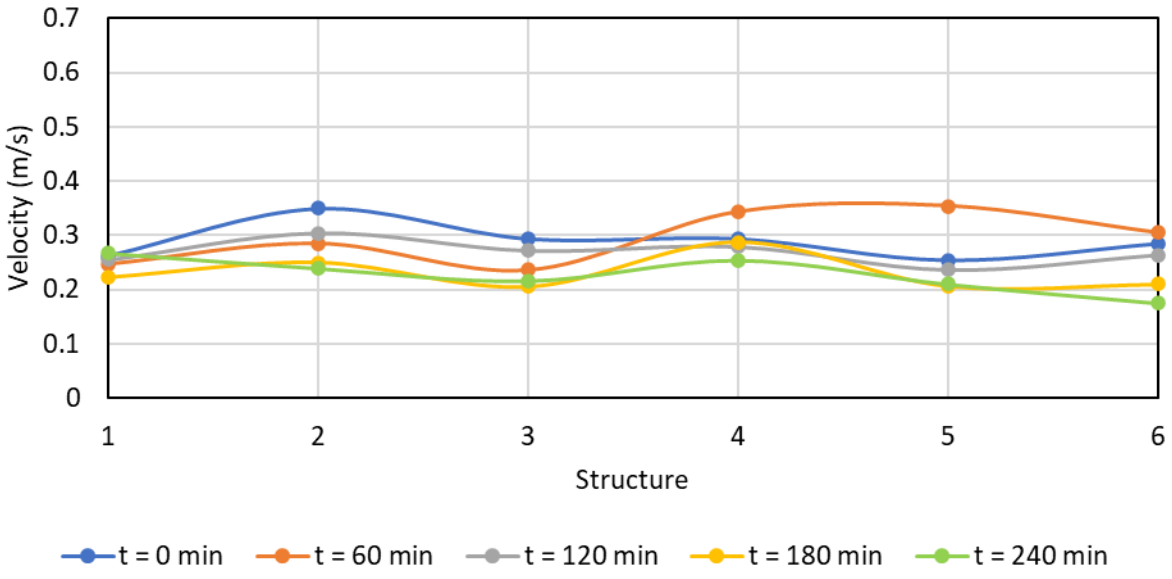

Figure 112. Outer bank y-velocity over time for the initial bed forming flow ($(\Delta y+H)/H$ = 1.25) in the curved flume from EXPT 9a.

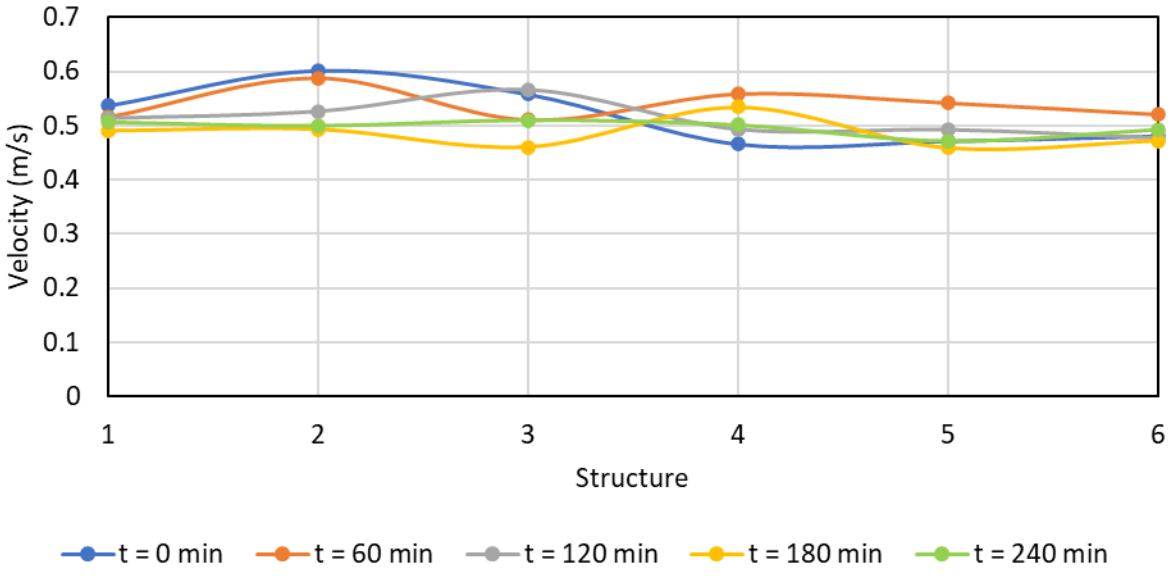

Figure 113. Outer bank maximum-velocity over time for the initial bed forming flow ($(\Delta y+H)/H$ = 1.25) in the curved flume from EXPT 9a.

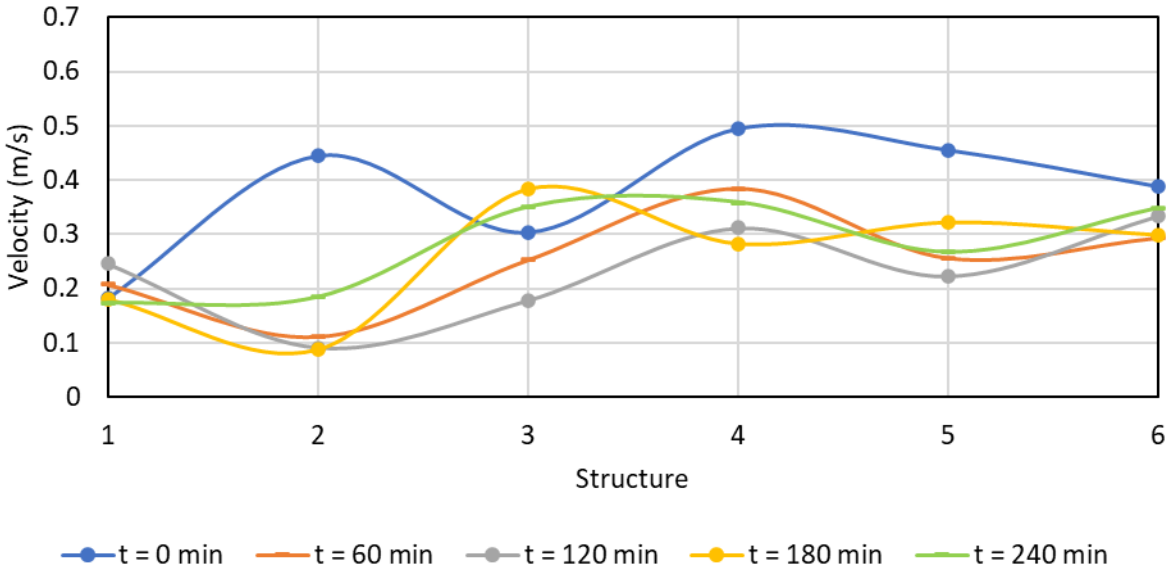

Figure 114. Structure tip x-velocity over time for $(\Delta y+H)/H$ = 0.75 in the curved flume from EXPT 10a.

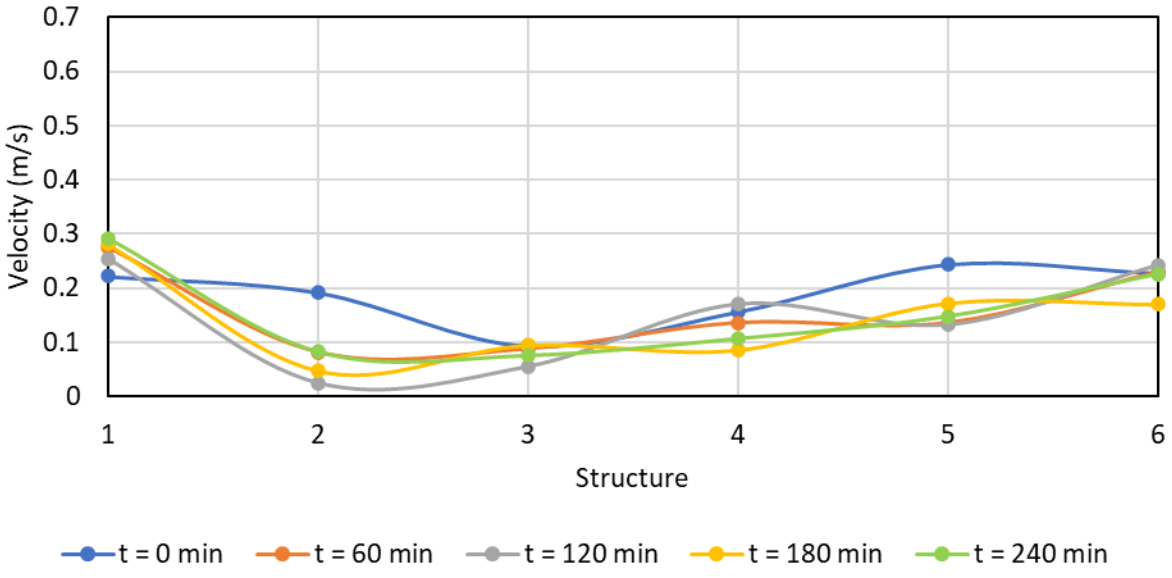

Figure 115. Structure tip y-velocity over time for $(\Delta y+H)/H$ = 0.75 in the curved flume from EXPT 10a.

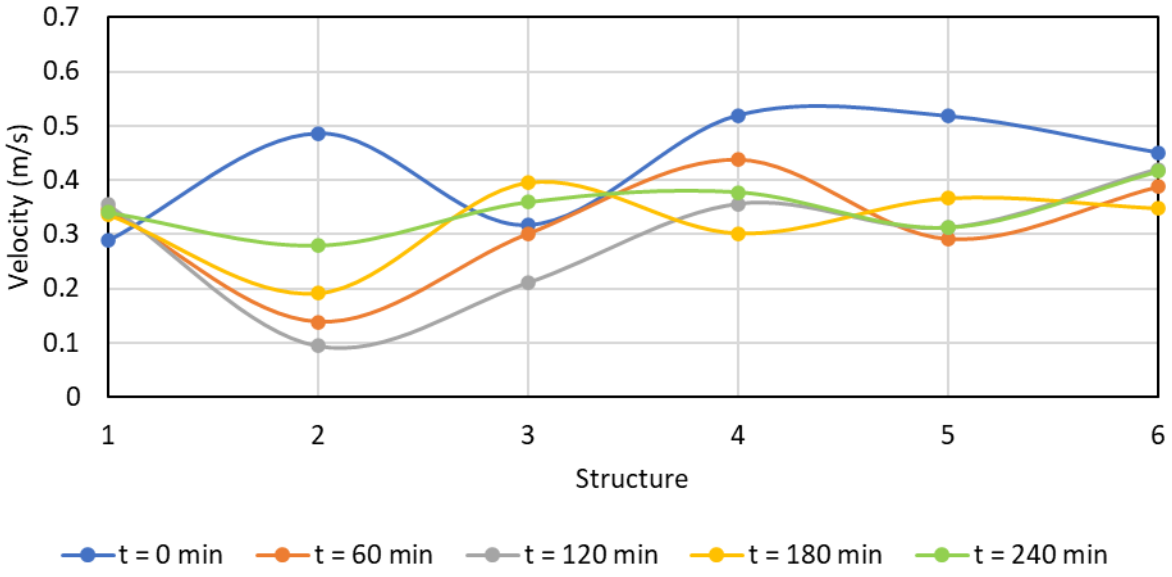

Figure 116. Structure tip maximum velocity over time for $(\Delta y+H)/H$ = 0.75 in the curved flume from EXPT 10a.

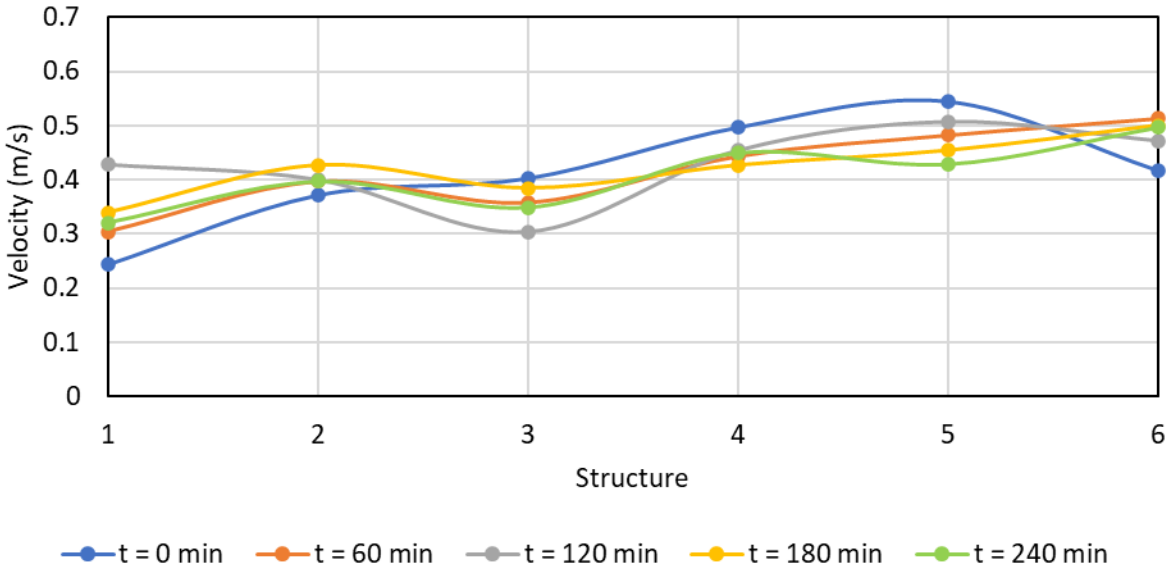

Figure 117. Bendway weir tip x-velocity over time for $(\Delta y+H)/H$ = 1.25 in the curved flume from EXPT 11a.

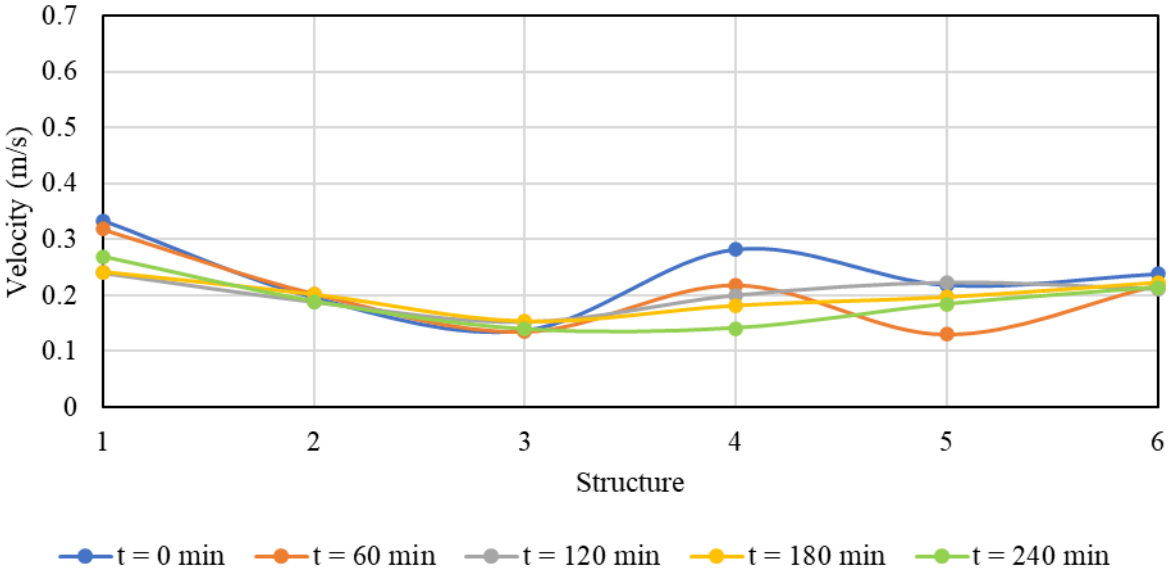

Figure 118. Bendway weir tip y-velocity over time for $(\Delta y+H)/H$ = 1.25 in the curved flume from EXPT 11a.

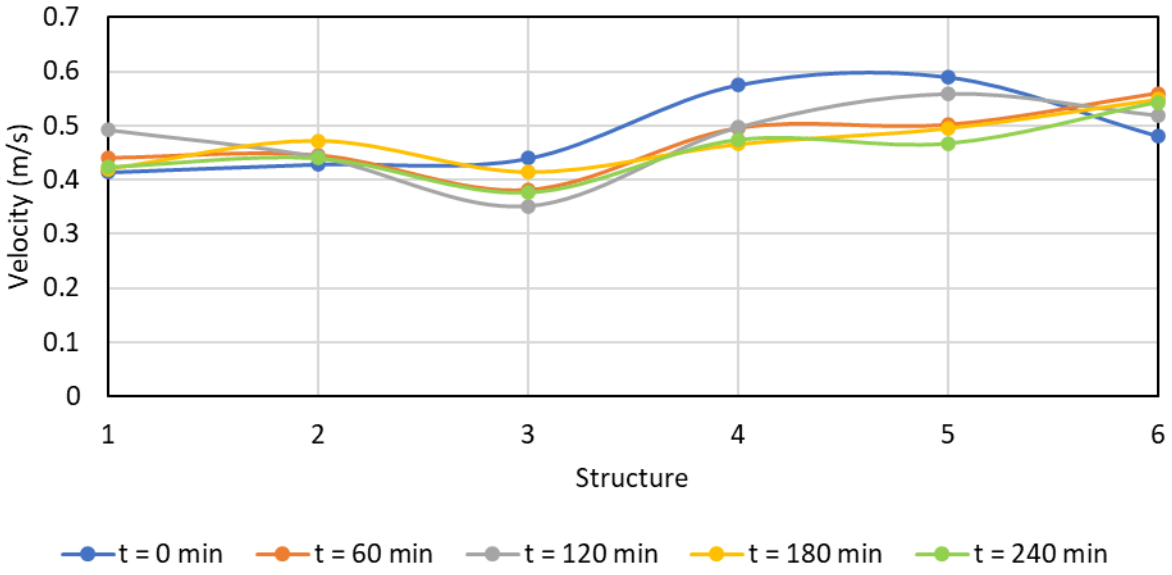

Figure 119. Bendway weir tip maximum velocity over time for $(\Delta y+H)/H$ = 1.25 in the curved flume from EXPT 11a.

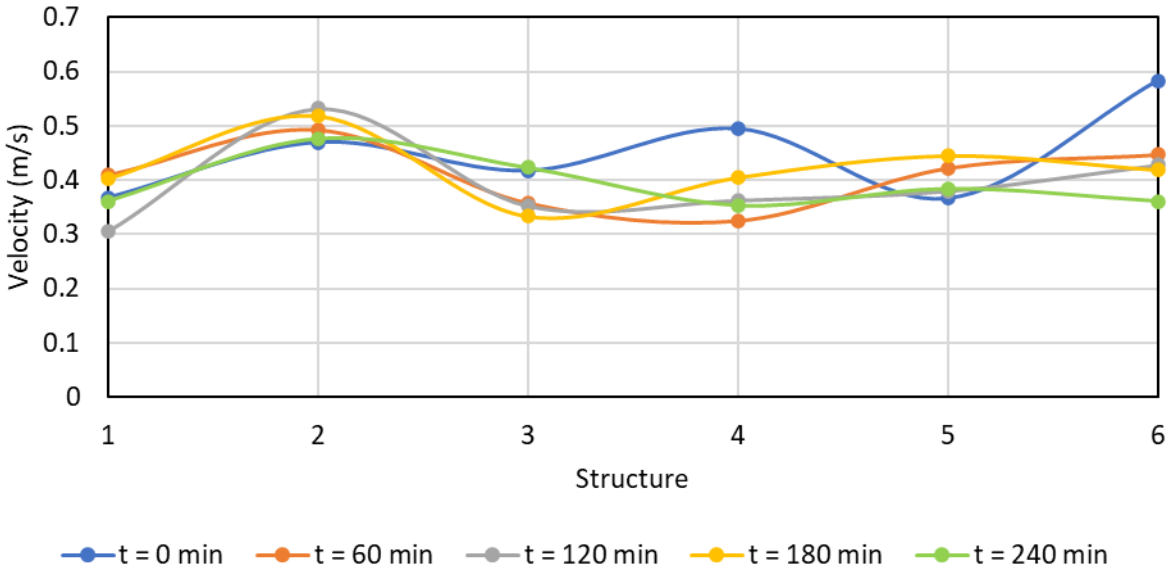

Figure 120. Bendway weir tip x-velocity over time for $(\Delta y+H)/H$ = 2.0 in the curved flume from EXPT 12a.

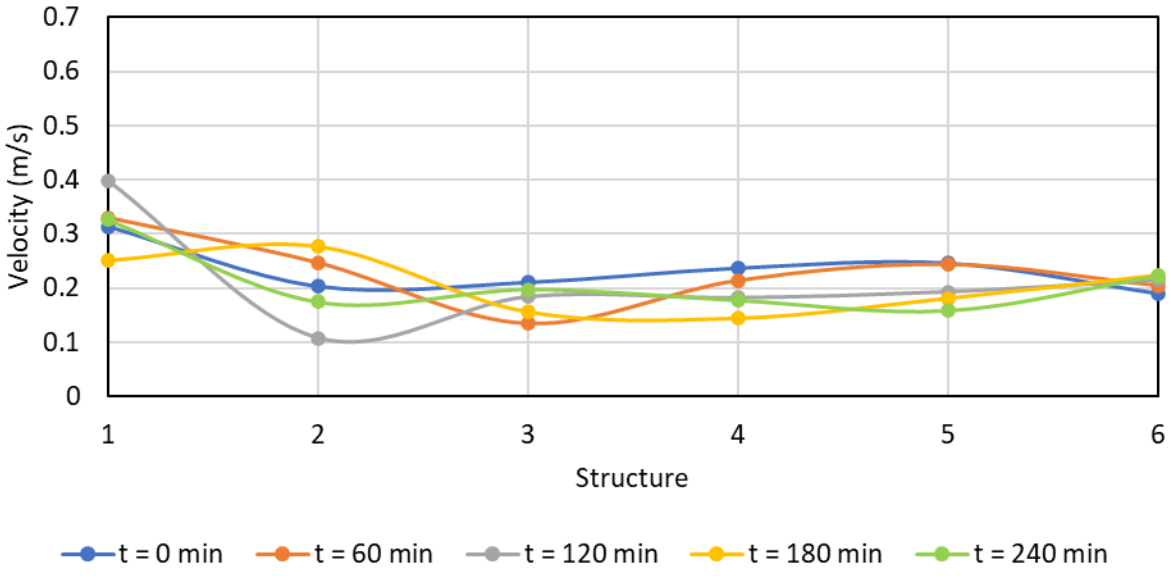

Figure 121. Bendway weir tip y-velocity over time for $(\Delta y+H)/H$ = 2.0 in the curved flume from EXPT 12a.

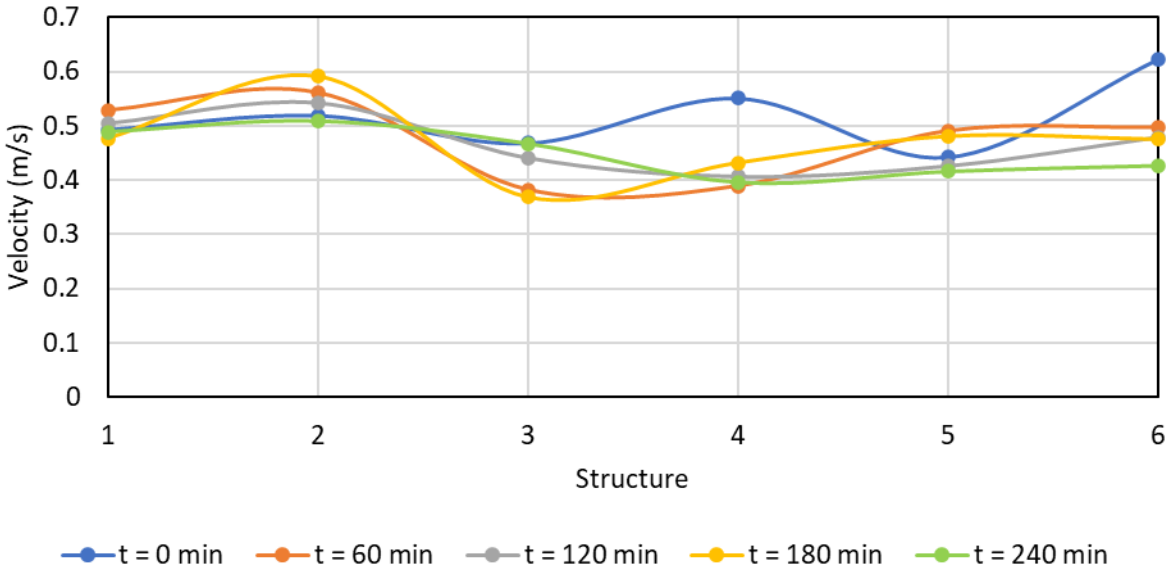

Figure 122. Bendway weir tip maximum velocity over time for $(\Delta y+H)/H$ = 2.0 in the curved flume from EXPT 12a.

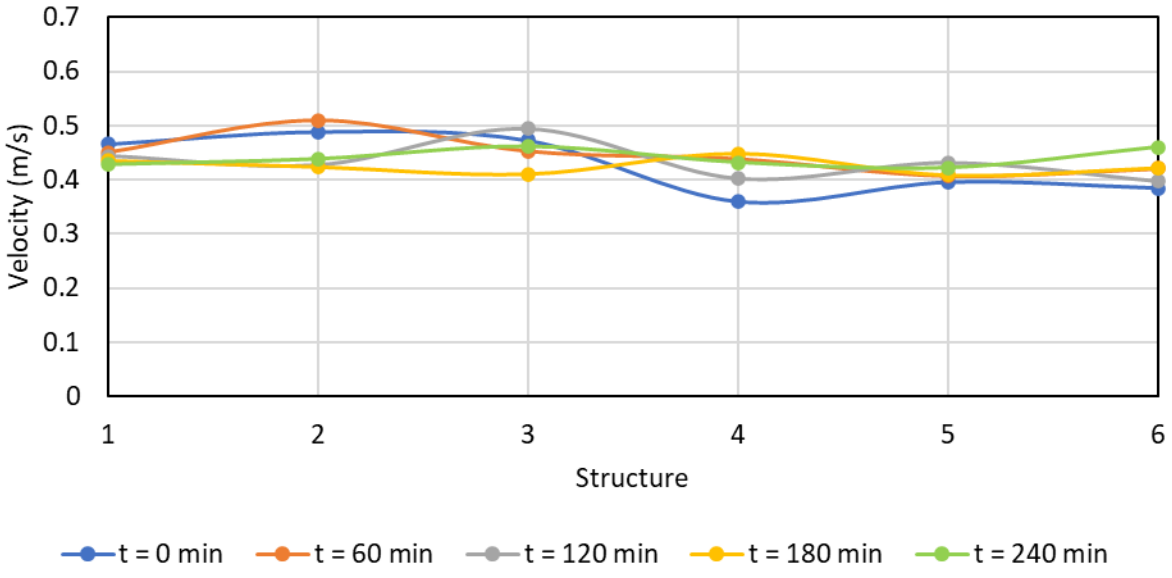

Figure 123. Outer bank x-velocity over time for the initial bed forming flow ($(\Delta y+H)/H$ = 1.25) in the curved flume from EXPT 13a.

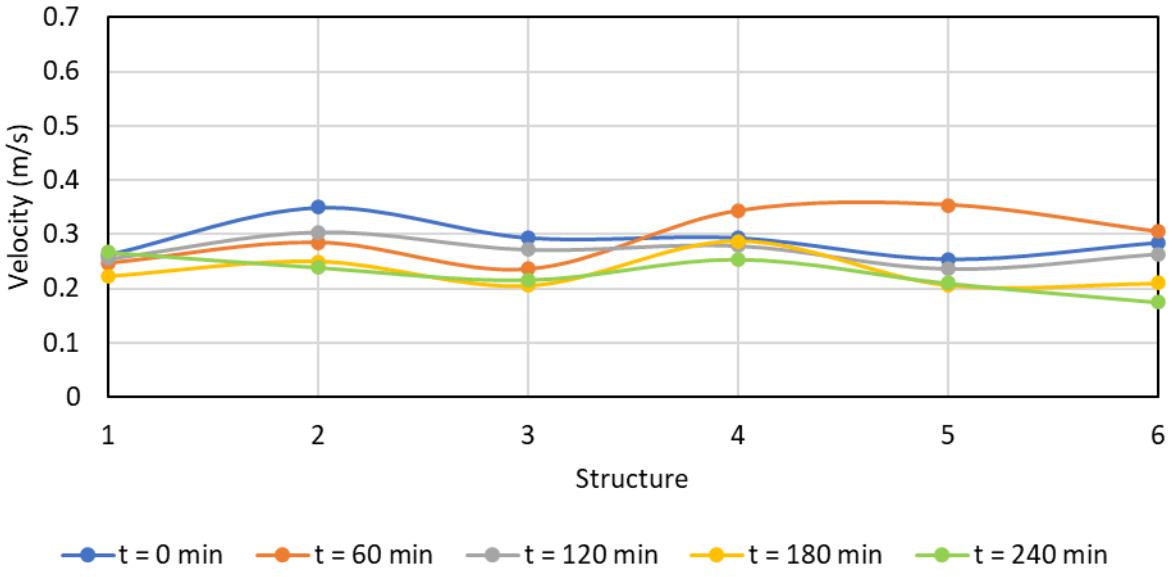

Figure 124. Outer bank y-velocity over time for the initial bed forming flow ($(\Delta y+H)/H$ = 1.25) in the curved flume from EXPT 13a.

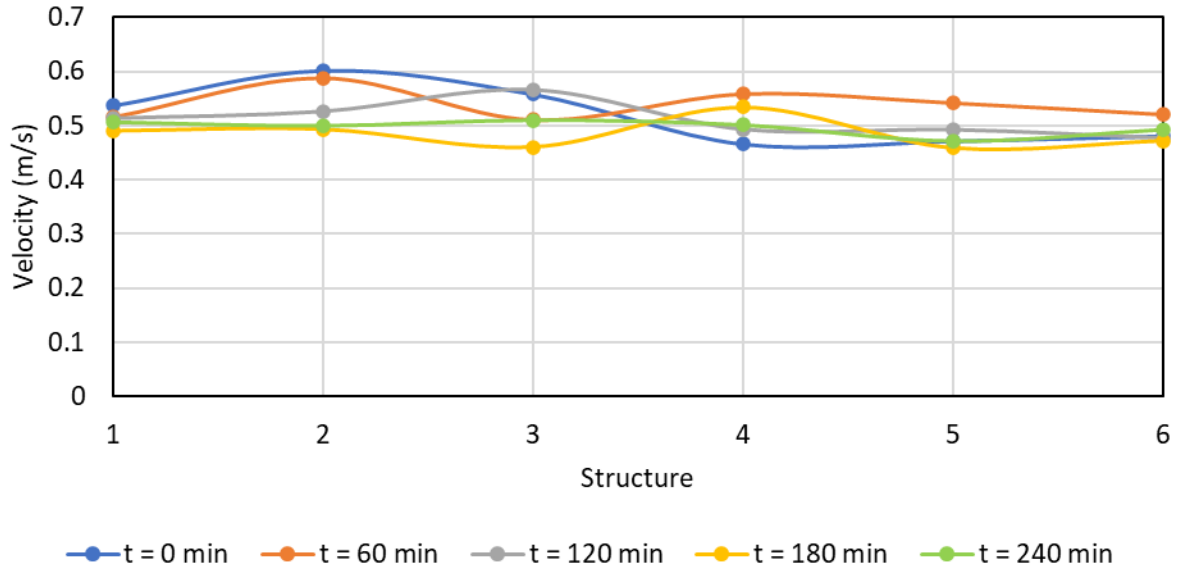

Figure 125. Outer bank maximum velocity over time for the initial bed forming flow ($(\Delta y+H)/H$ = 1.25) in the curved flume from EXPT 13a.

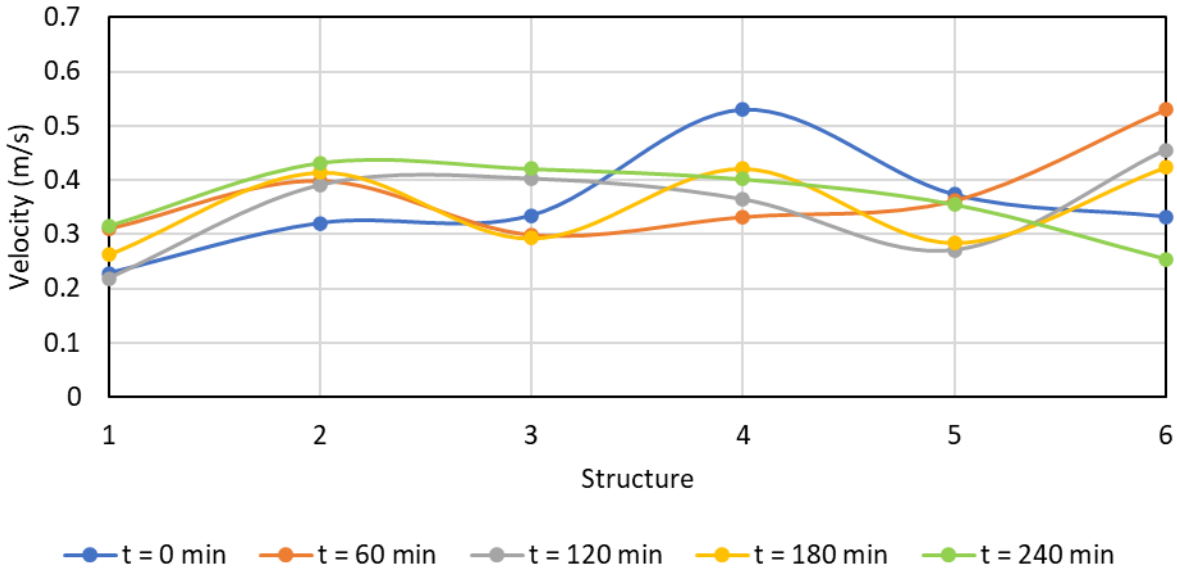

Figure 126. Rock vane tip x-velocity over time for $(\Delta y+H)/H$ = 0.75 in the curved flume from EXPT 14a.

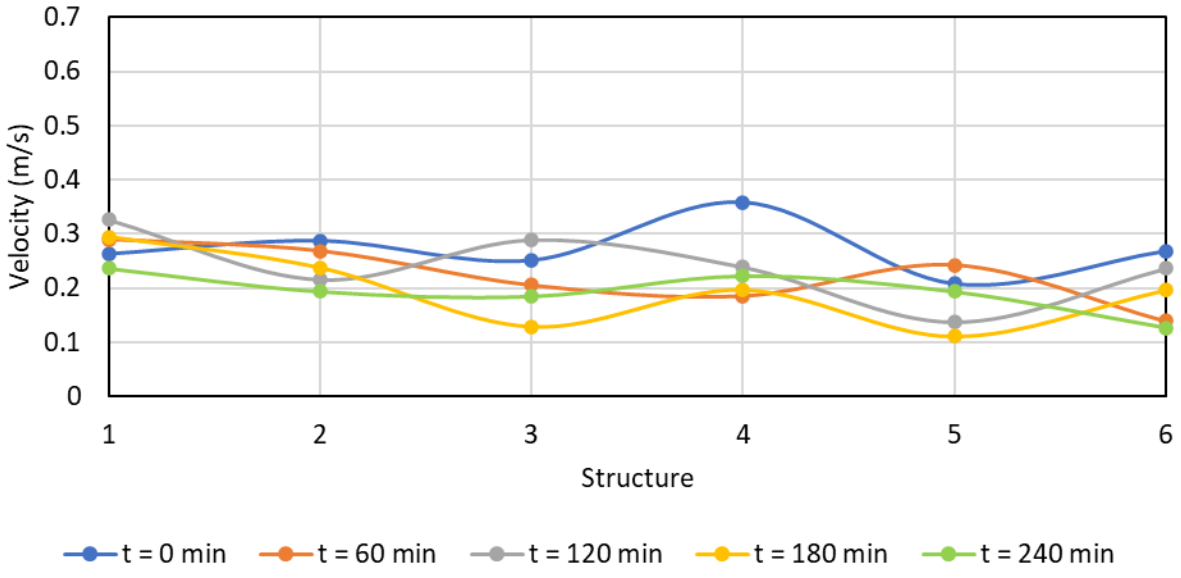

Figure 127. Rock vane tip y-velocity over time for $(\Delta y+H)/H$ = 0.75 in the curved flume from EXPT 14a.

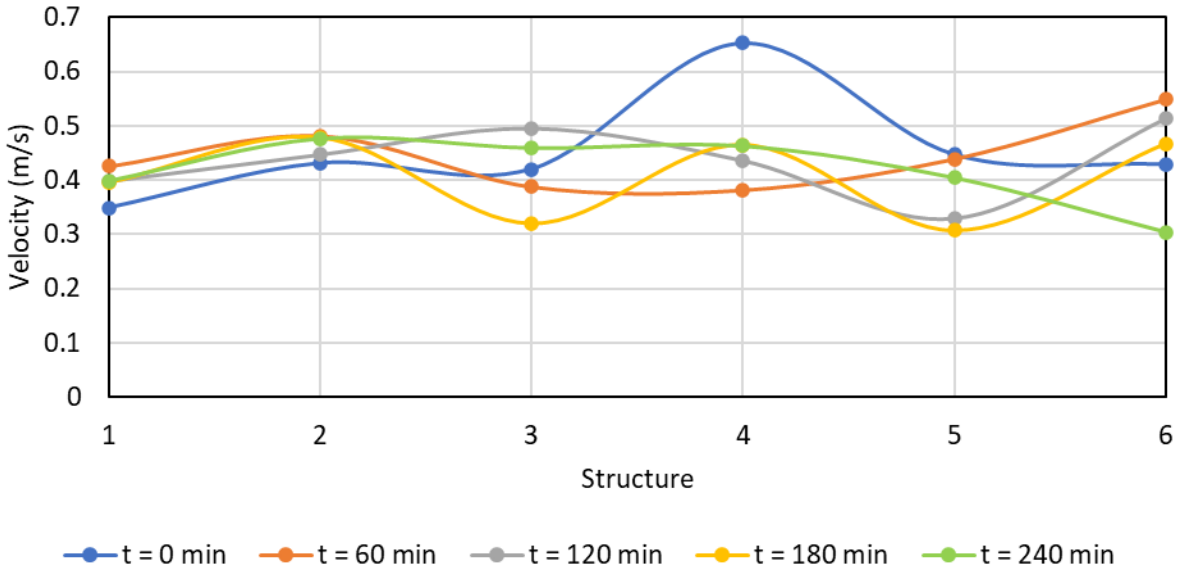

Figure 128. Rock vane tip maximum velocity over time for $(\Delta y+H)/H$ = 0.75 in the curved flume from EXPT 14a.

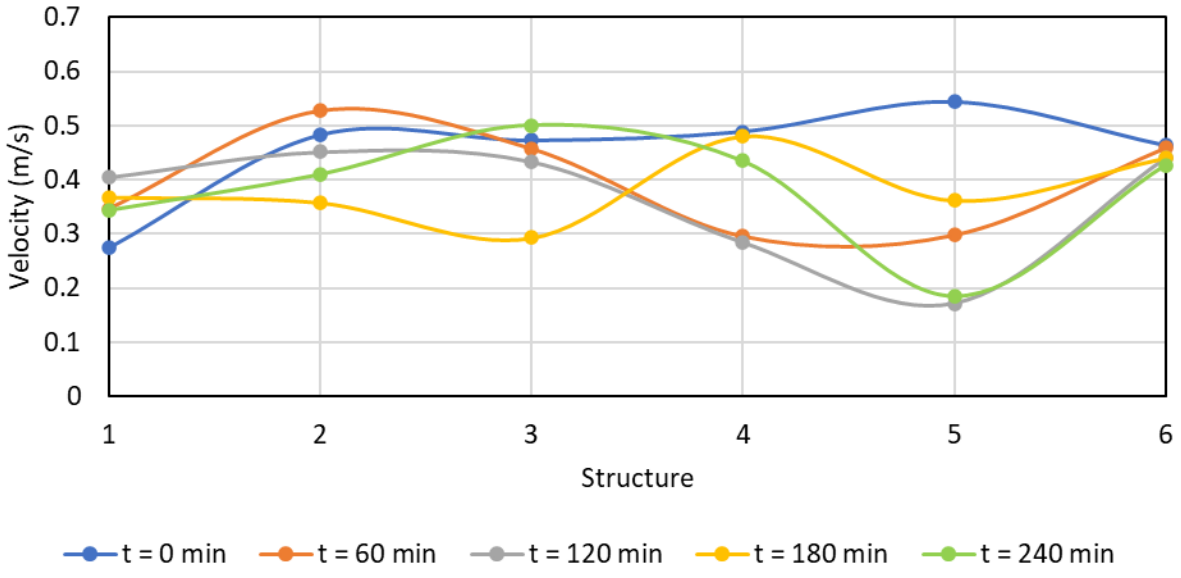

Figure 129. Rock vane tip x-velocity over time for $(\Delta y+H)/H$ = 1.25 in the curved flume from EXPT 15a.

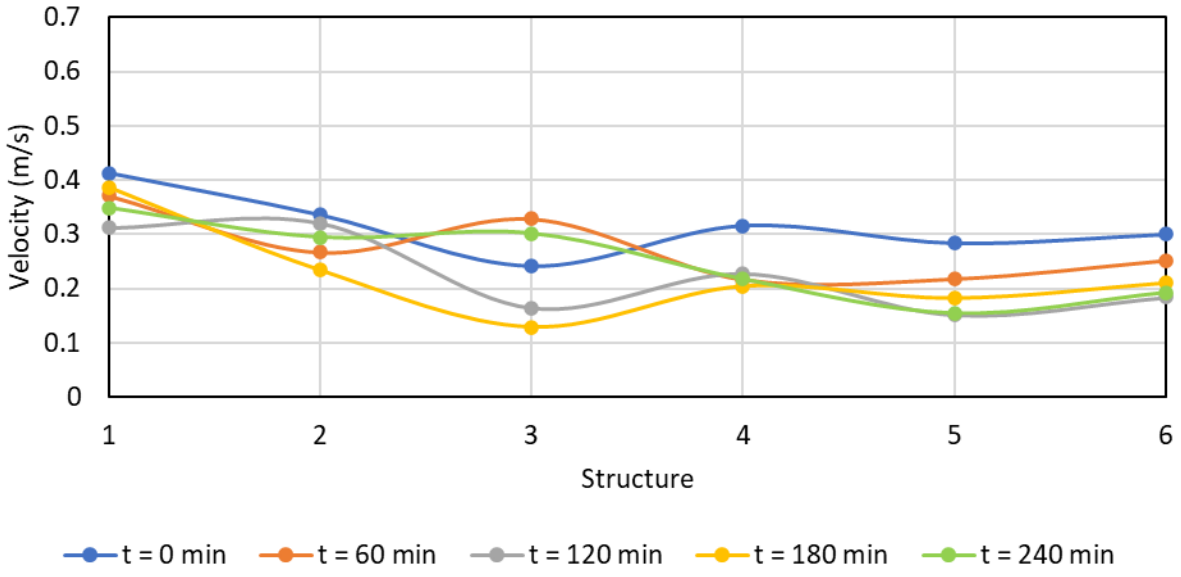

Figure 130. Rock vane tip y-velocity over time for $(\Delta y+H)/H$ = 1.25 in the curved flume from EXPT 15a.

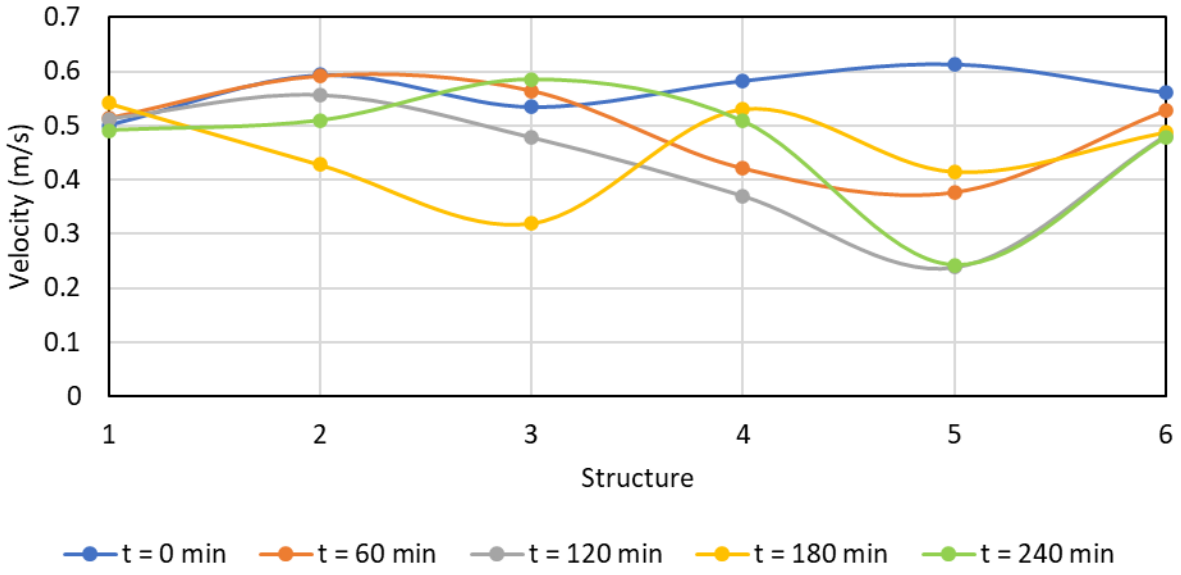

Figure 131. Rock vane tip maximum velocity over time for $(\Delta y+H)/H$ = 1.25 in the curved flume from EXPT 15a.

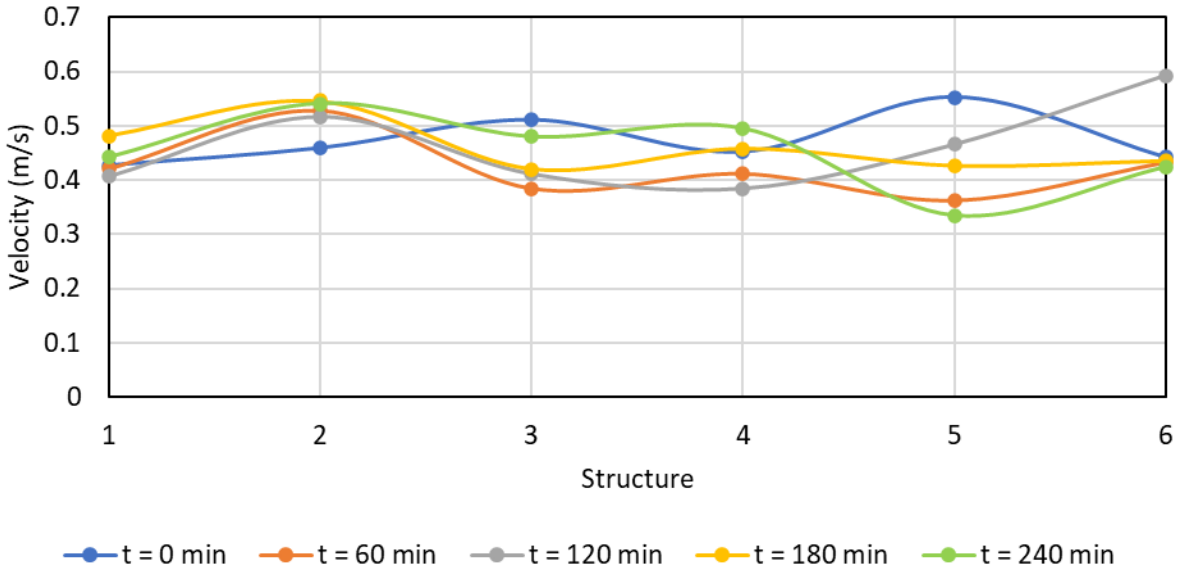

Figure 132. Rock vane tip x-velocity over time for $(\Delta y+H)/H$ = 2.0 in the curved flume from EXPT 16a.

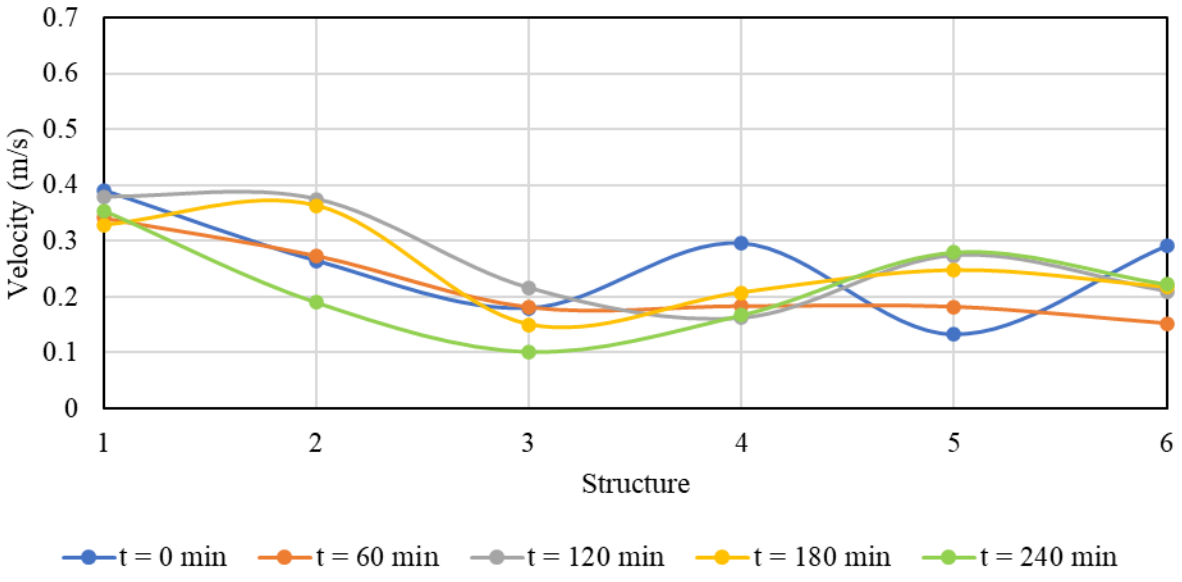

Figure 133. Rock vane tip y-velocity over time for $(\Delta y+H)/H$ = 2.0 in the curved flume from EXPT 16a.

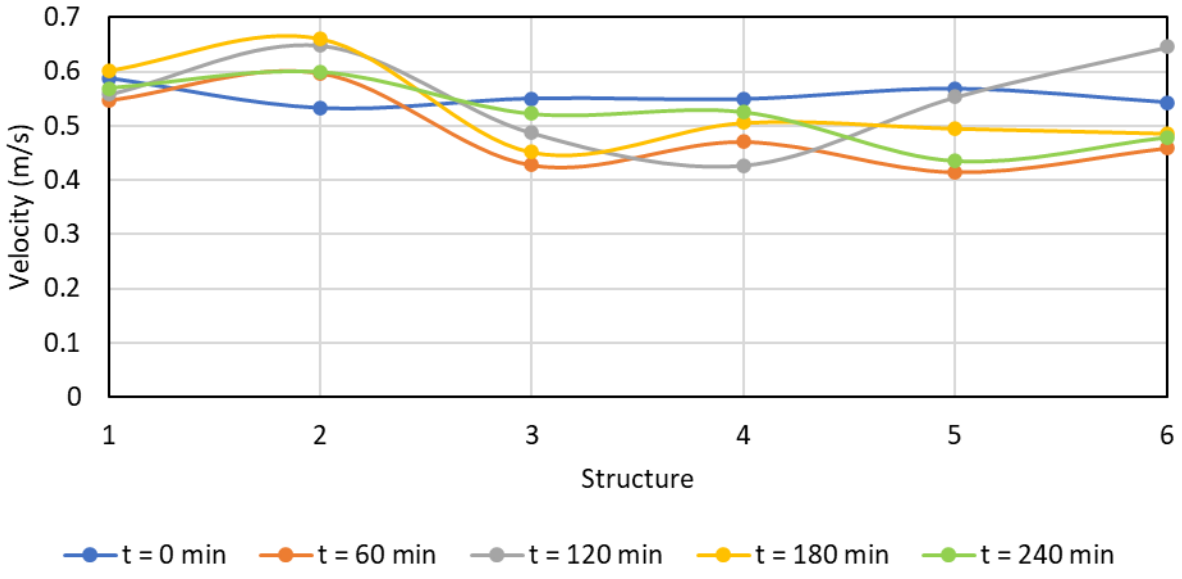

Figure 134. Rock vane tip maximum velocity over time for $(\Delta y+H)/H$ = 2.0 in the curved flume from EXPT 16a.

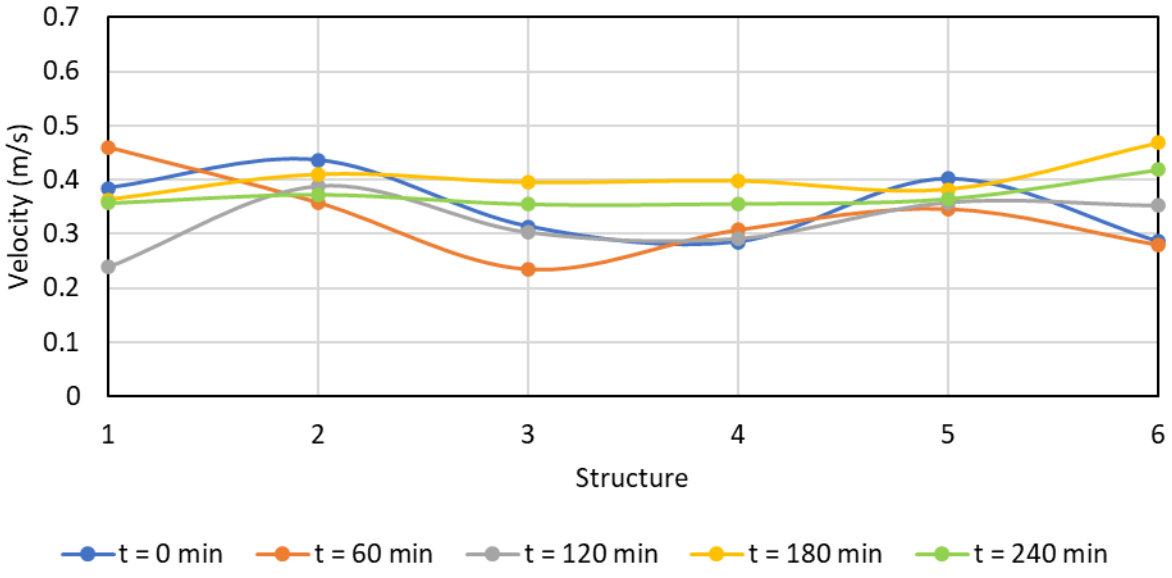

Figure 135. Outer bank x-velocity over time for the initial bed forming flow ($(\Delta y+H)/H$ = 1.25) in the curved flume from EXPT 17a.

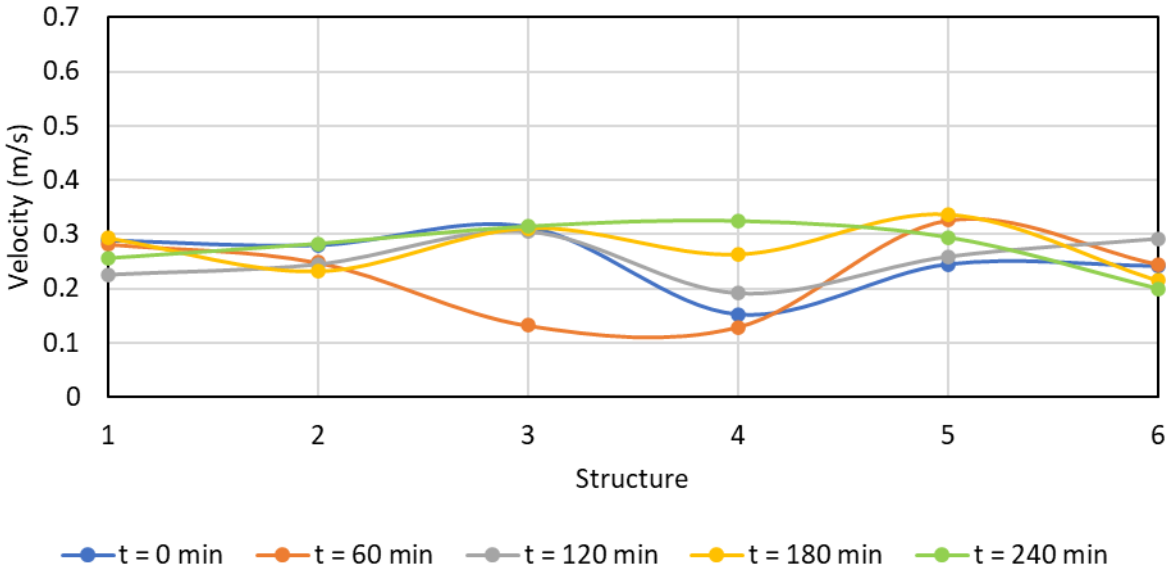

Figure 136. Outer bank y-velocity over time for the initial bed forming flow ($(\Delta y+H)/H$ = 1.25) in the curved flume from EXPT 17a.

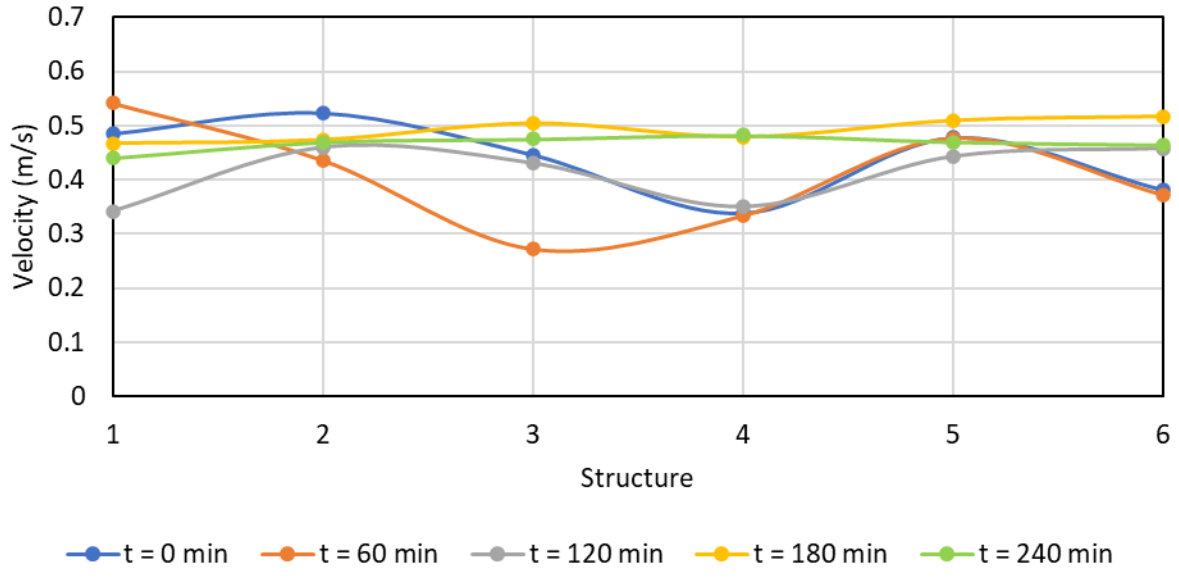

Figure 137. Outer bank maximum velocity over time for the initial bed forming flow ($(\Delta y+H)/H$ = 1.25) in the curved flume from EXPT 17a.

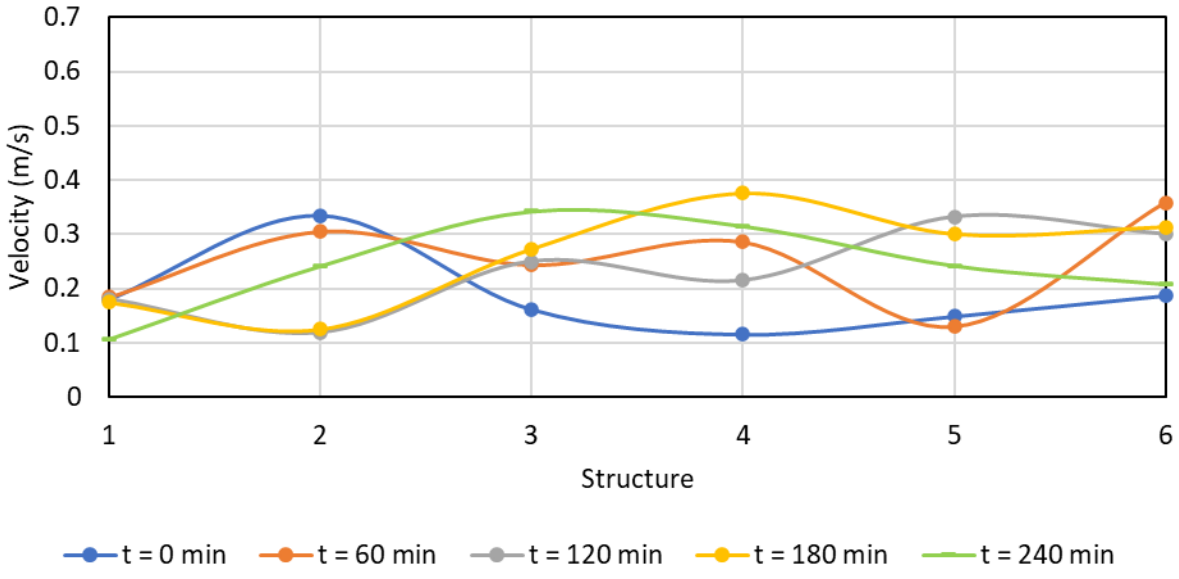

Figure 138. Bendway weir tip x-velocity over time for $(\Delta y+H)/H$ = 0.75 in the curved flume from EXPT 18a.

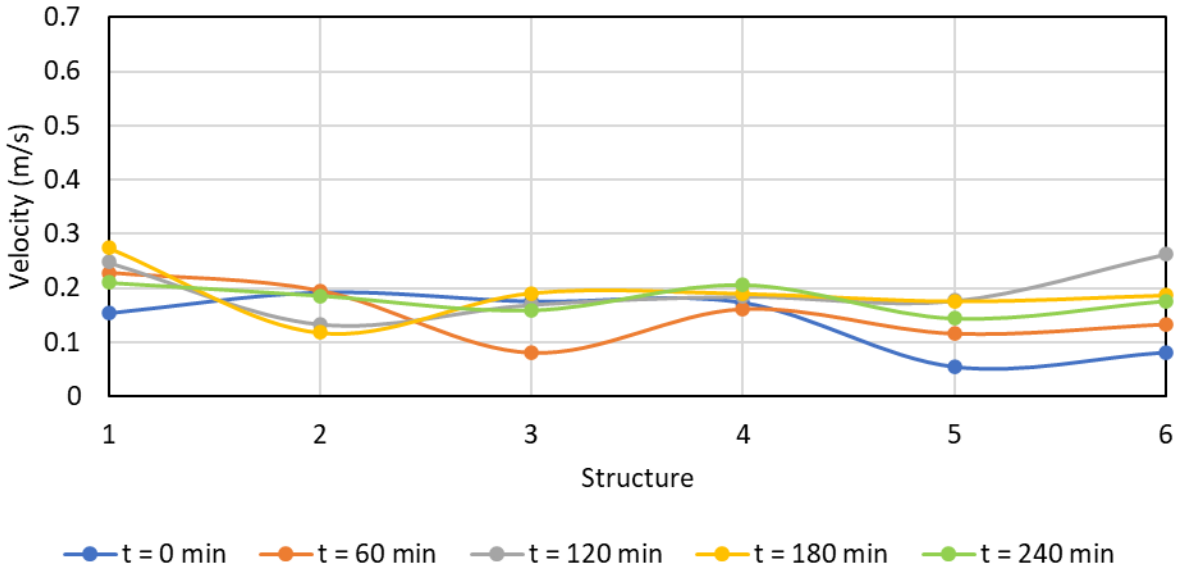

Figure 139. Bendway weir tip y-velocity over time for $(\Delta y+H)/H$ = 0.75 in the curved flume from EXPT 18a.

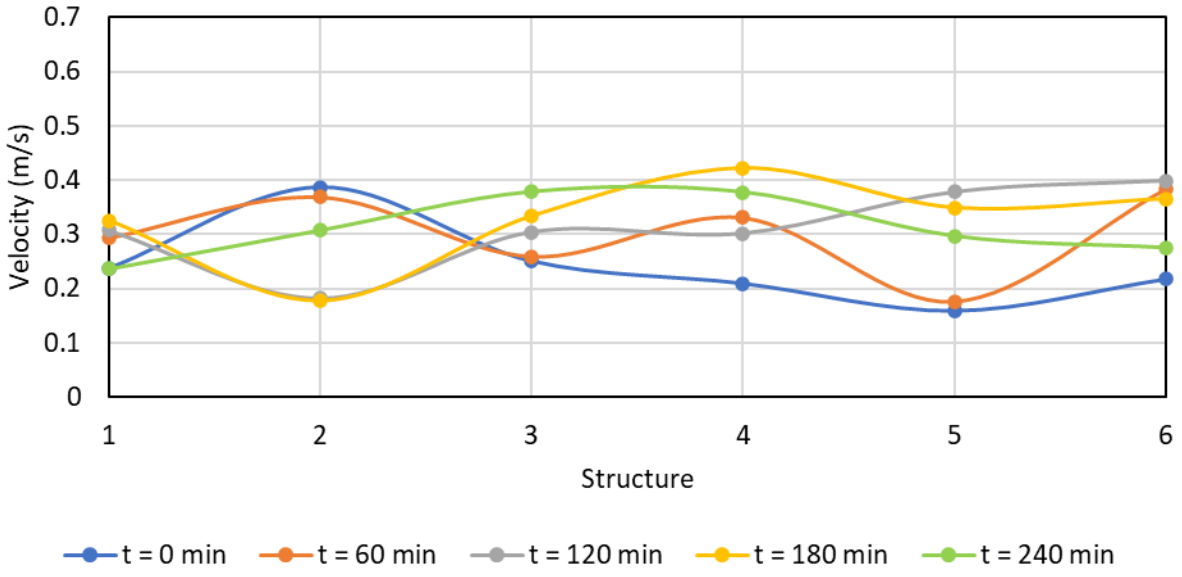

Figure 140. Bendway weir tip maximum velocity over time for $(\Delta y+H)/H$ = 0.75 in the curved flume from EXPT 18a.

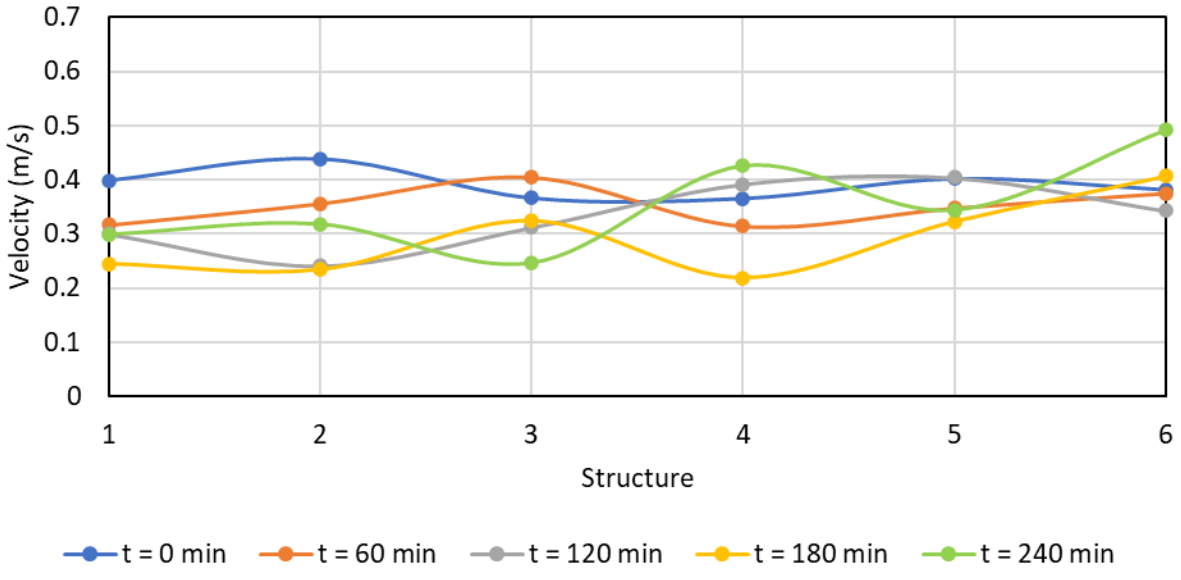

Figure 141. Bendway weir tip x-velocity over time for $(\Delta y+H)/H$ = 1.25 in the curved flume from EXPT 19a.

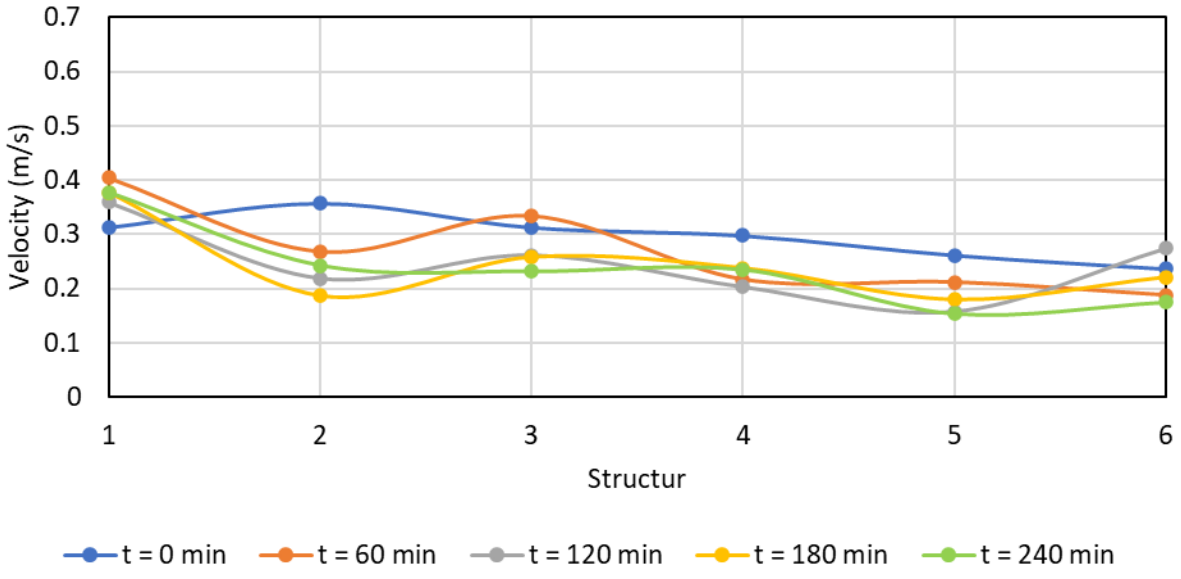

Figure 142. Bendway weir tip y-velocity over time for $(\Delta y+H)/H$ = 1.25 in the curved flume from EXPT 19a.

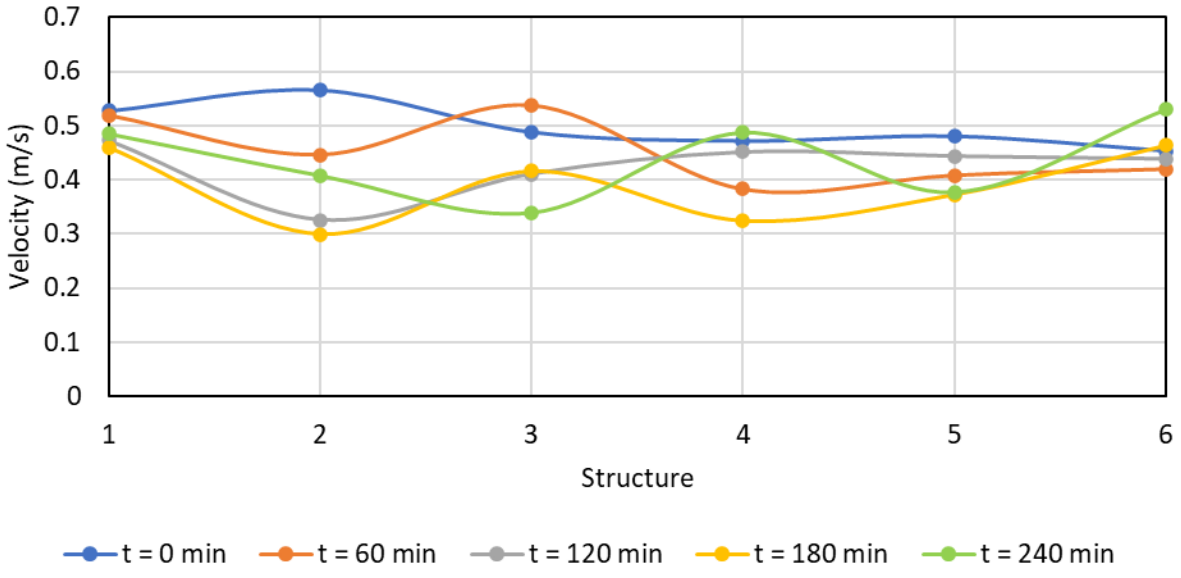

Figure 143. Bendway weir tip maximum velocity over time for $(\Delta y+H)/H$ = 1.25 in the curved flume from EXPT 19a.

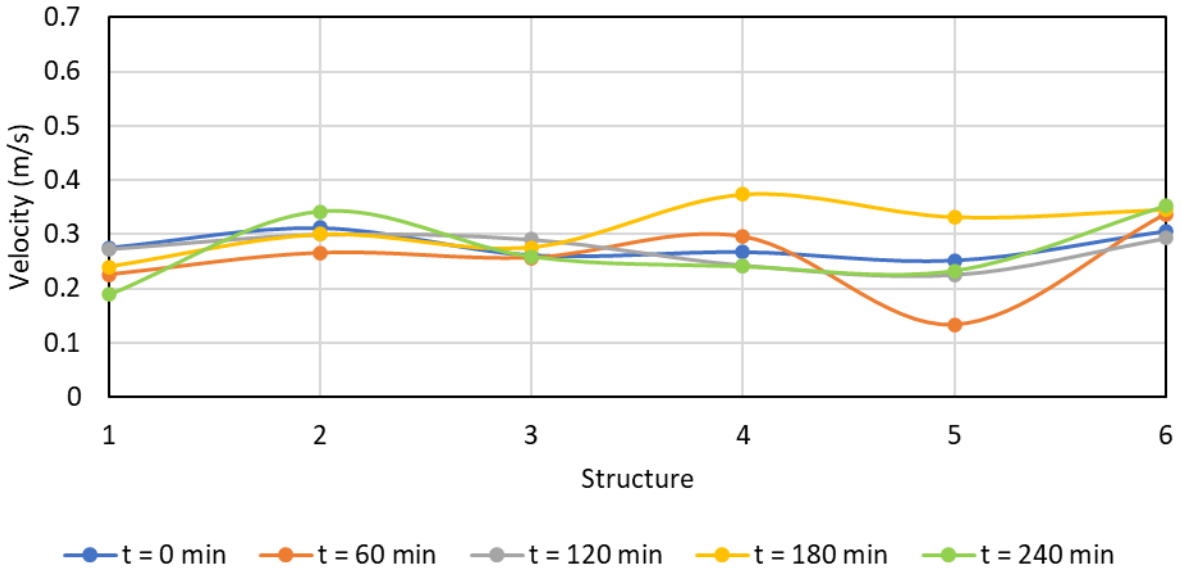

Figure 144. Bendway weir tip x-velocity over time for $(\Delta y+H)/H$ = 2.0 in the curved flume from EXPT 20a.

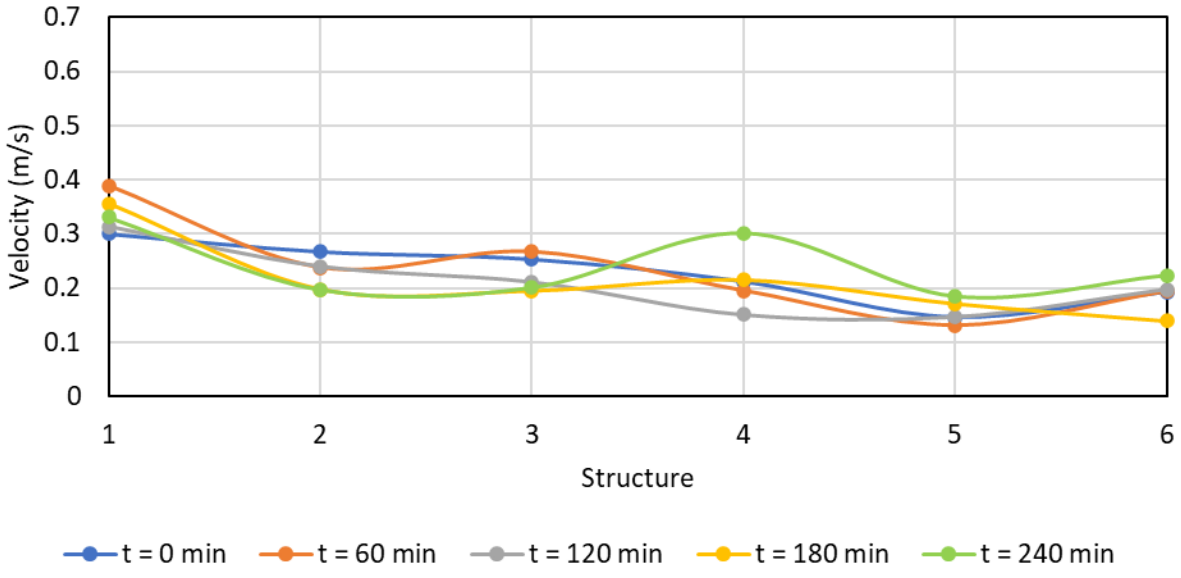

Figure 145. Bendway weir tip y-velocity over time for $(\Delta y+H)/H$ = 2.0 in the curved flume from EXPT 20a.

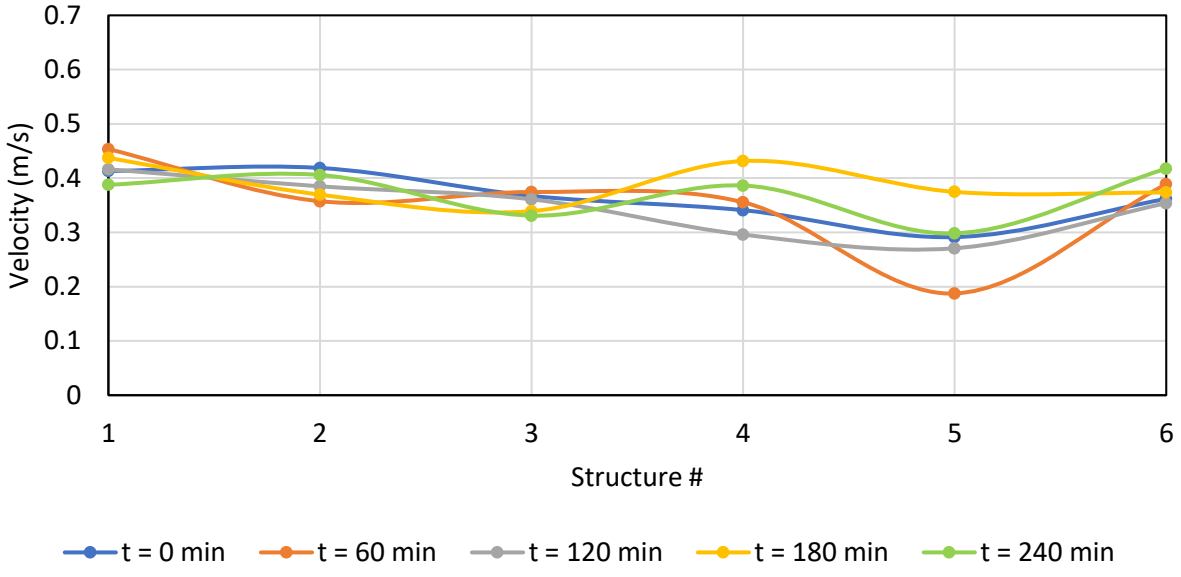

Figure 146. Bendway weir tip maximum velocity over time for $(\Delta y+H)/H$ = 2.0 in the curved flume from EXPT 20a.

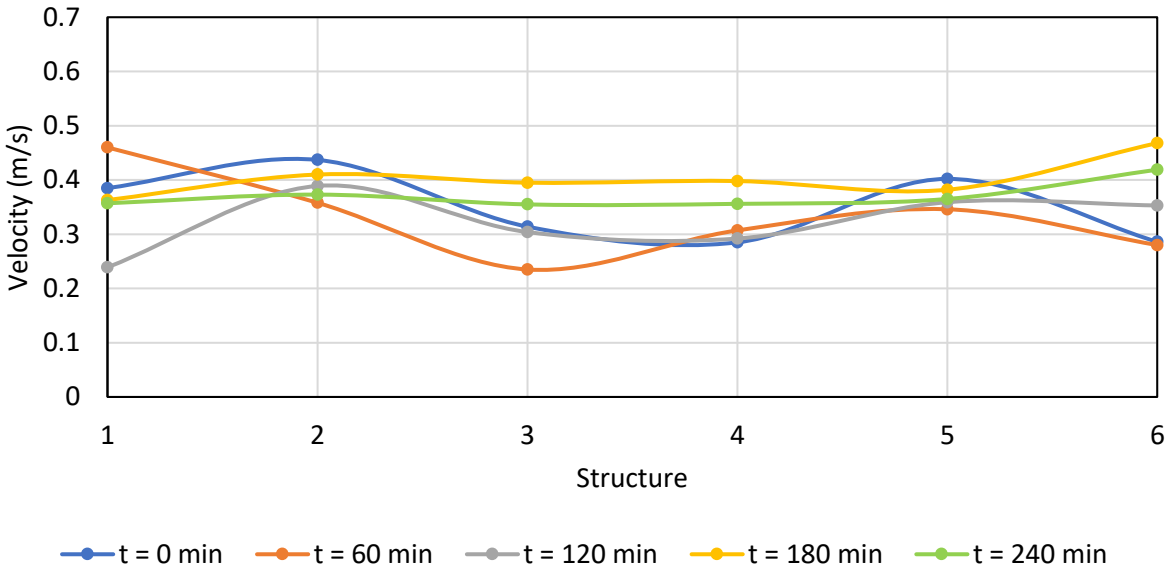

Figure 147. Outer bank x-velocity over time for the initial bed forming flow ($(\Delta y+H)/H$ = 1.25) in the curved flume from EXPT 21a.

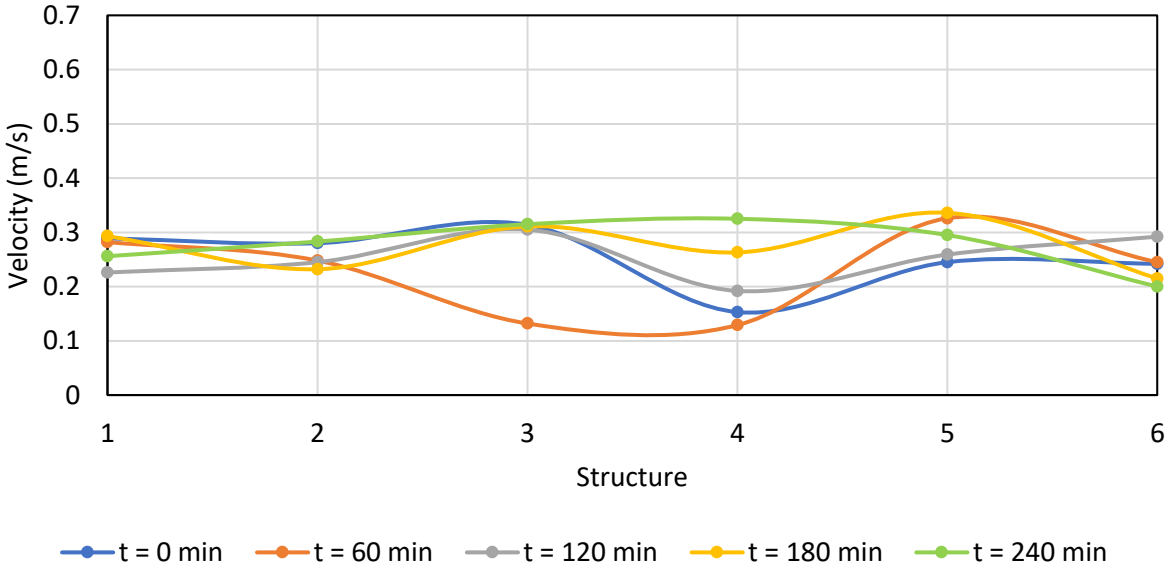

Figure 148. Outer bank y-velocity over time for the initial bed forming flow ($(\Delta y+H)/H$ = 1.25) in the curved flume from EXPT 21a.

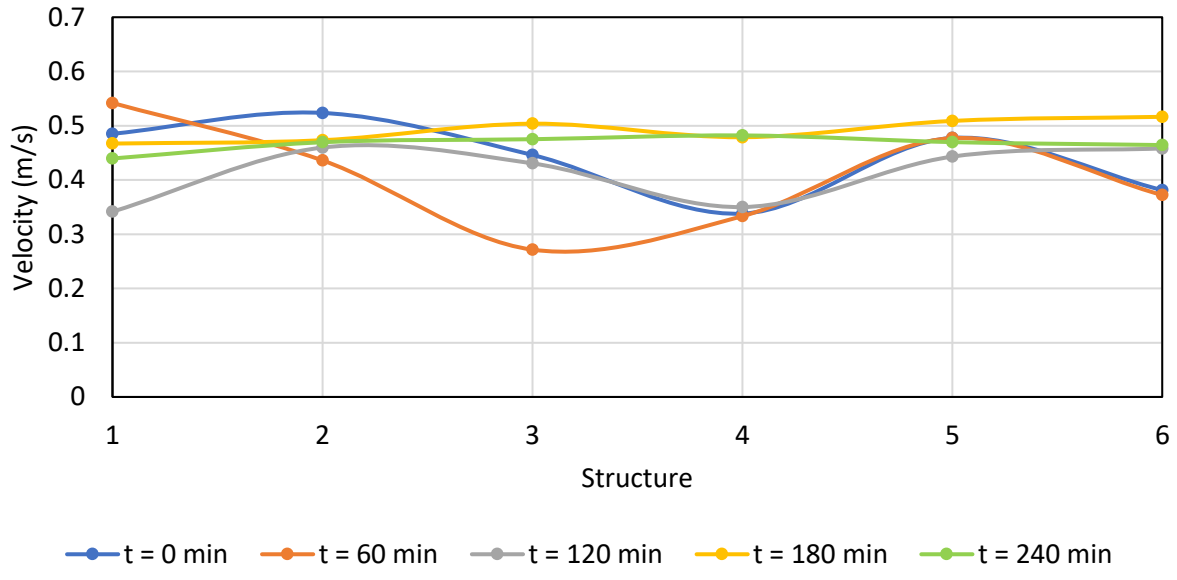

Figure 149. Outer bank maximum velocity over time for the initial bed forming flow ($(\Delta y+H)/H$ = 1.25) in the curved flume from EXPT 21a.

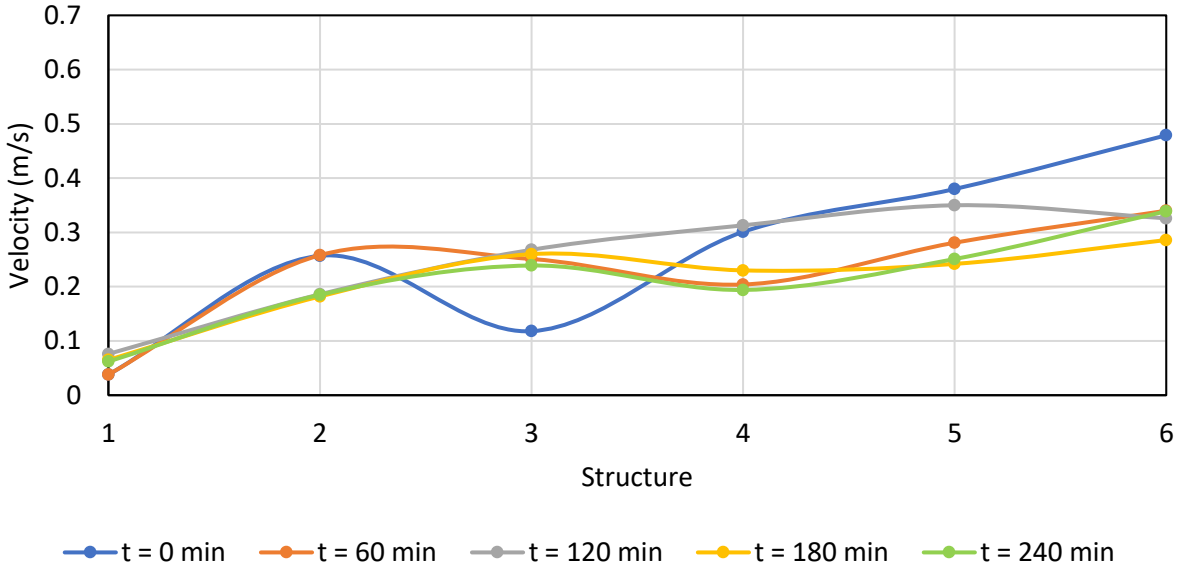

Figure 150. Rock vane tip x-velocity over time for $(\Delta y+H)/H$ = 0.75 in the curved flume from EXPT 22a.

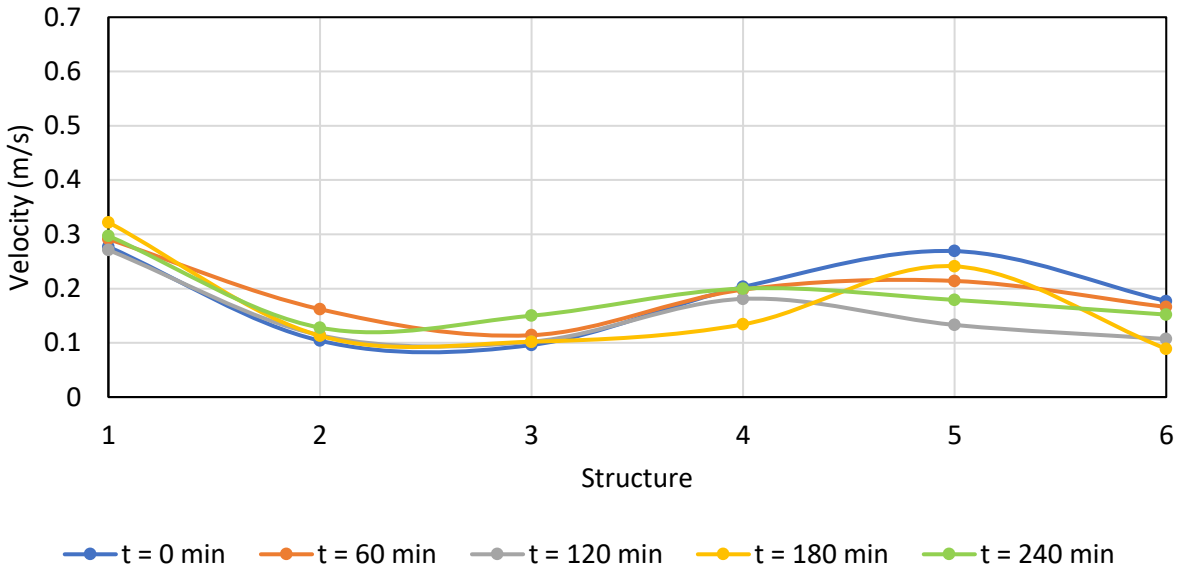

Figure 151. Rock vane tip y-velocity over time for $(\Delta y+H)/H$ = 0.75 in the curved flume from EXPT 22a.

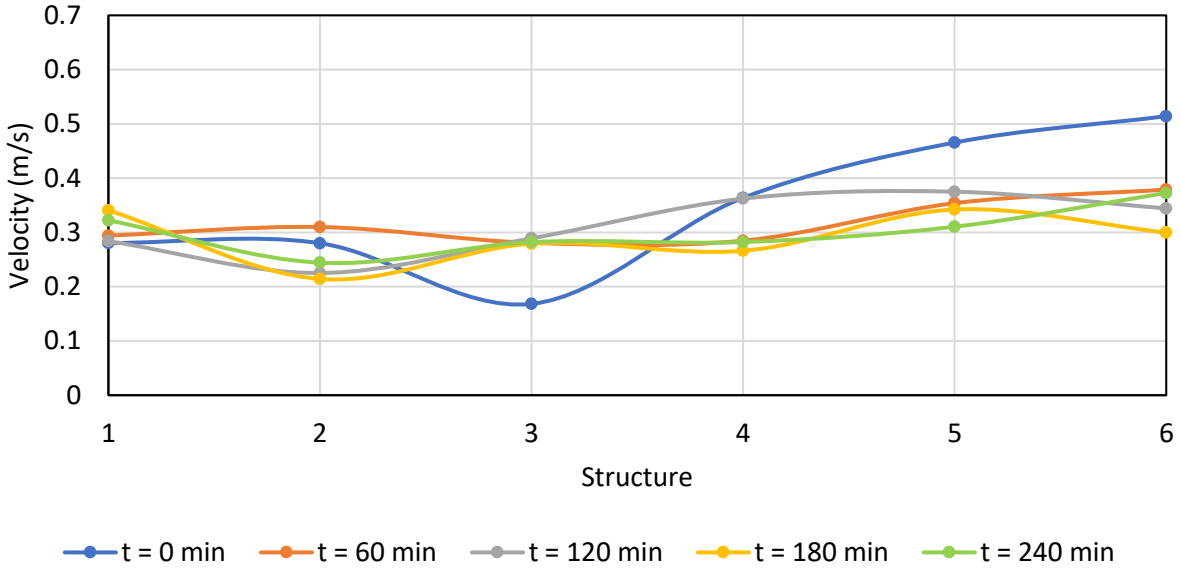

Figure 152. Rock vane tip maximum velocity over time for $(\Delta y+H)/H$ = 0.75 in the curved flume from EXPT 22a.

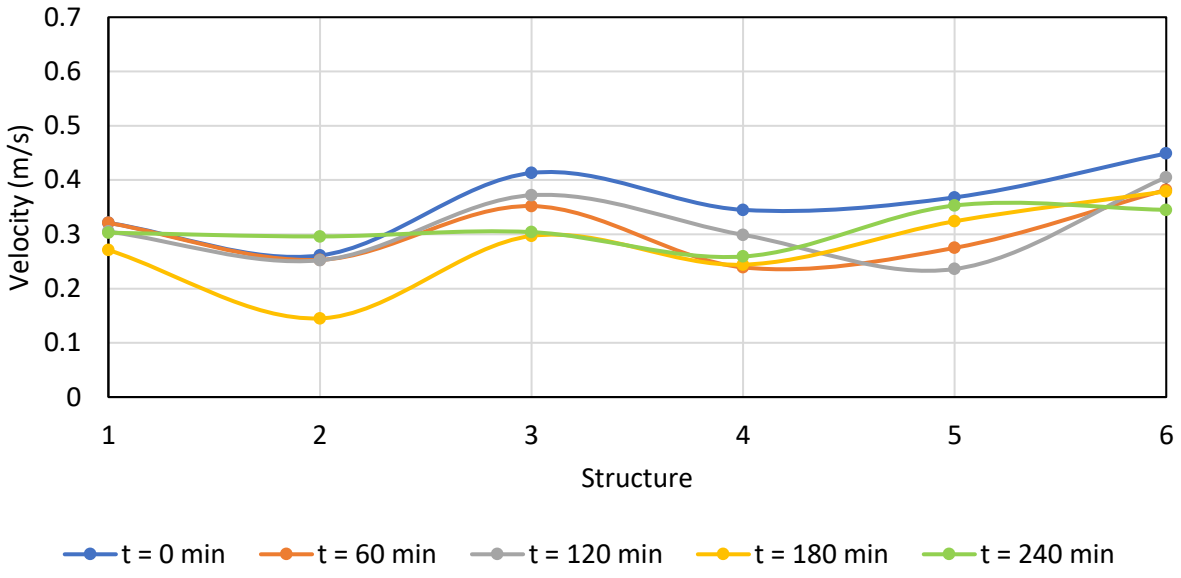

Figure 153. Rock vane tip x-velocity over time for $(\Delta y+H)/H$ = 1.25 in the curved flume from EXPT 23a.

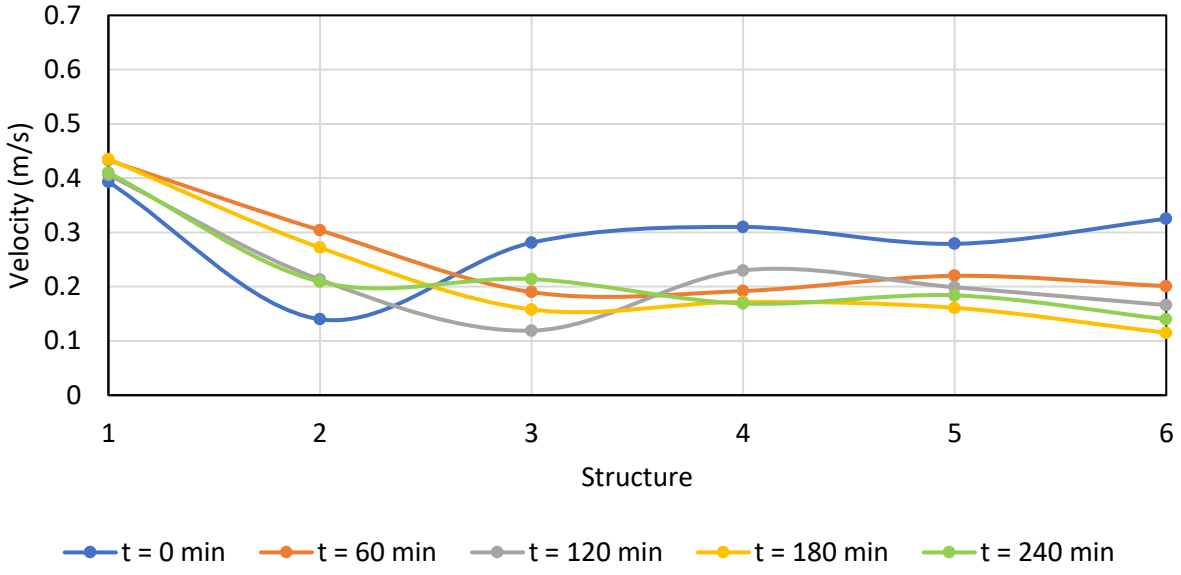

Figure 154. Rock vane tip y-velocity over time for $(\Delta y+H)/H$ = 1.25 in the curved flume from EXPT 23a.

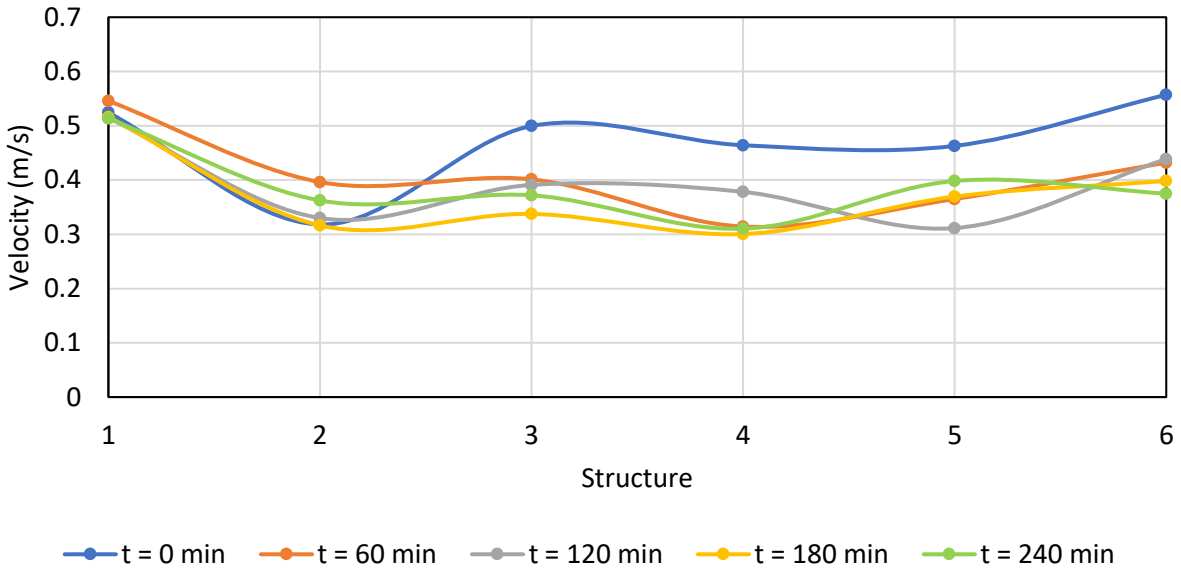

Figure 155. Rock vane tip maximum velocity over time for $(\Delta y+H)/H$ = 1.25 in the curved flume from EXPT 23a.

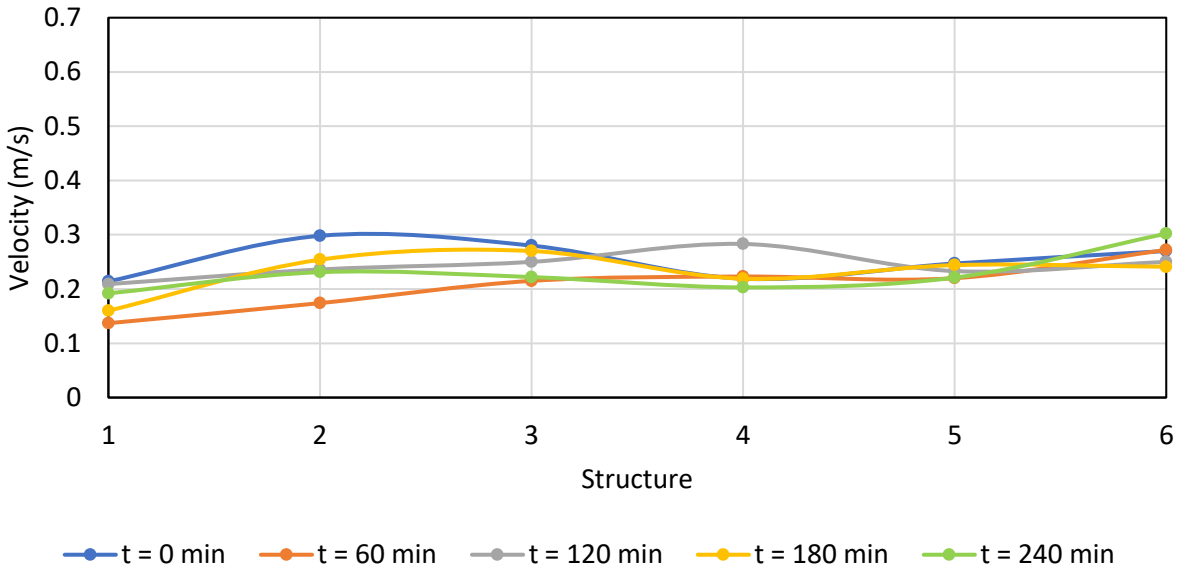

Figure 156. Rock vane tip x-velocity over time for $(\Delta y+H)/H$ = 2.0 in the curved flume from EXPT 24a.

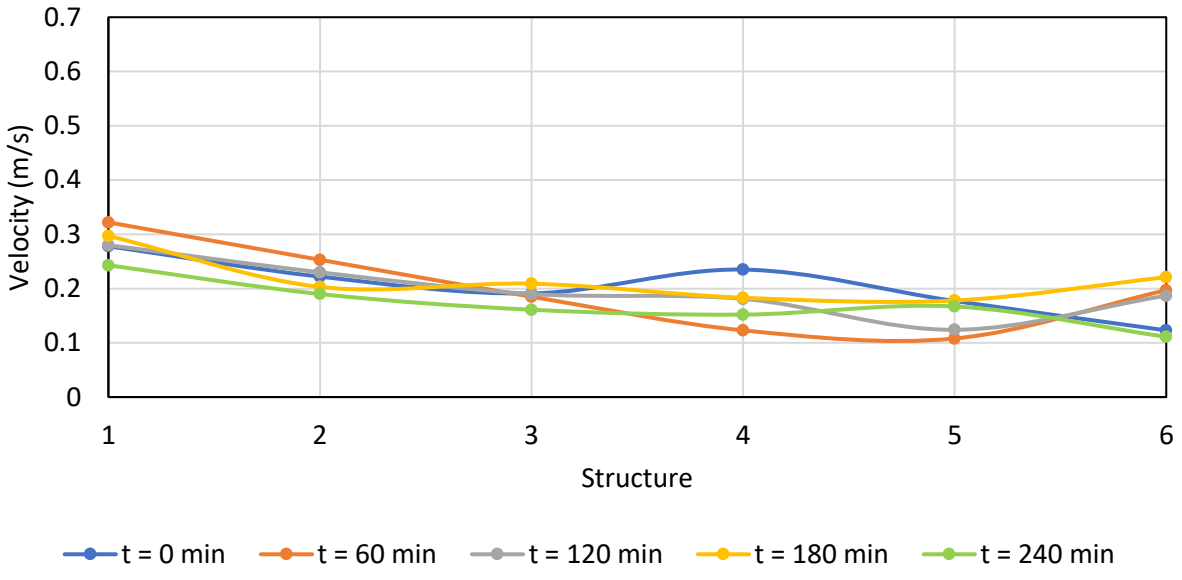

Figure 157. Rock vane tip y-velocity over time for $(\Delta y+H)/H$ = 2.0 in the curved flume from EXPT 24a.

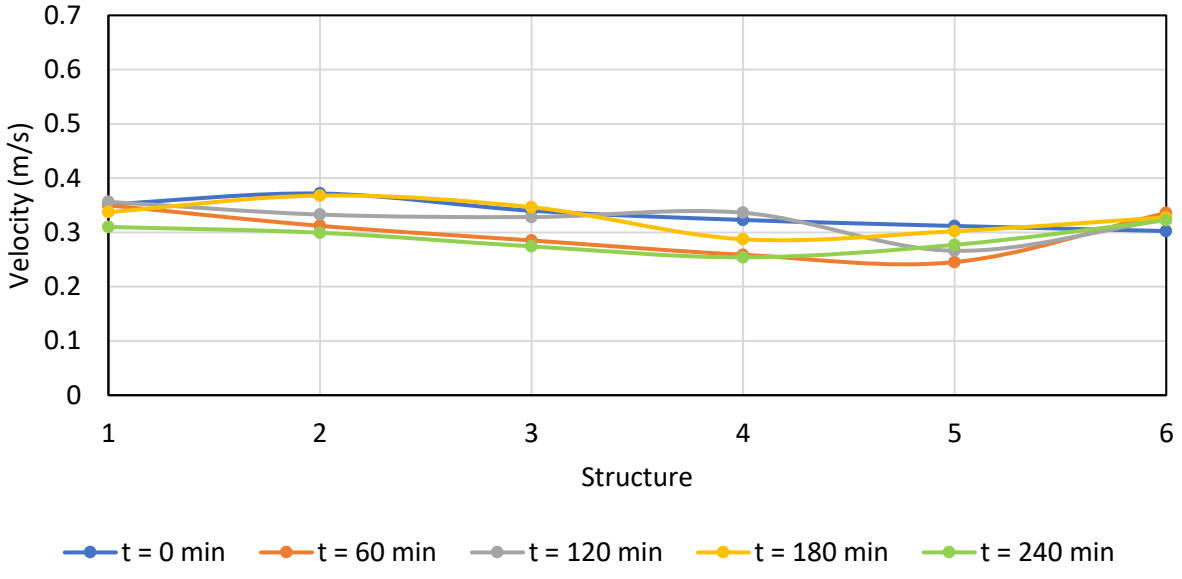

Figure 158. Rock vane tip maximum velocity over time for $(\Delta y+H)/H$ = 2.0 in the curved flume from EXPT 24a.

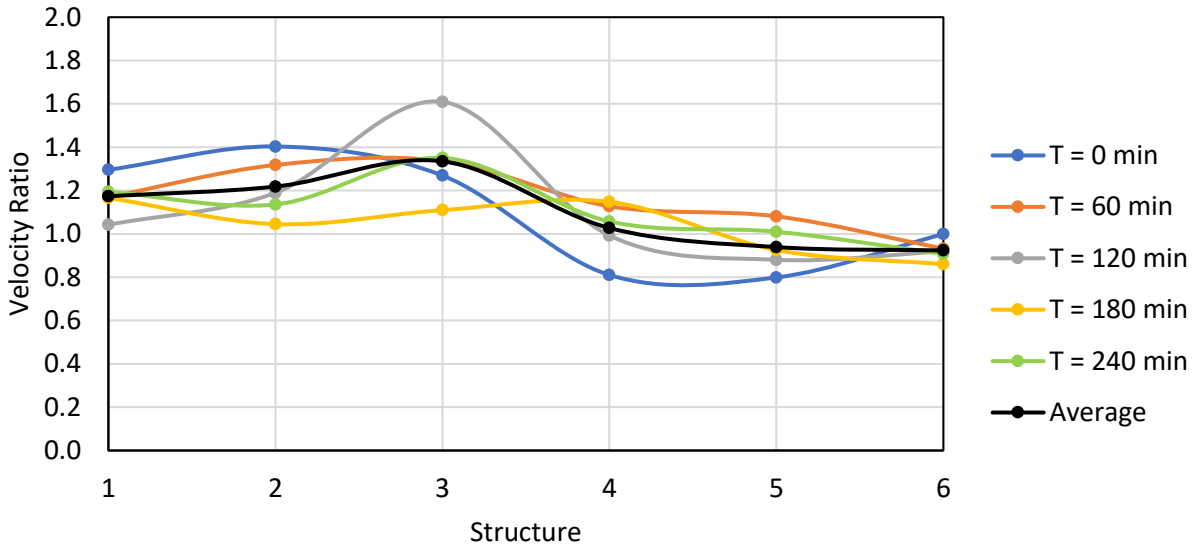

Figure 159. Velocity ratio of bendway weir tip velocity to outer bank velocity (with no structures) for $(\Delta y+H)/H$ = 1.25 in very coarse sand.

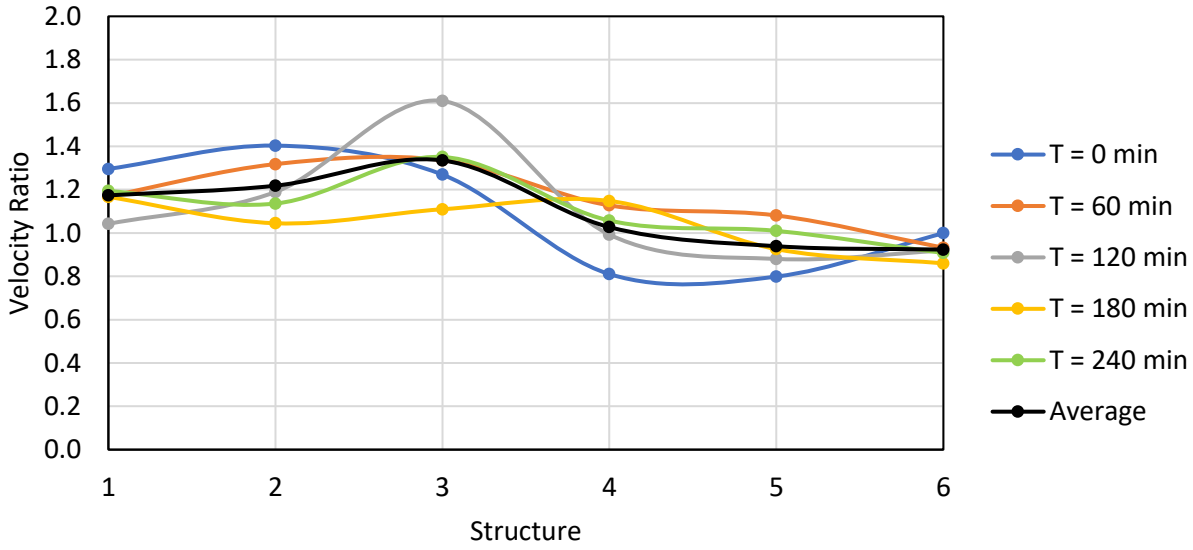

Figure 160. Velocity ratio of rock vane tip velocity to outer bank velocity (with no structures) for $(\Delta y+H)/H$ = 1.25 in very coarse sand.

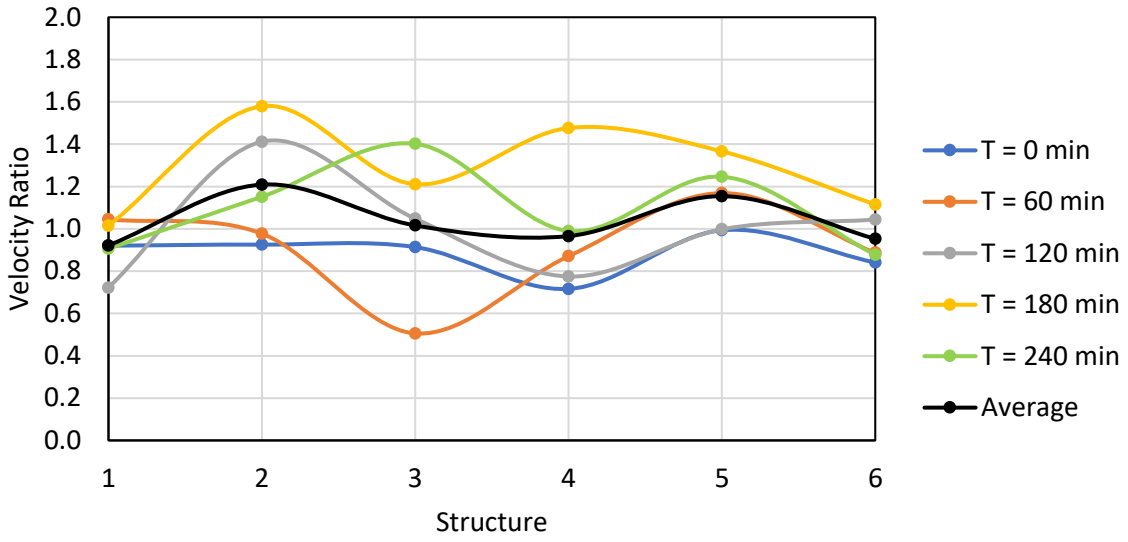

Figure 161. Velocity ratio of bendway weir tip velocity to outer bank velocity (with no structures) for $(\Delta y+H)/H$ = 1.25 in medium sand.

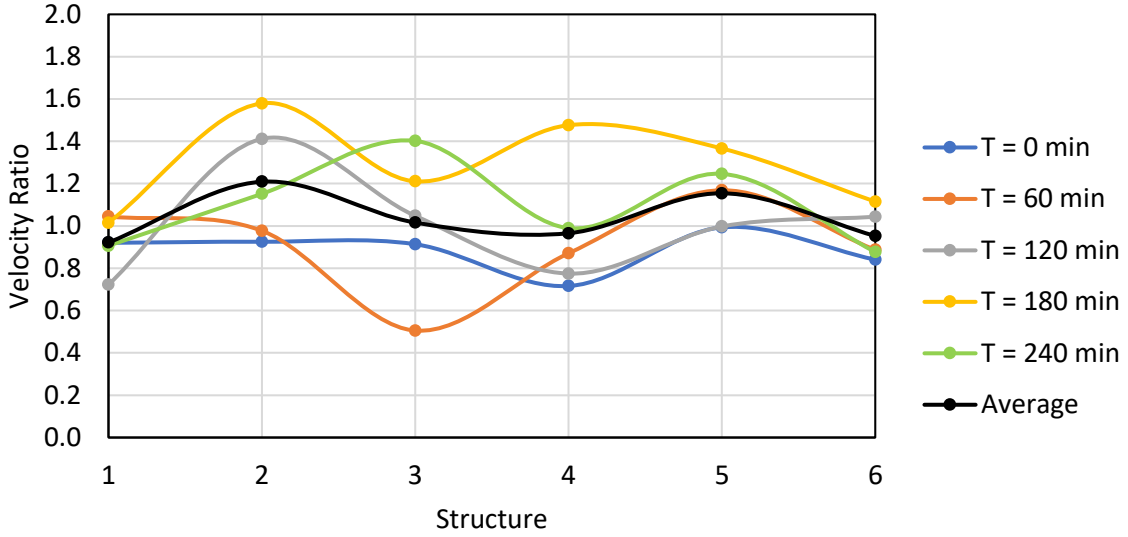

Figure 162. Velocity ratio of bendway weir tip velocity to outer bank velocity (with no structures) for $(\Delta y+H)/H$ = 2.0 in medium sand.

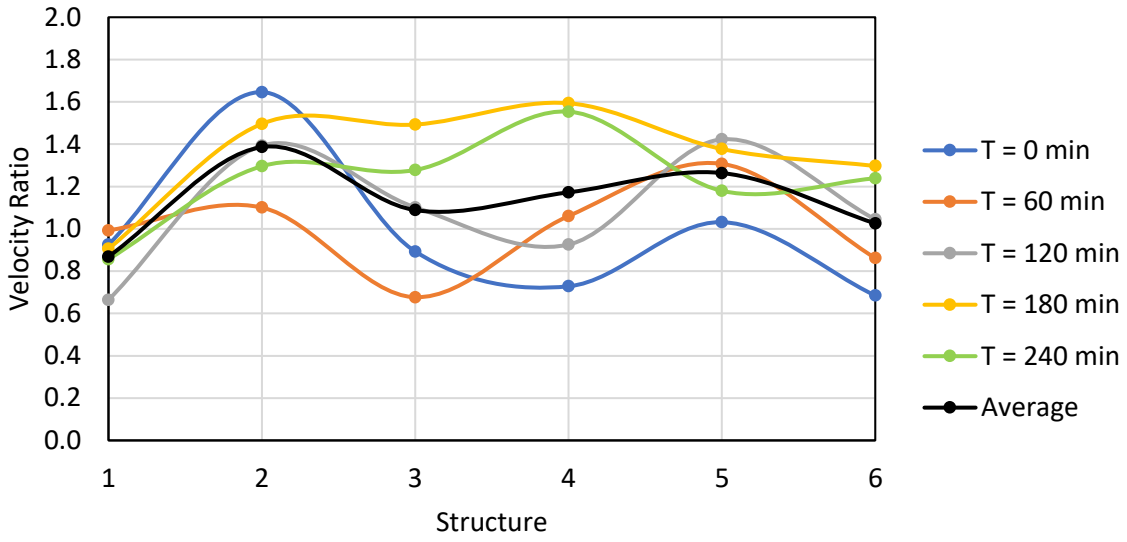

Figure 163. Velocity ratio of rock vane tip velocity to outer bank velocity (with no structures) for $(\Delta y+H)/H$ = 1.25 in medium sand.

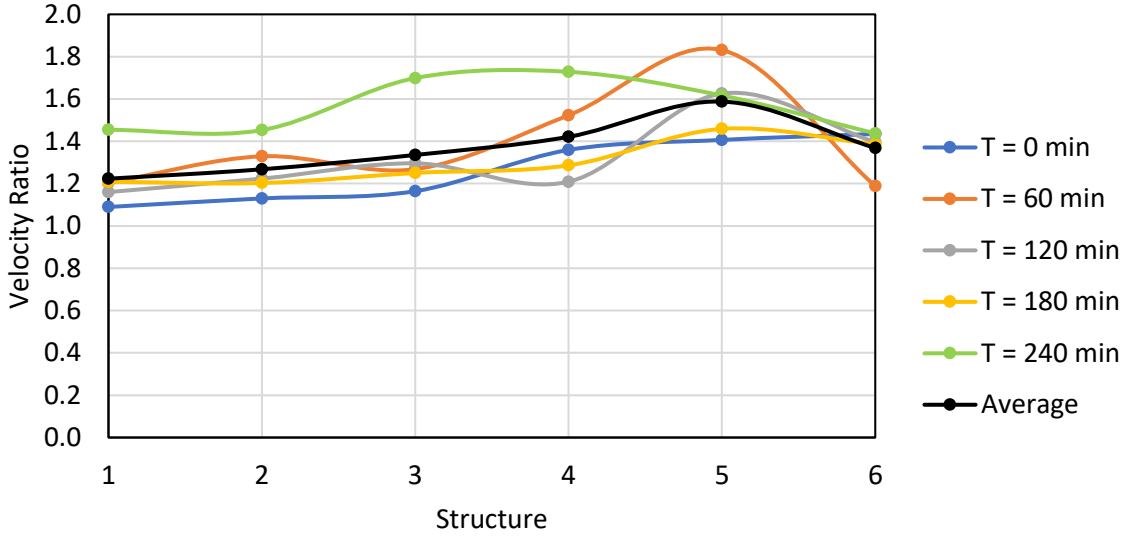

Figure 164. Velocity ratio of rock vane tip velocity to outer bank velocity (with no structures) for $(\Delta y+H)/H$ = 2.0 in medium sand.

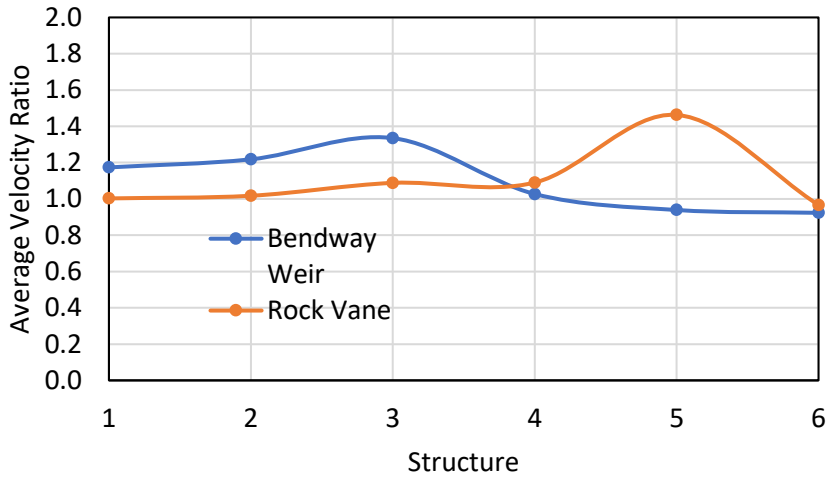

Figure 165. Comparison of average velocity ratio of rock vane/bendway weir tip velocity to outer bank velocity (with no structures) for $(\Delta y+H)/H$ = 1.25 in very coarse sand.

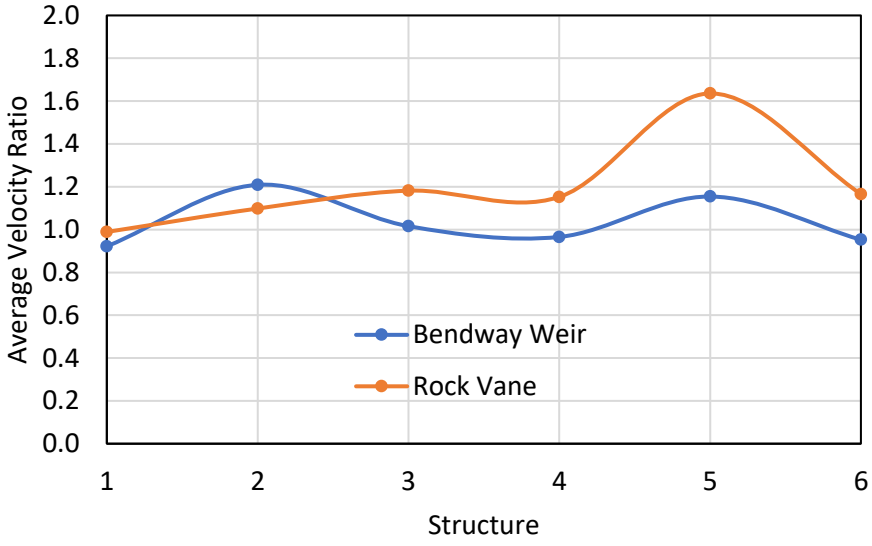

Figure 166. Comparison of average velocity ratio of rock vane/bendway weir tip velocity to outer bank velocity (with no structures) for $(\Delta y+H)/H$ = 1.25 in medium sand.

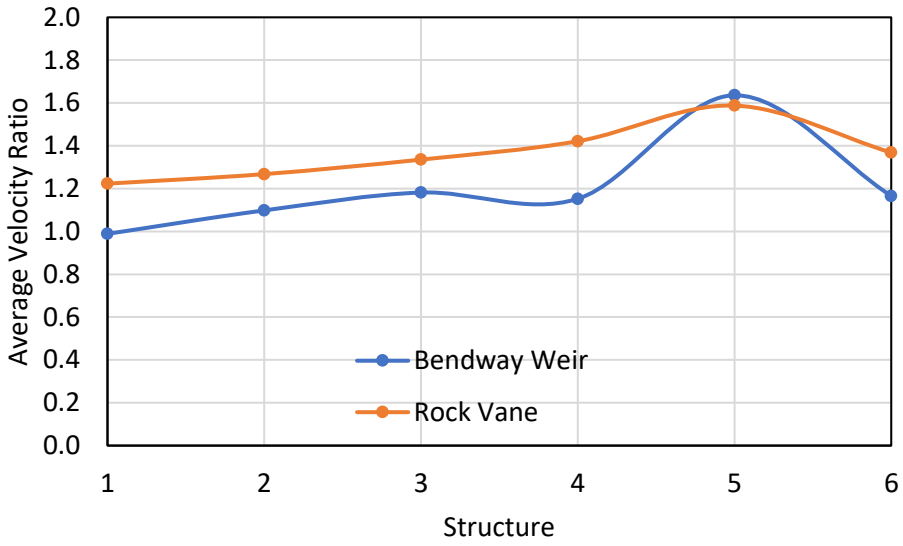

Figure 167. Comparison of average velocity ratio of rock vane/bendway weir tip velocity to outer bank velocity (with no structures) for $(\Delta y+H)/H$ = 2.0 in medium sand.

APPENDIX D. STRUCTURE MEASUREMENTS

Table 8d. Bendway weir dimension changes after running the hydrograph procedure in the curved flume with coarse sand.

$(\Delta y+H)/H$	Flow (m^3/s)	Structure	Orientation (°)	Crest L (cm)	H (cm)	Top Width (cm)	Scour Depth (cm)	Max Scour Depth (cm)
As built	0.07	1	60	52.1	7.62	7.62	0	NA
		2	60	52.1	7.62	7.62	0	
		3	60	52.1	7.62	7.62	0	
		4	60	52.1	7.62	7.62	0	
		5	60	52.1	7.62	7.62	0	
		6	60	52.1	7.62	7.62	0	
0.75	0.03	1	60	50.8	7.62	7.62	8.26	15.9
		2	60	50.8	7.62	7.62	12.7	
		3	60	52.1	7.62	7.62	6.35	
		4	60	47.0	7.62	7.62	3.81	
		5	60	50.8	7.62	7.62	3.18	
		6	60	48.3	5.08	15.2	3.18	
1.25	0.07	1	60	38.1	7.62	7.62	7.62	10.2
		2	60	47.0	7.62	7.62	8.26	
		3	60	47.0	7.62	7.62	7.62	
		4	60	40.6	7.62	7.62	6.99	
		5	60	47.0	7.62	7.62	5.72	
		6	60	47.0	2.54	15.2	0.64	
2.0	0.08	1	60	27.9	7.62	7.62	6.35	10.2
		2	60	33.0	7.62	7.62	5.72	
		3	60	30.5	7.62	7.62	5.72	
		4	60	25.4	7.62	7.62	5.72	
		5	60	40.6	7.62	8.89	5.72	
		6	60	40.6	2.54	15.2	5.08	

Table 9d. Rock vane geometry change after the hydrograph procedure in a curved flume with coarse sand.

$(\Delta y+H)/H$	**Flow** (m^3/s)	**Structure**	**α** (°)	**Crest L** (cm)	**H** (cm)	**Top Width** (cm)	**Scour Depth** (cm)	**Slope** (°)	**Max Scour Depth** (cm)
As built	0.07	1	60	52.1	7.62	7.62	0	15	NA
		2	60	52.1	7.62	7.62	0	15	
		3	60	52.1	7.62	7.62	0	15	
		4	60	52.1	7.62	7.62	0	15	
		5	60	52.1	7.62	7.62	0	15	
		6	60	52.1	7.62	7.62	0	15	
0.75	0.03	1	60	47.0	7.62	7.62	8.89	15	12.7
		2	60	47.0	7.62	7.62	9.53	15	
		3	60	47.0	7.62	7.62	6.35	15	
		4	60	47.0	7.62	7.62	5.08	15	
		5	60	48.3	7.62	7.62	2.54	15	
		6	60	43.2	5.08	15.2	1.27	12	
1.25	0.07	1	60	47.0	7.62	7.62	7.62	15	10.2
		2	60	47.0	7.62	7.62	8.89	15	
		3	60	45.7	7.62	7.62	8.26	15	
		4	60	40.6	7.62	7.62	6.99	15	
		5	60	45.7	7.62	7.62	6.99	15	
		6	60	43.2	5.08	15.2	4.45	12	
2.0	0.08	1	60	47.0	7.62	7.62	5.08	15	8.26
		2	60	45.7	7.62	7.62	5.72	15	
		3	60	35.6	7.62	7.62	5.72	15	
		4	60	33.0	3.81	12.7	5.72	20	
		5	60	40.6	7.62	8.89	5.72	15	
		6	60	43.2	7.62	15.2	5.08	12	

Table 10d. Bendway weir dimension changes after running the hydrograph procedure in the curved flume with medium sand.

$(\Delta y+H)/H$	Flow (m^3/s)	Structure	Orientation (°)	Crest L (cm)	H (cm)	Top Width (cm)	Scour Depth (cm)	Max Scour Depth (cm)
As built	0.07	1	60	52.1	7.62	7.62	0	NA
		2	60	52.1	7.62	7.62	0	
		3	60	52.1	7.62	7.62	0	
		4	60	52.1	7.62	7.62	0	
		5	60	52.1	7.62	7.62	0	
		6	60	52.1	7.62	7.62	0	
0.75	0.03	1	60	47.0	7.62	7.62	6.35	8.89
		2	60	50.8	7.62	7.62	7.62	
		3	60	45.7	7.62	7.62	5.72	
		4	60	43.2	7.62	7.62	1.27	
		5	60	45.7	7.62	7.62	5.08	
		6	60	52.1	7.62	12.7	3.81	
1.25	0.07	1	60	40.6	7.62	8.89	7.62	7.62
		2	60	45.7	7.62	7.62	7.62	
		3	60	40.6	7.62	7.62	7.62	
		4	60	38.1	7.62	7.62	6.99	
		5	60	43.2	7.62	7.62	6.35	
		6	60	47.0	7.62	12.7	5.72	
2.0	0.08	1	60	40.6	7.62	8.89	5.72	6.35
		2	60	44.5	7.62	7.62	5.72	
		3	60	39.4	7.62	7.62	5.72	
		4	60	35.6	7.62	7.62	5.72	
		5	60	40.6	7.62	7.62	5.72	
		6	60	47.0	7.62	12.7	4.45	

Table 11d. Rock vane dimension changes after running the hydrograph procedure in the curved flume with medium sand.

(Δy+H)/H	**Flow** (m^3/s)	**Structure**	**α** (°)	**Crest L** (cm)	**H** (cm)	**Top Width** (cm)	**Scour Depth** (cm)	**Slope** (°)	**Max Scour Depth** (cm)
As built	0.07	1	60	52.1	7.62	7.62	0	15	NA
		2	60	52.1	7.62	7.62	0	15	
		3	60	52.1	7.62	7.62	0	15	
		4	60	52.1	7.62	7.62	0	15	
		5	60	52.1	7.62	7.62	0	15	
		6	60	52.1	7.62	7.62	0	15	
0.75	0.03	1	60	50.8	7.62	7.62	9.53	15	10.2
		2	60	50.8	7.62	7.62	5.08	15	
		3	60	49.5	7.62	7.62	3.18	15	
		4	60	45.7	7.62	7.62	1.91	15	
		5	60	45.7	7.62	7.62	2.54	15	
		6	60	50.8	7.62	11.4	2.54	15	
1.25	0.07	1	60	47.0	7.62	10.2	6.35	15	8.89
		2	60	47.0	7.62	7.62	8.89	15	
		3	60	47.0	7.62	7.62	7.62	15	
		4	60	43.2	7.62	7.62	6.35	15	
		5	60	43.2	7.62	7.62	6.99	15	
		6	60	50.8	5.08	12.7	3.18	14	
2.0	0.08	1	60	43.2	7.62	10.2	7.62	15	3.25
		2	60	47.0	7.62	7.62	7.62	15	
		3	60	47.0	7.62	7.62	7.62	15	
		4	60	43.2	7.62	8.89	7.62	14	
		5	60	43.2	7.62	7.62	6.99	14	
		6	60	50.8	5.08	21.7	6.35	14	

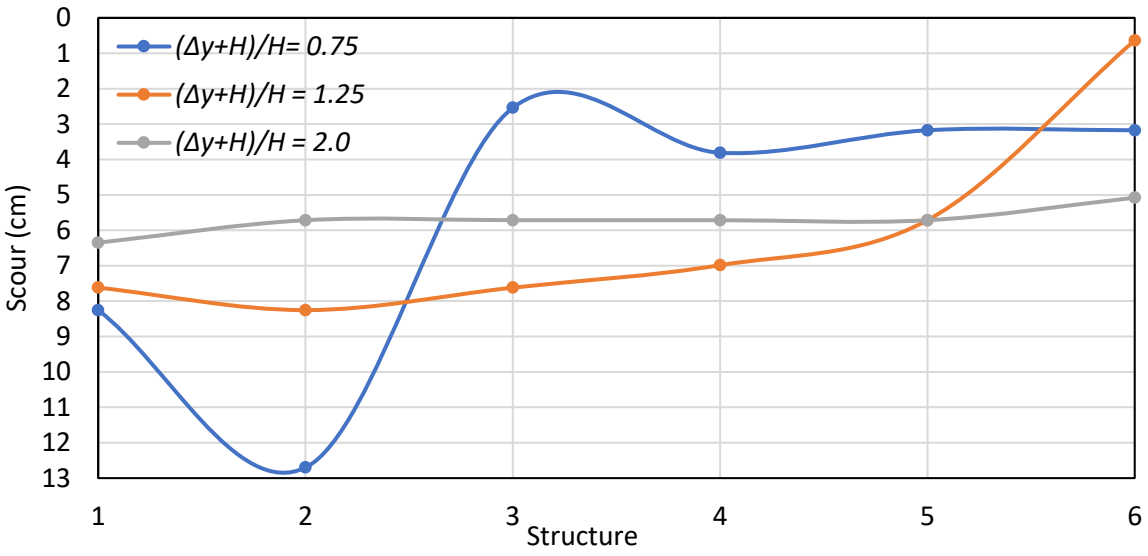

Figure 168. Bendway weir tip scour over varying flow depths in a curved flume with very coarse sand.

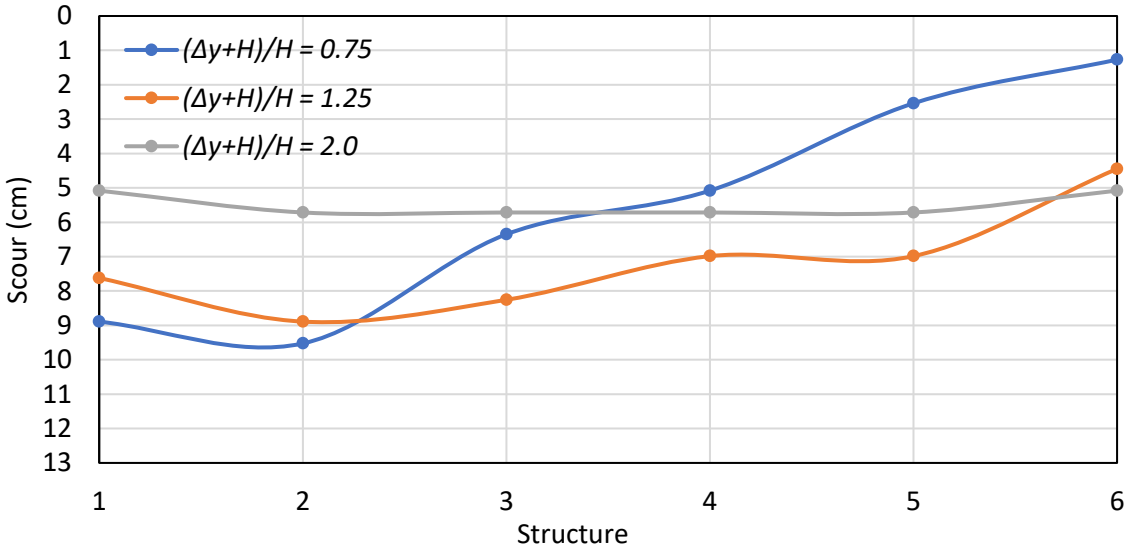

Figure 169. Rock vane tip scour over varying flow depths in a curved flume with very coarse sand.

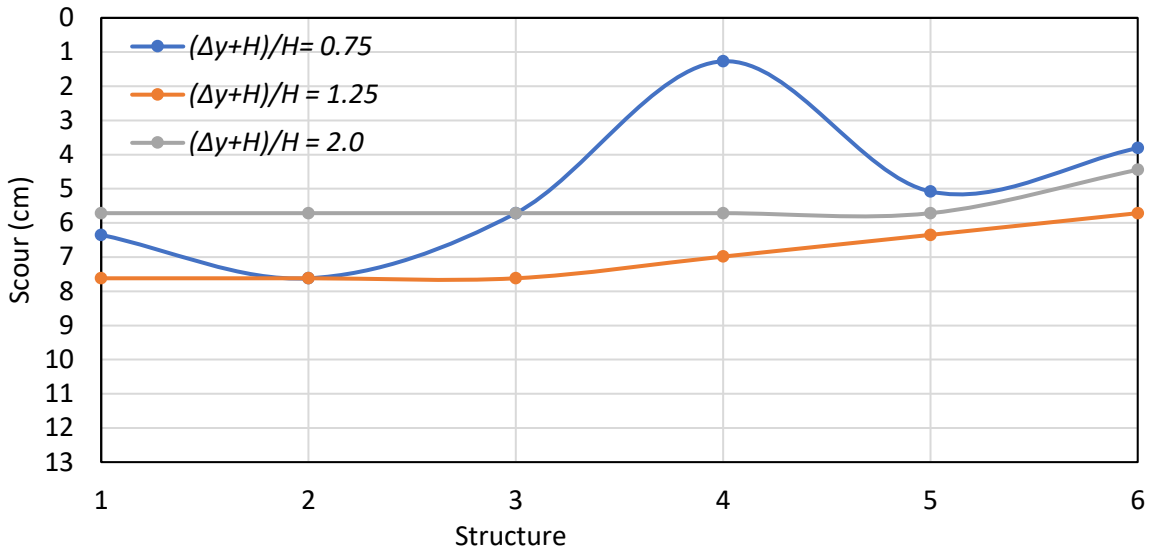

Figure 170. Bendway weir tip scour over varying flow depths in a curved flume with medium sand.

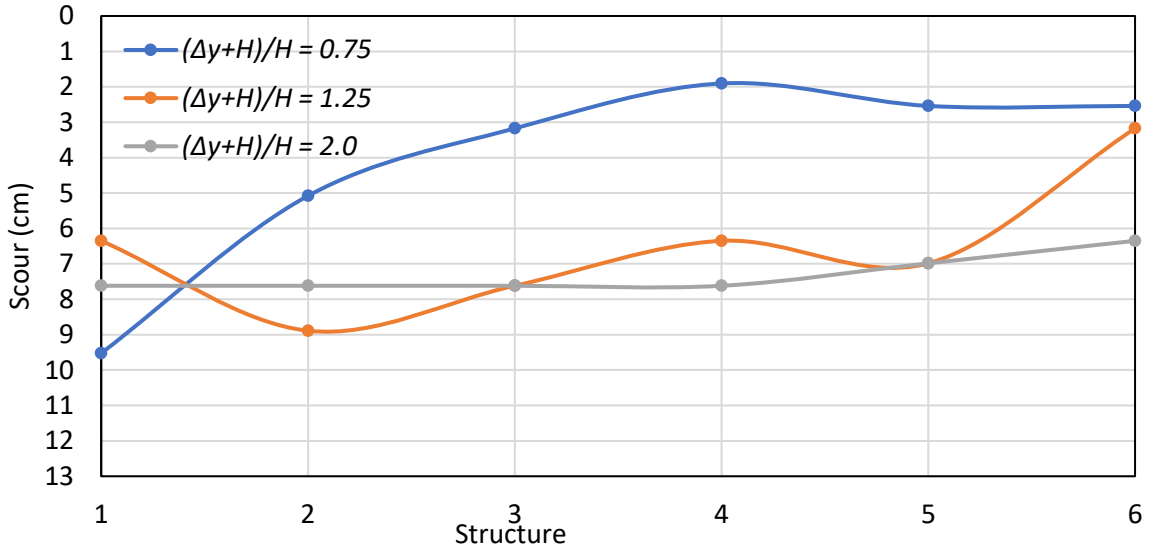

Figure 171. Rock vane tip scour over varying flow depths in a curved flume with medium sand.

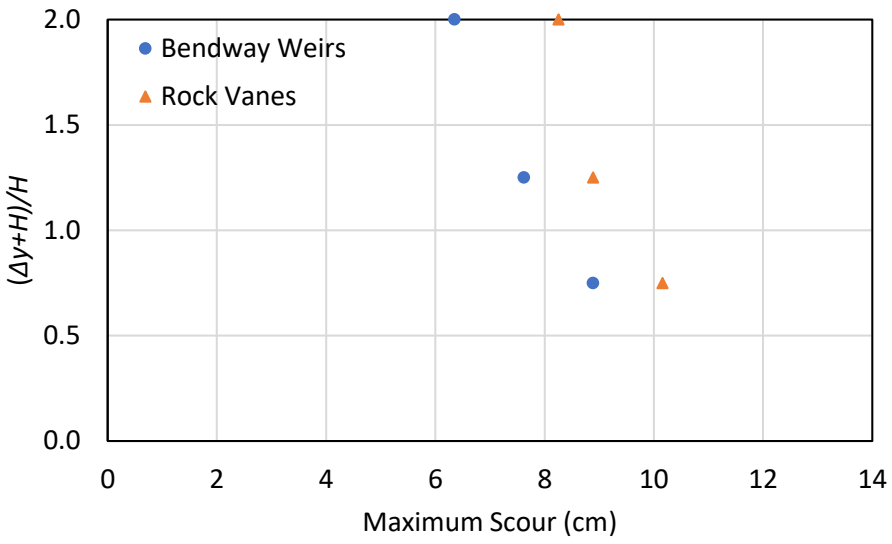

Figure 172. Maximum scour versus flow depth in medium sand.

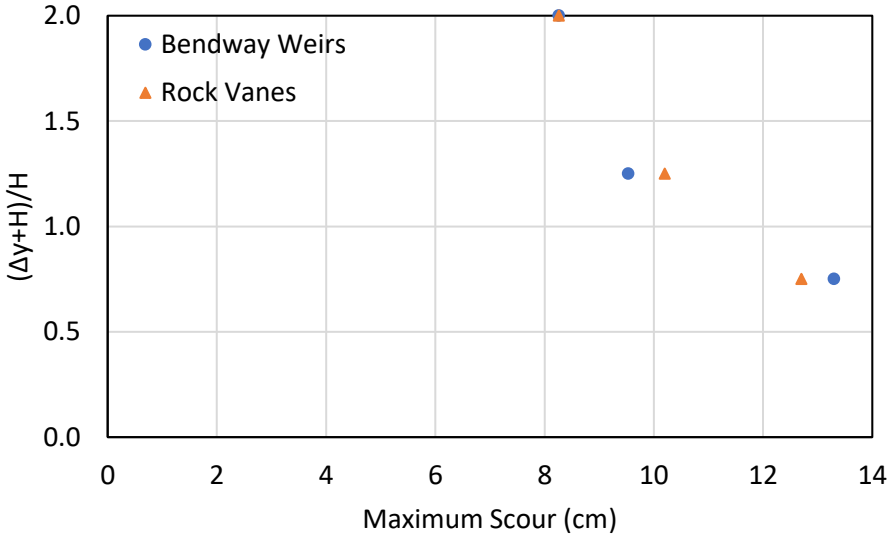

Figure 173. Maximum scour versus flow depth in very coarse sand.

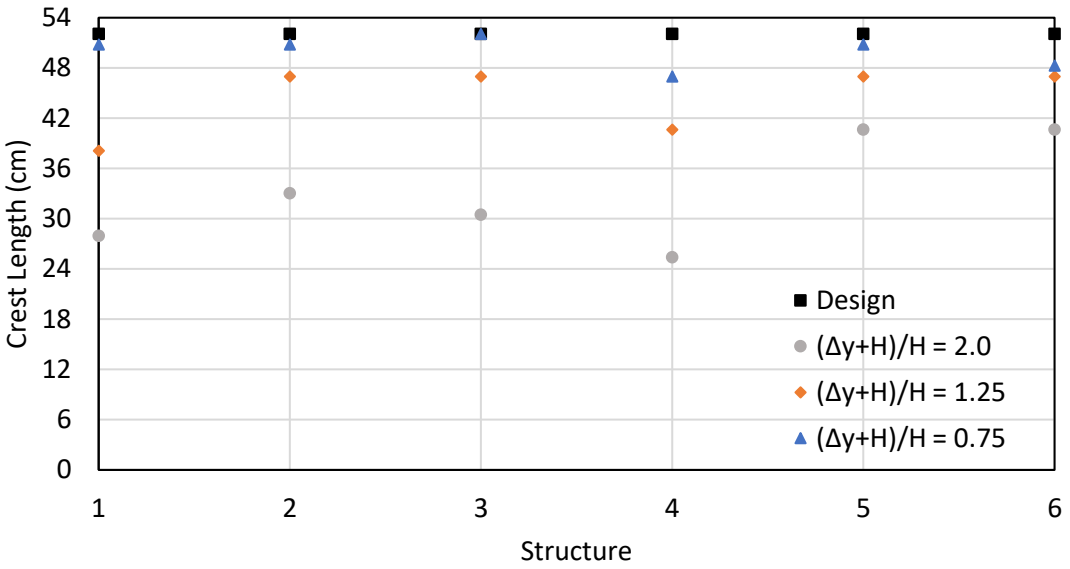

Figure 174. Bendway weir crest length change with flow depth in a curved flume with very coarse sand.

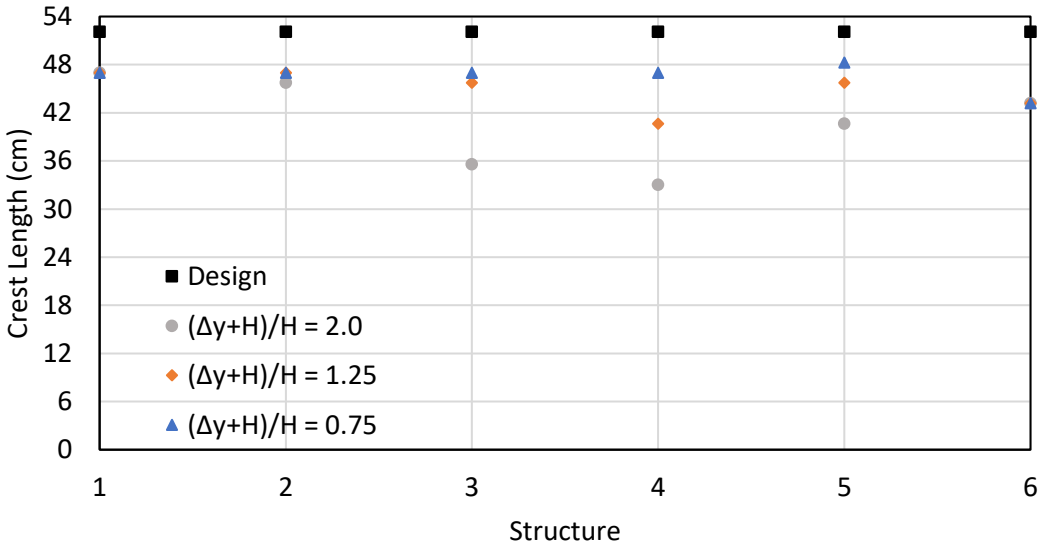

Figure 175. Rock vane crest length change with flow depth in a curved flume with very coarse sand.

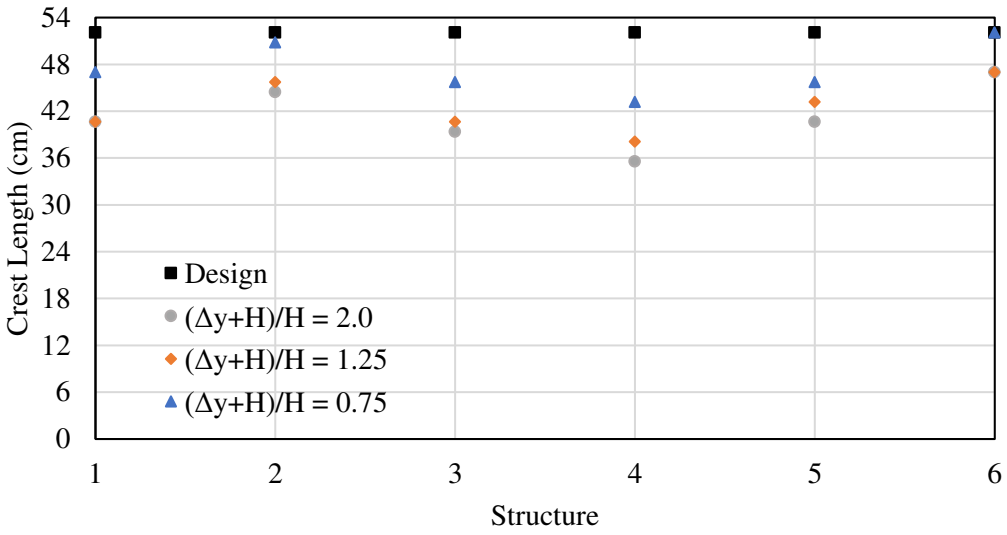

Figure 176. Bendway weir crest length change with flow depth in a curved flume with medium sand.

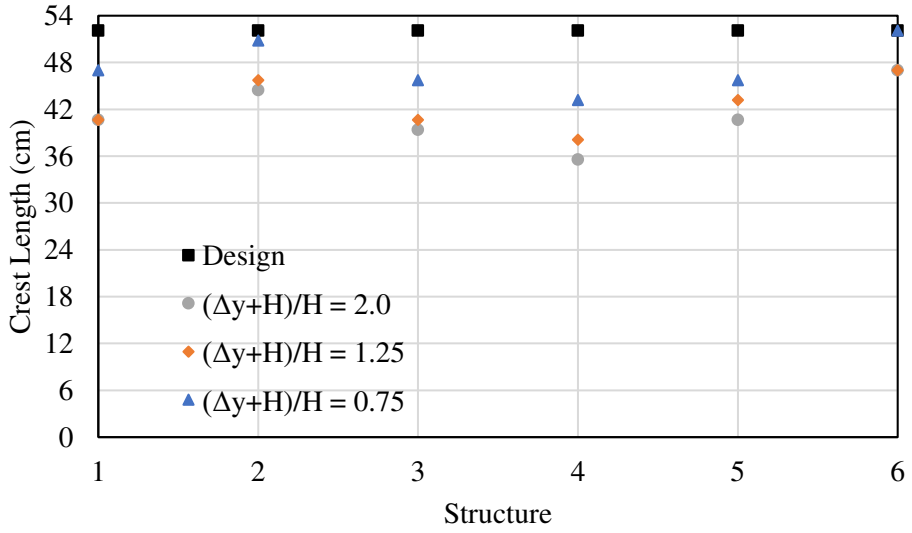

Figure 177. Rock vane crest length change with flow depth in a curved flume with medium sand.

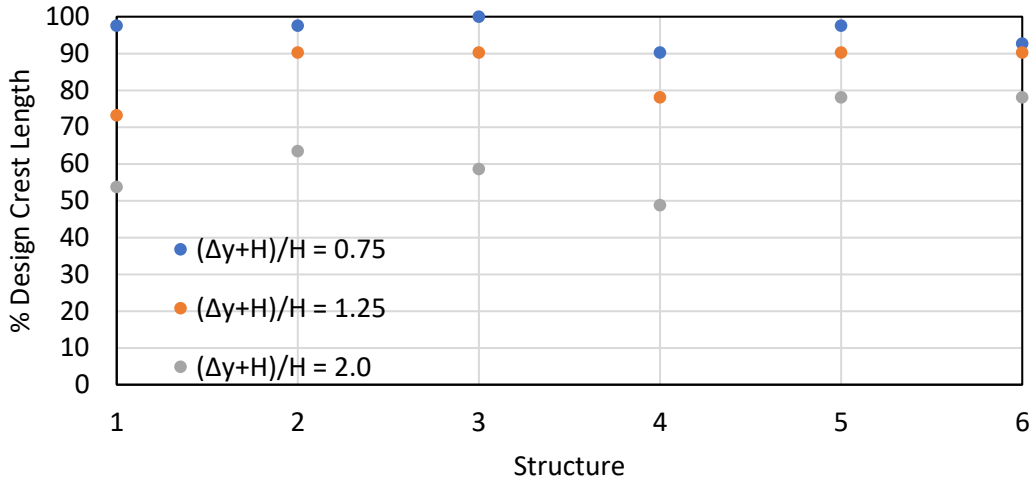

Figure 178. Bendway weir crest length variation with flow depth as a percent of the design crest length in a curved flume with very coarse sand.

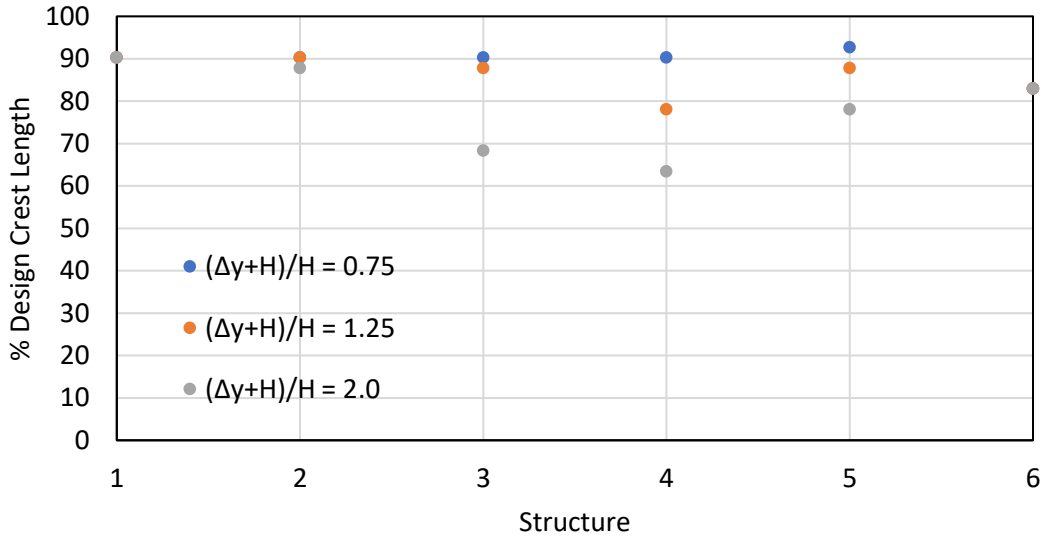

Figure 179. Rock vane crest length variation with flow depth as a percent of the design crest length in a curved flume with very coarse sand.

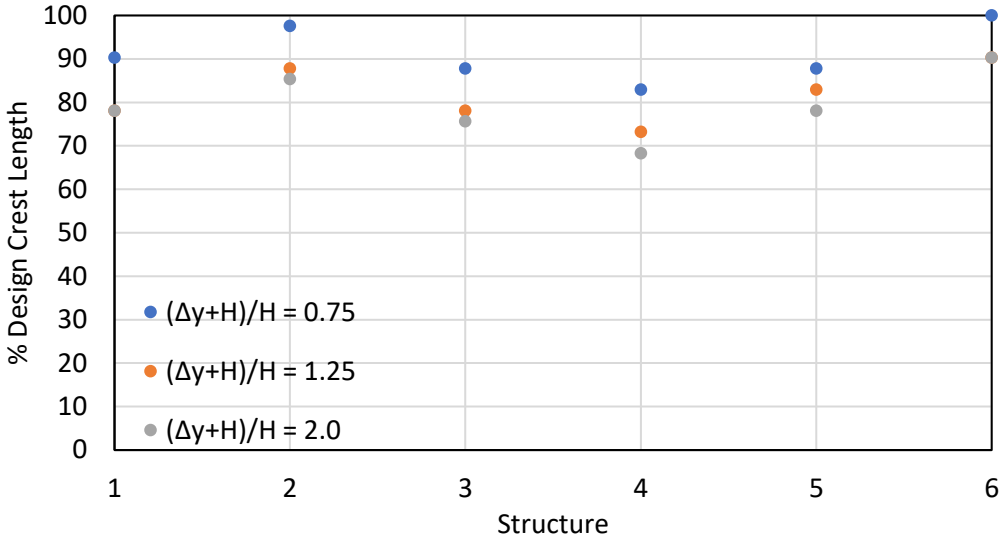

Figure 180. Bendway weir crest length variation with flow depth as a percent of the design crest length in a curved flume with medium sand.

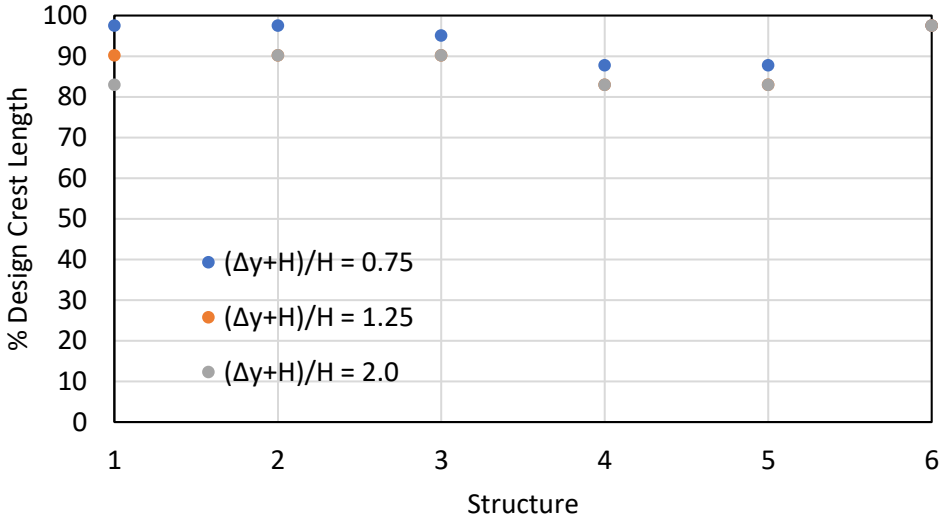

Figure 181. Rock vane crest length variation with flow depth as a percent of the design crest length in a curved flume with medium sand.

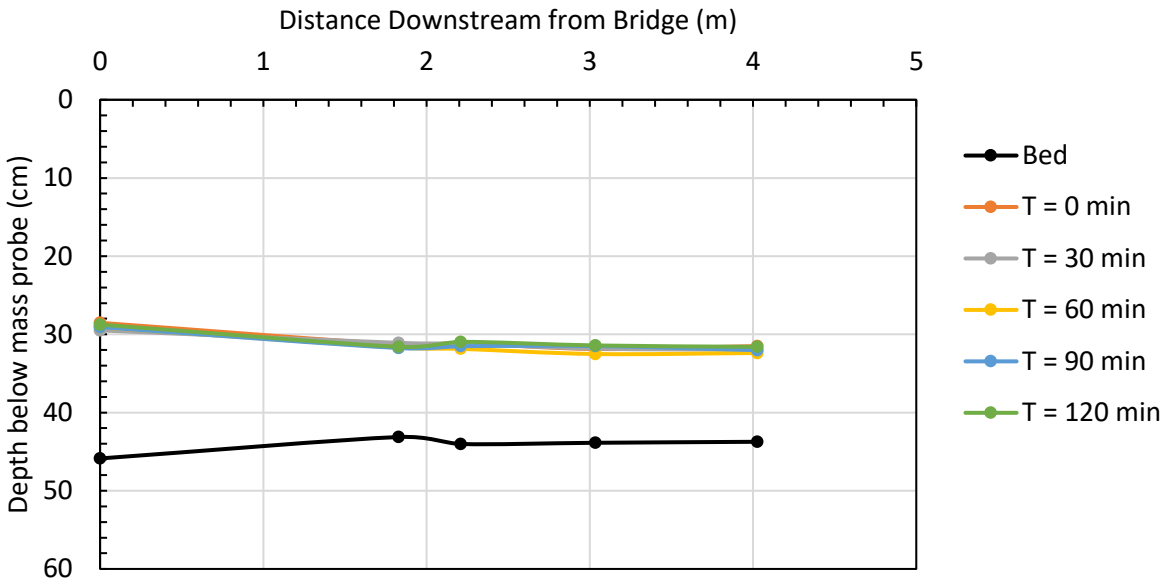

Figure 182. Massa probe WSE over time for EXPT 1a.

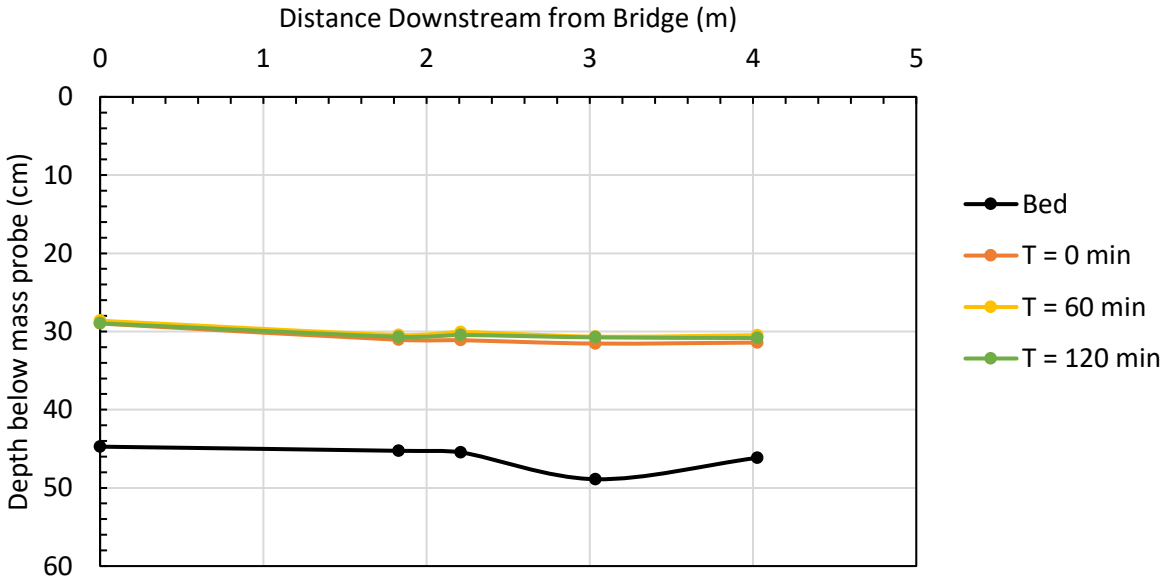

Figure 183. Massa probe WSE over time for EXPT 2a.

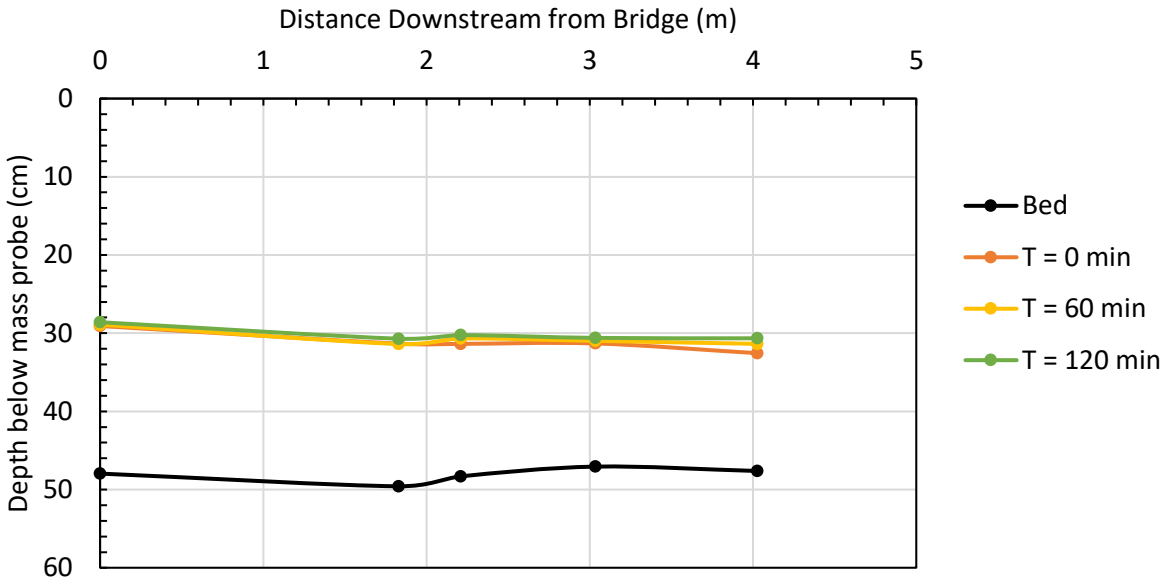

Figure 184. Massa probe WSE over time for EXPT 3a.

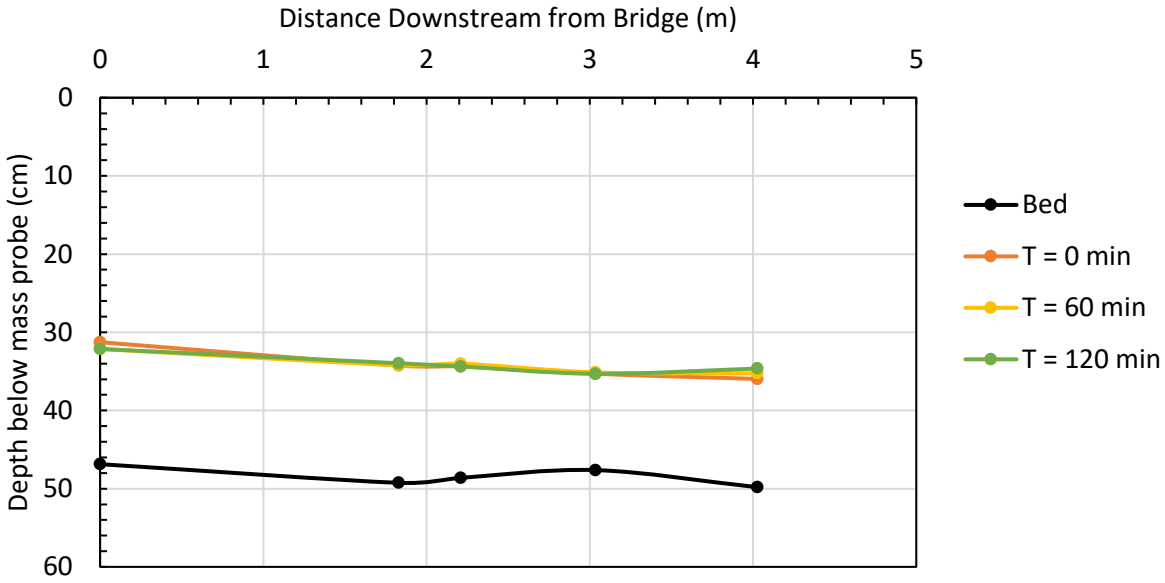

Figure 185. Mass probe WSE over time for EXPT 4a.

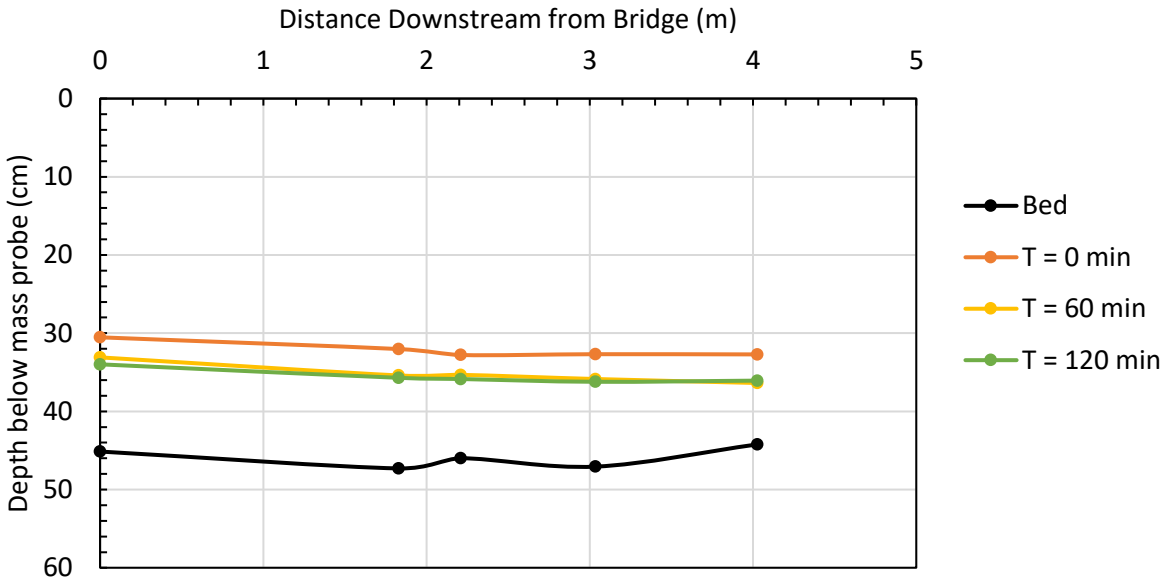

Figure 186. Massa probe WSE over time for EXPT 5a.

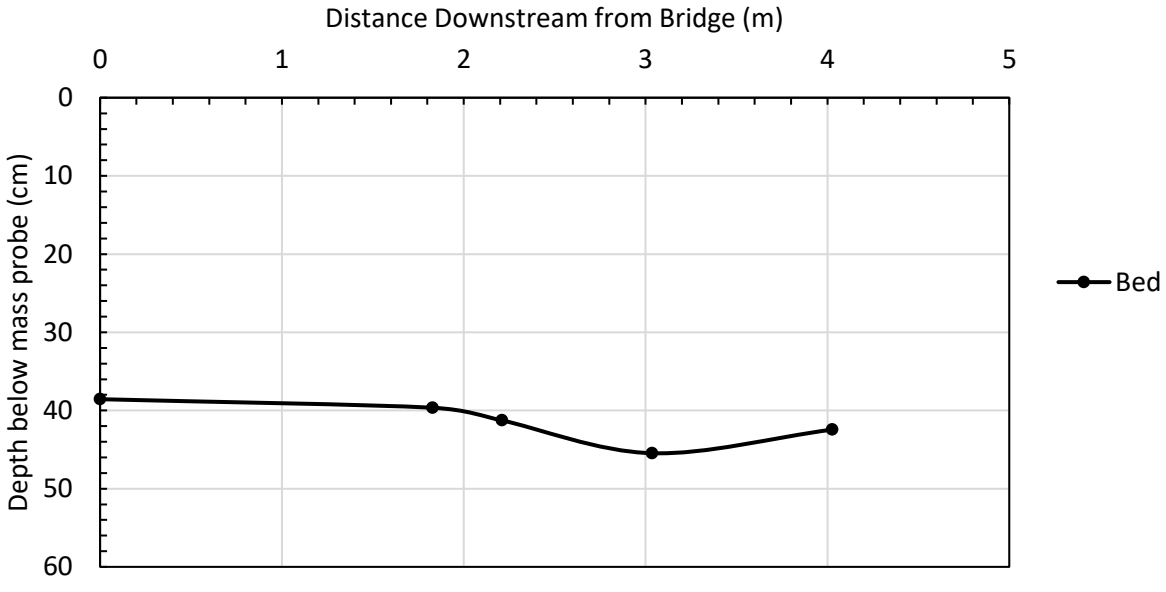

Figure 187. Massa probe bed elevation for EXPT 6a.

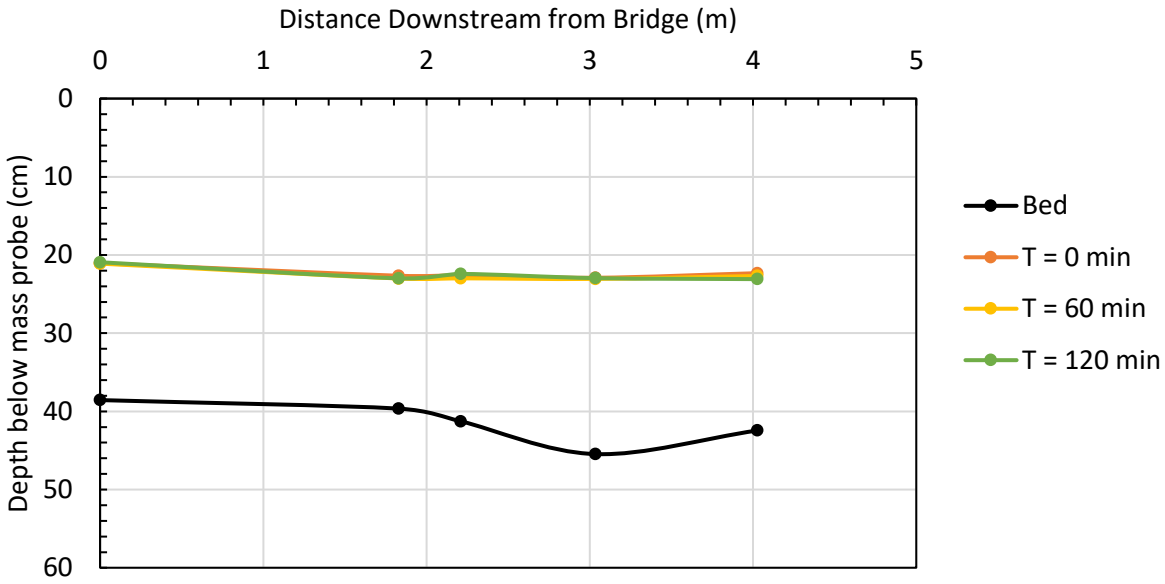

Figure 188. Massa probe WSE over time for EXPT 7a.

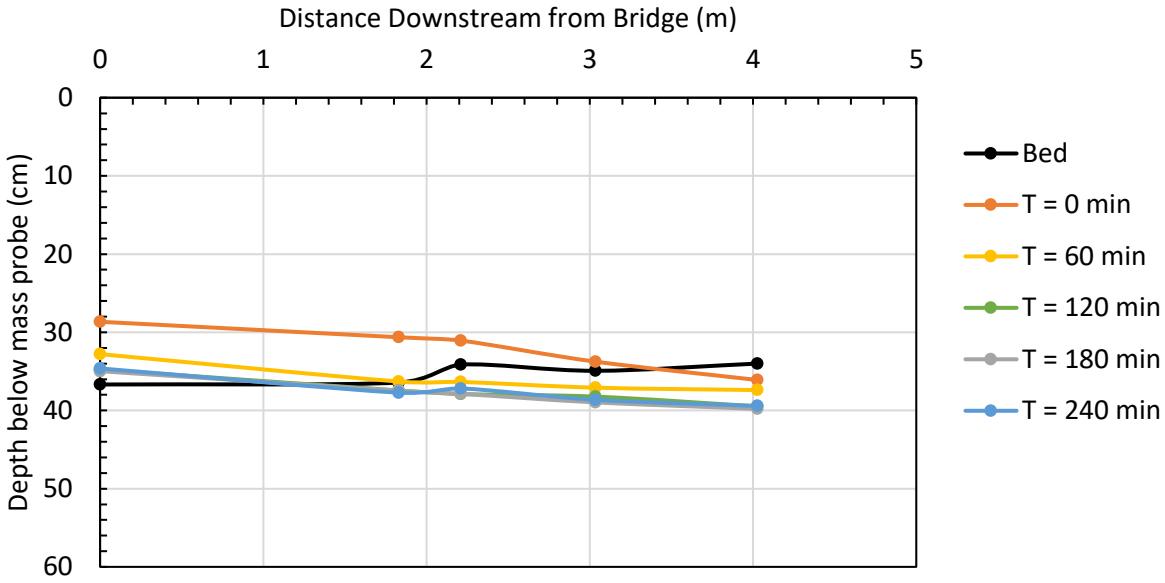

Figure 189. Massa probe WSE over time for EXPT 8a.

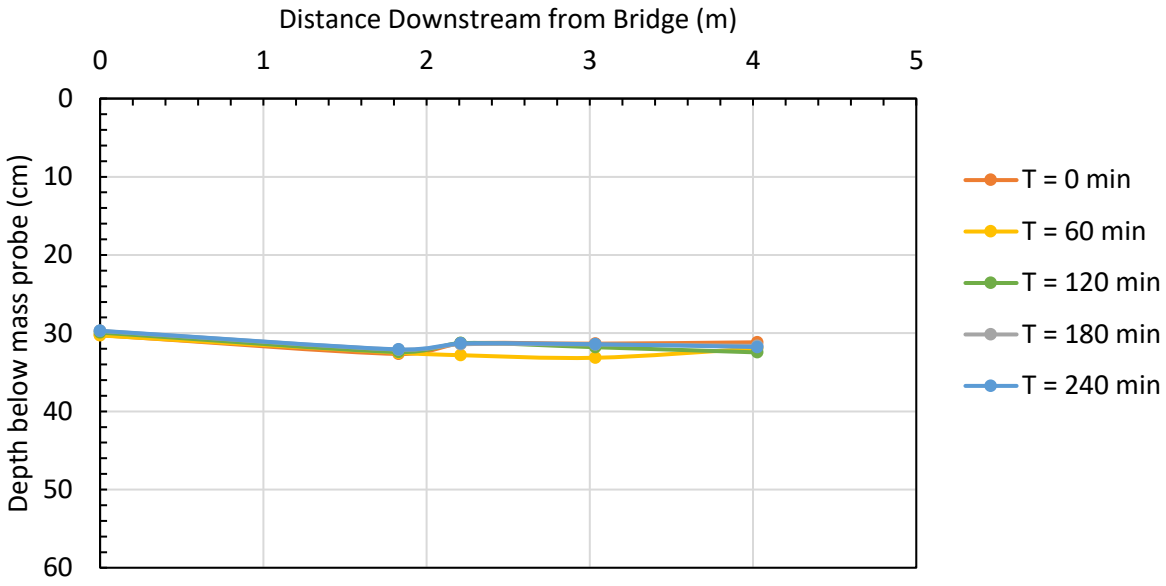

Figure 190. Massa probe WSE over time for EXPT 9a.

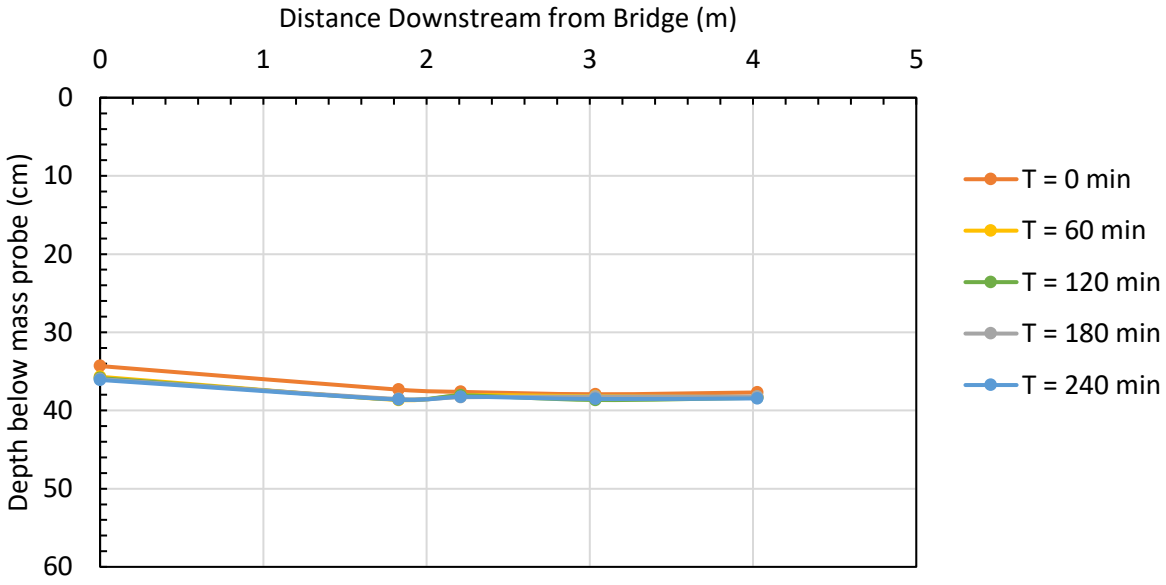

Figure 191. Massa probe WSE over time for EXPT 10a.

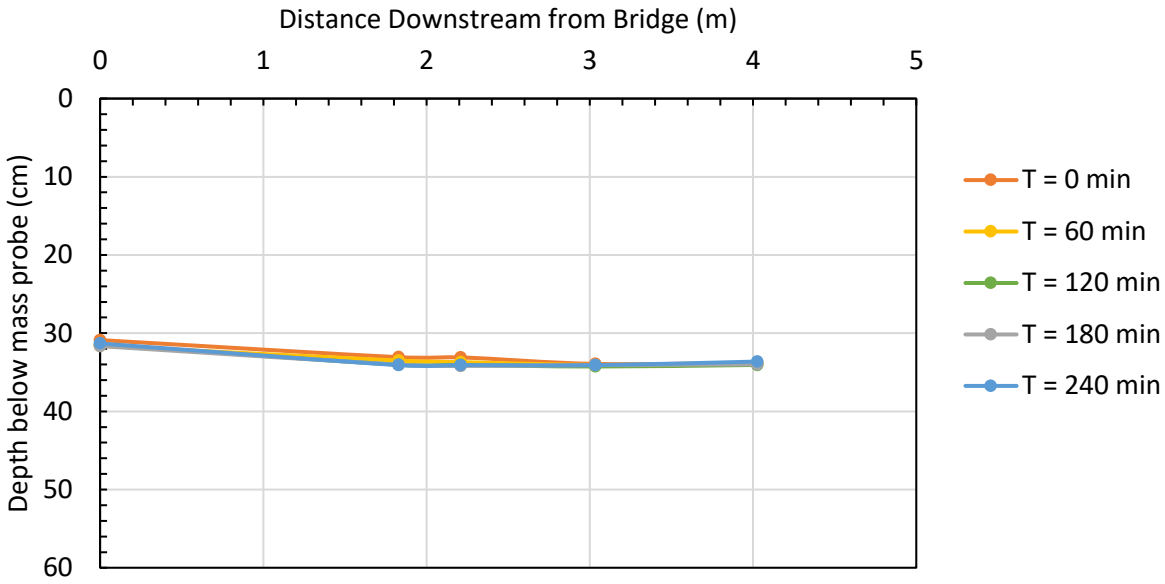

Figure 192. Massa probe WSE over time for EXPT 11a.

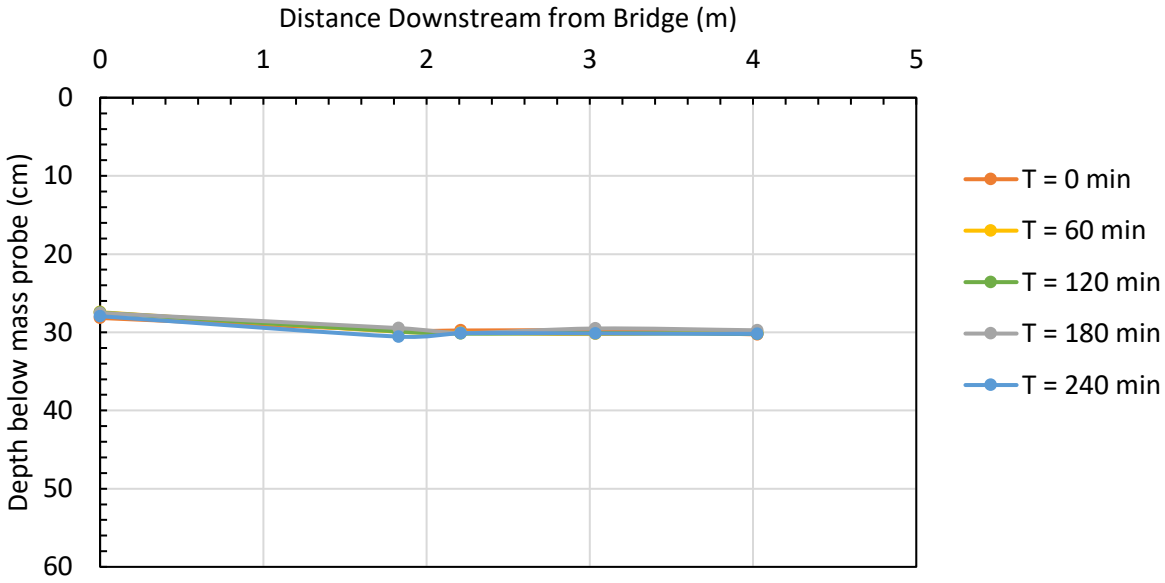

Figure 193. Massa probe WSE over time for EXPT 12a.

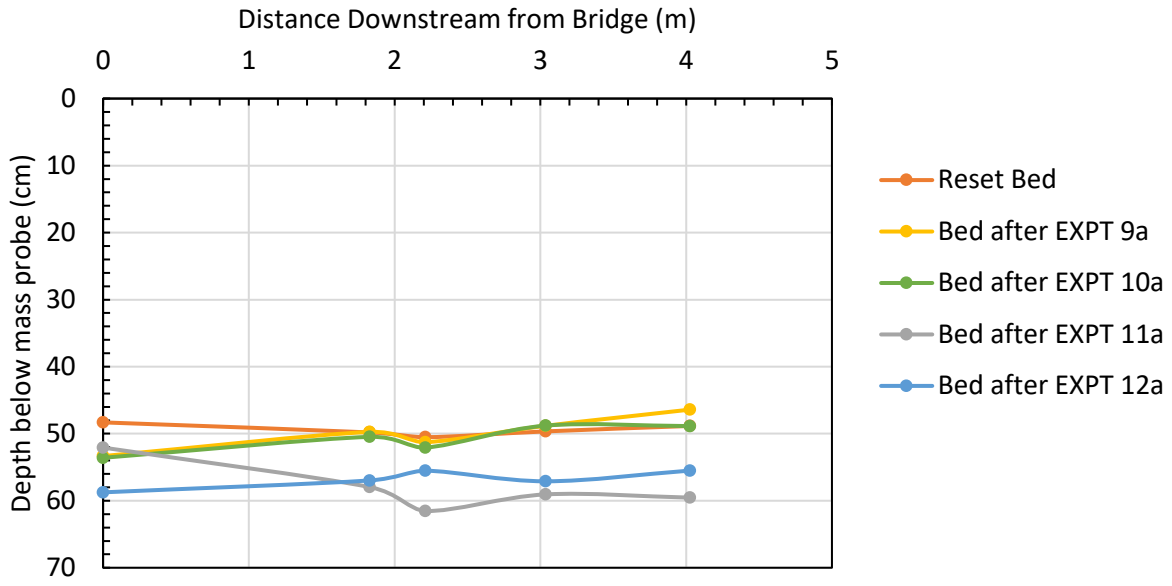

Figure 194. Massa probe bed elevation for the hydrograph procedure with bendway weirs and coarse sand.

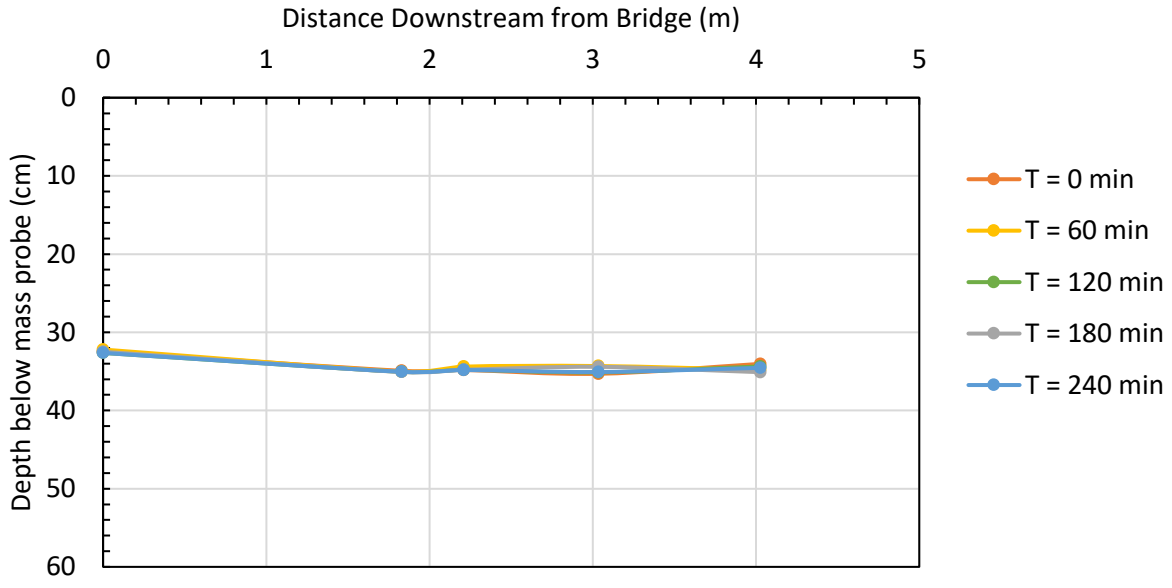

Figure 195. Massa probe WSE over time for EXPT 13a.

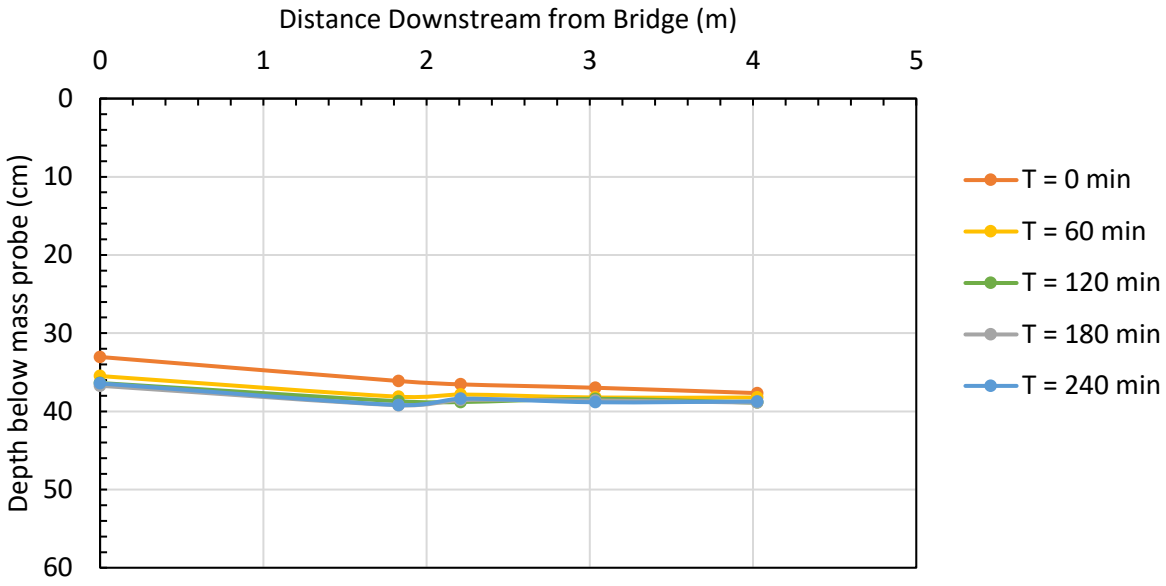

Figure 196. Massa probe WSE over time for EXPT 14a.

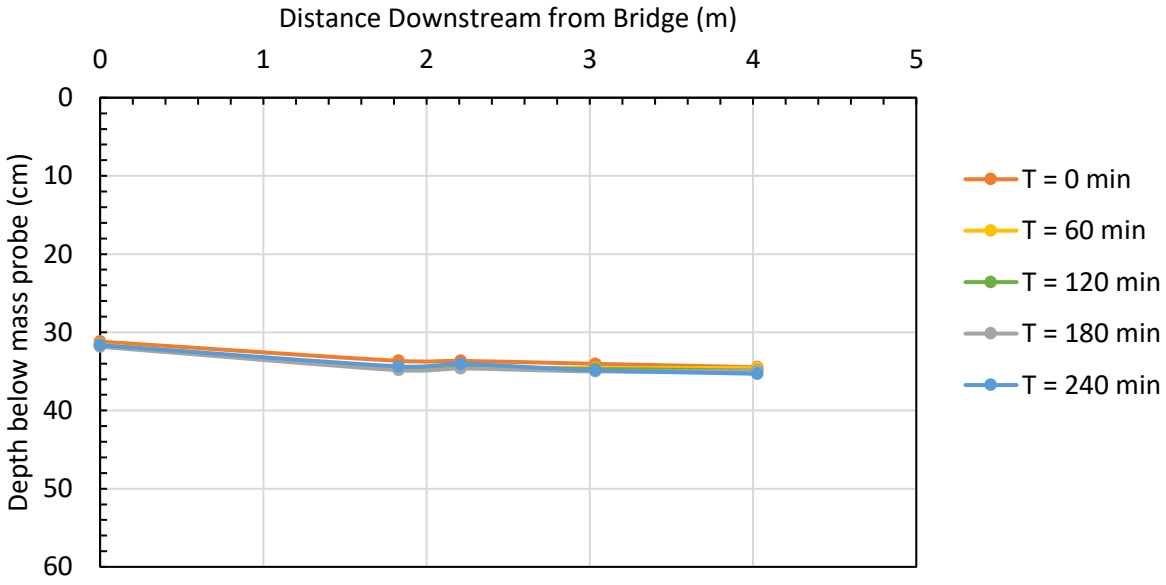

Figure 197. Massa probe WSE over time for EXPT 15a.

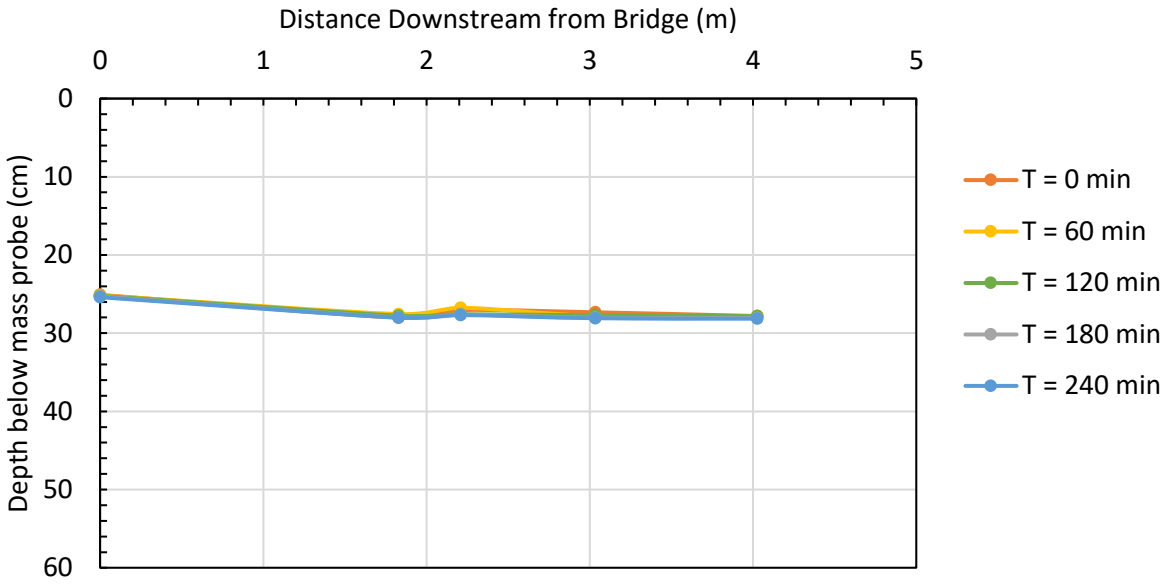

Figure 198. Massa probe WSE over time for EXPT 16a.

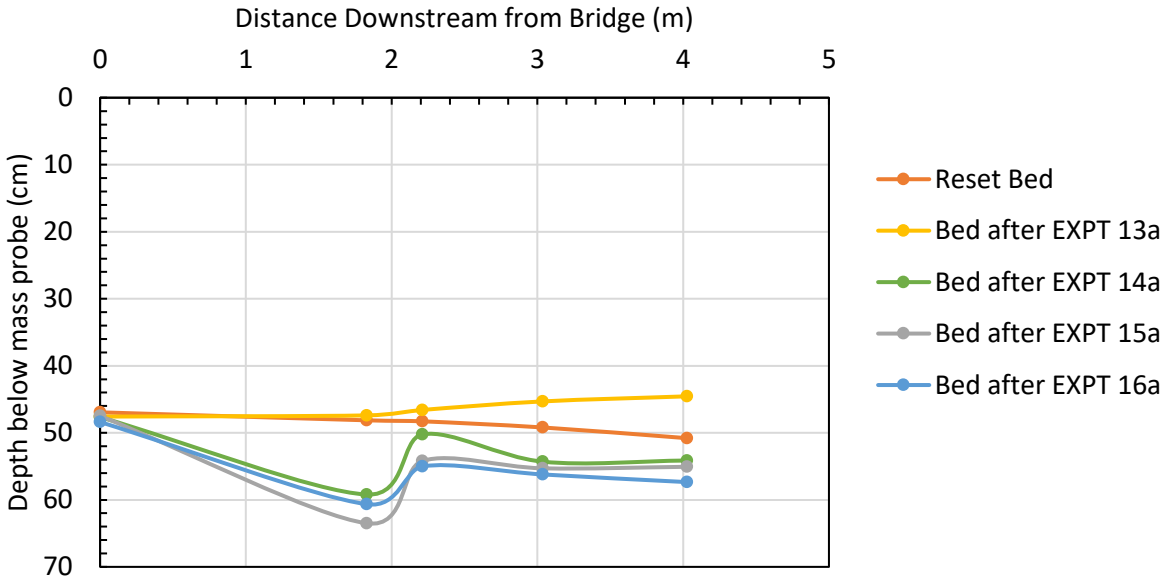

Figure 199. Massa probe bed elevation for the hydrograph procedure with rock vanes and coarse sand.

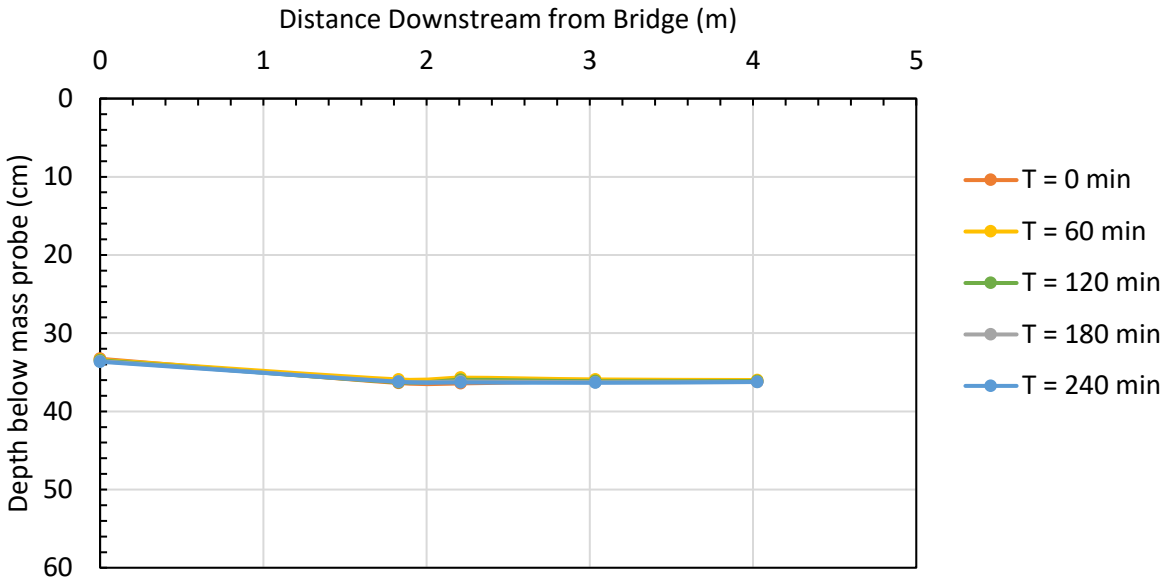

Figure 200. Massa probe WSE over time for EXPT 17a.

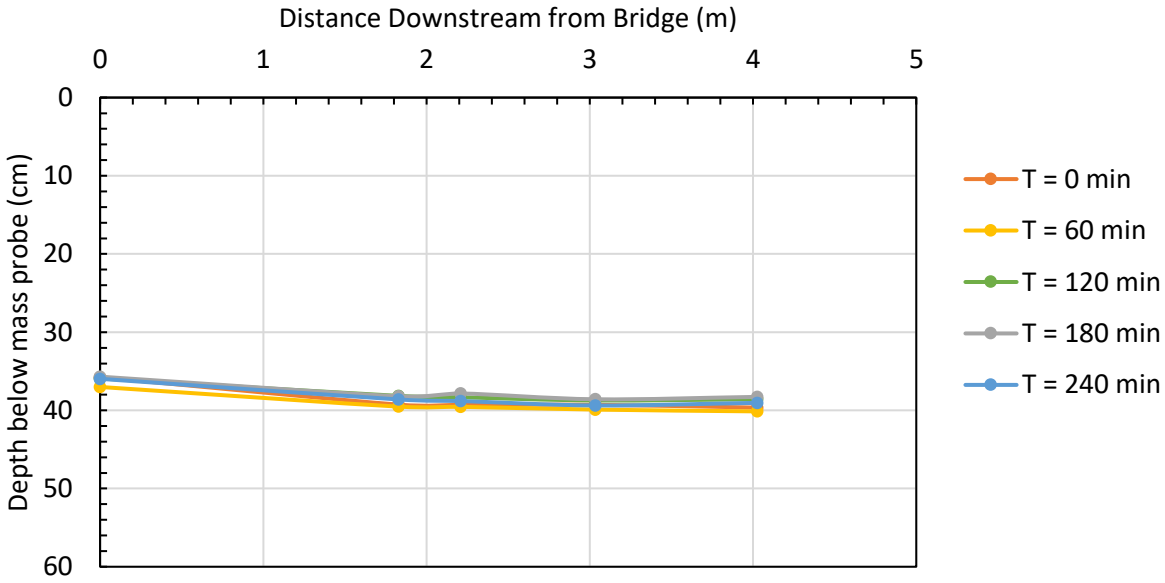

Figure 201. Massa probe WSE over time for EXPT 18a.

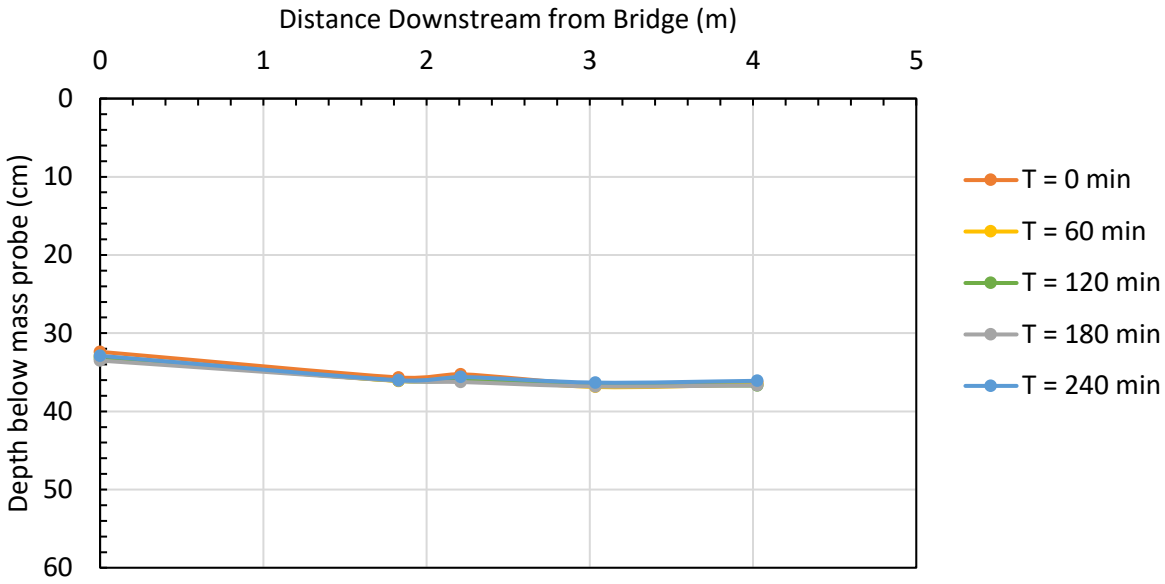

Figure 202. Massa probe WSE over time for EXPT 19a.

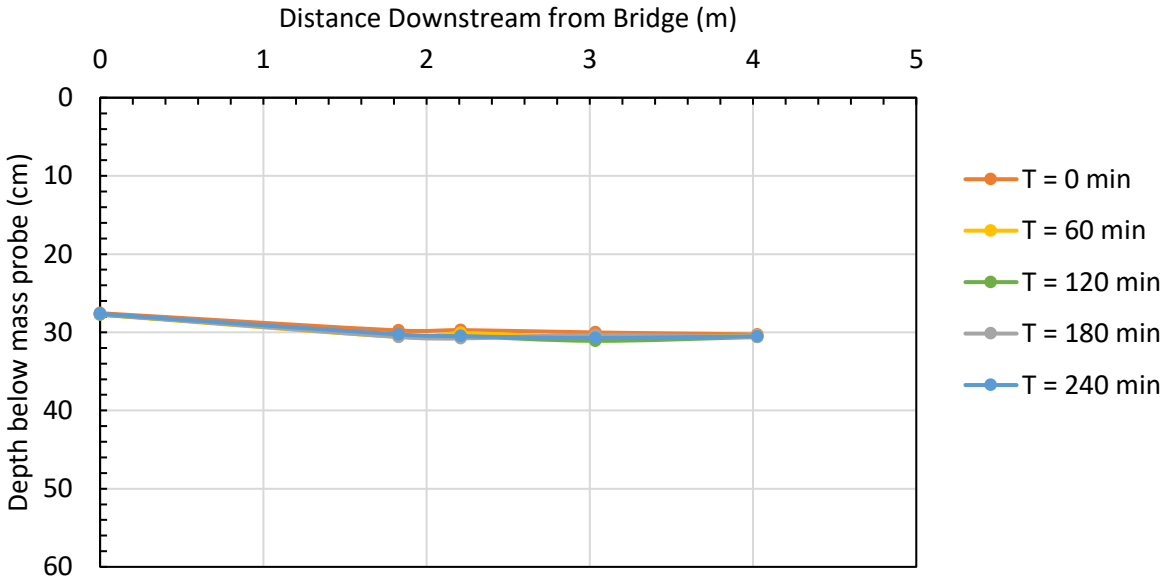

Figure 203. Massa probe WSE over time for EXPT 20a.

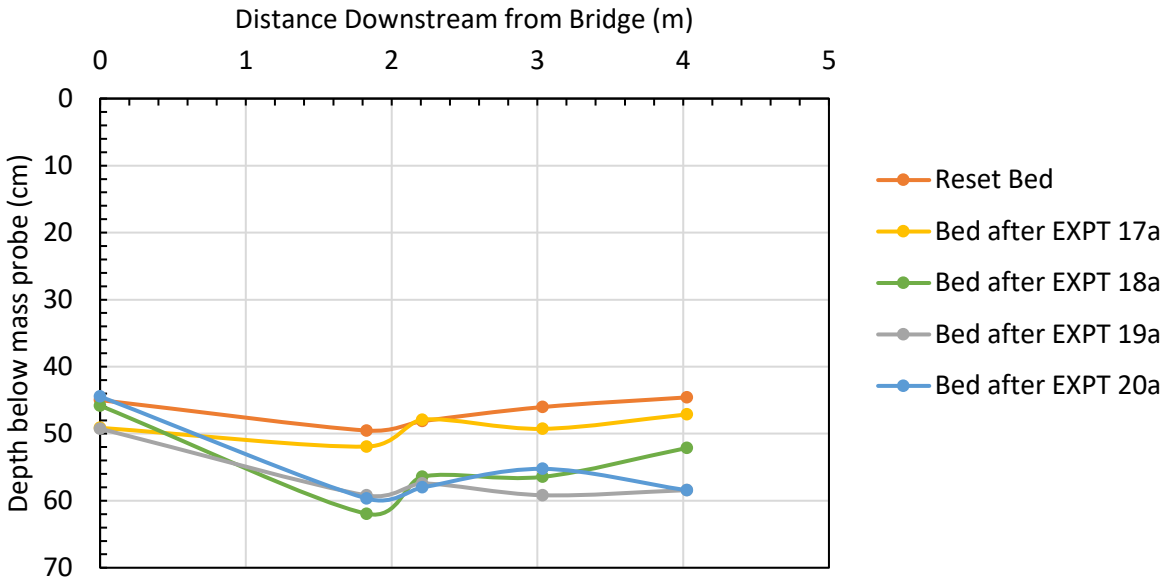

Figure 204. Massa probe bed elevation for the hydrograph procedure with bendway weirs and medium sand.

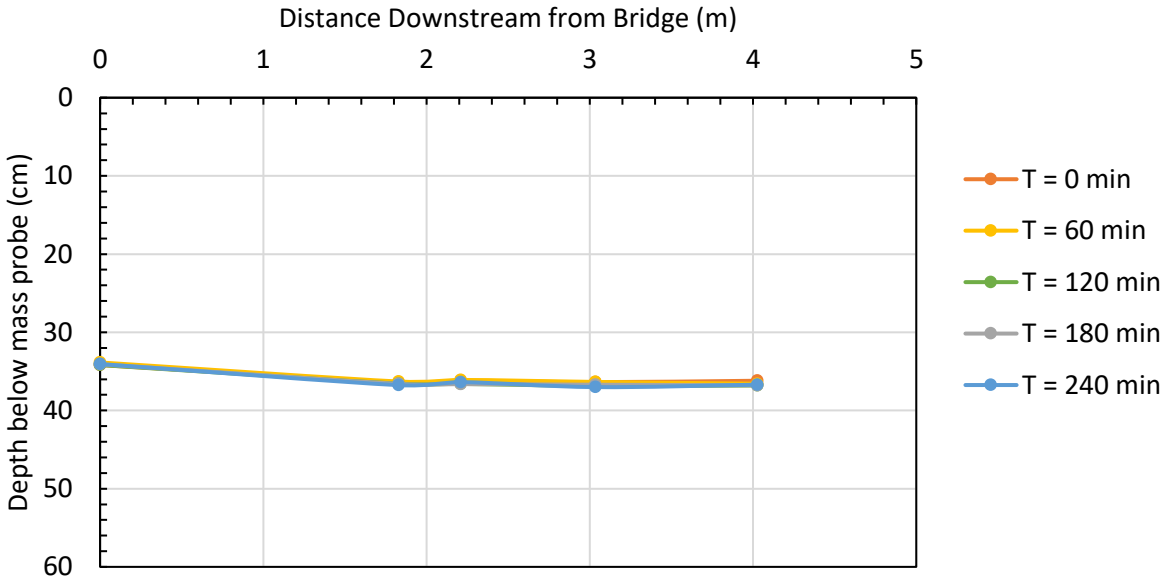

Figure 205. Massa probe WSE over time for EXPT 21a.

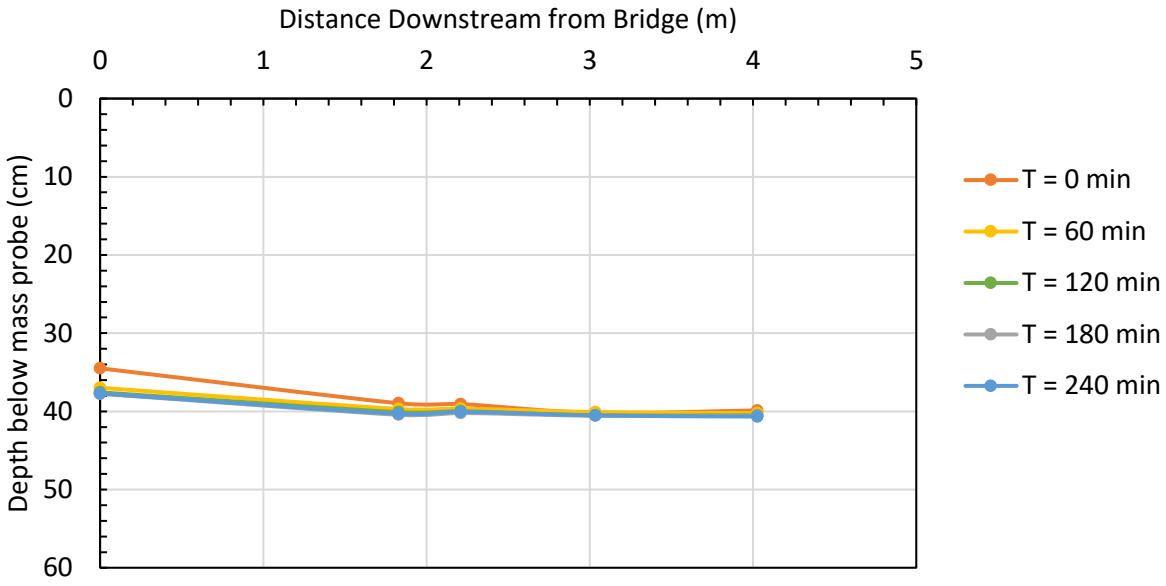

Figure 206. Massa probe WSE over time for EXPT 22a.

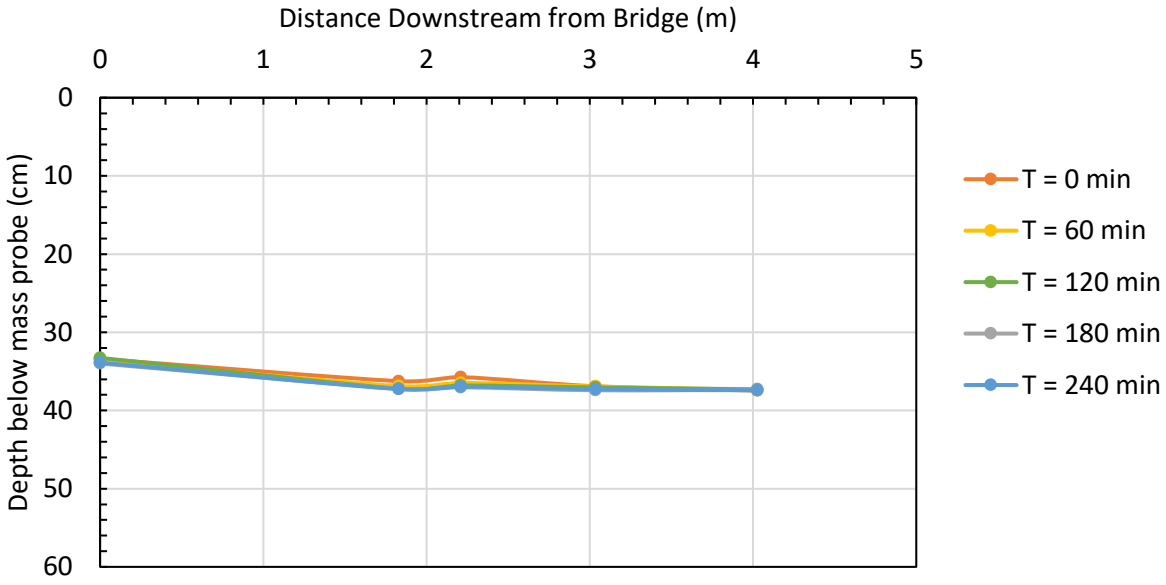

Figure 207. Massa probe WSE over time for EXPT 23a.

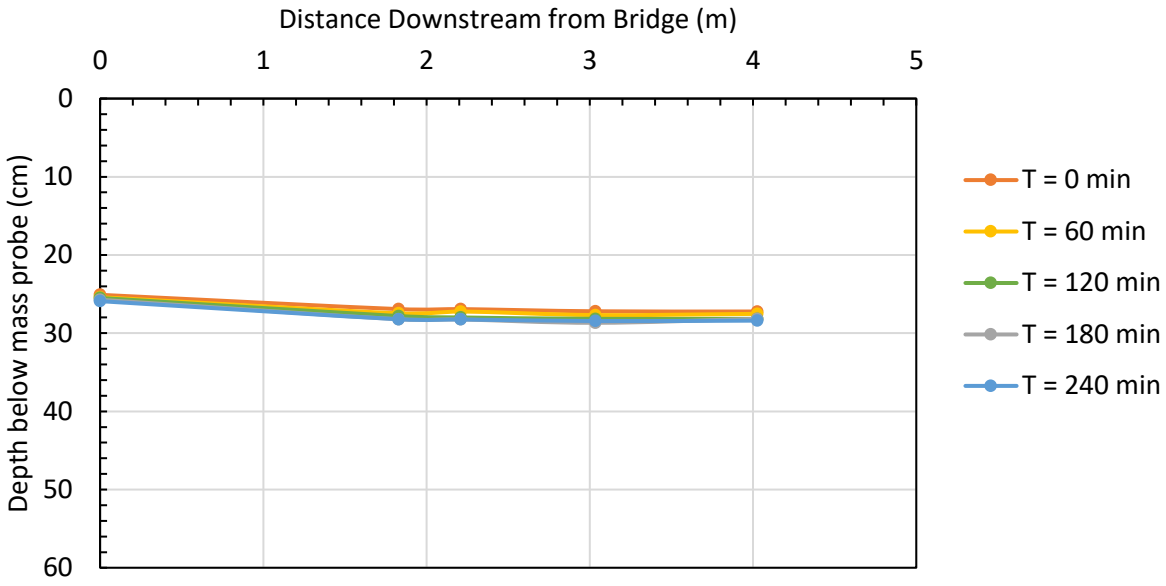

Figure 208. Massa probe WSE over time for EXPT 24a.

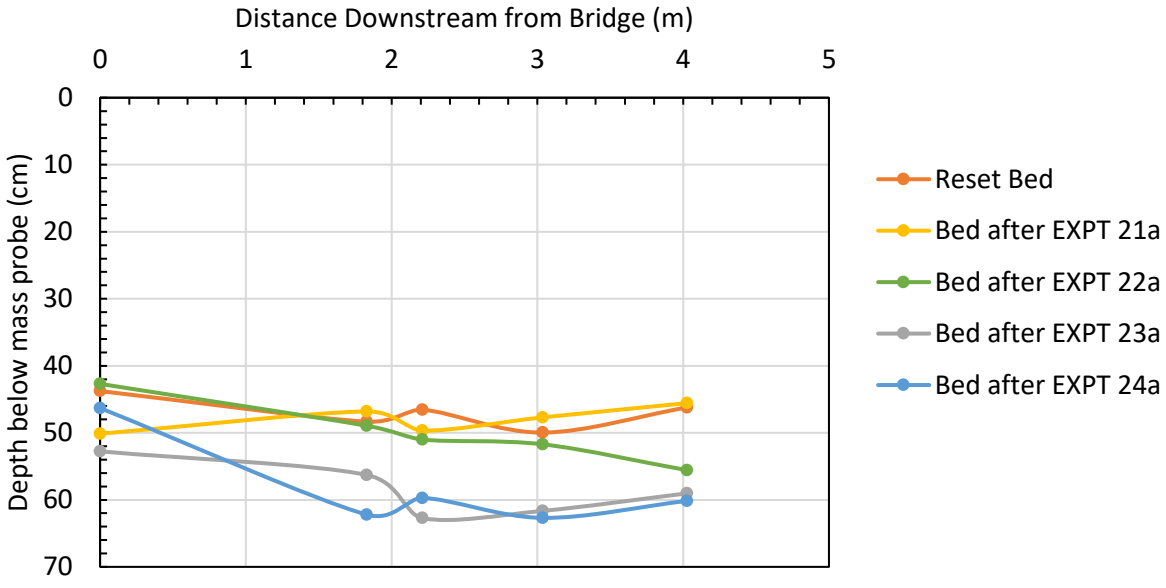

Figure 209. Massa probe bed elevation for the hydrograph procedure with rock vanes and medium sand.

ABBREVIATIONS

ADV	Acoustic Doppler Velocimetry
BOR	Bureau of Reclamation (U.S. Department of Interior)
CFD	Computational Flow Dynamics
CSU	Colorado State University
EXPT	Experiment
FLOW-3D	3D CFD model by Flow Science, Inc.
LiDAR	Light Detection and Ranging Survey System
LSPIV	Large-Scale Particle Image Velocimetry
MPM	Meyer-Peter & Müller
SRH-2D	Sedimentation and River Hydraulics – two dimensional
WSE	Water Surface Elevation